Analysis of perforated beams in fire using a virtual hybrid simulation approach

A thesis submitted to the Brunel University London,

for the degree of Doctor of Philosophy

By

Mustesin Ali Khan

Doctor of Philosophy

BRUNEL UNIVERSITY LONDON

2019

Abstract

This thesis is concerned with the behaviour of composite perforated beams in fire conditions, and a new virtual hybrid simulation approach is proposed to facilitate the investigation. Composite perforated beams are an increasingly popular choice in the construction of long-span floor systems as they provide a structurally and materially efficient design solution and allow space for building services. Most of the relevant research conducted to date has been focussed on isolated beam elements, assuming simply-supported boundary conditions. These simplifying assumptions are largely due to the complexity of modelling the whole structure in high definition, as well as the significant associated computational expense. However, testing and analysing isolated components inherently ignores any load redistributions which take place in the structure and does not provide an insight into the thermomechanical interactions which develop during a fire.

In this context, the two primary objectives of this work are to (i) develop a usable virtual hybrid simulation framework which assesses the response of individual structural elements subjected to fire, taking account of the surrounding structure and (ii) utilise this framework to investigate the behaviour of perforated beams exposed to fire including the effects from the surrounding structure in the form of axial and rotational restraint. In the virtual hybrid simulation method, the part of the structure which is exposed to fire is modelled in fine detail using shell and solid elements and the remaining surrounding structure is represented using simpler beam-column elements. The simulation is developed using a combination of the OpenSees, OpenFresco and Abaqus softwares and enables the user to investigate the behaviour of fire-exposed components while including the effect of the remaining structure without modelling the whole system in fine detail. The accuracy of the model is validated using available fire test data.

The behaviour of composite perforated beams in fire is analysed using the developed framework and then compared with the predicted response obtained by modelling isolated simply-supported beams. The results highlight the importance of including the effects from the surrounding structure in the analysis. The virtual hybrid simulation framework is then utilised to investigate the influence of the most salient parameters including the

type of fire, opening layout, restraint conditions as well as the material and geometric details.

In the final part of the thesis, the current ambient temperature design standards for perforated beams are modified to account for the effects of fire. A series of analytical expressions are developed to estimate the fire resistance of composite perforated beams with different opening layouts, and these predictions are compared with the fire resistance obtained from the numerical simulations. It is shown that the proposed analytical approach provides a good estimation of the fire resistance for the majority of cases.

Publications

The present PhD study has led to a list of journal papers, conference papers and technical presentations, as follows:

Journal Papers

1. **Khan, M. A.,** Jiang, L., Cashell, K. A., and Usmani, A. (2018). "Analysis of restrained composite beams exposed to fire using a hybrid simulation approach." *Engineering Structures*, 172, 956–966.
2. **Khan, M. A.,** Jiang, L., Cashell, K. A., and Usmani, A. "Virtual hybrid simulation of beams with web openings in fire" (under review with the *Journal of Structural Fire Engineering,* Manuscript Number JSFE-01-2019-0008)
3. **Khan, M. A.,** Cashell, K. A., and Usmani, A. "Analysis of restrained composite perforated beams during fire using a hybrid simulation approach**"** (accepted by the ASCE *Journal of Structural Engineering,* Manuscript Number STENG-7985)

Conference Papers

1. **Khan, M. A.,** Jiang, L., Cashell, K. A., and Usmani, A. (2018). "Analysis of composite beams exposed to fire using a hybrid simulation approach" published in conference proceedings of the *2nd Conference on Structural Safety Under Fire and Blast Loading*, Cobfab-2017, London, UK
2. **Khan, M. A.,** Jiang, L., Cashell, K. A., and Usmani, A. (2018). "Numerical modelling of the fire behaviour of restrained cellular beams using a hybrid simulation approach" published in conference proceedings of the 10th *Structures in Fire Conference***, SiF-2018,** Belfast, Ireland**.**
3. Cashell, K. A., Malaska, M., **Khan, M. A.**, Alanen, M. and Mela, K. (2019). "Numerical analysis of the behaviour of stainless steel cellular beam in fire – Submitted to the 14th *Nordic Steel Construction Conference*, Nordic Steel 2019, Copenhagen, Denmark.

Technical Presentations

1. **Khan, M. A.**, "Hybrid simulation approach in fire condition" Presented a poster at poster conference conducted by *Brunel University London 2016*, London, UK
2. **Khan, M. A.**, "Analysis of Cellular Beams in Fire Conditions using Hybrid Simulation" Presented a poster at 20th *Young Researcher Conference 2018*, conducted by the Institution of Structural Engineers (IStructE), London, UK
3. **Khan, M. A.**, "Analysis of perforated beams exposed to fire using virtual hybrid simulation" Presented the research at *Structure in Fire Forum 2019*, organised by University of Edinburgh at the Institution of Structural Engineers, London, UK

Acknowledgement

I would like to express my deepest gratitude to my principle supervisor Dr. Katherine Cashell for her dedication and knowledge, as well as for the support and patience throughout the duration of this study. I would also like to thank my second supervisor Prof. Asif Usmani, although not formally one of my supervisors, also provided invaluable advice, with considerable patience. It has been a privilege to work with both.

I would like to thank Dr. Liming Jiang (Hong Kong PolyU) for providing insightful comments and valuable suggestions. In addition, I wish to thank Prof. Pradeep Bhargava (IIT Roorkee) for his support, and encouragement to join a PhD.

I could not omit to express my gratitude for the PhD studentship received from the Brunel University London and funds that allowed me to attend two international conferences, thus gaining the experience of presenting my work to widely recognised audience.

Whilst at Brunel, I have been privileged to have had some wonderful colleagues, most notably Alaa Al-Isawi, Asif Mohammed, Rand Al-Janabi and Amy Flynn, whose company and friendship have proven to be invaluable.

I wish to thank my brother in law, Naushad Khan for taking care of everything back home when I was not there. I would also like to thank my father in law, Aijazuddin Sheikh for his support and always believing in me.

Special thanks goes to the closest person to me, my wife, Farheen Sheikh, whose love and support has always been an enormous source of inspiration and strength for me.

Above all, it is impossible to express how lucky I have been to have such a loving and supportive mother, Sanjeeda Parveen, I largely owe to her all I have achieved in my life. I would also like to thank my siblings Shagufta Anjum, Mohsin Ali Khan and Mohsina Anjum Khan who patiently and constantly supported me in the best possible way throughout my life.

Contents

List of figures

List of Tables

Notation

The following notation is used in the thesis. All symbols are initially defined within the text as it first appears and in the context in which it is used. Some symbols are followed by subscripts and superscripts referring to certain formulations. Those not defined below are explained in the text.

A	Area of cross-section
A_{bT}	Area of cross section of the bottom tee
A_f	Cross section are of the top flange
AR	Axial restraint
A_{sl}	Area of the tensile reinforcement
A_v	Area of the two tees
$A_{w,T}$	Cross section area of the web in top tee
$b_{eff,o}$	Effective width of the slab
b_f	Overall width of the tee
b_w	Effective width of the concrete flange in shear
c	Load-moment interaction coefficient
$dev(\sigma)$	Deviatoric stress
DOF	Degree of freedom
E	Young's modulus
$E_{a,\theta}$	Slope of the linear elastic range of steel at elevated temperature
E_θ	Young's modulus for concrete at elevated temperature
f'_{c20}	Compressive strength of concrete at 20 °C
f_{cd}	Design strength of concrete
f_{cr}	Tensile strength of concrete at room temperature
$f_{cr\theta}$	Tensile strength of concrete at elevated temperature

$f'_{c\theta}$	Concrete compressive strength at elevated temperature
$f_{p,\theta}$	Proportional limit stress at elevated temperature
f_y	Yield strength
$f_{y,\theta}$	Effective yield strength at elevated temperature
h	Depth of the steel I beam
h_c	Depth of concrete topping
h_d	Overall depth of the profiled deck
h_{eff}	Effective depth of the beam between the centroids of two tees
h_s	Depth of the flat part of the slab
HS	Hybrid Simulation
$h_{s,eff}$	Effective depth of the slab for punching shear
h_t	Depth of the top tee
$h_{w,T}$	Depth of the web of top tee
IP	Internet protocol
k_0	Reduction factor for the flexibility of the long opening
$k_{c.t}(\theta)$	Tensile strength reduction factor of concrete at elevated temperature
$K_{E,\theta}$	Slope of linear elastic range reduction factor for concrete at elevated temperature
$K_{p,\theta}$	Proportional limit reduction factor for concrete at elevated temperature
$K_{y,\theta}$	Effective yield strength reduction factor for concrete at elevated temperature
l	Span of the beam
l_{bd}	Encourage length for tensile reinforcement
l_o	Effective length of the opening
LTB	Lateral torsional buckling
M	Uniform bending moment applied on the beam

$M_{bT,RD}$	Bending resistance of the bottom tee
M_g	Moment due to gravity loads
$M_{o,Rd}$	Bending resistance of a perforated beam
$M_{p-\delta}$	Moment due to p-δ effect
M_{pl}	Plastic moment capacity of the section
$M_{tT,RD}$	Bending resistance of the top tee
M_u	Applied bending moment on a beam-column
$M_{vc,RD}$	Bending resistance due to the composite action of the top tee and the slab
MWO	Multiple web opening
$N_{bT,Rd}$	Tensile strength of the bottom tee
$N_{c,Rd}$	Compressive resistance of the slab
N_{ED}	Axial tensile force due to global bending action
$N_{pl,RD}$	Axial resistance of the tee section
n_s	Number of shear connectors above the opening
NS	Numerical substructure
n_{sc}	Number of shear connectors between the nearest support and the centre of the opening
$N_{wp,Rd}$	Buckling resistance of the web-post
P	Axial restraint developed due to restrained thermal expansion
P_{adpt}	Reaction force at the interface of the slave assembly
PNA	Plastic neutral axis
P_{rd}	Design resistance of the shear connector
PS	Physical substructure
P_u	Applied axial force on a beam-column
q	Yield strength of steel with hardening

$q_{t,d}$	Design value of fire load density
r	Radius of gyration of the section and reaction force matrix
S_0	Clear distance between the two openings
SWO	Single web opening
TCP	Transmission control protocol
t_f	Thickness of the flange
t_w	Thickness of the web
UB	Universal beam
UC	Universal column
u_{super}	Displacement at the interface node of master assembly
$V_{c,Rd}$	Shear resistance of the concrete slab in a perforated beam
$V_{pl,Rd}$	Shear resistance of a perforated steel beam
$V_{wp,ED}$	Shear resistance of the web-post
w	Uniformly distributed load applied on the beam
W_{pl}	Plastic failure load
x	Target displacement
Y	Eccentricity of the axial restraint from the centroid of the section
z_c	Depth of concrete in compression
Z_{pl}	Plastic section modulus of the section
z_{pl}	Distance of the extreme steel surface of the top flange from the plastic neutral axis
z_t	Distance of centroid of the top tee from the outer surface of the flange
$\delta_{midspan}$	Midspan deflection of the beam
ε	Strain
$\varepsilon_{o\theta}$	Strain at peak stress of concrete at elevated temperature

$\varepsilon_{p,\theta}$	Strain at the proportional limit of steel at elevated temperature
$\varepsilon_{t,\theta}$	Limiting strain of steel at elevated temperature
$\varepsilon_{u,\theta}$	Ultimate strain at elevated temperature
$\varepsilon_{y,\theta}$	Yield strain of steel at elevated temperature
λ	Slenderness ratio
$\sigma_{c\theta}$	Stress for concrete at elevated temperature
ΦP_n	Design axial force of a beam-column
ΦM_n	Design bending moment of a beam-column
$\emptyset(\sigma, q)$	Yield function for von Mises failure criteria

Chapter 1

Introduction

1. Motivation

Steel framed construction is one of the most common structural forms in the UK, owing to its many favourable attributes such as structural efficiency, ease of construction and ready availability of the required materials. One of the few perceived challenges with steel framed buildings is their behaviour during a fire, as the strength and stiffness of the material tends to decrease quite sharply with increasing temperature. In this context, engineers and researchers have focussed considerable efforts in recent years towards improving the understanding of what happens when a steel structure is exposed to fire conditions. Experimental testing is one of the best ways to understand the behaviour of structures in fire and to confirm the effectiveness of design methods for fire-resistant structures. However, only a few full-scale or large-scale fire tests have been performed on steel framed structures, where the whole system is investigated rather than just individual components. Large-scale structural fire tests are rare because they are costly and require specialized experimental facilities. Most of the experimental research into the behaviour of structures in fire has been carried out on isolated structural components, exposed to standard fire curves, in order to compare the fire performance under similar testing conditions. However, they do not represent real fires and building elements such as beams, floors, walls and columns are usually examined without taking into account the effect of the surrounding structural components. This is particularly important when a statically indeterminate structural assembly is subjected to fire because it experiences indirect loadings due to the restrained thermal deformations, i.e., a compressive force is induced in the member when it begins to expand. Upon failure of the fire exposed member in an indeterminate structure, the load is transferred to other members; this load redistribution may save the structure from collapse.

Testing isolated components such as beams or columns eliminates the possibility of load redistribution and does not provide an insight into the thermomechanical interaction with the remainder of the structure. New models and methodologies for simulating the behaviour of complex structures and advanced structural components are rapidly

emerging from the fields of high-performance engineering and computing. However, it is essential to utilize the available results from experimental tests to validate and calibrate the new models and methodologies. In light of the benefits and challenges of structural fire testing, hybrid simulation has emerged as a promising technique in that it combines testing of isolated components with simulation of the global response. Hybrid simulation is quite common in the seismic engineering community but is a new approach for analysing the behaviour of structures subjected to fire.

In hybrid fire simulation, the fire exposed component is tested in the laboratory as a physical substructure (or assembley) and the surrounding structure is modelled numerically as a numerical substructure. Both the physical and numerical substructures interact at the interface at fixed intervals of time to investigate the whole system behaviour. Performing hybrid fire simulation is a complex process, but any challenges can be minimised and understood if the hybrid simulation framework is verified numerically before testing the physical specimen in the laboratory. In this context, the objective of the current work is to establish and validate a virtual hybrid simulation framework where the physical specimen is replaced by a detailed numerical model. The fire-exposed part of the structure is modelled in great detail using shell and solid elements in the so-called "slave assembly". On the other hand, the surrounding structure is modelled using simpler beam-column elements, in the "master assembly". Both the assemblies are made to communicate with each other after every integration step using a middleware software. The communication between the two assemblies takes place in a similar way as the physical specimen communicates with the numerical model of the surrounding structure in a real hybrid test. Establishing a virtual hybrid simulation framework helps in understanding the complexities and possible errors in performing a physical-numerical hybrid test. Once validated, this approach can be utilised to conduct real hybrid fire tests by replacing the numerical model of fire exposed component with a physical specimen. This approach investigates the behaviour of the fire-exposed components while including the effect of the remaining structure without modelling the whole system in 3D. In other words, it provides a computationally efficient methodology for analysing the whole structural system in fire.

The behaviour of steel beams with web openings (perforated beams) in fire is quite complex compared with regular steel beams without web openings owing to the unique

failure modes which can develop, e.g., web-post buckling and Vierendeel bending. In addition, the development of axial and rotational restraint in fire due to the presence of the surrounding structure makes the perforated beam behave differently than simply supported perforated beams. The proposed virtual hybrid simulation approach is utilised in this thesis to study the fire behaviour of perforated beams while including the effects of the surrounding structure to give accurate and efficient results without needing to model the whole structure in 3D.

1.1. Research background

The hybrid simulation approach is now quite common in seismic engineering, and its benefits have been widely accepted. In a general hybrid simulation approach, the whole system is divided into two substructures. The substructure which is expected to experience large deformations or whose seismic performance needs to be evaluated in fine detail is tested physically in the laboratory and is known as the physical substructure (PS). The rest of the structure is modelled using a standard FE software in the other substructure which is referred to as the numerical substructure (NS). The main purpose of the numerical substructure is to implement the surrounding structural effects at the boundaries of the physical specimen. These two substructures interact with each other at the interface nodes by transferring the forces and displacements after every integration step. In this way, this approach simulates the behaviour of the whole structural system without testing the whole system in the laboratory.

There are only a few examples in the literature for full-scale hybrid fire testing which are described in more detail in Chapter 2 of this thesis. Most of the recent hybrid testing was performed at the National Research Council Canada's (NRC) testing facilities in Ottawa (Mostafaei 2012, 2013). In these studies, the interaction between the physical and numerical substructures was not automatic but was user-controlled, meaning that the user paused the physical test every five minutes to log the numerical data and then the simulation was re-started. The accuracy of this approach was compromised due to the manual nature of the test. The number of responses communicated between the two assemblies was also limited. Only the axial displacements and axial reaction forces were communicated between the test and the model, by assuming that the column was axially loaded and the geometry was symmetrical.

However, due to the challenges involved in conducting hybrid testing and simulation in fire conditions, it is sensible to develop and verify a framework in a fully numerical environment. The successful implementation of a virtual hybrid simulation framework eliminates the requirement for manual involvement between the two assemblies and this framework can then be employed in the future by replacing the detailed FE model with a physical substructure. In this approach, many different responses can be controlled and communicated at the interface between the two substructures.

The majority of research studies on perforated beams to date have concentrated on beams with simply-supported boundary conditions (e.g., Ellobody and Young 2015; Nadjai et al. 2007a, 2016; Wong et al. 2009). However, it has been noted that most perforated beams in practice experience some degree of both axial and rotational restraint (Najafi and Wang 2017a). Moreover, the behaviour of the beams during a fire is very much dependent on the type and magnitude of the restraint developed by the surrounding structure (Najafi and Wang 2017a; 2017b). The proposed virtual hybrid simulation framework can be utilised to analyse the response of restrained perforated beams in fire conditions. This approach eliminates the need to model the whole structural system using 3D complex elements which enhances the computational efficiency of the simulation technique and helps to develop an understanding of the fire response of the perforated beams by considering the effects from the surrounding structure.

1.2. Objectives and scope

The aim of this study is to establish a virtual hybrid simulation methodology for structures exposed to fire and to understand the behaviour of perforated beams exposed to fire using this technique. In this study, a usable virtual hybrid simulation framework is developed which can assesses the response of individual structural elements subjected to fire by taking account of the surrounding structure. This framework is intended to be used to conduct real hybrid test for the structural components exposed to fire by replacing the detailed numerical model with the physical specimen in the laboratory while utilising the rest of the framework. The virtual hybrid simulation approach includes the whole system behaviour rather than just the behaviour of a single component. Hybrid simulation is a relatively new technique and has rarely been applied in the field of structural fire engineering. The methodology for conducting fully automated hybrid simulation in fire is established in this study and the procedure is validated by comparing the results with

the fire test performed on a full-scale steel frame at Cardington (Lennon 1997). Once verified, this methodology can be applied to conduct the real hybrid fire test in the laboratory with fully automatic communication between the physical and numerical substructure at every integration step, using a middleware software.

The research involves the utilisation of the virtual hybrid simulation framework to analyse the behaviour of composite perforated beams exposed to fire considering the effect of the surrounding structure. The modelling technique is verified by comparing the results with the fire test results performed on an administrative building in Mokrosko (Wald et al. 2011). A study has been carried out using the validated model to understand the behaviour of unrestrained and restrained composite perforated beams under different fire scenarios. The virtual hybrid simulation framework in fire is further modified to analyse the performance of composite perforated beams with different opening arrangements, as well as various load levels and steel grades. For this study, the hybrid fire simulation framework is established using two different softwares, namely Abaqus for the fire-exposed part of the structure and OpenSees for the rest of the structure. The use of Abaqus for the fire-exposed beam strengthens the methodology as it can capture any local buckling or local yielding behaviour (web-post buckling) that may occur. The availability of an excellent visual interface in Abaqus also helps to analyse the results and understand the behaviour accurately. In addition, the ambient temperature analytical equations proposed by the Steel Construction Institute (SCI) in publication P355 (Lawson and Hicks 1998) for the analysis and design of beams with web openings are modified to incorporate the effects of elevated temperature.

1.3. Outline of the thesis

Chapter 1

This thesis comprises seven chapters that include the development of a virtual hybrid simulation framework and numerical studies, as well as the analytical solution for fire exposed perforated beams. The first chapter introduces the thesis, and the contents of the remaining six chapters are briefly summarised below.

Chapter 2

Chapter 2 provides a general literature review to provide the background for the main topics addressed in the thesis. The mechanical properties of steel and concrete are studied

in the first section. The behaviour of various structural elements at elevated temperature is then discussed. The literature corresponding to the overall structural response of perforated steel and composite beams has been studied, both at ambient and elevated temperature. Attention is then given to full-scale tests involving beams with web openings. An introduction of hybrid simulation in the analysis of seismic problems and hybrid simulations performed in the field of structural fire engineering are also presented. A more specific and detailed description of relevant literature is given at appropriate stages in other parts of the thesis.

Chapter 3

Chapter 3 investigates the behaviour of unrestrained and restrained steel perforated beams at elevated temperature. This chapter includes details of the numerical modelling, such as the element types, boundary conditions, mesh sensitivity and imperfections. The numerical model is validated with results from available experimental programmes and simulations performed on axially restrained and unrestrained solid and perforated steel beams.

Chapter 4

In this Chapter, the importance of the location of axial restraint in perforated beams exposed to fire is highlighted. A study on axially restrained perforated steel beams is conducted by varying the most salient parameters, such as the location of axial restraint and the slenderness ratio of the beams.

Chapter 5

Chapter 4 covers the development and validation of a virtual hybrid simulation framework by modelling both the slave and master assemblies using beam-column elements. Recent developments made in the OpenSees material models are discussed and validated. The modified J2PlasticityThermal material in OpenSees is used to perform a 3D thermo-mechanical analysis and to perform a 2D-3D virtual hybrid simulation in fire. The computational efficiency of the virtual hybrid simulation framework is highlighted.

Chapter 6

This chapter provides details of the implementation of the virtual hybrid simulation model to analyse the behaviour of perforated beams using OpenSees and the middleware

software, OpenFresco. The test conducted on an administrative building comprising of perforated beams in Mokrsko (Wald et al. 2011) is used to validate the model. Moreover, a study is carried out using the same model to analyse the effect of different numerical approaches and different fire scenarios on the thermo-mechanical response of restrained composite perforated beams.

Chapter 7

The virtual hybrid simulation framework is further developed in this chapter by replacing the 3D detailed OpenSees model with a 3D detailed Abaqus model to capture the local phenomena such as web-post buckling, lateral torsional buckling, buckling of bottom tee and Vierendeel bending. The modified virtual hybrid simulation approach is successfully validated with the available test results. The validated model is used to analyse the effect of different openings arrangements, steel grade and load level on the response of perforated steel beam under fire. Various stages of the behaviour of perforated beams in fire have been analysed as well as the different local failure modes associated with perforated beams, such as web-post buckling, Vierendeel bending, flange buckling and lateral torsional buckling. The commonly-employed SCI design guidance, P355 (Lawson and Hicks 1998) for designing perforated beams at ambient temperature is discussed and extended in this thesis, for use at elevated temperature. The fire resistance of the perforated beams is found using the developed analytical model and FE simulations. The fire resistance obtained from the FE parametric study is compared with the fire resistance calculated using the design methods and a reasonably good agreement is obtained.

Chapter 8

Chapter 8 summarises the primary outcomes and conclusions from this work, together with recommendations for future research on related topics.

Chapter 2

Literature Review

2. Introduction

This chapter provides an overview of previous work carried out on the response of composite perforated beams exposed to fire. Whilst the behaviour of perforated beams in fire has been the subject of considerable research interest in recent years, the focus herein is given to work which is of particular relevance to the research dealt with in this thesis. Firstly, the important features of the material stress-strain behaviour of steel and concrete at elevated temperature are discussed. Then, emphasis is given to the overall response of perforated beams exposed to fire, with different support conditions. Finally, this chapter addresses work related to the use of hybrid simulation approach in fire. Other, more specific, reviews of the literature are included within other chapters of the thesis, where appropriate.

2.1. Material properties at elevated temperature

The mechanical properties of concrete and steel used in this research are in accordance with those in the Eurocodes (EN-1994-1-2 2005; EN 1992-1-2 2004; EN 1993-1-2 2005). The mechanical properties of these materials are highly dependent on temperature and the coefficient of thermal expansion is also of great interest to structural engineers. The constitutive relationships for structural building materials are not linear, but generally, at elevated temperatures, a reduction in the strength and stiffness of the materials is observed, whereas the coefficient of thermal expansion remains relatively constant. Significant research has been done to understand the behaviour of building materials at elevated temperature and incorporated in the design standards such as the Eurocodes (EN-1994-1-2 2005; EN 1992-1-2 2004; EN 1993-1-2 2005) and the AISC Specification for Structural Steel Buildings (AISC 2016). The material properties defined in the Eurocodes at elevated temperature are widely used in the literature e.g., (Hicks et al. 2012; Najafi and Wang 2017a; Usmani et al. 2000, etc) and this research also adopts the Eurocode guidelines, as discussed below.

2.1.1. Steel

Generally, the material behaviour of steel at ambient temperature is considered relatively simple as it is ductile in nature and the same stress-strain behaviour can be assumed in both tension and compression. Although, this isotropic characteristic of the material behaviour remains the same even at elevated temperature, the material properties of steel at elevated temperature are significantly different from those at room temperature. Tests for the high temperatures strength properties are conducted in mainly two ways: anisothermal and isothermal tests (Cooke 1988; Kirby 1988). In anisothermal tests, the test specimen is subjected to a constant load and then exposed to uniformly increasing temperature. Temperature and strain are recorded continuously under constant stress. Thermal strain evaluated from a separate test is subtracted from the total measured strain (Outinen and Mäkeläinen 2004). In the anisothermal tests, the heating rate has a great influence on the strain rate, and thus different heating rates produce different strain rates. Heating rate of steel under fire conditions depends on the nature of the fire as well as on insulation and steel section properties.

On the other hand, the isothermal tests are generally faster and easier to conduct than the anisothermal tests. In the isotherml tests, the test specimen is heated to a specific temperature and after that a tensile test is carried out. Stress and strain values are recorded continuously under constant temperature. The test can be either load-controlled (loading rate is constant or strain controlled) strain rate is constant (Anderberg 1988; Outinen and Mäkeläinen 2004). Generally, tensile strength tests are conducted to obtain elastic modulus and yield strength of steel. There is a lack of experiments on the modulus of steel under compression. However, it is generally assumed that the modulus of elasticity for steel, derived based on tensile strength tests, is the same for compression state. Originally, the Eurocode temperature-stress-strain curves were derived based on anisothermal tests under slow heating rates (Anderberg 1988; Twilt 1991).

The stress-strain behaviour of steel and the reduction factors corresponding to high temperature used in this study are defined in accordance to Eurocode 3 (EN 1993-1-2 2005), as shown in Fig. 2.1. Eurocode 3 divides the response into four regions, as shown in Fig. 2.1, based upon the following parameters:

$f_{y,\theta}$ Effective yield strength at temperature θ

$f_{p,\theta}$ Proportional limit at temperature θ

$E_{a,\theta}$ Slope of the linear elastic range at temperature θ

$\varepsilon_{p,\theta}$ Strain at the proportional limit at temperature θ

$\varepsilon_{y,\theta}$ Yield strain at temperature θ

$\varepsilon_{t,\theta}$ Limiting strain for the yield strength at temperature θ

$\varepsilon_{u,\theta}$ Ultimate strain at temperature θ

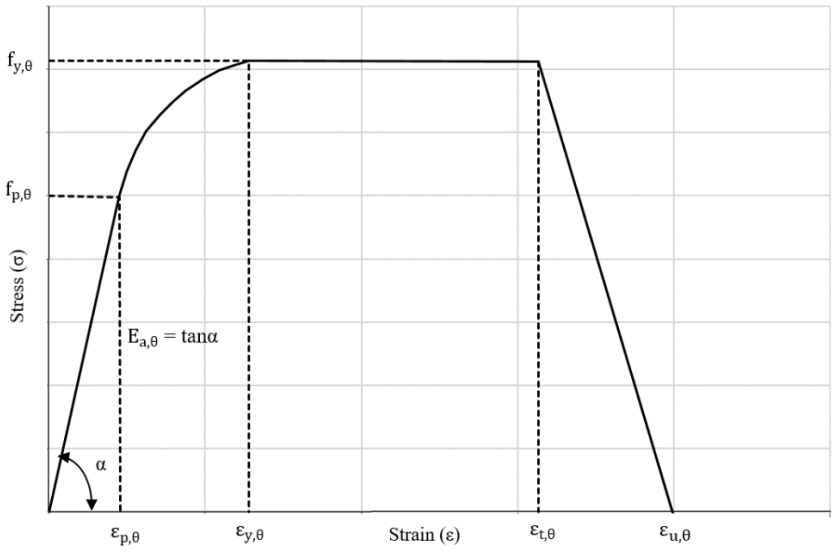

Fig. 2.1 Stress-strain relationships of steel (reproduced from EN 1993-1-2 2005)

The reduction factors are proposed to take into account the effect of high temperatures on the mechanical properties of the steel. According to Eurocode 3, the reduction factors for the proportional limit $k_{p,\theta}$, the effective yield strength $k_{y,\theta}$ and the slope of the linear elastic range $k_{E,\theta}$ are presented in Fig. 2.2.

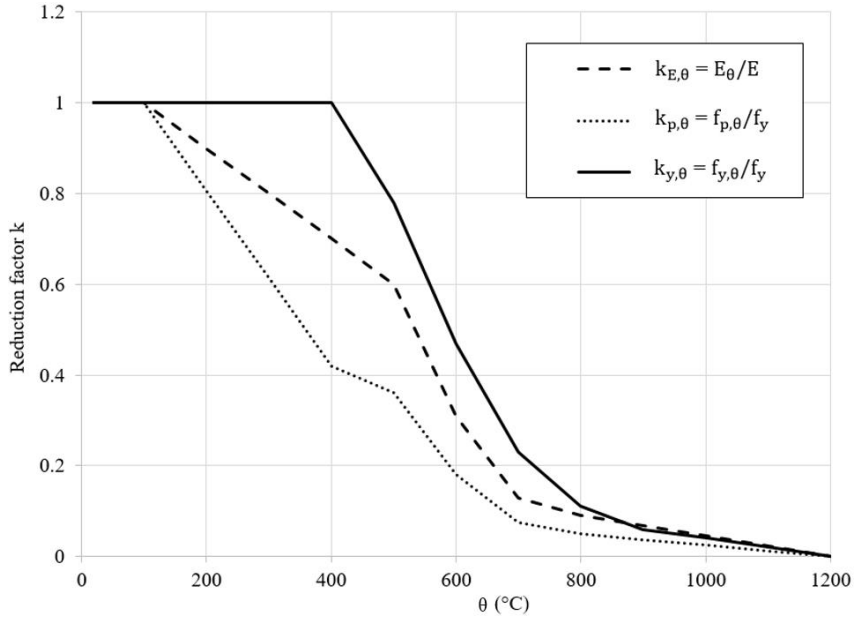

Fig. 2.2 Reduction factors for steel at elevated temperatures

2.1.2. Concrete

Similar to steel, there are different methods to determine the stress strain behaviour of concrete at elevated temperatures i.e., anisothermal and isothermal (Schneider 1988). In anisothermal testing methods, the concrete specimen is loaded under a mechanical load and then temperature is increased uniformly. This procedure is repeated under various loading magnitudes to obtain the stress-strain relationship at elevated temperatures. It has been reported that the stress stain behaviour of concrete is dependent on method of testing used (Schneider 1988). This implies that the data used to understand the behaviour of concrete components at elevated temperature should be derived from anisothermal testing as it is a true representation of a fire scenario.

2.1.2.1. Concrete in compression

Compressive strength of concrete at an elevated temperature is of primary interest in fire resistance design. Compressive strength of concrete at ambient temperature depends upon water-cement ratio, aggregate-paste interface transition zone, curing conditions, aggregated type and size, admixture types, and type of stress (Mehta and Monteiro 2006). At high temperature, compressive strength is highly influenced by room temperature strength, rate of heating, and binders in batch mix (such as silica fume, fly ash, and slag). Unlike thermal properties at high temperature, the mechanical properties of concrete are well researched. The strength degradation in HSC is not consistent and there are significant variations in strength loss, as reported by various authors. The stress-strain relationship used in this study is in accordance to Eurocode 2 (EN 1992-1-2 2004).

According to Eurocode 2 (EN 1992-1-2 2004), the compression behaviour of concrete at elevated temperatures is governed by the following three parameters:

(1) Compressive strength ($f'_{c\theta}$)

(2) Strain at Peak stress ($\varepsilon_{o\theta}$) and

(3) Ultimate strain ($\varepsilon_{u\theta}$)

The ascending branch of the stress-strain behaviour of concrete is governed according to the Eq. 2.1 as is graphically represented in Fig. 2.3:

$$\sigma_{c\theta} = [3\varepsilon f'_{c\theta}/\varepsilon_{o\theta}(2 + (\varepsilon/\varepsilon_{o\theta})^3)] \quad \text{when} \quad \varepsilon \leq \varepsilon_{o\theta} \tag{2.1}$$

For numerical modelling, a linear or non-linear descending branch is permitted by the Eurocode. The effect of elevated temperatures on the mechanical properties of concrete is incorporated in the form of reduction factors proposed in Eurocode. The reduction factor for the compressive strength at elevated temperature($f'_{c\theta}$), strain at peak stress at elevated temperature ($\varepsilon_{o\theta}$) and ultimate strain at elevated temperature ($\varepsilon_{u\theta}$) are presented in Table 2.1.

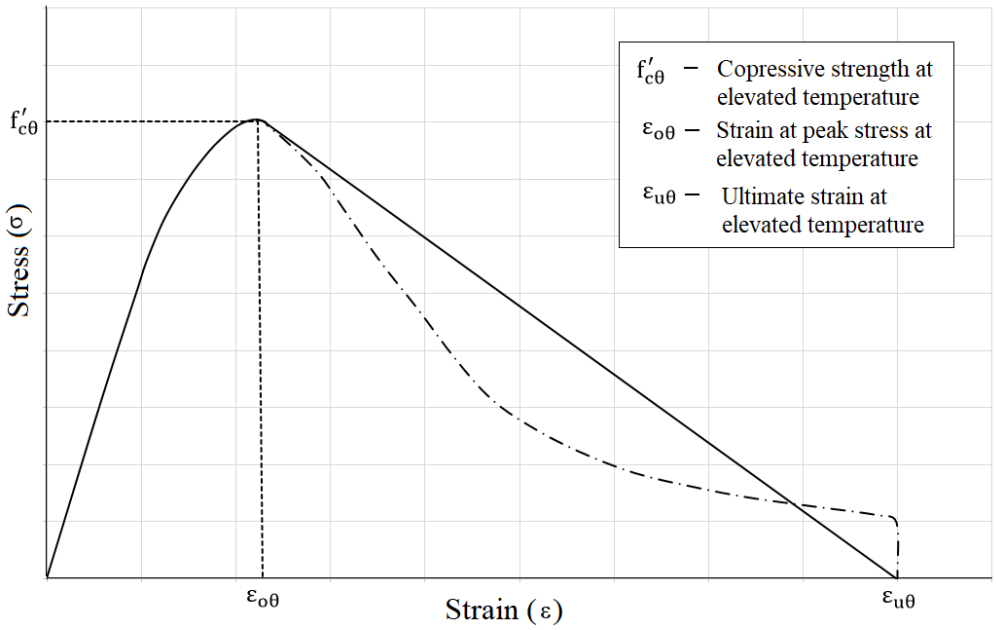

Fig. 2.3 General compressive stress-strain relationship at elevated temperature (reproduced from EN 1992-1-2 2004)

Table 2.1 Reduction factors for the main parameters of the stress-strain relationship of concrete at elevated temperatures according to Eurocode 2 (EN 1992-1-2 2004)

Temperature (°C)	$(f'_{c\theta})/(f'_{c20})$	$\varepsilon_{o\theta}$	$\varepsilon_{u\theta}$
20	1.00	0.0025	0.0200
100	1.00	0.0040	0.0225
200	0.95	0.0055	0.0250
300	0.85	0.0070	0.0275
400	0.75	0.0100	0.0300
500	0.60	0.0150	0.0325
600	0.45	0.0250	0.0350
700	0.30	0.0250	0.0375
800	0.15	0.0250	0.0400

900	0.08	0.0250	0.0425
1000	0.04	0.0250	0.0450
1100	0.01	0.0250	0.0475

2.1.2.2. Concrete in tension

The tensile strength of concrete is much lower than compressive strength, due to ease with which cracks can propagate under tensile loading (Mindess et al. 2003). Concrete is weak in tension, and for normal strength concrete (NSC), tensile strength is only 10% of its compressive strength and for high strength concrete (HSC), tensile strength ratio is further reduced. Thus, tensile strength of concrete is often neglected in strength calculations at room and elevated temperatures. However, it is an important property, because cracking in concrete is generally due to tensile stresses and the structural damage of the member in tension is often generated by progression in microcracking (Mindess et al. 2003). Under fire conditions tensile strength of concrete can be even more crucial in cases where fire induced spalling occurs in a concrete structural member (Khaliq and Kodur 2012). Tensile strength of concrete is dependent on almost same factors as compressive strength of concrete (Shah 1991).

The tensile behaviour of concrete and the reduction factors corresponding to high temperature are also defined in Eurocode 2 (EN 1992-1-2 2004). The reduction of the characteristic tensile strength of concrete is allowed for by the coefficient $k_{c.t}(\theta)$ as defined in Eqs. 2.2 - 2.4. The graphical variation of the tensile strength reduction factor of concrete with temperature is illustrated in Fig. 2.4.

$$f_{cr\theta} = k_{c,t}(\theta)\, f_{cr} \tag{2.2}$$

$$k_{c,t}(\theta) = 1 \qquad \text{for } 20\,^{\circ}\text{C} \leq \theta \leq 100\,^{\circ}\text{C} \tag{2.3}$$

$$k_{c,t}(\theta) = 1 - \left(\frac{\theta-100}{500}\right) \qquad \text{for } 100\,^{\circ}\text{C} \leq \theta \leq 600\,^{\circ}\text{C} \tag{2.4}$$

where

$f_{cr\theta}$ is the tensile strength of concrete at elevated temperature; f_{cr} is the tensile strength of concrete at room temperature; and $k_{c,t}(\theta)$ is the eduction factor at elevated temperature

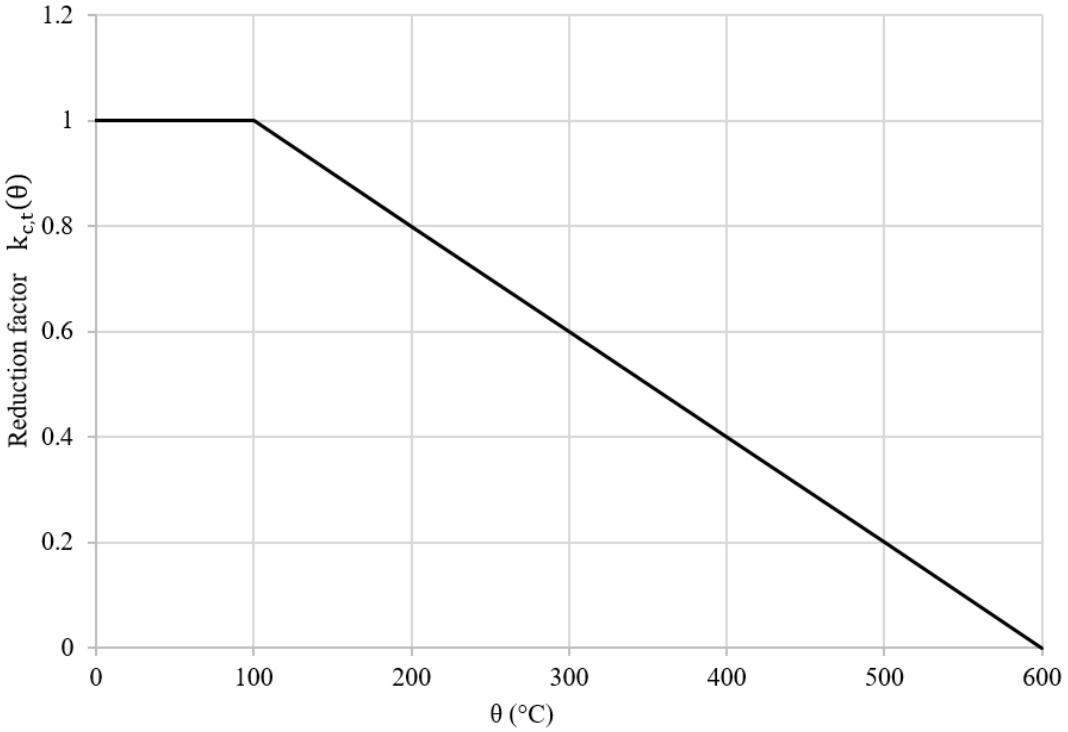

Fig. 2.4 Reduction factor for the tensile strength of concrete at elevated temperature

2.2. Behaviour of solid steel beams in fire conditions

In this section, the behaviour of simply supported, rotationally restrained, and axially and rotationally restrained solid steel beams exposed to fire is discussed.

2.2.1. Simply supported solid steel beams in fire

When simply supported solid steel beams are exposed to fire, no axial force is induced due to the axially unrestrained support conditions, thus the applied bending moment at a particular section remains constant for the whole duration of fire. A rise in temperature reduces the plastic bending moment capacity of the steel beams. The temperature at which the applied bending moment becomes equal to the reduced plastic bending moment capacity of the section is known as the critical temperature of the beam. In other words, the failure of a beam exposed to fire occurs when the maximum bending moment at a section reaches the plastic bending moment capacity of the section.

In the initial stages of a fire, the midspan deflection of the beam is relatively low. This is due to the fact that the beam is allowed to expand freely and the reduction in the material strength is not significant. The main contributing factor for the midspan deflection in the early stages of a fire is thermal bowing. During the later stages of a fire, at higher

temperatures, there is a significant reduction in the strength and stiffness of the material which causes tensile yielding of the bottom flange. Under high compressive stress, yielding of the top flange also occurs which leads to the formation of a plastic hinge in the section. The presence of a plastic hinge at the midspan results in the formation of a mechanism causing a sudden increase in midspan deflection (a runaway) and the beam is considered to be failed at this stage (Moss et al. 2004).

The overall behaviour of simply supported steel beams with a slab is similar to that of the steel beams without a slab (Wang 2002). Two full-scale fire tests on simply supported composite beams with steel sheeting perpendicular and parallel to the steel section were conducted by Jiang et al.(2017). Both specimens were observed to fail by the formation of a plastic hinge at the mid-span and large mid-span deflections were observed. The only difference is that under the same applied load, the composite beam shows better fire resistance due to the increased bending moment capacity of the composite section (Wang 2002).

2.2.2. Rotationally restrained solid steel beams in fire

Steel beams with rotational restraint and without axial restraint experience free elongation similar to simply supported beams and consequently the initial deflections at low level of elevated temperature are due to thermal bowing and stiffness degradation. Initially, the hogging moment at the supports develop due to the presence of rotational restraint and effectively resists the increase of midspan deflection. As the temperature increases, the yield strength reduces which results in the yielding at the support. The hogging moment at the support increases until the start of yielding and formation of a plastic hinge (Usmani et al. 2001). After this stage, a further rise in temperature results in a noticeable increase in midspan deflection. For the beam to be in equilibrium, the support moment is redistributed to the span. As soon as the beam reaches the reduced moment capacity due to rise in temperature, the formation of a plastic hinge at the span also takes place (Wang 2002) which confirms the formation of a mechanism and considered as beam failure. Various researchers (e.g., Burgess et al. 1991; El-Rimawi et al. 1997; Lawson 1990; Liu 1998, 1999; Wang and Burgess 2008) have also conducted studies to analyse the behaviour of rotationally restrained and axially unrestrained beams in fire and similar behaviour is obtained.

2.2.3. Axially and rotationally restrained solid steel beams in fire

Various studies have been conducted to analyse the response of axially and rotationally restrained solid beams in fire and it has been observed that the behaviour of a beam with axial restraint is much more complex than those without axial restraint (Gillie et al. 2001; Lennon 1997; Li and Guo 2008). The behaviour of axially restrained steel beams in fire is explained in various stages. The typical behaviour of axially and rotationally restrained steel beams in fire is represented in Fig. 2.5 (Dwaikat and Kodur 2011).

In the first stage, when the temperature starts to rise, the temperature of the bottom flange increases at a more rapid rate compared with rest of the beam, which causes downward thermal bowing. Due to restrained thermal expansion, a compressive force and a hogging moment are also induced in the section. The hogging moment at the support increases and the sagging moment at midsection reduces until yielding at the support takes place. This occurs due to the combination of high hogging moments and axial compression force and local buckling of the lower flange is also observed on some occasions (Dwaikat and Kodur 2011).

In the second stage, due to the redistribution of loads, the hogging moments then start to reduce gradually and the mid-span moment starts increasing. Further heating reduces the plastic moment capacity of the beam at the midsection. As soon as the reduced moment capacity due to rise in temperature becomes equal to the applied moment, a plastic hinge forms at the midsection and a runaway deflection is observed. At this stage, unloading of the axial compression starts and the compressive axial force in the section changes to a tensile axial force (Dwaikat and Kodur 2011), as shown in Fig. 2.5.

In the third and final stage, the deflection increases at a slower rate and the restrained beam continues to carry the applied load under a catenary action. In this way, the catenary action helps the beam to resist high temperatures without experiencing a collapse. In the catenary stage, the transition of the load-bearing mechanism from flexural to cable (tensile) takes place and the temperature at which this transition occurs is known as the transition temperature (Dwaikat and Kodur 2011). Further, increase in the temperature results in the rupture of the beam or failure of the connections (Dwaikat and Kodur 2011; Gillie et al. 2001; Lamont et al. 2007; Tan and Huang 2005; Wang et al. 2016; Yin and Wang 2004). Moreover, the transition temperature is greatly dependent on the load level.

A rise in the load level reduces the transition temperature of the beam and results in a low fire resistance (Lamont et al. 2007; Wang et al. 2016).

(a) Layout of restrained steel beam

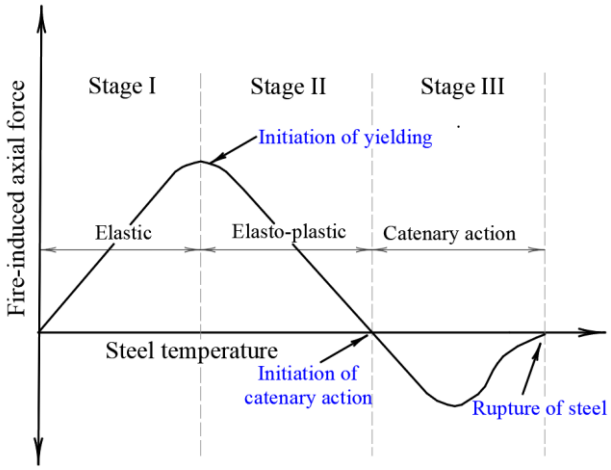

(a) Fire-induced axial force

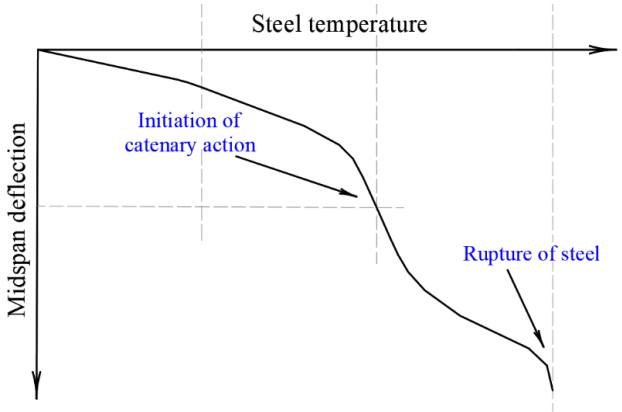

(b) Midspan deflection

Fig. 2.5 Typical fire response of restrained steel beams in fire (reproduced from Dwaikat and Kodur 2011)

2.2.4. Steel beams with different location of axial restraint in fire

The behaviour of restrained steel beams is greatly influenced by various factors including, the magnitude and location of axial restraint. Significant axial force develops in a restrained steel beam when it is exposed to fire. Dwaikat and Kodur (2010) conducted a numerical study to analyse the effect of location of axial restraint on the performance of solid steel beams. This study showed that if the location of axial restraint is shifted towards the bottom flange than it develops moment in the opposite direction to the moment developed due to the applied vertical load. This effect is reported analogous to

the tensile force in a pre-stressed concrete beam. In this way, it was found that it could enhance the fire performance of the solid steel beams with low slenderness ratio ($L/r \leq 30$) but the effect is minimum and less appreciated on high slender beams ($L/r \geq 60$). Due to the presence of openings in the web, the axial stiffness of the beams reduces significantly and buckling of the perforated beams can occur at a lower temperature as compared to the beams without web openings. Moving the location of axial restraint towards the lower flange may accelerate the buckling of the lower tee and may result in the early failure. So, similar conclusions cannot be drawn for perforated beams and the effects of location of axial restraint on the behaviour of perforated beams need to be investigated.

2.2.5. Steel beams exposed to different fire scenarios

Most of the studies conducted in the past investigated the behaviour of structural members assuming standard fire exposure. However, when a structural member is exposed to a natural fire scenario, it may behave differently. The effect of different fire scenario on the response of restrained steel beams was investigated by Dwaikat and Kodur (2010) by comparing the performance of a beam when exposed to standard fire and Eurocode design fires (EN 1991-1-2 2005). Different types of fires used in this study are explained in the next section. It was noticed that when the beam is exposed to a standard fire, it failed after developing a catenary action. Whereas, in case of design fire, the beam did not fail and continued to carry the loads. The reason for this behaviour was the decay phase of the design fire (absent in standard fire) during which steel regained much of its strength and stiffness.

Alam et al. (2017) conducted a study to analyse the effect of different fire scenario on the behaviour of slim floor beams. Three fire exposures were considered in that study, i.e., standard fire, a slow parametric fire and a fast parametric fire. During a standard fire exposure, the temperature increases for the whole duration of fire due to the absence of descending branch, whereas in parametric fire exposures, the temperatures of the slim floor beams decrease to ambient temperature after reaching a maximum value. It was observed that during the early stage of fire, the average temperature and the thermal gradient developed due to a fast parametric fire exposure was more severe compared with a standard fire and slow parametric fire exposure. Moreover, it was concluded that the thermo-mechanical behaviour of slim floor beams depends on the average temperature

across the steel section and the effect of thermal gradient across the section of slim floor beams is less significant. In most of the previous studies, the perforated beams are analysed under standard fire exposure despite the fact that factors such as the thermal gradient and the average temperature of the section may influence the behaviour significantly. Hence, their response to natural fire scenarios still deems further examination and is investigated in this study.

2.2.5.1. Different types of fires

In structural fire engineering, the two most common design approaches are the prescriptive design approach and performance based design approach. On the basis of these design approaches, different types of fire exposures are defined in design standards i.e., standard fire and parametric fire. In prescriptive approach, a standard fire test is conducted. The basic principle of the standard fire test, that may more properly be known as the standard furnace test, is that a structural element is loaded to produce the same stresses that would be induced in that element when in place in the structure of which is considered a representative part. The element is then heated under load with the measured temperature regime in the furnace following a prescribed time-temperature relationship until failure of the element occurs. Traditionally, beams and slabs are heated from beneath, while columns are heated on all four sides and walls heated from one side only. The standard furnace test is regulated on an international basis by ISO 834 (EN 1991-1-2 2005)which has been subject to subsequent amendments. Traditionally, most building structure fires have been considered to occur with the bulk of the combustible material taken as cellulosic and the resultant standard furnace time- temperature curve established on this basis. For such fire tests, the time- temperature curve specified for the furnace is

$$\theta = 20 + 345\log(8t + 1)$$

where θ is the furnace temperature (°C) and t is the time (min).

Unlike the time- temperature response in a furnace test that is imposed by the standard to which the test is carried out, the time- temperature response in a fire compartment is a function of compartment size, type of compartment, available combustible material, and air supply available for combustion. This situation is often designated a natural or real fire (the former term is preferred here, although eurocode (EN 1991-1-2 2005) uses parametric fire), and the heat it generates may be calculated from basic principles. However, attempts have been made to represent the solution to the natural compartment

time- temperature response by empirical curves; one such is given in eurocode (EN 1991-1-2 2005). The development of compartment fires can be broken down into three phases: pre-flashover (also known as growth period); post-flashover (fully developed fire); and the decay period (Fig. 2.6).

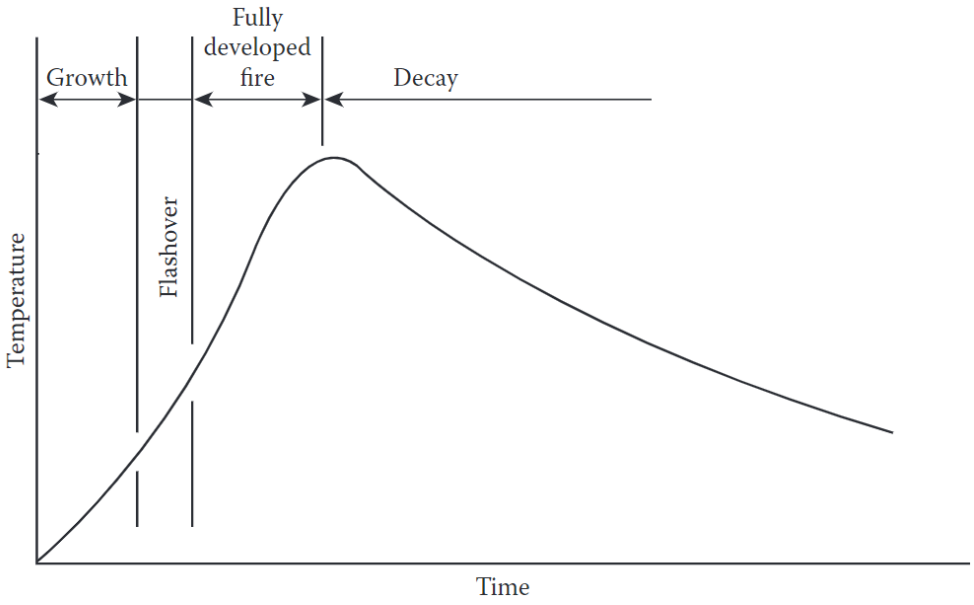

Fig. 2.6 Phases of a parametric fire (reproduced from Purkiss and Li 2013)

In the pre-flashover period, combustion is restricted to small areas of the compartment; therefore, only localized rises in temperature can occur. It should be noted that such rises may be substantial. The overall or average rise in temperature within a bounded fire compartment will be very small and indeed at this stage there may be no obvious signs of a fire. A large number of incipient fires never get beyond the stage of pre-flashover because of insufficient fire load or air supply (ventilation) to allow the fire to grow beyond pre-flashover. In many cases, human intervention causes flashover, for example, by opening a door or window and thereby suddenly increasing the air supply. The pre-flashover stage is often ignored in the calculations of the compartment time- temperature response since the overall effect on the compartment is small even though the pre-flashover period can be long compared to the subsequent stages of a fire. Flashover occurs when fire ceases to be a local phenomenon within the compartment and spreads to all the available fuel within the compartment. Propagation of flames through any unburnt gases and vapours collected at ceiling level then ensues.

In this period, the rate of temperature rise throughout the compartment is high as the rate of heat release within the compartment reaches a peak. The rate of temperature rise

continues until the rate of generation of volatiles from the fuel bed begins to decrease as the rate of fuel consumption decreases or when insufficient heat is available to generate such volatiles. Once the rate of temperature rise reaches a peak, the fire continues into its decay phase. Decay phase, as its name suggests, the temperature in the compartment starts to decrease as the rate of fuel combustion decreases. Due to thermal inertia, the temperature in the structure will continue to increase for a short while in the decay period; i.e., there will be a time lag before the structure starts to cool.

2.3. Perforated beams

In modern construction of steel framed buildings, there is an increasing tendency towards the specification of long-span floor systems which enable larger open plan spaces to be achieved. Perforated or cellular beams acting compositely with a reinforced concrete floor slab is a popular choice for such floor systems. Perforated beams can be made either by cutting and welding hot-rolled steel sections to provide the desired shape or by fabricating the section from steel plates similar to plate girders. The openings may be designed in any shape but the most popular shapes are circular (giving a cellular beam), rectangular, elongated and sinusoidal openings. These are separated by solid web-posts and the web-post size varies according to the dimensions of the openings. Generally, perforated beams are preferred in multi-storey buildings to regular I sections as they allow for longer spans to be achieved which, in turn, leads to more flexible column-free space and shorter erection times. In addition, they can reduce the overall height of the building owing to the integration of services within the structural frame as shown in Fig. 2.7. It has been shown that using these types of beam can be very economical and reduce the total weight of steelwork significantly (Nadjai et al. 2017).

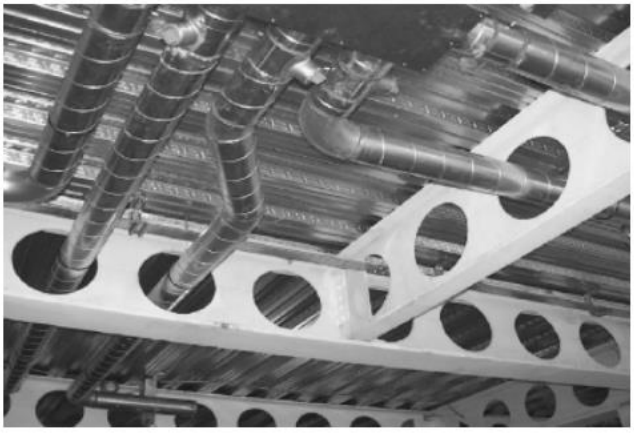

Fig. 2.7 Service pipes through webs of cellular beams (Boissonnade et al. 2013)

2.3.1. Perforated beams at the room temperature

The behaviour of perforated beams at room temperature is well documented in various analytical and experimental studies (e.g., Chung et al. 2001; Lawson et al. 2006; Pachpor et al. 2014; Tsavdaridis and D'Mello 2011a). The presence of the openings in the web makes the structural behaviour of the beam different in a number of aspects from that of solid steel beams. In solid beams, the behaviour is mostly dominated by the reduction of bending moment capacity due to increase of temperature at the location of the maximum bending moment. However, various new possible failure modes are introduced in beams with web openings at the openings and the web-posts. In this section, the ambient temperature behaviour of perforated beams is discussed, a brief description of failure modes which are associated with perforated beams is provided.

2.3.1.1. Global bending failure

If the opening is present at the location of maximum bending moment, i.e., at midspan for simply supported beams, the beam fails when the applied moment exceeds the plastic moment capacity of the section at the location of the opening. In this failure mode, the yielding of the bottom and top tees takes place under the bending tension and compression, respectively. Toprac and Cooke (1959) have studied that when a section at the opening is subjected to a pure bending moment, the yielding of tees above and below the opening occurs similar to that of beams with solid webs. Fig. 2.8 shows the global bending failure of a perforated beam with an opening at the centre.

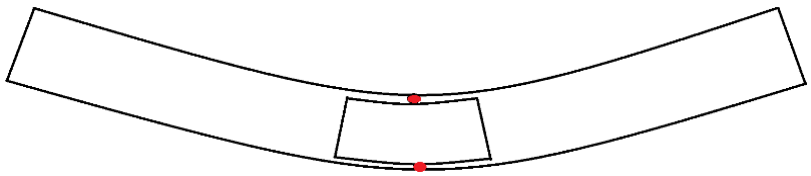

Fig. 2.8 Global bending failure mode in perforated beams

2.3.1.2. Global shear failure

Generally, openings fail due to the combined effect of bending and shear but the presence of opening at the location of high shear, reduce the shear capacity of the section by eliminating the web area, this may lead to the failure in pure shear. Shear failure of perforated beams is rare and limited to very small length of opening, which is located in the region of very high shear (Chung et al. 2003). Generally, the failure occurs due to the

combined effect of shear and bending moment but in uniformly loaded simply supported beams, if the opening is present near the support, the possibility of failure due to pure shear increases.

2.3.1.3. Vierendeel bending

The Vierendeel bending in perforated beams is discussed by various researchers (Halleux 1967; Toprac and Cooke 1959) and it is reported that the structural response of a perforated beam is similar to Vierendeel girder. In this mechanism, secondary bending moment is generated due to the transfer of vertical shear across the opening. The high magnitude of stress develops in the elements surrounding the opening due to the combined effect of global bending moment, shear force and secondary bending moment from Vierendeel action. Due to this complex state of stress, plastic hinges at the corners of an opening starts developing to form a mechanism. Formation of this Vierendeel mechanism causes excessive plastification at the plastic hinge locations and noticeable distortion of the section is observed in the manner of a parallelogram as shown in Fig. 2.9. For perforated beams, this failure mode is typically considered the most critical.

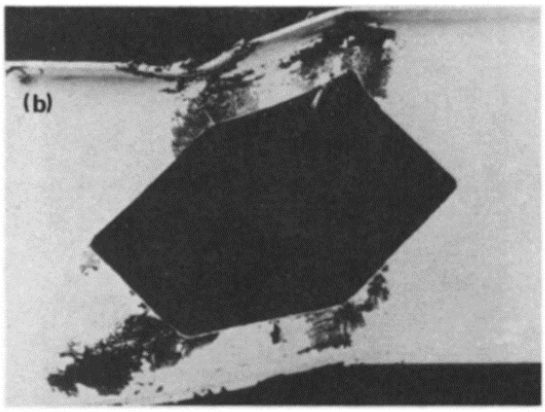

Fig. 2.9 Vierendeel bending failure mode (Kerdal and Nethercot 1984)

2.3.1.4. Lateral torsional buckling

Generally, failure due to lateral torsional buckling (LTB) occurs when the lateral support to the compression flange of the steel beam is inadequate (Deng et al. 2015; Menkulasi et al. 2017; Tsavdaridis and D'Mello 2011b). If the steel beams have insufficient lateral support and are not axially loaded than LTB failure mode will govern the behaviour (Kerdal and Nethercot 1984). The typical lateral torsional buckling in a cellular beam is shown in Fig. 2.10. Tests are conducted by researchers to analyse the difference in the

LTB behaviour of solid beams and cellular beams. Same smooth continuous laterally buckled profile with no web-post buckling is observed in both types of beams (Kerdal and Nethercot 1984; Kuchta and Maślak 2015). Therefore the guidelines to estimate the lateral torsional buckling strength of solid beams could also be used for perforated beams, using the cross-section properties of the section at the location of the opening (Kuchta and Maślak 2015).

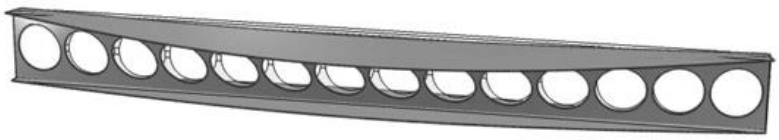

Fig. 2.10 Lateral torsional buckling failure mode (Sonck et al. 2011)

In recent research (Ellobody 2012; Kwani and Wijaya 2017; Sonck and Belis 2015), it was observed that lateral torsional buckling is one of the primary failure mode in perforated steel beams and this decreases the failure load considerably. Whereas for composite perforated beams, where the compression flange is laterally restrained due to the presence of slab, a dominance of lateral torsional buckling is rarely observed.

2.3.1.5. Web-post failure

Beams with single web opening and individual openings at a sufficiently large distance minimise the possibility of web-post buckling. However, for closely spaced openings, there is an unavoidable interaction between the openings and various other failure mechanism related to web-post buckling may develop. The web-post buckling is a local instability which is observed experimentally by many researchers (Halleux 1967; Redwood et al. 2007). This instability is characterized by an out of plane displacement of the web-post which could lead to the failure of the perforated beams, whereas the introduction of web stiffeners can reduce the extent of web-post buckling. The presence of stiffeners increases the failure load by 10 to 40% and proved to be effective in improving the web-post buckling resistance (Redwood et al. 2007).

Generally, two types of web-post buckling are most common in perforated beams, i.e., lateral torsional buckling due to the combination of vertical and horizontal shear and web crippling under concentrated loads. The web crippling failure mode can be avoided by not placing a high concentrated load directly above the web-post region. Whereas, in the

lateral torsional buckling failure mode, a combination of the horizontal and vertical shear forces acts on the tees which result in the development of diagonal tensile and compressive forces in the web-post as shown in the Fig. 2.11. Under this compressive force, the web-post buckles and lateral torsional buckling is also initiated as shown in Fig. 2.12.

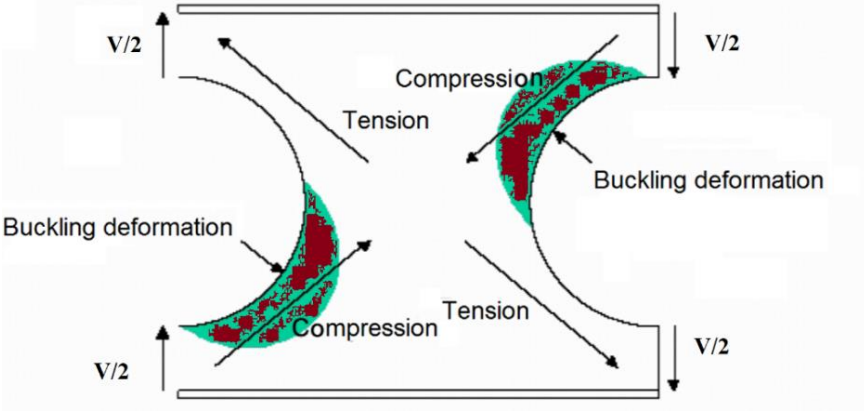

Fig. 2.11 Diagonal stresses in web-post buckling failure mode (reproduced from Lawson 2006)

Fig. 2.12 Web-post buckling failure mode (Durif et al. 2013)

2.3.2. Perforated beams in fire condition

Despite the numerous amount of research publications on the fire behaviour of restrained beams with solid web, there are only a few research published on the fire response of restrained beams with web openings. Most of the studies carried out in the past assume simply supported perforated beams. Moreover, ignoring the effect of restrained thermal expansion, the behaviour is found to be similar to that of ambient temperature behaviour and the influence of fire is not specifically noticed.

A series of tests were carried out by Nadjai et al. (2007) on simply supported composite perforated beams in fire. The main findings of the tests highlighted the importance of web-post in perforated beams because the web-post buckling failure mode was observed as the dominating failure mode in all the tests. A 3D nonlinear finite element model of the composite perforated beam was developed, and a numerical study was carried out by Wong et al. (2009). The numerical model was validated using the results from the fire tests conducted at Ulster University (Nadjai et al. 2007b) by predicting all the failure modes. The available analytical model for the design of composite beams with web openings at ambient temperature was used to calculate the fire resistance by incorporating the reduced sectional properties at elevated temperature. Moreover, web-post buckling and Vierendeel bending (as shown in Fig. 2.13) were the two failure modes considered in the analytical model. The results predicted using the analytical model were conservative and show a close agreement with the test results and FE analysis.

Fig. 2.13 Web-post buckling and Vierendeel bending in perforated beams exposed to fire (Nadjai et al. 2016)

A detailed finite element model of the perforated beam was developed by Vassart et al. (2010), the accuracy of the model was validated with the results from full-scale fire experiments performed in Northern Ireland (Nadjai et al. 2011). Using the FE model, an extensive parametric study was conducted to develop an analytical model for predicting the critical temperature of beams with web openings. The analytical model was developed according to the design guidelines available in Eurocodes (EN 1992-1-2 2004; EN 1993-1-2 2005). The design model incorporates various failure modes, i.e., Vierendeel bending web-post buckling, global shear and global bending. A software called ACB+ was developed using this analytical model to design cellular beams which is available at the ArcelorMittal website (Vassart 2009).

A simplified method for analysing frames comprising cellular beams which are subjected to fire has been proposed (Abu et al. 2009). In this method, the web openings are not directly incorporated but their effect is represented using an equivalent web thickness, resulting in a solid beam. However, various failure modes associated specifically with perforated beams such as web-post buckling and Vierendeel bending cannot be realistically predicted using this approach. In summary, there is a lack of data and analysis on the behaviour of restrained composite perforated beams in fire conditions in the literature. Accordingly, the current study aims to study this behaviour using a virtual hybrid simulation numerical approach. In this method, the structure is divided into two sub-sections or assemblies, and the area which is expected to undergo large deformations (i.e., the perforated beam which is subjected to fire) is modelled in fine numerical detail in one assembly whilst the surrounding structure which should behave elastically is modelled in another assembly at a much lower computational cost. A middleware or interaction software such as OpenFresco (Kwon et al. 2007; Takahashi and Fenves 2006) is used to connect the two assemblies at the interface. This modelling method is employed because it is capable of analysing the whole structure in an accurate yet computationally efficient manner. In addition, hybrid simulation combining physical testing with numerical analysis has been receiving greater attention in recent years, especially in earthquake engineering applications, and its value and efficiency have been recognised (Pegon and Pinto 2000). Although physical tests are not included in the current study, an important objective of the work is to establish and scrutinise a hybrid simulation framework for fire conditions in a virtual environment, which can later be used in combination with real fire testing.

2.3.3. Full-scale compartment tests with perforated beams

In the past, only a few full-scale compartment tests with perforated beams have been conducted. The most cited full-scale compartment tests are the tests conducted by the Czech Technical University and the University of Ulster (Nadjai et al. 2011; Wald et al. 2011). Details and findings of these tests are summarised below.

2.3.3.1. Czech Technical University test (Wald et al. 2011)

This fire test was conducted on an administrative building in Mokrsko, Poland by Czech Technical University. The structural system comprises of one floor of a steel and concrete composite office building, which consists of four bays with dimensions of 9 m × 6 m

each. “Angelina” composite perforated beams developed by Arcelor-Mittal with sinusoidal web openings were used in this test as shown in Fig. 2.14. A static load of 3.0 kN/m^2 was applied on the slab using sandbags, and the calculated self-weight from the structure was 2.6 kN/m^2.

Fig. 2.14 Fire test on an administrative building in Mokrsko (Wald et al. 2011)

The fire load was created by unwrought cribs of 50×50 mm with 1 m length of softwood. It is observed that midspan deflection of the Angelina beams increases slowly for the initial duration of fire. However, after 61 minutes of fire exposure, most of the structure collapsed. This experiment presents the only full-scale structural fire testing which has experienced a structural collapse. The failure of the Angelina beams initiated due to the occurrence of Vierendeel bending across the first two openings from the support as shown in Fig. 2.14. Whereas, after 50 minutes, lateral torsional buckling (folding of the beams along its longitudinal axes) starts to dominate and leads to the collapse of the beams.

2.3.3.2. Ulster University tests (Nadjai et al. 2011)

Researchers at Ulster University also carried out a full-scale fire test in 2010 on a 15 m long and 9 m wide compartment as shown in Fig. 2.15. The primary objective of this test was to study the membrane action of the concrete slab and the composite behaviour of the secondary perforated beams. The effect of the interaction with the surrounding

structures on the behaviour of the perforated beam was also investigated as opposed to the isolated testing of the beams with simple support without axial and rotational restraint. It was found that at low temperature (less than 500 °C), the deflection was dominated by thermal bowing. Whereas at higher temperature, the deflection is controlled by mechanical deflection due to the reduction in steel strength and stiffness. At high temperatures, the web-post buckling occurs, and then the bottom flange starts to displace in the lateral direction. At 800 °C, the transition of load carrying mechanism from bending to catenary action takes place, and only the top flange resist the applied load under tensile action.

Fig. 2.15 Full-scale compartment test conducted at Ulster University (Nadjai et al. 2011)

2.4. Hybrid Simulation

Traditionally, the fire resistance of structural elements is determined using prescriptive methods. These methods evaluate the fire endurance of individual structural elements, as single elements, without considering the effects from the surrounding structure. A single element testing method has limitations in terms of providing a realistic estimation for the fire performance of the element since the interactions between the single element specimen and the rest of the building are disregarded in the assessment. The behaviour of various structural elements can be assessed either by building and testing a full-scale building in fire or performing a reliable FE analysis of the whole building. However, the

full-scale testing methods are very expensive and require significant efforts, time as well as large laboratory space and facilities. On the other hand, modelling the whole structural system in 3D is also a complex and computationally expansive task. An alternative approach to the full-scale testing could be a hybrid simulation (HS), but with significantly less time, space and cost required.

Hybrid simulation is most commonly employed by earthquake engineers to study the seismic behaviour of structures. In this computational method, the structure is divided into two assemblies or substructures. The assembly which is expected to experience large deformations or whose seismic performance needs to be evaluated in fine detail is tested physically in the laboratory and is known as the physical substructure (PS). The rest of the structure is modelled using a standard FE software in the other assembly which is referred to as the numerical substructure (NS). Both assemblies interact with each other at each time step of the response using a communication software, e.g., OpenFresco (Schellenberg et al. 2007).

It is a method in which the structural displacements due to the earthquake and other extreme loads can be calculated computationally using a stepwise integration procedure and applied quasi-statically to the test specimen in the laboratory. The resulting resistance forces are measured and fed back to the computational model as part of the input for the next calculation step. Hybrid simulations performed in the past were mainly performed with structures subjected to dynamic loads. In general, each time-step in a hybrid testing consists of four distinct phases (see Fig. 2.16): (i) The target displacement for the first integration step is calculated at the interface of the numerical substructure; (ii) The target displacement is imposed at the interface of the physical substructures; (iii) The reaction forces from the PS is measured and fed to the numerical substructures; and (iv) The equations of motion for the current step are solved to get the next value of the target displacement. Nevertheless, each of the four phases is essential in hybrid simulation and repeated until the experiment is complete.

Moreover, HS would provide more flexibility and more test data compared with the full-scale testing method. As such, computer simulations could be revised simply, with almost no cost, and for any new configuration, only building a small specimen would be required.

While in the full-scale testing, for any new study scenario, a new full-scale specimen would be required. Furthermore, the computer simulation could provide details of the building performance components, such as internal load, deformation, stress and strain, which would be impractical or very difficult to measure during the full-scale testing.

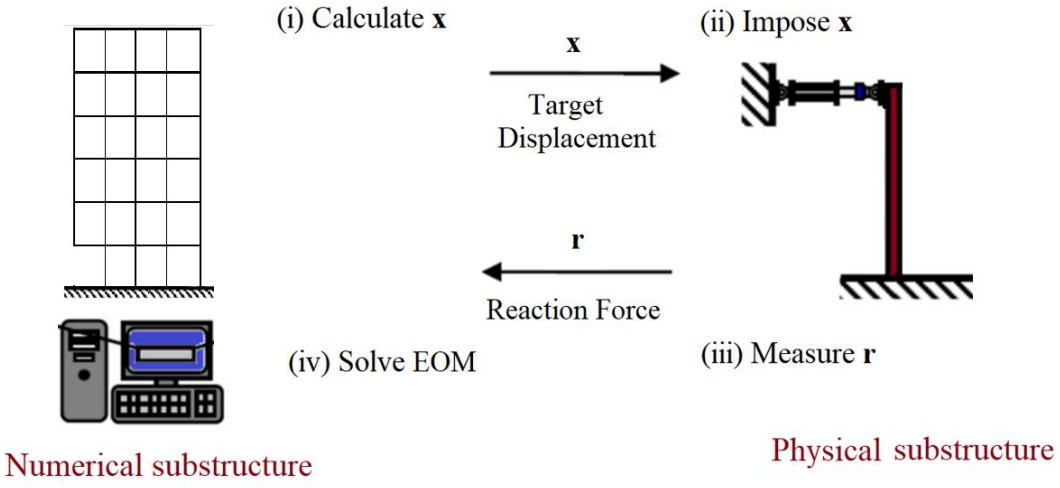

Fig. 2.16 Basic Hybrid Testing Approach (Nakata et al. 2007)

In the general hybrid simulation set-up, structure is divided in to master and slave assemblies. The part of the structure whose behaviour is to be evaluated is termed as slave assembly and the surrounding structure is termed as master assembly. The master assembly implements the boundary conditions on the slave assembly and the slave program (or programs) return the reaction forces to the master program (Schellenberg et al. 2008a). The boundary conditions that are transferred at the interface degrees-of-freedom from the master to the slave assembly can be defined as displacements and rotations. A middleware software is required to connect the master and slave programs. Such software solves the issues such as data storage, communication methods, system control, optimisation and data transformations. The middleware used in this work is OpenFresco. OpenFresco software was originally developed to perform hybrid testing (also referred to as hybrid simulation), in which the physical specimen in the laboratory is linked to the FE software to execute the tests but in the study presented here, it is utilised to simply link two FE models. The following section provide the details of hybrid simulations conducted for analysing seismic and fire engineering problems in previous researches.

2.5. Hybrid simulation in seismic engineering

The hybrid simulation approach was developed under the US-Japan Cooperative Earthquake Programme in the early 1980s (Dermitzakis and Mahin 1985; Takanashi and Nakashima 1988). For a comprehensive review of development made in the field of hybrid simulation, more information is available in the publication of Schellenberg et al. (2009). The first studies about numerical algorithms for the integration of the equation of motion in hybrid simulation have been conducted by Shing and Mahin (1984). They investigated the implementation of stable explicit schemes, included Newmark method (Newmark 1959). During the experiments it has been observed that the damage occurred in limited and specific regions of the entire structure. Consequently, Dermitzakis and Mahin (1985) suggested using substructuring technique, meaning that a structure needs to be divided into experimental and numerical substructures to perform partitioned hybrid simulations. A summary of the all the activities in hybrid simulations, performed in U.S., have been published by Mahin and Shing (1985). The paper described the basic approach to the pseudo-dynamic testing method, and this includes the numerical integration algorithms, details about the implementation and also the capabilities and the limitation of the technique.

A comprehensive summary of all the field activities developed in Japan have been presented by Takanashi and Nakashima (1987). Meanwhile, in U.S., Thewalt and Mahin (1987) presented the research about the first multi-directional hybrid simulation, developed as force, mixed force and displacement control strategies, and proposed the "effective force" dynamic testing method.

The complexity of the structural systems increased as well as the growing number of partitioned hybrid simulations. Nakashima et al. (1992) present the first implementation of hybrid simulation for real-time testing. The dynamics actuators and a digital servo-mechanism were used in the implementation. Campbell and Stojadinovic (1998) proposed geographically distributed structural subassemblies where the individual sited are connected through Internet. The new developments and activities in hybrid simulation made at the European Laboratory for Structural Assessment (ELSA) have been presented by Magonette and Negro (1998). Pan et al. (2005) developed an architecture where the physical test was conducted in one place while the numerical analysis was performed in a different location, where the communication between the substructure has been done

via Internet. The reason was to take advantage of different existing testing sites. Following sections describe the software components used for conducting hybrid simulations.

2.5.1. OpenSees

OpenSees, the Open System for Earthquake Engineering Simulation, is a software framework for simulation applications, originally for earthquake engineering applications, using finite element methods. It was originally developed at the University of California, Berkeley (McKenna 1997), and was later extended to perform structural fire analysis by researchers at the University of Edinburgh (Usmani et al. 2010). OpenSees is an object-oriented software implemented in the C++ language, through an open-source development process and uses the 'Tcl' scripting language as the platform. It is a collaborative program which is constantly being developed by numerous researchers (Jiang and Usmani 2018a; Kolozvari et al. 2018; Zhu et al. 2018). Globally, a collaborative framework such as OpenSees can be a valuable tool as it offers a standard program-developing environment and thereby optimizes the structural engineering problem-solving strategies. The main advantage of using this particular finite element software for hybrid simulation, besides the fast computation capabilities, comes from the possibility of directly linking OpenSees to any hybrid simulation setup through the middleware software OpenFresco. Moreover, the object-oriented and open-source approach allows any developer to add components to fit their particular needs in specific areas of engineering research, and simultaneously disseminate the development to potential users.

For instance, the seismic community of OpenSees has made significant developments in regards to geotechnical modelling of structures by simulating the full soil-structure interaction. It has also been developed to carry out a structural reliability and a sensitivity analysis which offers many reliability calculation tools. In addition to its availability as an analysis tool, OpenSees also presents a favourable software platform for the US Nees network because it allows engineers to organise and communicate data required to perform remote experiments and hybrid simulations. The OpenSees community is the largest community of this kind in the field of geotechnical and structural engineering. In the context of this study, it brings together the best of structural fire engineering computational capabilities under one platform which is accessible to all users. It also

facilitate new collaborations across geographical boundaries to solve ever more challenging problems.

There are mainly three types of problems encountered in structural analysis, a) steady-state problems, b) transient problems, and c) eigenvalue (stability) problems. Each of these analyses can be further classified as linear or nonlinear analysis. Following are the basic steps involved in the structural analysis of linear problems with OpenSees:

(1) The structural problem is discretised into nodes and elements.
(2) The element stiffness matrices are formulated.
(3) The system of equations is formulated in the third step.
(4) Suitable boundary conditions are employed.
(5) The system of equations is solved for the nodal degrees-of-freedom (DOF)
(6) Responses are computed within each element from calculated values for the DOFs

Different types of equilibrium equations are formed to achieve the required responses for three basic types of problems. For nonlinear problems, the system of equations formed is nonlinear and to obtain a solution an iteration scheme is generally utilised, e.g., Newton-Raphson method.

2.5.1.1. Class hierarchy in OpenSees

The classes in OpenSees are grouped into four major categories (McKenna 1997):

1. Modelling classes: These classes are used to prepare a finite element model for a given structural analysis problem.

2. Finite Element Model classes: These classes are used to describe the finite element model and stores the results of the analysis.

3. Analysis classes: The governing equations are formed and solved using these classes.

4. Numerical classes: The numerical operations involved in the solution procedure are taken care of by these classes.

Any of the four classes can access other classes to obtain a solution of a given structural problem. In the Step (1) of the analysis, various components, i.e., node, element and constraint, etc. are built through Modelling classes. Step (2) is performed by the Finite Element Model classes. The Analysis classes and Numerical classes are used to implement Steps (3) to (6) as described in the previous section.

2.5.1.2. Fire models for heat transfer analysis in OpenSees

A growing library of fire models has been made available in OpenSees Thermal. For fire scenarios where a uniform compartment gas-temperature is assumed to exist at an instant of time, models such as the standard fire and parametric fire (EN 13501-1 2007), etc., can be employed to define the gas temperature evolution, which is usually considered to be reasonable for small compartments. In recent years, localized burning and travelling fire behaviour in large compartments have attracted greater attention. Localized fire models have been provided in the Eurocode (EN 13501-1 2007) and Structural Fire Protection Engineering (SFPE) handbook, and travelling fire models are beginning to appear in the technical literature in this field (Dai et al. 2017; Stern-Gottfried 2011; Stern-Gottfried and Rein 2012). These advanced fire models are based upon applying a time history of heat flux at all spatial coordinates of the exposed surfaces of structural members resulting in fully characterizing the thermal loading demand on the structure corresponding to any given fire scenario.

The thermal impact on structural members caused by the fire exposure can be calculated in heat transfer analyses. The 'Heat Transfer' module in OpenSees Thermal can be deployed to run one-dimensional (1D) to three-dimensional (3D) heat transfer analyses. The basic architecture of heat transfer module follows the original OpenSees convention, which stores the modelling objects (heat transfer nodes, elements, and boundary conditions) in a HeatTransferDomain and performs the calculation in the HeatTransferAnalysis object. Tcl scripting commands have been provided for the heat transfer analysis as well, which utilise a mesh tool to discretise the structural members or sections into heat transfer nodes and elements. Commonly used structural materials such as steel and concrete have been added to the material library to perform a heat transfer analysis. Detailed heat transfer analysis procedure is explained in Chapter 6.

2.5.1.3. Thermo-mechanical analysis in OpenSees

When temperatures obtained from heat transfer analysis are applied at various locations in the structure and a stress analysis is performed, this type of analysis is termed as thermo-mechanical analysis. The thermo-mechanical analysis of structures subjected to fire is performed using beam-column (or frame) elements and shell elements in a 3D structural model or using both types of elements (a multi-scale model). The class hierarchy of the thermo-mechanical element implementation is illustrated in Fig. 2.17,

where Material, SectionForce Deformation, Element, and ElementalLoad are all abstract classes (base classes). Fig. 2.17 also shows the dependencies that these have between each other. The frame element can be formulated based on displacement interpolation or force interpolation, while its cross section is discretised into a number of fibres associated with uniaxial material models. A range of models for structural materials are added to the UniaxialMaterial collection which adopts the temperature dependent material properties from the Eurocodes.

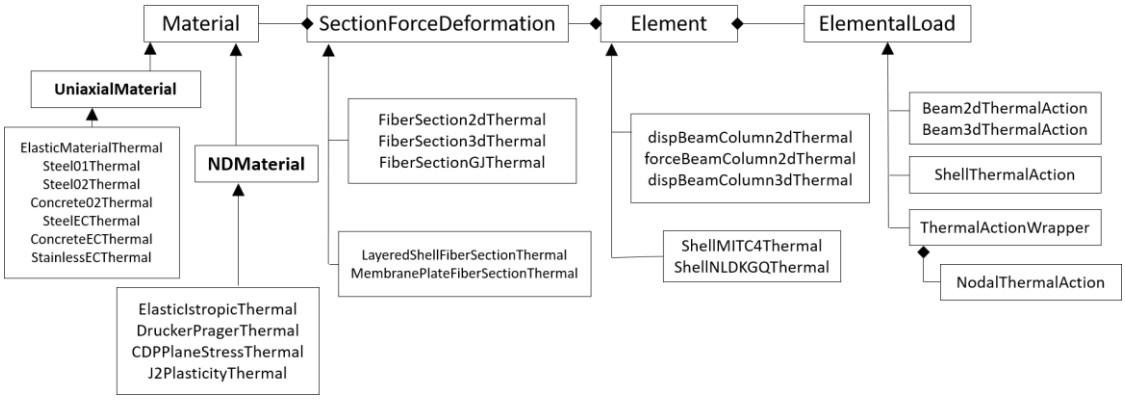

Fig. 2.17 Classes developed in OpenSees for thermo-mechanical analysis

Thermo-mechanical shell elements (ShellMITC4Thermal and ShellNLDKGQThermal) are developed to model a thin plate such as beam flanges and concrete slabs. Both shell elements adopt a layered plate section, which can be either simply defined as a MembranePlateFiberSectionThermal of five layers of consistent material, or an advanced LayeredShellFiberSectionThermal which accepts various number of layers and different material type for each layer. Currently, the thermo-mechanical versions of multi-axial materials (NDMaterial) for shell elements are available as elastic models with stiffness degradation and thermal elongation (ElasticIstropic3dThermal), steel models defined as rebar meshes (PlateRebarMaterialThermal) or plane stress layers (J2PlasticityThermal) and a plane stress form of concrete damaged plasticity model (CDPPlaneStressThermal).

2.5.2. OpenFresco

There are a number of different approaches for enabling the two assemblies to communicate with each other. The more traditional method is to use a file exchange system, as has been used in a number studies (Kwon et al. 2007; Wang et al. 2006). In this system, first, the trial displacements and rotations are estimated by the master FE

code at the interface node and saved in the form of data files. Then, the saved quantities are applied as boundary conditions in the slave assembly and the reaction forces at the interface node are estimated. These responses are also stored in a similar way in data files. Finally, the stored reaction forces are applied at the interface node in the master assembly to determine the new displacements and rotations for the next time step. The above steps are repeated for each integration time step until the end of the analysis. Although the file exchange system provides an excellent means for transferring data between the two assemblies, the main disadvantage is that the two FE models cannot run concurrently and therefore it is not very computationally efficient.

In the current study, the data is transferred between the two codes using a middleware software called OpenFresco which defines a super element and an adapter element in the master and the slave programmes respectively. Using OpenFresco for data communication between the two programmes enables both the FE codes to run simultaneously and concurrently, without restarting the analysis after every time step. This reduces the complexity and enhances the computational efficiency of the process, compared with the file exchange system.

The hybrid simulation architecture of OpenFresco uses the master and slave assemblies. OpenFresco comprises four different software classes. The first object is an experimental element (ExpElement), which represents the part of the structure that is physically tested and provides the interface between the FE software and the experimental software framework. The experimental site (ExpSite) is the second software class which is used to store the data. The third object is the experimental setup (ExpSetup) which transforms the data between the experimental element degrees of freedom and the actuator degree of freedom in the laboratory. The final object is the experimental control (ExpControl), which relates to the control and data acquisition systems. In the current study, OpenFresco facilitates the storage, transformation and transfer of data between the master and slave assemblies.

2.6. Hybrid simulation in fire

Although this approach is relatively common in seismic engineering, there are few examples in the literature where hybrid simulation is applied to analyse structures exposed to fire. The first hybrid simulation in fire was conducted by Korzen et al. (1999, 2010). A column was tested physically in the laboratory and the remaining building was

modelled using an FE software in the computer. The two assemblies communicated only through single degree-of-freedom, i.e., the axial column force computed from the model was adjusted and applied to the physical specimen at every integration step. Displacement control method was used to implement the calculated force to the physical specimen. Therefore, the required axial force was achieved by adjusting the displacement at the interface. The resultant displacement at the interface of the physical specimen was measured and fed to the FE model for next step calculation of axial column force. These steps were repeated until the test was complete.

Recently, Mostafaei (2013) has also conducted a hybrid simulation of a reinforced concrete frame, including a fire test of the first-floor central column as a physical substructure (PS). The rest of the structure was modelled in the non-linear finite element software SAFIR (Nwosu et al. 1999) as a numerical substructure (NS). Utilising the symmetry of the structure, the substructures interacted with each other through manual control of the axial force at the column ends. The interaction between the physical and numerical substructures was not automatic but was user-controlled, meaning that the user paused the physical test every five minutes to log the numerical data and then the simulation was re-started. The axial force and the axial displacement were recorded for the PS and NS. The applicability of this approach was limited due to control and communication of a single degree of freedom and the manual nature of the test.

Hybrid simulation in a real fire testing scenario is very complex, particularly if it is necessary to apply manual control to more than one interface. There are up to six unknowns (i.e., degrees of freedom in the NS and forces and moments in the PS) requiring control and communication at each interface. Manual control of these quantities increases the complexity of the tests and can introduce error into the process. So, before conducting a hybrid simulation in fire it is necessary to establish a hybrid simulation framework in a numerical environment. This means replacing the physical testing element of the hybrid simulation with another numerical model which uses high-resolution elements such as 3D shell and solid elements to create a so-called virtual hybrid simulation approach. The successful implementation of a virtual hybrid simulation framework eliminates the requirement for manual involvement between the two assemblies and this system can then be employed with a physical substructure in place of the detailed FE model in future

work. In this approach, a multiple numbers of responses can be controlled and communicated at the interface between the two assemblies.

2.7. Seismic vs Fire hybrid simulation

As presented in this chapter, the hybrid simulation in seismic field was widely studied and important improvements were done. Some main differences between the seismic field and fire field when performing hybrid simulations have been presented. It has been underlined that the direct implementation of the existed methods is not straightforward but nevertheless the development done in seismic field are a good source of inspiration for the specific problems of hybrid simulation in fire field.

There are various differences between the two fields when performing hybrid simulations. The first difference between the two fields is the equation that needs to be solved during the hybrid simulation. For the seismic field a dynamic equation governs the procedure while in the fire field the static equation needs to be solved. When the physical structure is exposed to fire, it expands slowly in time. Therefore, a dynamic approach is not required to conduct hybrid simulation in fire conditions.

One of the main challenges of hybrid fire testing is related to the necessity to conduct the hybrid fire simulation in real time; except for metallic elements in which a uniform temperature distribution can develop, the temperature distribution in most elements is highly non-uniform and time dependent and cannot be scaled down in time (this is particularly significant for concrete or timber elements). In seismic field, reduced scale tests are possible (similitude theory is needed in this case).

Real time testing is needed in fire field compared to seismic field, where slow tests, rapid tests, real time tests and smart shaking table tests are possible. In fire field, except for some specific elements, i.e. pure metallic unprotected structures, the evolution of the thermal gradient in the section of the PS continues even if the fire stops. This requests a real time testing and a fast interaction between the substructures during the hybrid simulation. In seismic field, the slow tests can be executed on extended time-scales of up to two orders of magnitude slower than the actual time-scale.

In fire fields, the structural elements are tested in furnaces, exposed to different fire load. This means that the structural elements need to be assembled (positioned) in such a way

to build a closed space where the load fire can be reproduced properly. The structural elements can be totally or partially exposed to fire. The transfer system and data-acquisition system must be protected from the fire exposure whereas in seismic field no protection is needed since the test is performed at ambient temperature.

2.8. Summary of the literature review and originality of this research:

(1) An axially restrained perforated beam behaves in a completely different way compared with an identical axially unrestrained perforated beam. The unrestrained perforated beams fail due to the loss of the bending moment capacity at elevated temperature and a sudden increase in midspan deflection (runaway) is observed. On the other hand, the restrained perforated beams can develop a catenary action on achieving large deflections even after losing the bending moment capacity, provided a sufficient axial restraint is developed. The location of this axial restraint have a significant influence on the fire behaviour of the steel beams, but the effect of location of axial restraint in case of perforated beams has not been given much attention and this aspect needs to be investigated.

(2) In the literature, most of the numerical and experimental studies to investigate the behaviour of perforated beams in fire ignore the whole structure behaviour and focus mainly on a single element. Considering the surrounding structure during the fire can considerably affect the behaviour of perforated beams. A computationally inexpensive yet accurate approach needs to be developed to analyse the behaviour of restrained perforated beams in fire by incorporating the effect of surrounding structure in the analysis.

(3) In hybrid fire simulation, the whole structure is divided into two substructures, i.e., PS and NS. On the other hand, the virtual hybrid simulation method presented in this thesis uses a fully numerical environment for both the substructures. To validate this approach, the whole structure can also be simulated in a single analysis (without sub-structuring) and results can be compared to check the accuracy of the proposed virtual hybrid simulation approach.

(4) Most previous numerical investigations on restrained composite perforated beams in fire are limited to standard fire exposure. Different fire scenarios may pose a different rate of heating and cooling as a result of which the beams may experience

different thermal gradients. The influence of different fire scenarios on the performance of the restrained perforated beams is investigated in this research.

(5) The methodology of virtual hybrid simulation can be extended to a modified virtual hybrid simulation framework by coupling different FE software for different parts of the structure. This can enable the user to use the modelling capabilities of multiple software, i.e., fire exposed portion can be modelled in Abaqus and the surrounding structure can be modelled in OpenSees. Local failure modes, which are essential in analysing the behaviour of restrained perforated beams can be traced more accurately using Abaqus modelling features. On the other hand, the travelling fire models available in the latest version of OpenSees can also be utilised in the same simulation.

Chapter 3

Behaviour of perforated steel beams in fire

3. Introduction

This chapter starts by providing the details about the numerical modelling procedure including the solver type, element type, mesh sensitivity analysis, residual stresses and the implementation of imperfections. Thereafter the numerical modelling calibration is carried out by modelling the isolated structural components such as solid steel beams and perforated steel beams exposed to fire with and without axial restraint. All the validations are performed by comparing the results against experimental data and finite element analysis performed by other researchers. Various types of structural members exposed to uniform and non-uniform temperature distribution are modelled and validated in this chapter.

3.1. Numerical modelling using Abaqus

In this section, key aspects related to numerical modelling in Abaqus are discussed.

3.1.1. Solver type

The Abaqus general solver is employed for all the transient state analysis of structural elements exposed to fire. However, due to temporary numerical instabilities, there may be convergence problems with the general solver. This problem is minimised by including artificial damping in the model. In Abaqus, the artificial damping can be applied by checking the "dissipated energy fraction" while defining the step. The value of the dissipated energy fraction is chosen carefully so that it can bypass the issue of temporary instabilities and does not change the response of the beams significantly. A typical value of 1×10^{-10} is used in this study. Various other researchers (e.g., Chen and Wang 2012; Dai et al. 2010; Elsawaf et al. 2011) have utilised the same technique.

3.1.2. Element type

In finite element modelling, there are various types of elements that can be used to model structures exposed to fire. The most common types of elements used in previous studies are solid or continuum, shell, beam and truss elements. Both shell and solid elements can be utilised to model the perforated beams in fire but the use of beam-column elements is limited to modelling solid beams and cannot be used for perforated beams as the geometry of the section varies along the length of the beam. S4 and S4R are the full and reduced integration quadrilateral shell elements offered by Abaqus. Frequent use of both types of shell elements is observed in the literature to model the solid and perforated steel beams (e.g., Ellobody 2011; Sofias et al. 2014; Wang et al. 2014). General purpose S4R shell elements are used in this study to model the perforated steel beams in fire. S4R are the first order shell elements and have six degrees of freedom at each node (three translations and three rotations).

Using first order elements for modelling pure bending problems in finite element analysis may result in two problems, which are shear locking and an hourglassing phenomenon. These problems should be carefully considered and addressed while modelling. The shear locking phenomenon may arise owing to the implementation of full integration scheme and the hourglass phenomenon may occur due to the use of reduced integration scheme.

The problem of shear locking arises when pure bending cases are modelled using a full integration scheme. It allows the generation of shear deformations instead of bending deformations as shown in Fig. 3.1(a). It allows the angle between the edges of the element to become non-90° and generation of shear strain is observed. This problem results in an over stiff behaviour of the elements and known as shear locking. Generally, shear locking is minimised by using a finer mesh and using reduced integration elements.

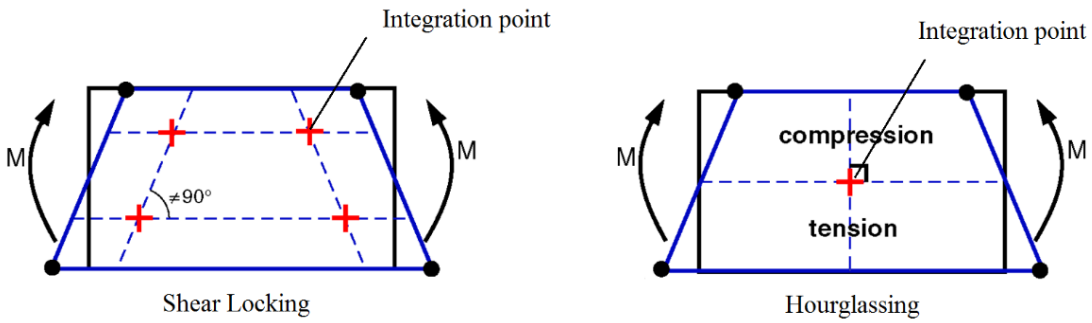

(a) (b)

Fig. 3.1 Shear locking and hourglass phenomenon

On the other hand, the use of reduced integration elements to model the pure bending eliminates the shear locking but could induce the hourglass phenomenon as shown in Fig. 3.1(b). Using a single element across the depth of the section may not capture bending strain and develops zero energy mode. The length of the element remains the same with zero strain as illustrated in Fig. 3.1(b). This problem may be eliminated if three or more elements are used and each element can capture either compressive or tensile strains.

3.1.3. Boundary conditions

Fig. 3.2 shows the boundary conditions used in the simulation models. A reference point is defined in the space, which lies on the centroidal axis of the section. All the nodes at the beam end are constrained to this reference node through distributing coupling constraint available in Abaqus. The desired boundary conditions are assigned to the reference node directly in the instance of complete axial restraint as shown in Fig. 3.2(b). However, in order to model partial axial restraint, similar to the previous reference point, another reference point is defined lying on the centroidal axis of the member and a spring is defined between the two reference points as shown in Fig. 3.2(c). A variable stiffness value can be assigned to the spring to simulate the different magnitude of axial restraint.

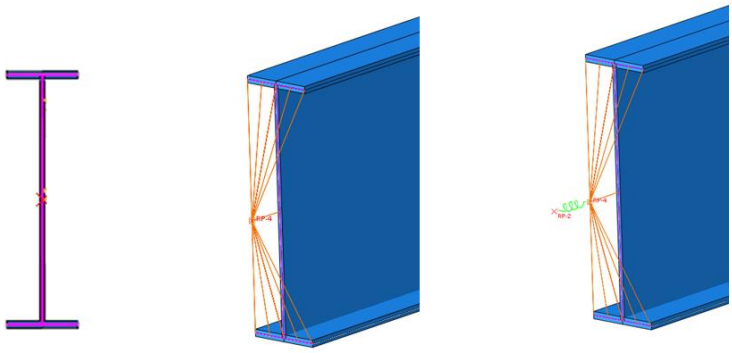

(a) (b) (c)

Fig. 3.2 Boundary conditions applied in Abaqus (a) Steel section (b) Coupling constraint for fixed axial restraint (c) Coupling constraint for partial axial restraint

3.1.4. Mesh sensitivity

To achieve accurate results, a sufficiently fine mesh is required in finite element modelling. A coarse mesh may result in inaccurate solutions, whilst a finer mesh will advance the solution towards a more precise result but at higher computational cost. The mesh is refined until an accurate solution is obtained, and any further decrease in the mesh

size does not improve the accuracy of the solution; then the mesh is considered to have converged. A mesh sensitivity analysis should be carried out by selecting an optimum mesh size to achieve a fairly accurate solution and simultaneously keeping the computational time to minimal. To conduct a mesh convergence study, a simply supported beam using section W24×76 is modelled with 8 m span. The beam is analysed under uniform moment and uniformly distributed load. In both types of loading, the uniform bending moment or uniformly distributed load is applied and increased until the failure of the beam. The stress-strain relationship for steel is used according to the Eurocode guidelines (EN 1993-1-2 2005) with a yield strength of 275 N/mm^2 and Young's modulus of 2.1×10^5 N/mm^2. The mesh density is varied from a large element size of 100 mm to a small element size of 10 mm. The load-midspan deflection and moment-midspan deflection behaviours are presented in Fig. 3.3 and Fig. 3.4, respectively. The accuracy of the FE solution is also checked against the analytical solution which is obtained using the following equations.

The plastic moment capacity of a section is given by

$$M_{pl} = Z_{pl} \times f_y \tag{3.1}$$

where M_{pl} is the plastic moment capacity of the section, Z_{pl} is the plastic section modulus of the section and f_y is the yield strength of steel.

For simply supported beams subjected to a UDL, the failure load is defined as follows,

$$W_{pl} = 8M_{pl}/l^2 \tag{3.2}$$

where l is the beam span and W_{pl} is the failure load.

For a beam under a uniformly distributed load “w”, the linear elastic curve can be plotted using the following relation.

$$\delta_{midspan} = 5wl^2/\,384EI \tag{3.3}$$

where $\delta_{midspan}$ is the deflection at midspan.

If the beam is under uniform moment “M”, the linear elastic curve is plotted using the following relation.

$$\delta_{midspan} = Ml^2/\,8EI \tag{3.4}$$

The plastic failure moment and plastic failure load are obtained using Eq. 3.1 and 3.2, respectively. In the first simulation, the beam is loaded under a UDL until the failure is

achieved and the load-midspan deflection behaviour is obtained. The maximum failure load and the initial linear elastic slope are also plotted using the above equations and shows a good agreement with the FE simulations as shown in Fig. 3.3. In the second simulation, the beam is loaded under a uniform moment and the moment is applied at the reference nodes as shown in Fig. 3.2(b). The maximum failure moment and the initial linear elastic slope are also plotted using the above equations. A show very good conformity is obtained with the FE simulations as illustrated in Fig. 3.4. The above FE analysis is repeated with different mesh sizes and the results obtained using different mesh sizes implies that there is a negligible effect of mesh density on the overall behaviour of the beams. In this particular instance, any of the 100 mm, 50 mm, 25 mm and 10 mm mesh sizes can be selected to predict the desired load-midspan deflection behaviour accurately. However, a mesh coarser than 50 mm cannot be used as it will result in two elements across the flange width, one on either side. If it is required to trace the stresses, strains and other parameters across the flange width than use of one element is not appropriate. On the other hand, using a smaller mesh size, e.g., 10 mm, will increase the computational time without any significant improvement in the results. Therefore, a mesh size of 25 mm can be used in this instance.

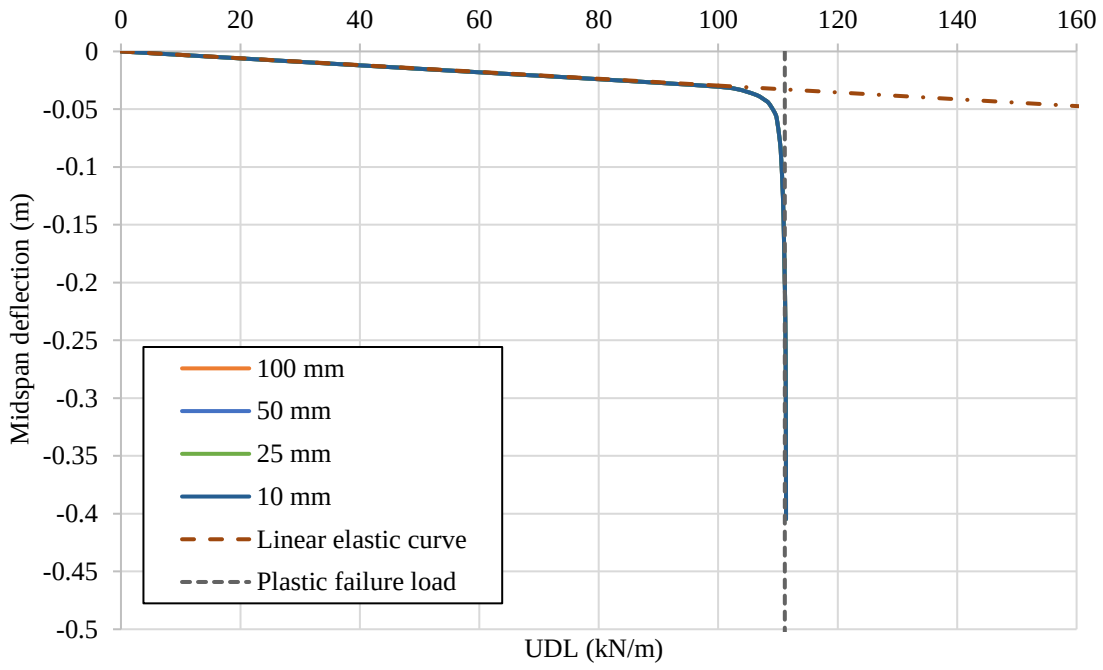

Fig. 3.3 W24×76, 8 m span beam under a uniformly distributed load

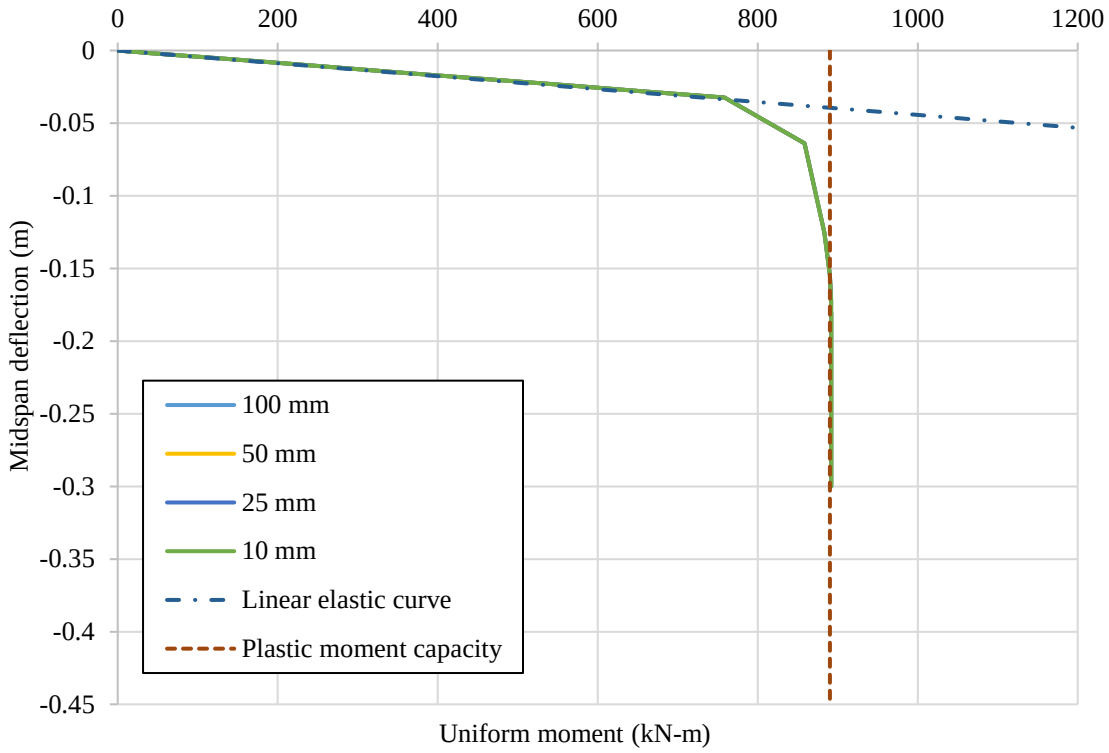

Fig. 3.4 W24×76, 8 m span beam under a uniform moment

The main objective of this study is to analyse the behaviour of perforated beams. The mesh density can have a great influence in predicting important phenomenon in perforated beams such as web-post buckling. So, a cellular beam from the literature is also modelled to conduct a mesh sensitivity analysis and to capture the web-post buckling behaviour. Warren (2001) conducted a study by testing 8 cellular beams (1A, 1B, 2A, 2B, 3A, 3B, 4A, 4B). Out of these 8 beams, web-post buckling was observed only in beam 4B. A UB305×102×25 section was used as a parent section to develop this beam. The schematic of the beam is shown in Fig. 3.5. Further details are available in the detailed test report (Warren 2001).

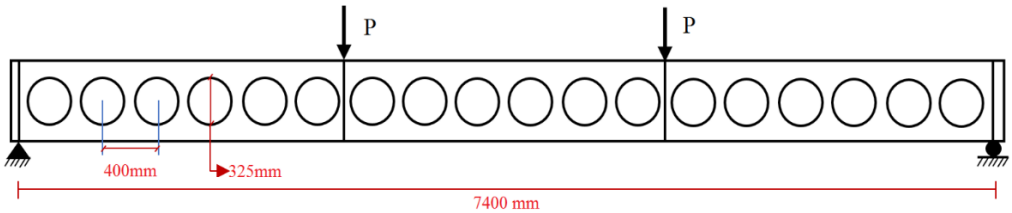

Fig. 3.5 Details of beam 4B tested by Warren (2001)

Fig. 3.6 shows the load-deflection curves for beam 4B with different mesh densities. In this case, the effect of mesh density can be observed and refining the mesh from 150 mm to 25 mm improve the accuracy of the results but reducing mesh size beyond 25 mm does

not result in any improvement of the accuracy of the result, hence a mesh size of 25 mm is selected.

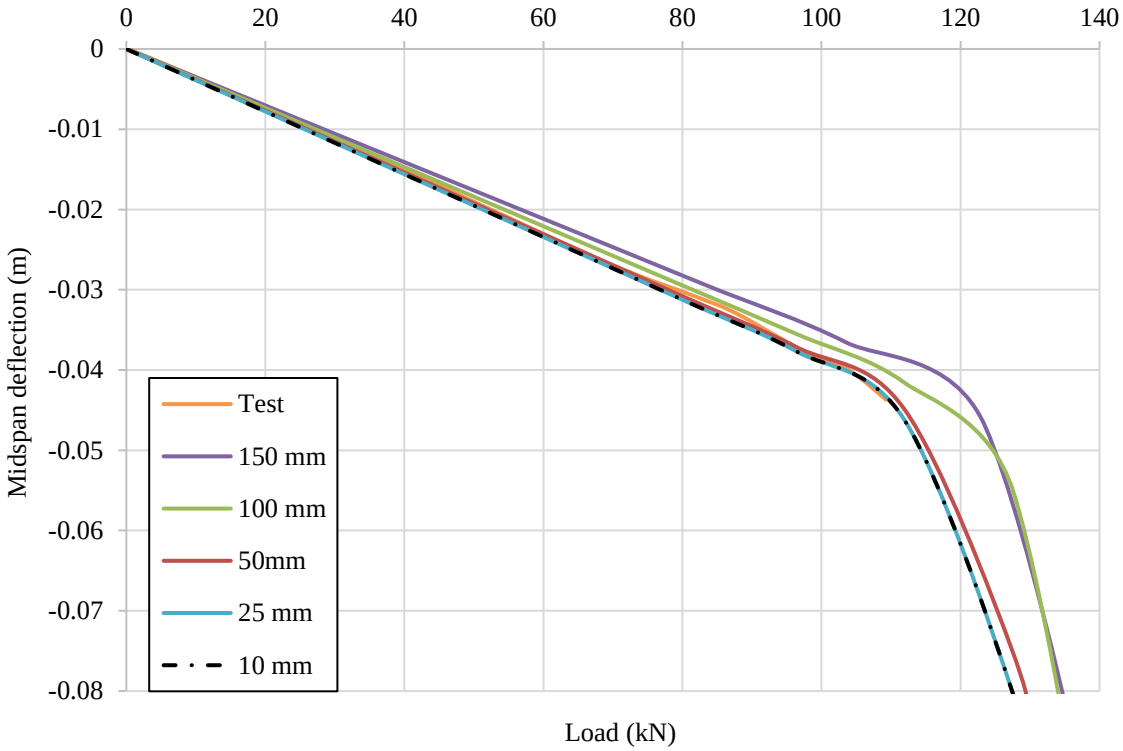

Fig. 3.6 Mesh sensitivity analysis for beam 4B tested by Warren (2001)

3.1.5. Imperfections

Real structural components have geometric imperfections in the form of deviations from the ideal geometry. Introduction of geometric imperfections in modelling perforated beams is vital because, during the manufacturing process of perforated beams, operations like cutting and fabrication develop initial imperfections in the member. Therefore, to assume a perforated beam without imperfections may be far from reality. So, to include the effect of geometric imperfections, the perturbations in the geometry are introduced in the FE model.

There is not a perfect guideline to assign the shape and the magnitude of the initial imperfection in the FE models of the perforated beams. To assign initial web-post imperfection, SCI report RT1187 (Simms 2008) on the design of steel beams with web openings suggests that the shape of the imperfection should be in the form of a half sine wave with a maximum amplitude of h/600, where h is the height of the section. For lateral buckling, Eurocode (EN 1993-1-1 2005) suggests a value of l/500 as the imperfection at midspan to investigate the lateral buckling behaviour, where l is the length of the member.

In this study, a linear elastic buckling analysis is carried out in order to identify the possible buckling modes of the structure. Multiple buckling modes are superimposed to incorporate the local and global imperfections. The imperfections are applied to the perfect geometry by applying a scale factors to the buckling mode shapes of the member. This procedure is used to apply the imperfections to the geometry for most of the simulations performed in this study.

A cellular beam tested by Surtees and Liu (1995) is modelled to investigate the importance of imperfection on the behaviour. Fig. 3.7 illustrates the load-midspan deflection behaviour using the various magnitude of imperfections (h/10000, h/1000 and h/h), where h is the height of the section. It is observed that introducing a large imperfection of 1 mm (h/h) improves the accuracy of the results significantly. It is noteworthy that the web-post buckling behaviour can be traced in perforated beams if appropriate imperfections are applied. Beams without initial imperfections show stiff behaviour and are able to sustain higher loads without noticing any web-post buckling.

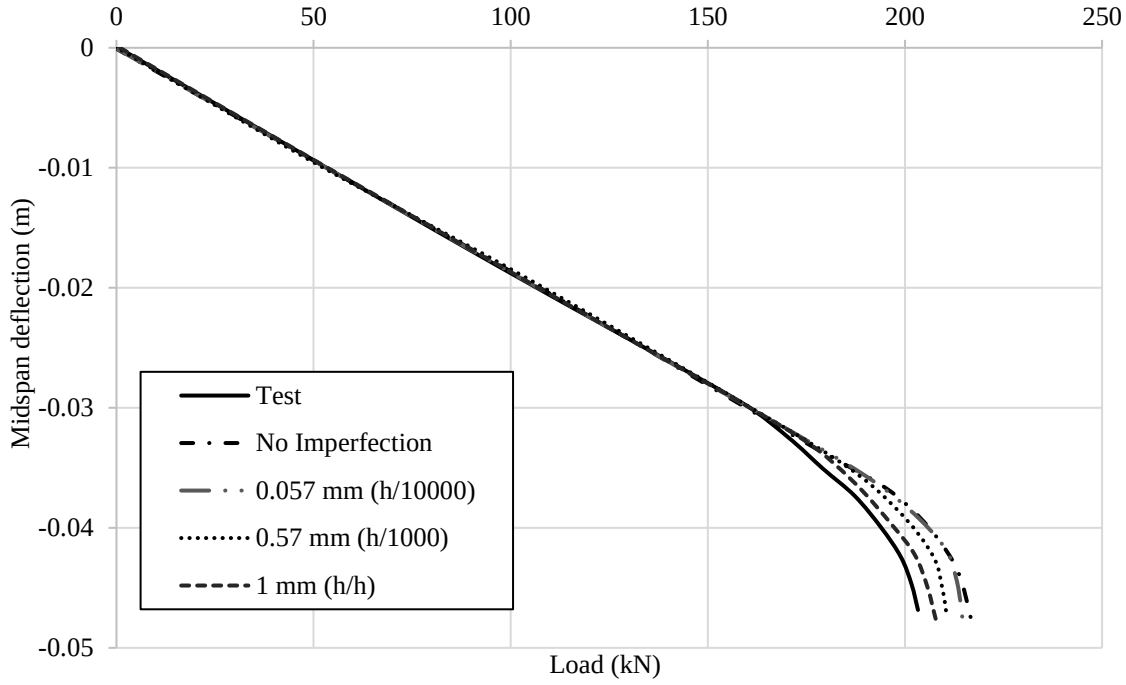

Fig. 3.7 Imperfection sensitivity for Surtees and Liu (1995)

3.1.6. Residual stresses

Residual stresses developed in a structural member are a self-equilibrating set of stresses in its unloaded state (Withers and Bhadeshia 2001). They are present in most types of

structural steel sections and they are induced due to various types of manufacturing operations such as welding, cutting and non-uniform cooling. In hot-rolled steel sections, non-uniform cooling is the main cause of the development of residual stresses. These stresses can have a significant influence on the formation of yield at a certain section. The structural stiffness, stability and fatigue strength of a structure is also affected due to their presence and should be considered carefully.

Generally, in a hot rolled I section, the edges of the flange cool rapidly compared to the middle part. Due to this differential cooling rate, the edge of the flange is left in residual compression whereas the middle portion is under residual tension. For webs, the web-to-flange junction is generally found in residual tension due to slower cooling than the middle part of the web. In the current study, it is noteworthy that the influence of the residual stresses decreases with increasing temperature (Manal 2017). Moreover, the imperfection values used in the Eurocode curves take account of residual stresses and geometrical imperfections, whereas only geometrical imperfections are introduced into the Abaqus models (Najafi 2014). However, the geometrical imperfections used in this study are quite severe and may be considered to compensate for the omission of direct inclusion of residual stress (Najafi 2014).

3.2. Behaviour of axially unrestrained solid beams exposed to fire

An extensive numerical study was conducted by Burgess et al. (1991) to understand the behaviour of various structural elements exposed to different fire scenarios. Four beams are selected from that study to be validated here. Two 4 m simply supported beams under a uniformly distributed load of 45.8 kN/m are selected. One of the beams is exposed to uniform temperature distribution while the other beam is under a thermal gradient as shown in Fig. 3.8. Another set of rotationally fixed and axially unrestrained beams with 8 m span and under a UDL 11.46 kN/m and 17.18 kN/m are chosen for validation. Both these beams are exposed to non-uniform temperature distribution according to Fig. 3.8. All four of the beams use the same section UB254×146×43, with a steel strength of 275 N/mm^2 and Young's modulus of elasticity of 2.1×10^5 N/mm^2 at ambient temperature. The mechanical and thermal properties of steel are defined according to the Eurocode guidelines (EN 1993-1-2 2005), and a constant value of 1.4×10^{-4}/ ºC for the coefficient of thermal expansion is used. To avoid lateral torsional buckling and web-post buckling, the web is laterally restrained along the span. Najafi and Yin (Najafi 2014; Yin 2004)

have also simulated these beams to validate their model and their results are also compared. A good agreement is shown between the FE model and the results of Burgess et al. (1991) and Najafi (2014) as illustrated in Fig. 3.9 to Fig. 3.12.

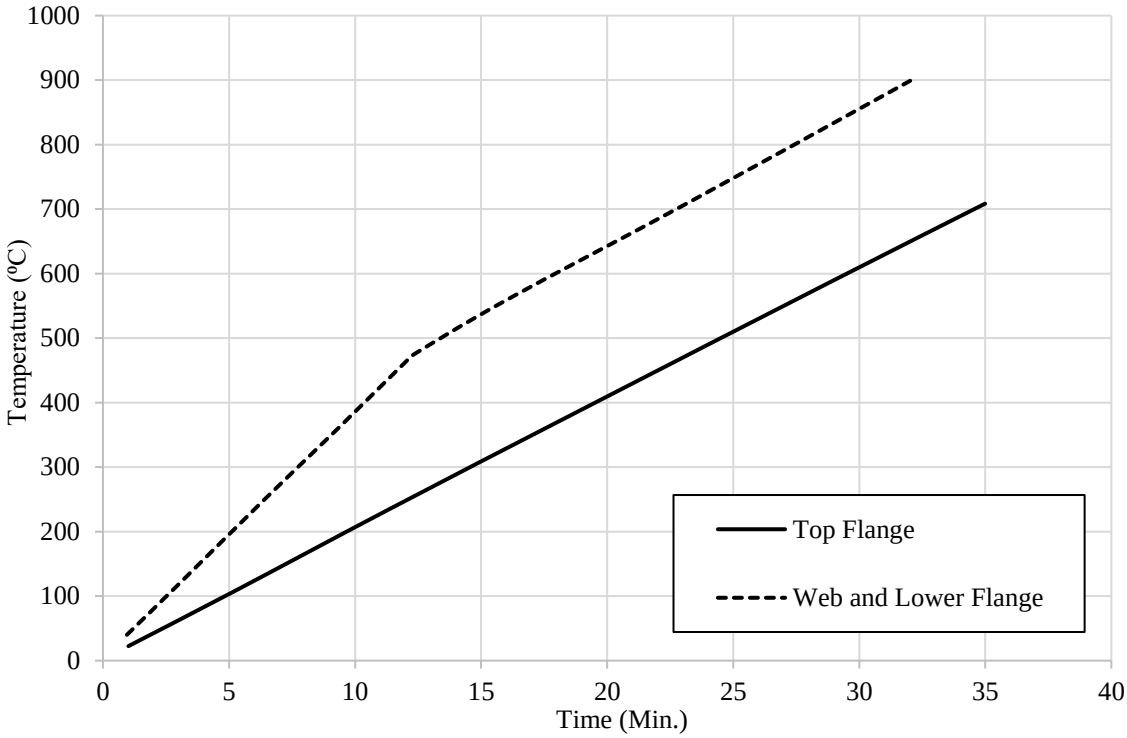

Fig. 3.8 Assumed temperatures in the numerical models of Burgess et al. (1991)

The midspan deflection for unrestrained beams exposed to fire mainly comprises of two components which are thermal bowing deflection (due to thermal gradient) and mechanical deflection (due to a loss in the strength at high temperature). In the case of uniform heating, up to 400 ºC, there is a negligible increase in the deflection because of the absence of thermal bowing and no reduction in the material strength. When the temperature reaches beyond 500 ºC, the mechanical strength of the material reduces considerably which leads to the compression buckling of the top flange as shown in Fig. 3.13 (a). Due to the buckling of the top flange, the midspan deflection increases suddenly as shown in Fig. 3.10. However, in the case of non-uniform temperature distribution, there is an increase in the deflection for the initial duration of fire, which is mainly due to the thermal bowing effect. At higher temperatures, similar to uniform temperature distribution, a sudden increase in the mechanical deflection is observed (see Fig. 3.11) which is due buckling of the top flange as illustrated in Fig. 3.13 (b). In case of 8 m rotationally restrained beams, yielding near the supports is observed due to restrained rotations as shown in Figs. 3.13 (c) and (d). Lateral torsional buckling of 8 m rotationally

restrained beams is observed which is attributed to a high magnitude UDL of 17.18 kN/m as shown in Fig. 3.13 (d).

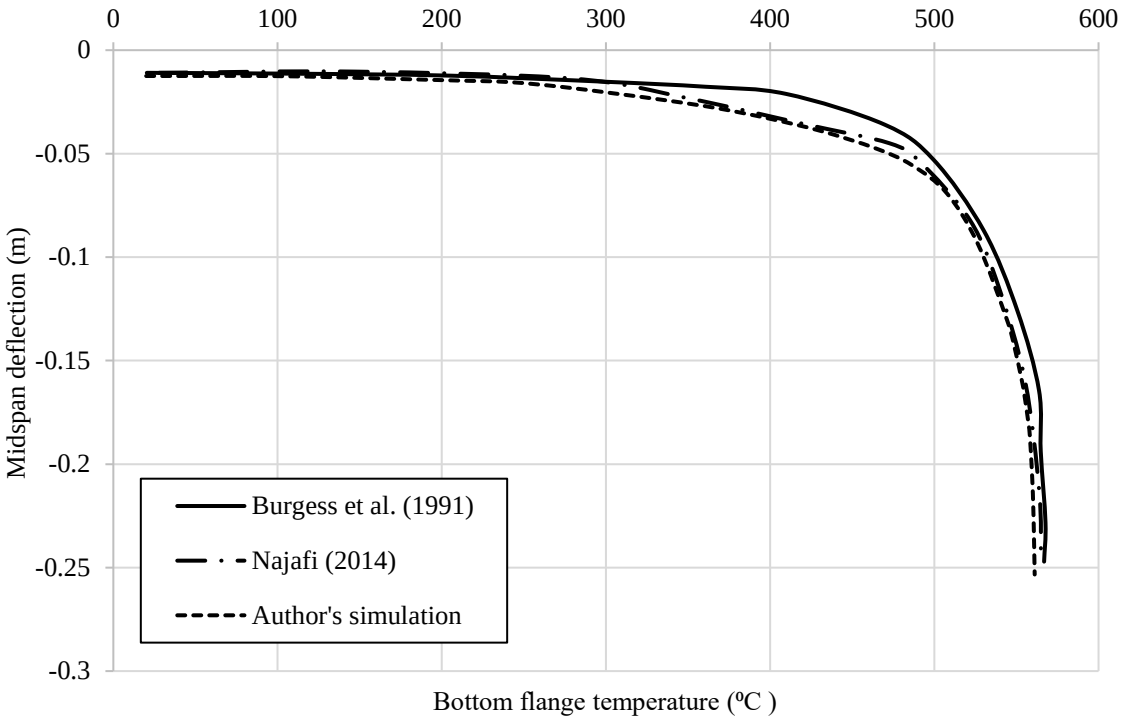

Fig. 3.9 Simply supported solid beam with a span of 4 m under a uniform temperature distribution

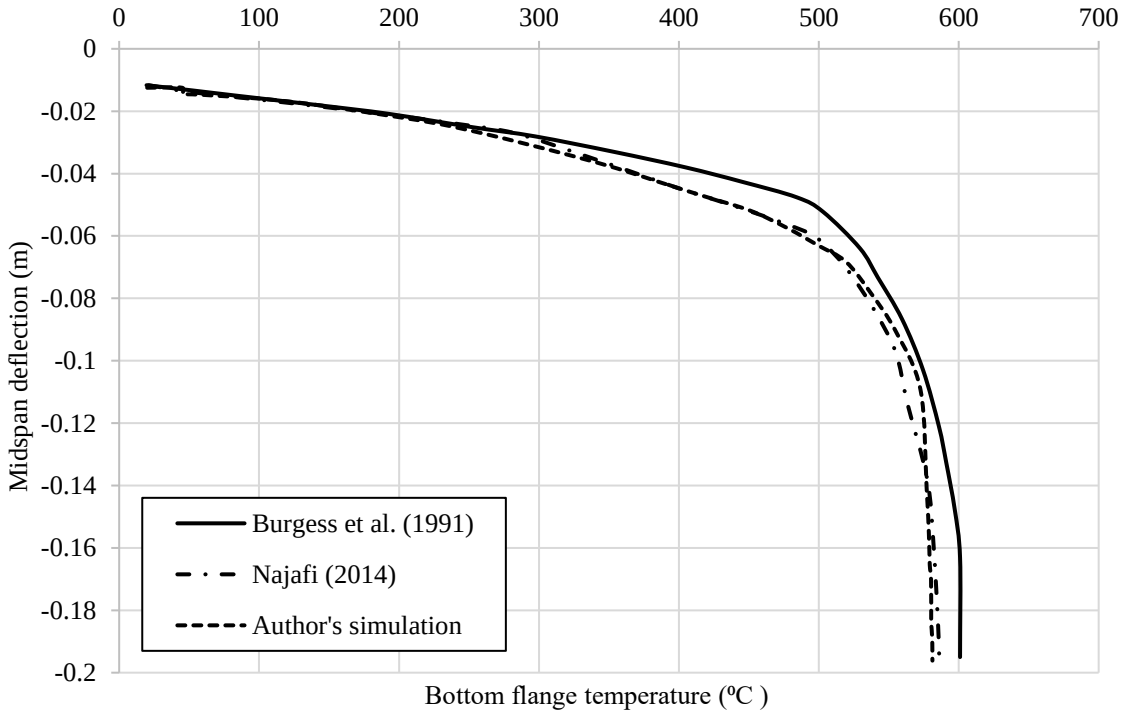

Fig. 3.10 Simply supported solid beam with a span of 4 m under a non-uniform temperature distribution

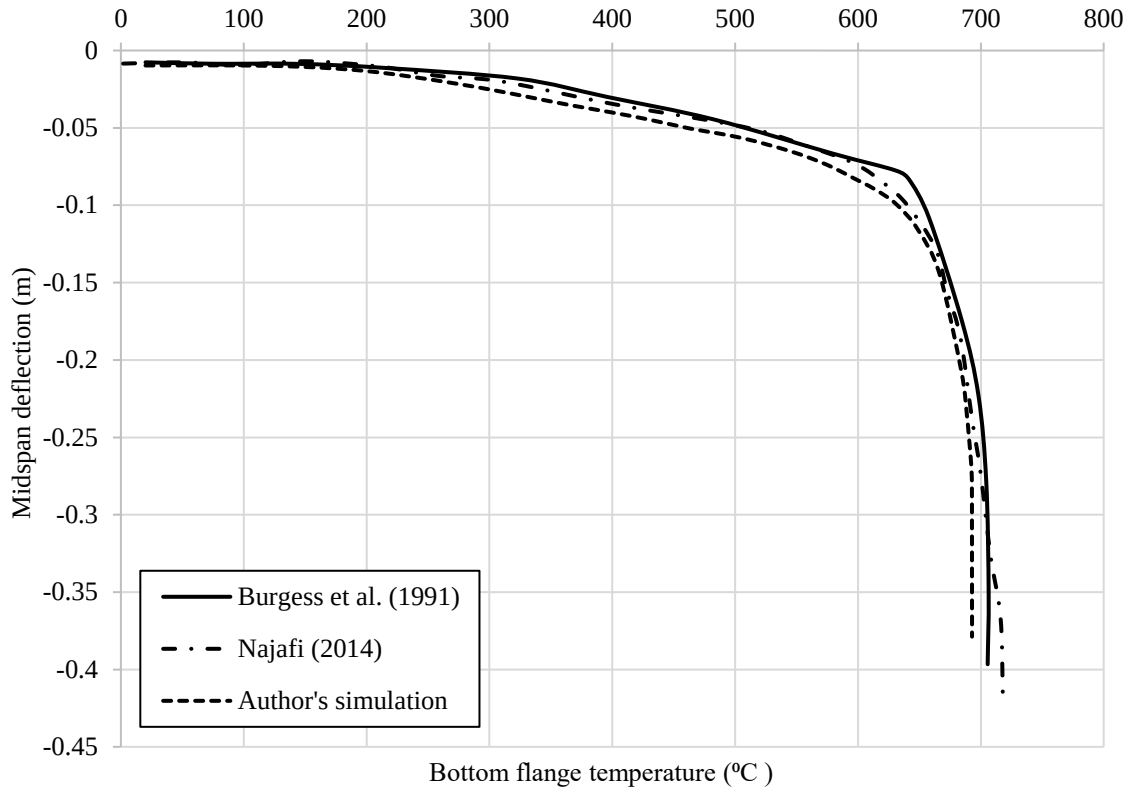

Fig. 3.11 Rotationally restrained and axially unrestrained beam of 8 m span under a UDL of 11.46 kN/m

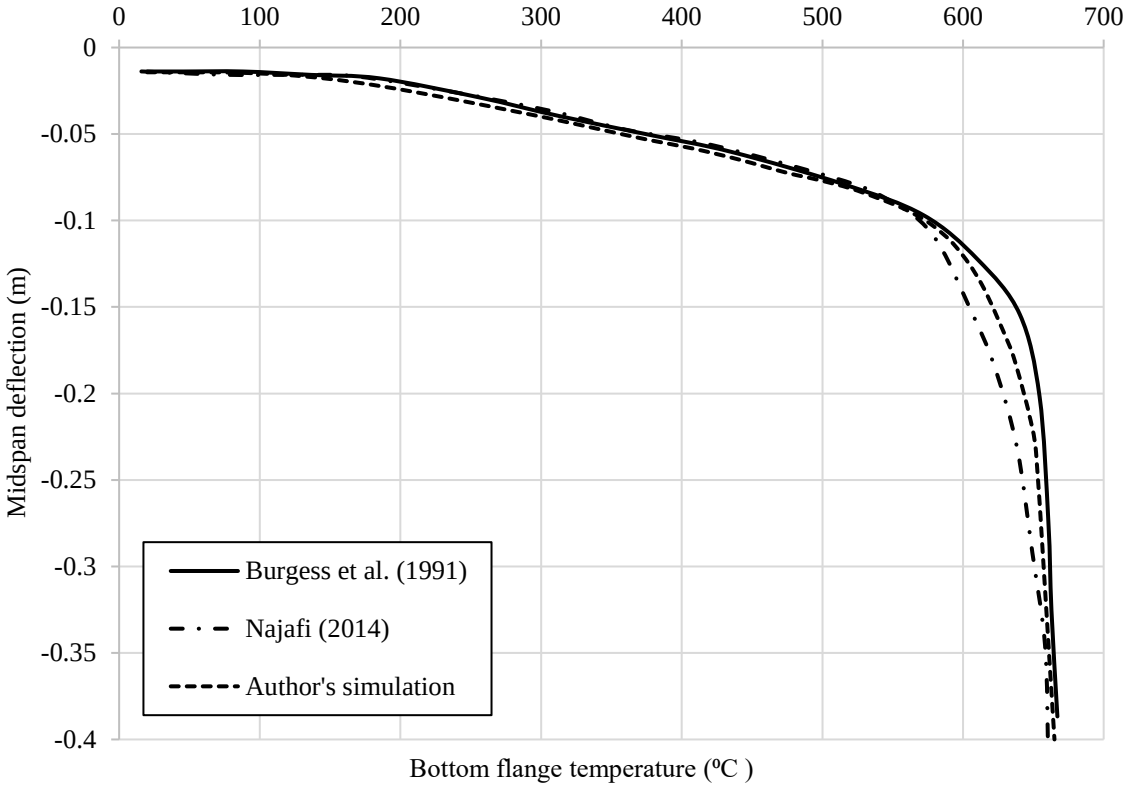

Fig. 3.12 Rotationally restrained and axially unrestrained beam of 8 m span under a UDL of 17.18 kN/m

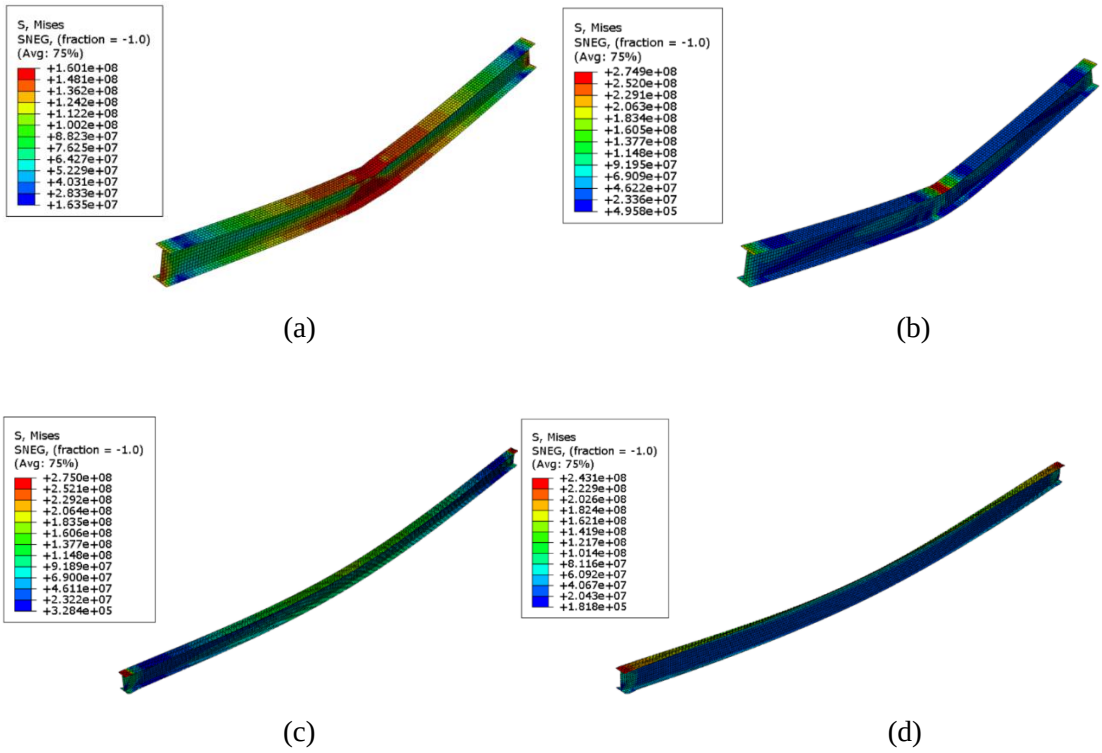

Fig. 3.13 Failure modes for solid steel beams exposed to fire (a) 4 m unrestrained beam exposed to uniform temperature (b) 4 m unrestrained beam exposed to non-uniform temperature (c) 8 m rotationally restrained beam under a UDL of 11.46kN/m (d) 8m rotationally restrained beam under a UDL of 17.18 kN/m

3.3. Behaviour of axially restrained solid beams exposed to fire

An extensive parametric study was conducted by Najafi (2014) to analyse the behaviour of axially restrained solid beams exposed to elevated temperature. All beams were fully axially restrained so that a catenary action develops in the beam at high temperature. The web was laterally restrained to avoid the lateral torsional buckling and web buckling in all the simulations. The effect of various parameters was investigated in that study, e.g., load ratio, level of axial restraint and different temperature distributions in the cross-section. Here in this section, only a group of the axially restrained and rotationally free beams are simulated and validated.

A UB457×152×60 (S275) section is utilised in modelling all the beams in the group. All beams are simulated for three-point loading arrangement and a uniform temperature distribution is assumed across the depth of the beams. In this section, two beams of 5 m length are simulated under load ratios of 0.4 and 0.7 with central concentrated loads of 111.6 kN and 195.3 kN, respectively. Another set of beams are simulated with a span length of 8 m and under a central concentrated load of 69.8 kN and 122.1 kN with load

ratios of 0.4 and 0.7, respectively. The analysis is carried out in two steps. In the first step, the static load is applied and in the second step, the thermal load is applied. During the application of thermal temperatures in the second step, the static load is kept constant. Fig. 3.14 and Fig. 3.15 illustrate the temperature-midspan and temperature-axial reaction behaviour comparison with the Najafi's results for all beams simulated in this section and a very good agreement has been obtained.

The overall behaviour of 5 m and 8 m axially restrained beams is the same. During the initial stage of fire (up to 500 ºC), the rate of deflection is very slow and the main cause of deflection is the thermal bowing and restrained expansion of steel as shown in Fig. 3.14. In the later stage (beyond 600 ºC), the midspan deflection increases at a rapid rate and the main reason for this high rate of deflection is the loss of material strength at elevated temperature. It is noteworthy that due to high slenderness of 8 m beams compared to 5 m beams, they buckles at a lower axial compressive force and this buckling initiates the compressive unloading of the section as illustrated in Fig. 3.15. It is also observed that an increase in load ratio causes an early transition of the axial reaction from compression to tension. Fig. 3.16 represents the deformed shapes of these beams at failure.

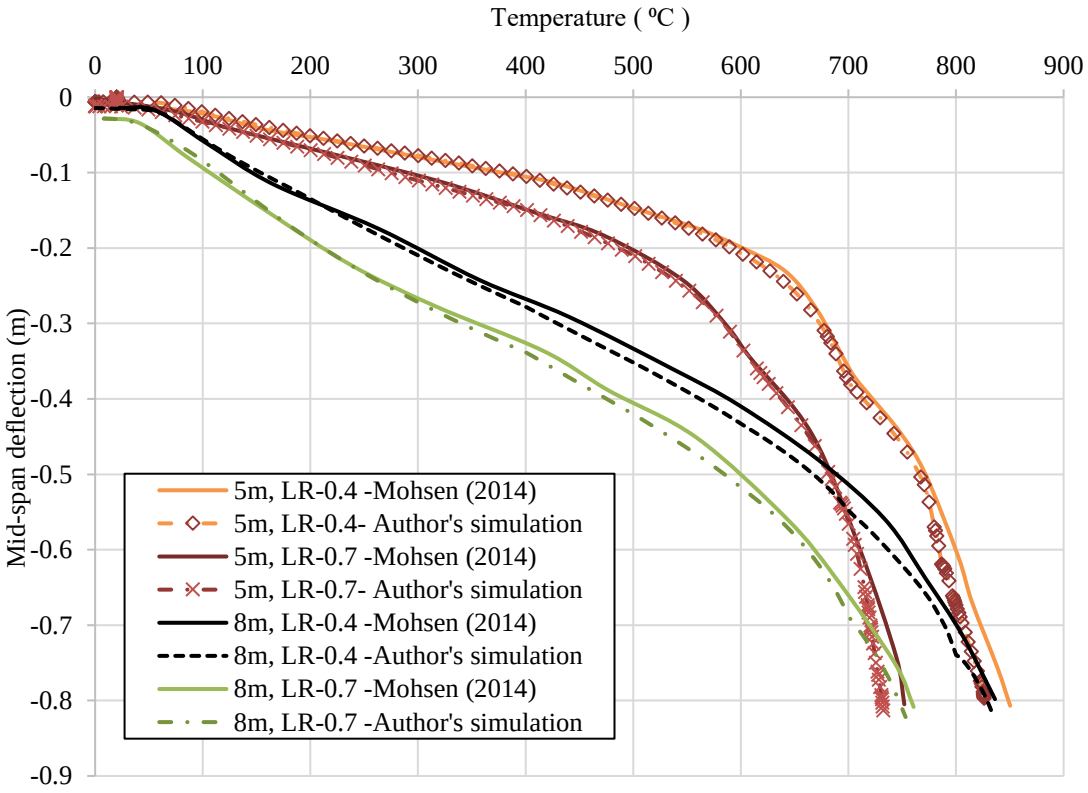

Fig. 3.14 Temperature- midspan deflection behaviour for axially restrained beams under uniform temperature distribution

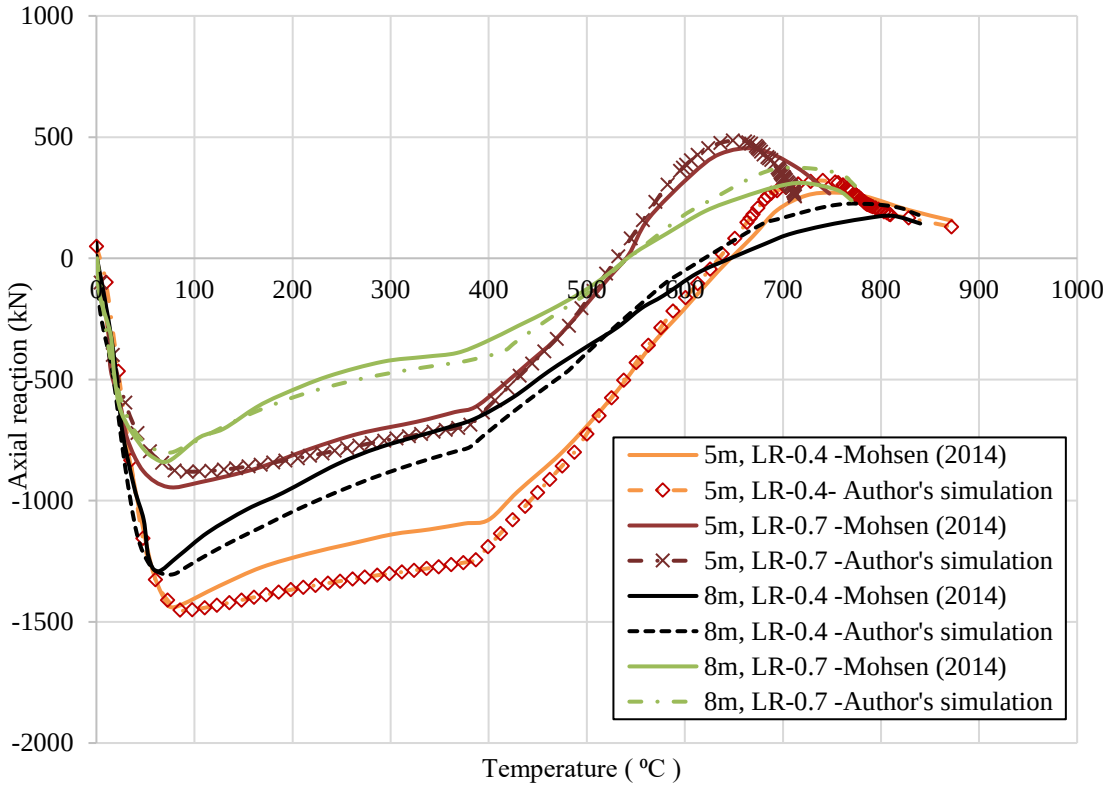

Fig. 3.15 Temperature- axial reaction behaviour for axially restrained beams under uniform temperature distribution

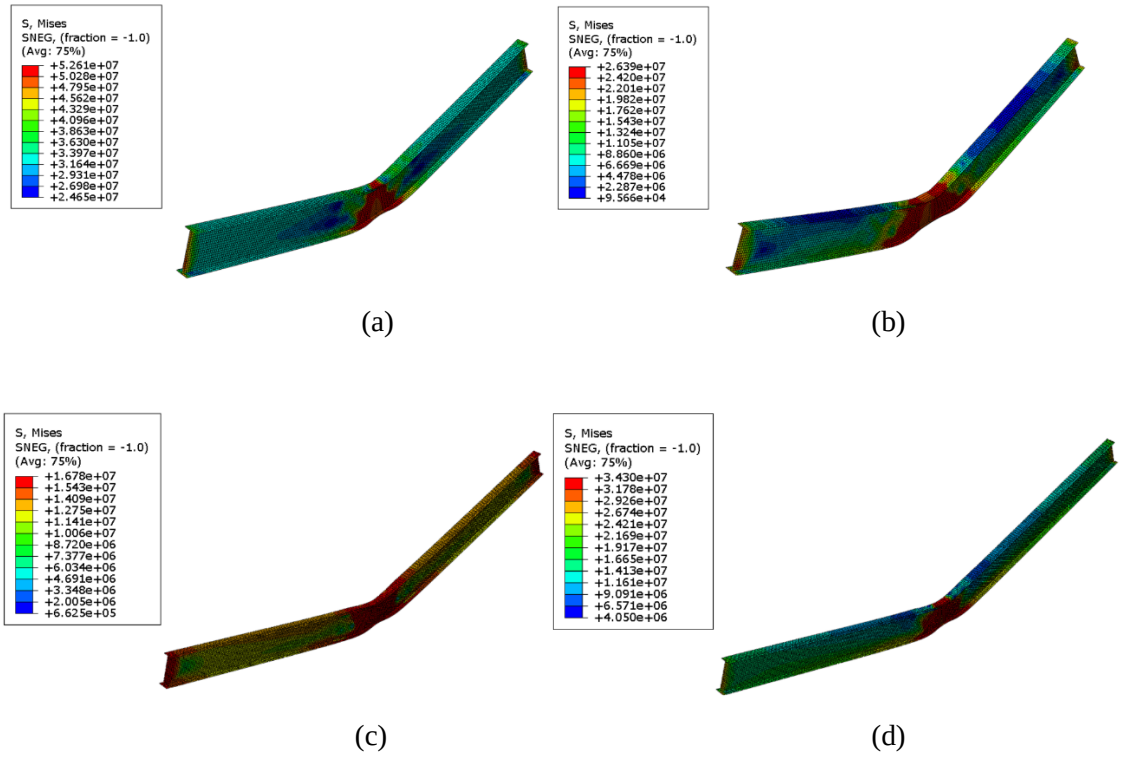

Fig. 3.16 Failure modes for axially restrained solid steel beams exposed to uniform temperature distribution (a) 5m beam under a LR 0.4 (b) 5 m beam under a LR of 0.7 (c) 8 m beam under a LR of 0.4 (d) 8 m beam under a LR of 0.7.

3.4. Behaviour of unrestrained perforated beams exposed to fire

In this section, the unrestrained perforated beams are simulated and the model is validated using the instances from a study conducted by Yin and Wang (2006). The perforated beams modelled in this section uses a UB457×152×60 (S275) steel section with a span of 8 m. The beams are modelled without any web opening (NWO), with different size of single web opening (SWO 1, SWO 2 and SWO 3) and an instance of multiple web openings (MWO) is also modelled as shown in Fig. 3.17. Openings in all the simulated cases are symmetrical to geometric centreline of the beam. A uniformly distributed load of 35 kN/m with a load ratio of 0.7 (based on the ambient temperature capacity of the solid section) is applied to all the cases. All beams are exposed to a uniform temperature distribution.

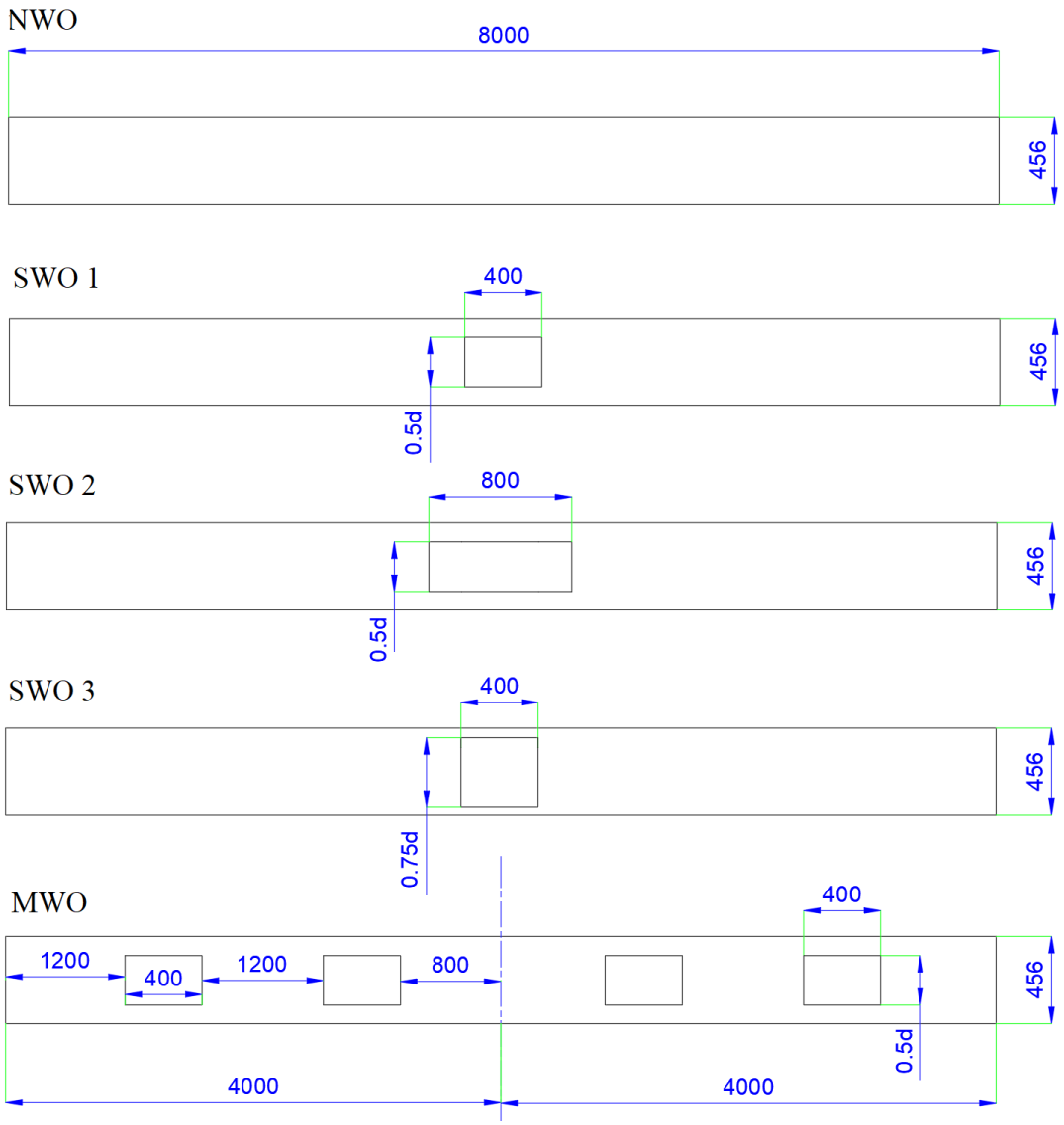

Fig. 3.17 Schematic for location and size of openings (all dimensions are in mm)

Three arrangements of MWO (with the same opening size) were simulated by Yin and Wang (2006) in his study. It is noticed that in the cases of multiple openings, the behaviour is analogous to the beams without opening, this is due to the fact that openings are not placed at the critical section and are relatively small in size to interfere with each other. Therefore, only one instance of multiple web openings is modelled in this section. The analysis is conducted in two steps. In the first step, the static load is applied and in the second step, a uniform temperature distribution across the cross-section is applied.

Fig. 3.18 shows the temperature-midspan deflection behaviour for these unrestrained perforated beams. There are two stages in the fire behaviour of unrestrained steel perforated beams. In the initial stage of fire, the increase in midspan deflection is negligible and this is due to the two reasons. Firstly, the deflection due to thermal bowing is absent as no thermal bowing is observed due to the uniform temperature distribution across the section. Secondly, these beams are free to expand and no increase in midspan deflection is noticed due to the thermal expansion. In the later stage of fire, due to a significant decrease in material strength, the top tee buckles under high compression and a runaway deflection behaviour is observed as illustrated in Fig. 3.18. The temperature at runaway deflection is known as the limiting temperature.

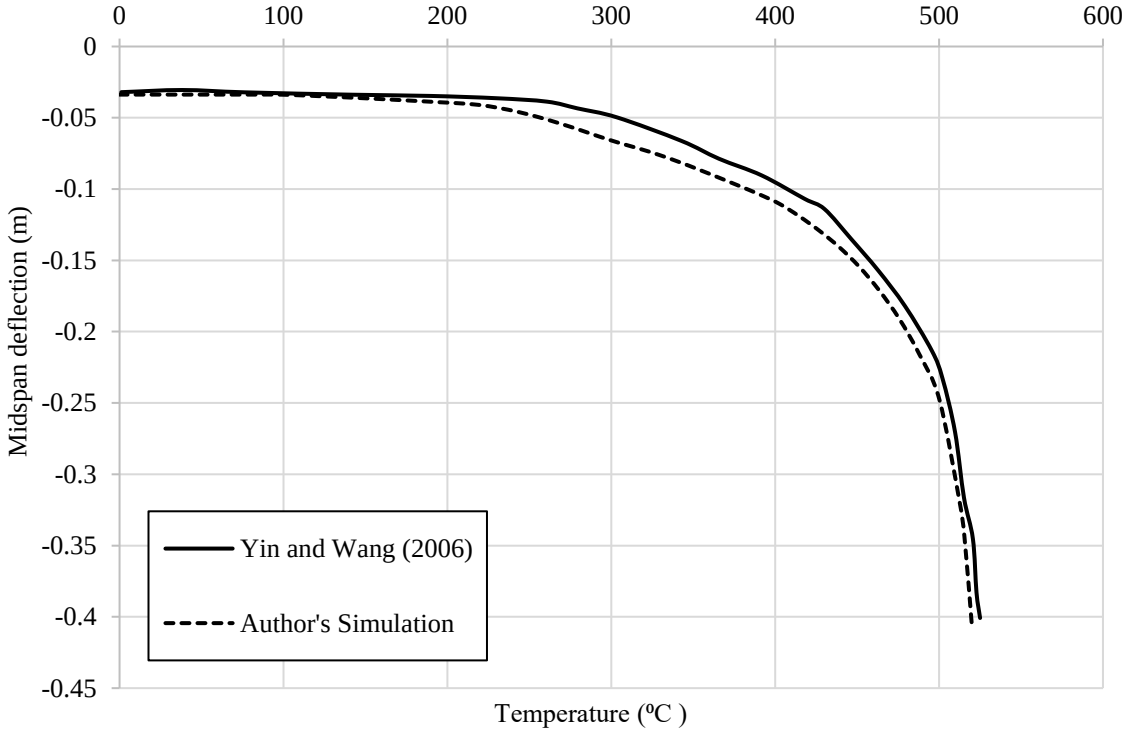

(a)

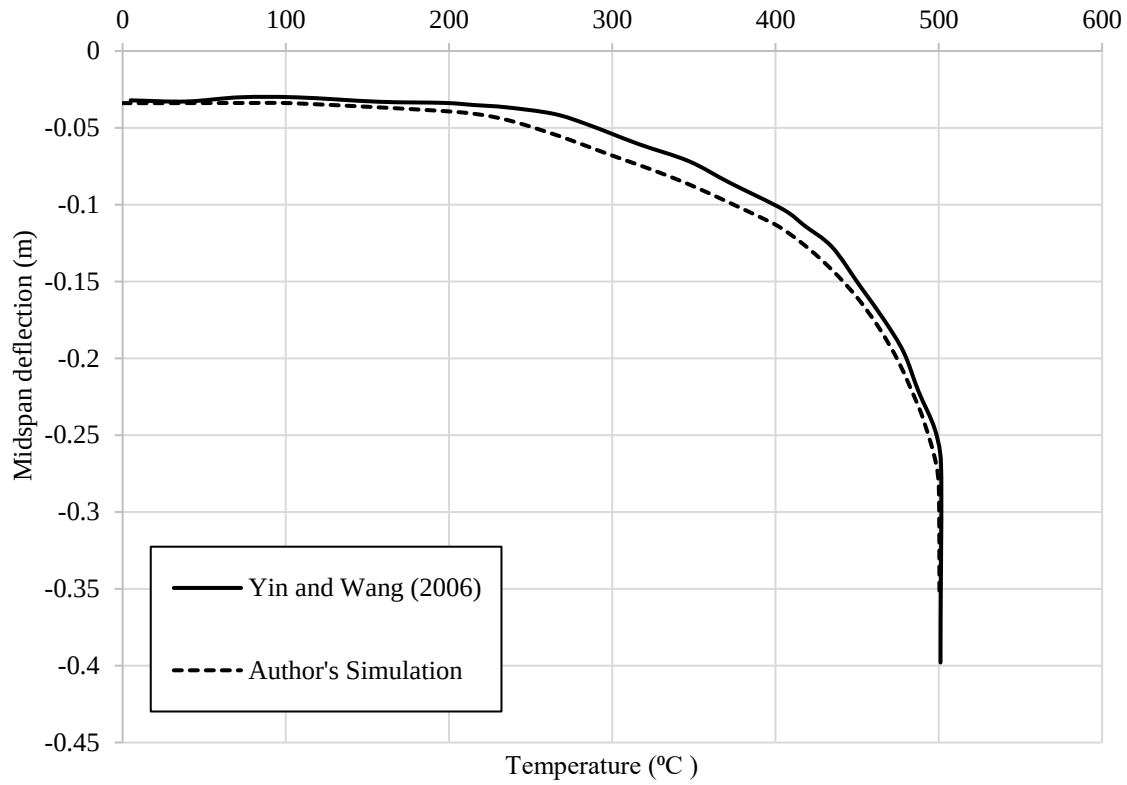
0
100
200
300
400
500
600
0
-0.05
-0.1
-0.15
-0.2
-0.25
-0.3
-0.35
-0.4
-0.45
Midspan deflection (m)
Yin and Wang (2006)
Author's Simulation
Temperature (ºC)

(b)

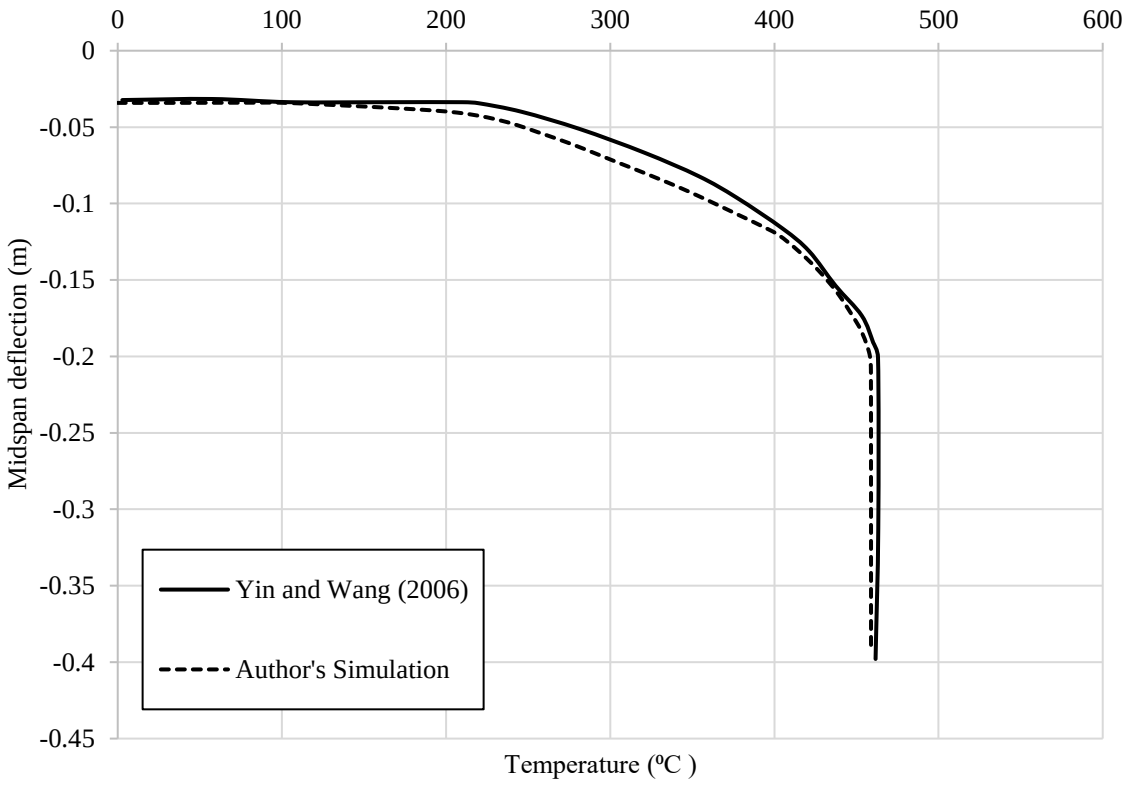
0
100
200
300
400
500
600
0
-0.05
-0.1
-0.15
-0.2
-0.25
-0.3
-0.35
-0.4
-0.45
Midspan deflection (m)
Yin and Wang (2006)
Author's Simulation
Temperature (ºC)

(c)

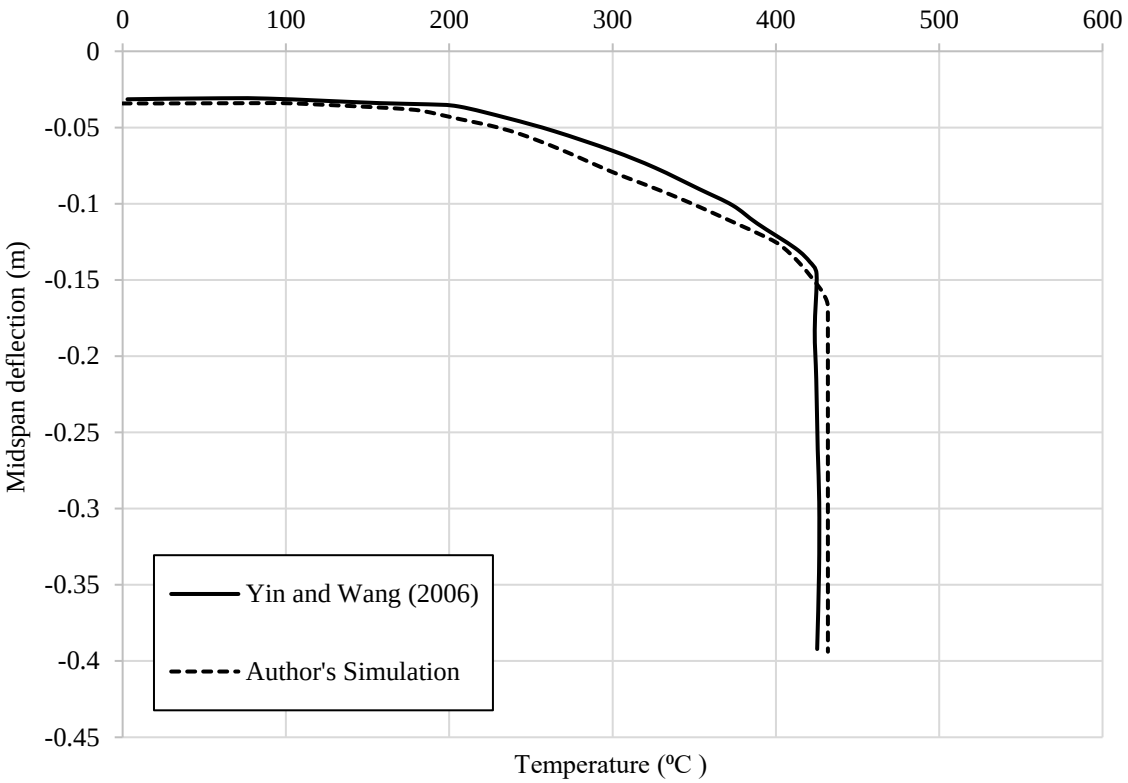

(d)

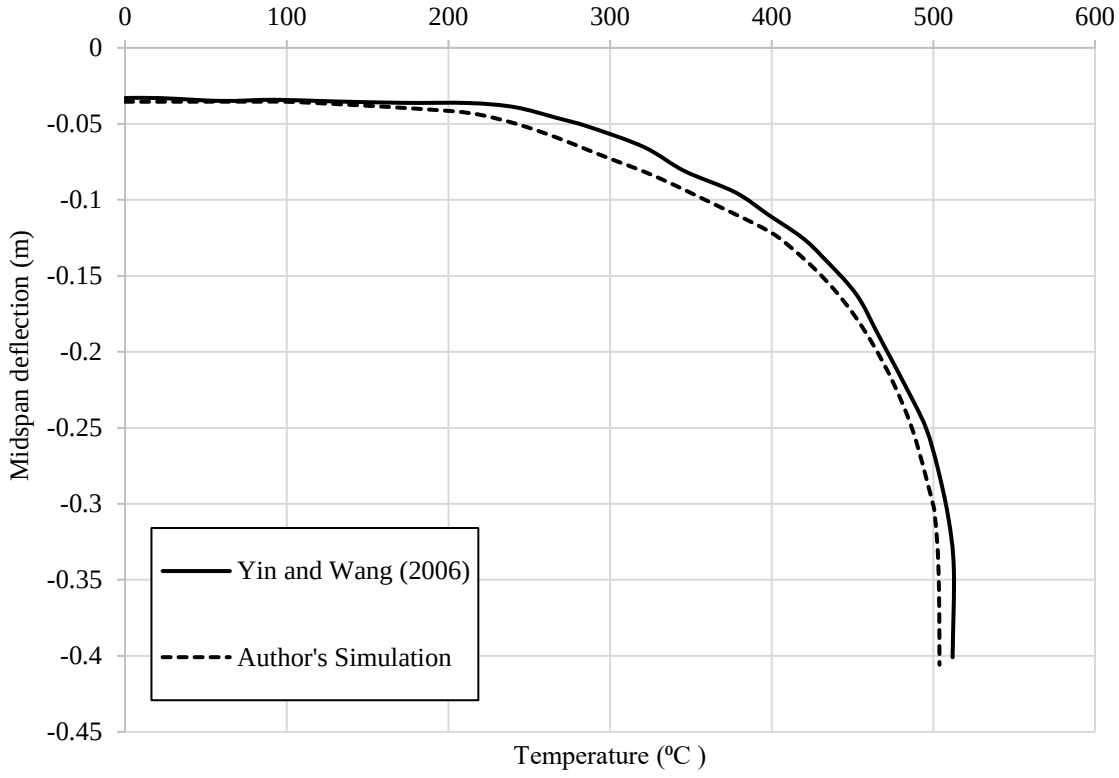

(e)

Fig. 3.18 Comparison between the author's simulation results with those of Yin and Wang (2006) for axially unrestrained beams (a) NWO (b) SWO 1 (c) SWO 2 (d) SWO 3 (e) MWO

3.5. Behaviour of axially restrained perforated beams exposed to fire

In this section, the behaviour of axially restrained perforated beams under fire is analysed and the results are compared with the results of Yin and Wang (2006). Fig. 3.19 compares the temperature-midspan deflection and temperature-axial reaction behaviour. Overall, a reasonably good agreement is achieved with the literature results. The stages of behaviour for axially restrained perforated steel beams observed in this study are similar to those obtained by Yin and Wang (2006). In the initial stage of fire, a compressive force is developed in the whole section due to the restrained thermal expansion and this causes the midspan deflection to increase rapidly. It is observed that all the beams with opening at the centre failed due to the buckling of the top tee-section under high compression as shown in Fig. 3.20. The buckling of the top tee occurs in the early stages of fire in restrained perforated beams and this initiates the compressive unloading of the section. In restrained perforated beams, the axial reaction changes from compression to tension at a much lower temperature compared to the beam without web opening as illustrated in Fig. 3.19 (b). Since all the steel perforated beams are designed considering axially and rotationally unrestrained conditions, the connections do not experience any tensile force at limiting temperature.

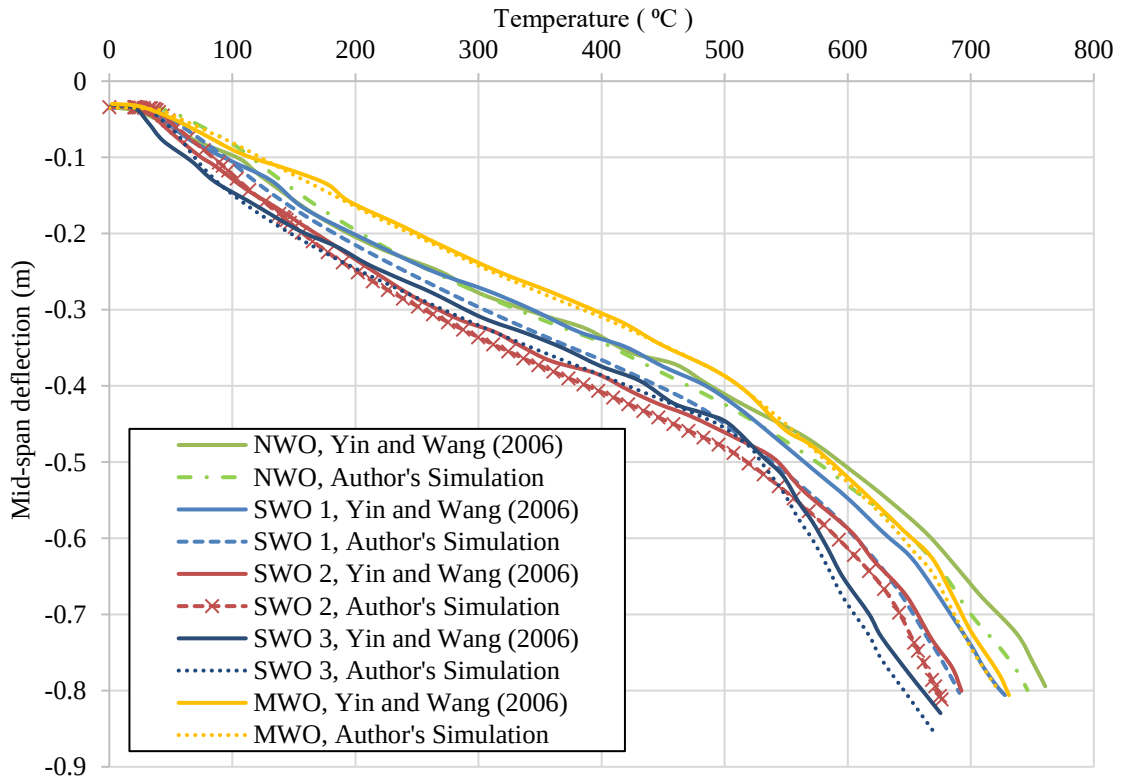

(a)

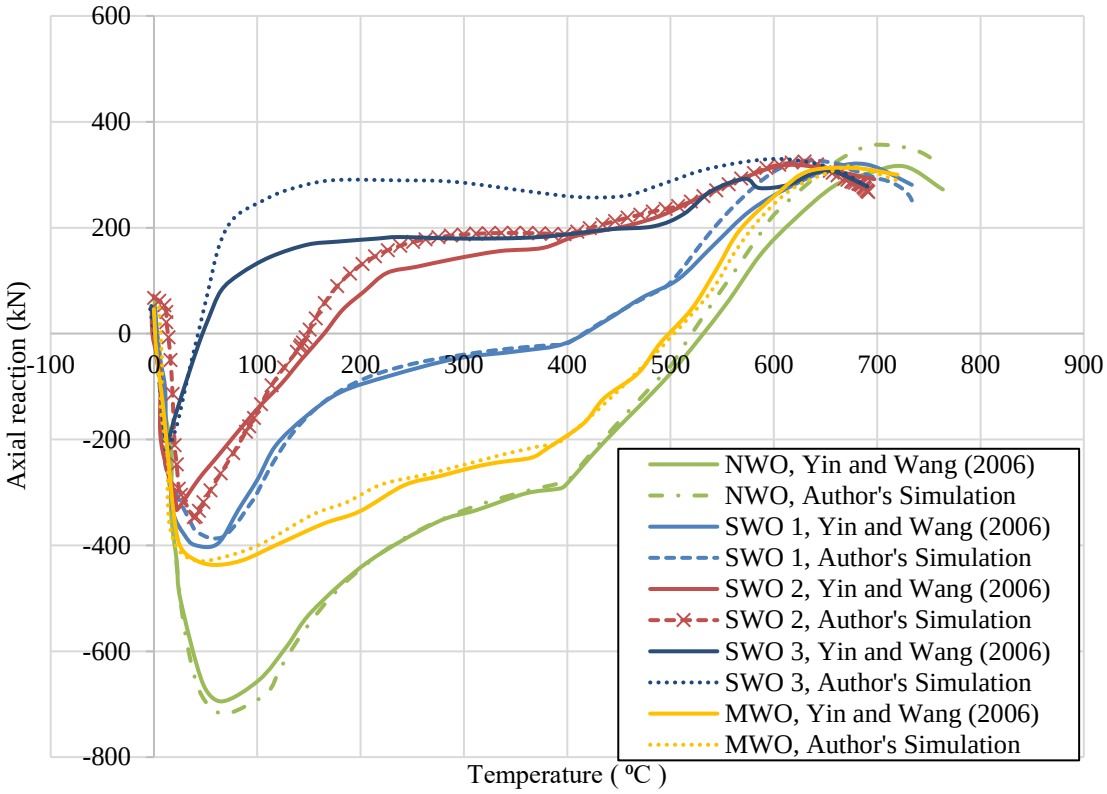

(b)

Fig. 3.19 Comparison between the author's simulation results with those of Yin and Wang (2006) for axially restrained beams (a) Midspan deflection (b) Axial reaction

However, in case of restrained perforated beams, the connections may generally be subjected to a high tensile force (see Fig. 3.19 b) which should be taken in to account while designing the connections.

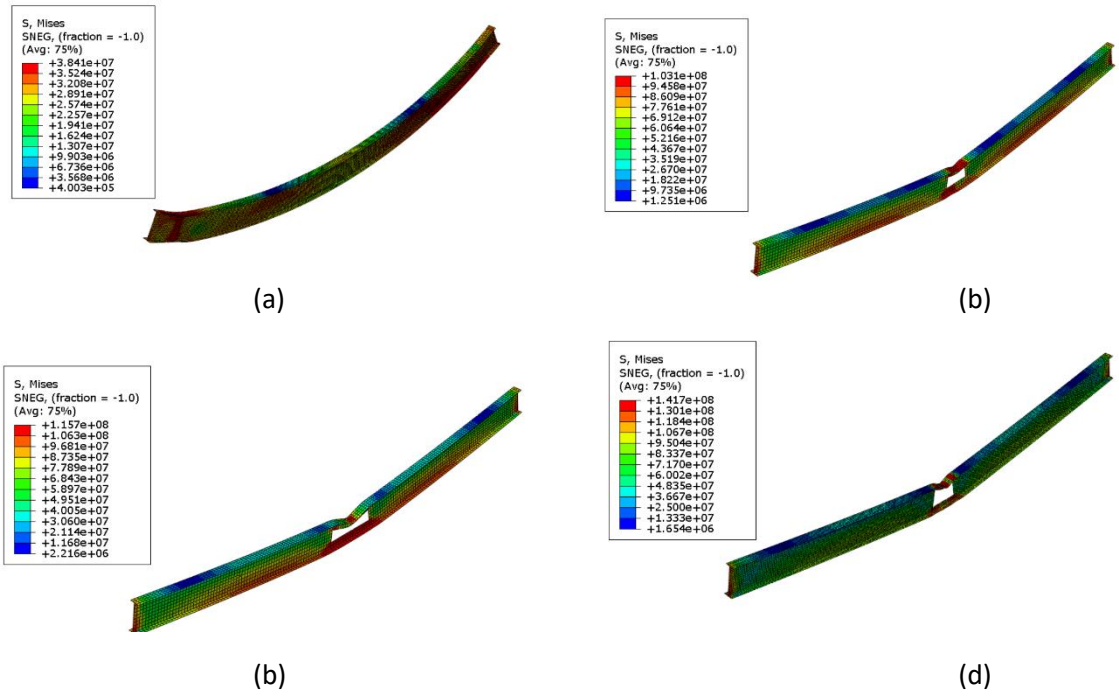

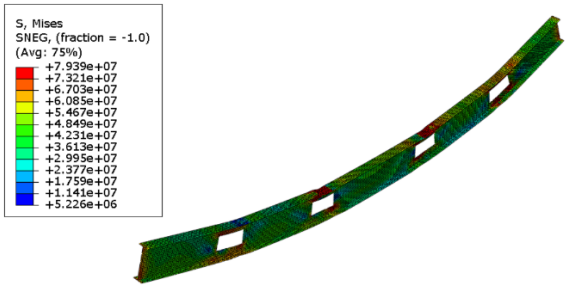

(e)

Fig. 3.20 Buckling of top tee under high compression for axially unrestrained beams (a) NWO (b) SWO 1 (c) SWO 2 (d) SWO 3 (e) MWO

3.6. Concluding remarks

This chapter presents the numerical validation studies for solid beams and perforated beams with and without axial restraint by comparing the results with the numerical studies and experiments conducted by other researchers. The study presented here showed a good agreement with the results from other authors in all aspects, i.e., temperature–midspan deflection, temperature–axial reaction behaviours, and for the detailed deformation patterns of the beams. Buckling of the top flange under high compression is observed as the main failure mode in unrestrained solid beams while for more slender solid steel beams loaded under high load ratio, lateral torsional buckling is also observed. Tensile catenary action is successfully captured in case of axially restrained solid steel beams. In case of axially restrained perforated beams, yielding near the support starts under high axial compression which results in the formation of plastic hinges at the support and buckling of top flange above the opening leads to the formation of plastic hinge in the span. After the formation of mechanism, the compressive axial force in the beam changes to tension and the beam continues to carry load under a tensile catenary action.

Chapter 4

Influence of axial restraint on the fire behaviour of perforated beams

4. Introduction

Structural steel frame systems are quite popular in the construction of building structures due to the superior material properties, i.e., high ductility and high strength of structural steel, compared to other conventional construction materials. For ambient temperature design, restrained perforated beams in a structure are not expected to experience a significant amount of axial force. On the other hand, a significant amount of axial compression is induced in the steel perforated beams due to restrained thermal expansion at elevated temperature. Development of this high axial compression changes the beam behaviour from pure flexural (beam behaviour) to compression-flexural (beam-column) behaviour.

At ambient temperature, due to the very small compressive forces, no load-moment interaction is observed and the flexural capacity of the beam is independent of the axial compression. Whereas at elevated temperature, due to high axial forces, the load-moment interaction plays a vital role in assessing the behaviour of the beams. To obtain a realistic design, the design capacity of the beam-column is calculated by considering the interaction between the applied forces, i.e., bending moment and the axial force. The typical load-moment interaction relationship is as follows (AISC 2005).

$$\frac{P_u}{\Phi P_n} + c\frac{M_u}{\Phi M_n} \leq 1.0 \qquad (0.1)$$

where P_u and M_u are the applied axial force and bending moment, ΦP_n and ΦM_n are the design axial force and bending moment capacities, and c is an interaction coefficient, respectively. According to the above load-moment interaction equation, if a significant amount of axial compression is developed in the beam due to restrained expansion in fire then it could adversely affect the flexural capacity of the beam. In the fire situation, a high

axial compressive force can reduce the moment carrying capacity of a section as can be seen from Eq. 4.1.

Despite the numerous amount of research publications on fire behaviour of restrained solid steel beams, there are only a few research published on fire response of restrained beams with web openings. Fire tests on axially restrained cellular beams exposed to fire were conducted by The Ulster University (Nadjai et al. 2017) and the extent of axial forces developed in the cellular beams was significant. In another numerical study, Najafi and Wang (2017a) investigated the effect of the magnitude of axial restraint on the behaviour of perforated steel beams and the transition of axial forces from compression to tension was appreciated, which does not allow the beams to collapse even at high temperatures. Based on this study, a simplified analytical approach was proposed by Najafi and Wang (2017b) to predict the behaviour of restrained steel perforated beams subjected to fire. In the literature, most of the studies assume that the axial force developed due to restrained thermal expansion acts at the geometrical centroid of the perforated beam and the effect of the development of the axial force at other location (across the depth of the section) on the behaviour of perforated beams has been neglected.

Due to various connection configurations, e.g., single plate shear connection and welded angle seat connection as shown in Fig. 4.1, the location of axial force can vary across the depth of a beam exposed to fire (Dwaikat and Kodur 2010). In the majority of the studies, the location of the thermally induced axial force is assumed to be at the geometric centroid of the perforated beam, and therefore no moment is generated around the beam support and no effect on the sagging moment at the centre of the beam is observed.

However, if the axial restraint develops at an eccentric location to the geometric centre of the beam due to different connection types, then a significant amount of bending moment might develop near the support. This thermally induced bending moment can greatly influence the behaviour of the perforated beams and can transform the beam into a beam-column. The assumption of developing an eccentric axial force in fire exposed perforated beams is not valid for single plate shear connection as shown in Fig. 4.1(a) which is designed to avoid the development of the moment at the support. However, for welded angle seat connection, a significant amount of bending moment might develop at the support due to the eccentric axial forces as shown in Fig. 4.1(b).

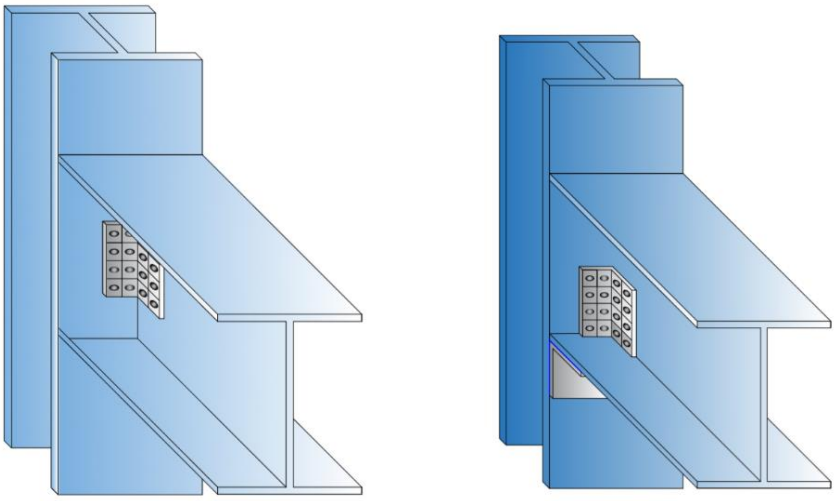

(a) (b)

Fig. 0.1 Connection types (a) Single plate shear connection (b) Welded angle seat connection

Various studies show that the magnitude of the axial force developed due to restrained thermal expansion depends on various factors, i.e. fire scenario and the level of axial restraint. However, varying the location of axial restraint and the slenderness ratio of the beam influence the fire behaviour of perforated beams and were not considered in the previous studies. Hence, a parametric study is conducted here; the parameters investigated in this study are the location of axial restraint and the slenderness ratio of the beam.

4.1. Effect of the magnitude of axial restraint

Before conducting a study to analyse the effect of location of axial restraint, the effect of the magnitude of axial restraint on the fire response of perforated beams is investigated in this section. This aspect is studied by conducting a study on a 10 m perforated beam, which is made up using a section W24×76. The perforated beam chosen for this illustration has 7 rectangular openings of size 500×300 mm at equal intervals and the schematic of the beam is shown in Fig. 4.2. The level of axial restraint (AR) is varied as a percentage of axial stiffness of the section (AE/L), i.e. AR = 0, 10%, 20%, 30%, 50% of AE/L and infinity. Initially, the beam is loaded under a UDL of 30% of its ambient load carrying capacity and then the beam is exposed to a standard fire exposure (EN 1991-1-2 2005). Fig. 4.3 shows the time-temperature variation at different locations of the beam, i.e., web, bottom flange and top flange. The temperature-midspan deflection behaviour of the perforated beam is shown in Fig. 4.4.

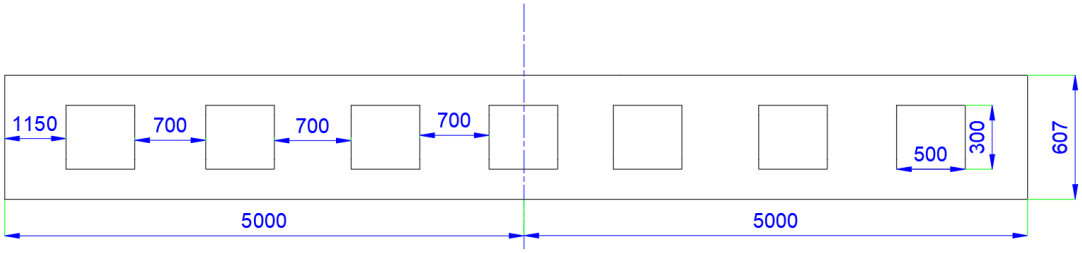

Fig. 0.2 Schematic for the beam used for studying the effect of the magnitude of axial restraint (all dimensions are in mm)

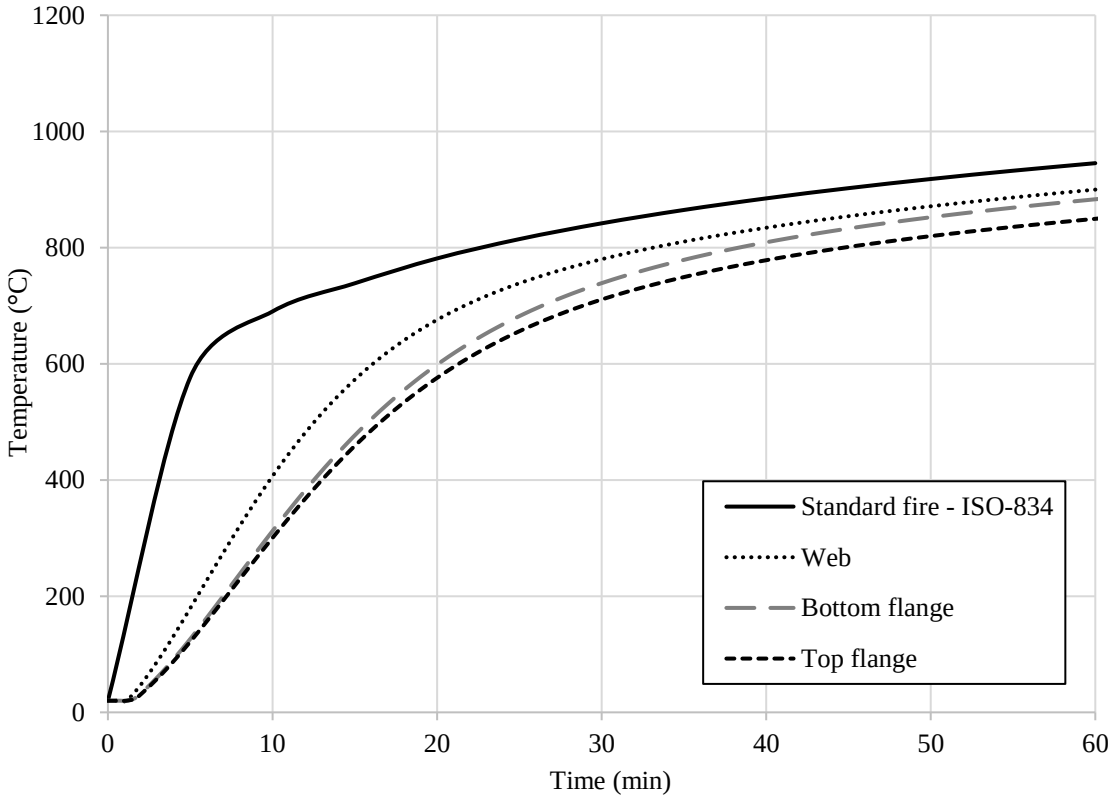

Fig. 0.3 Temperatures in steel section resulting from Standard Fire

The midspan deflection in an unrestrained perforated beam (AE/L = 0) exposed to fire occurs mainly due to thermal bowing and loss of strength and stiffness at high temperature. In the initial stage of fire, the major part of the deflection is due to the thermal bowing as very less reduction in the strength and stiffness is observed. However, in the later stage of fire, the deflection is dominated by the second factor which is due to a reduction in the mechanical strength of steel. For beams with a lower level of axial restraint, in the initial stage of fire (up to 515 °C in this case), the midspan deflection and the rate of increase of deflection is less compared to the beams with a higher level of axial restraint. This is due to the fact that the beams with lower axial restraint are allowed to

expand more compared to the beams with a higher level of axial restraint. Increasing the level of axial restraint, arrest the horizontal movement of the beam, which results in increased midspan deflection and a higher rate of increase of midspan deflection during the initial stage of fire as illustrated in Fig. 4.4. However, the results in Fig. 4.4 illustrates that an increase in the level of axial restraint results in the improved overall performance of the perforated beams with lesser midspan deflections. At later stages of fire exposure (beyond 515 °C in this case), the loss of mechanical strength is significant due to the exposure to high temperature. At this stage, the load carrying mechanism of the beams transforms from flexural action to tensile action if the sufficient amount of axial restraint is provided; this behaviour can be confirmed in Fig. 4.5. The catenary action is absent in the beam without any axial restraint and the midspan deflection of this beam increases suddenly at high temperature which leads to the collapse of the beam.

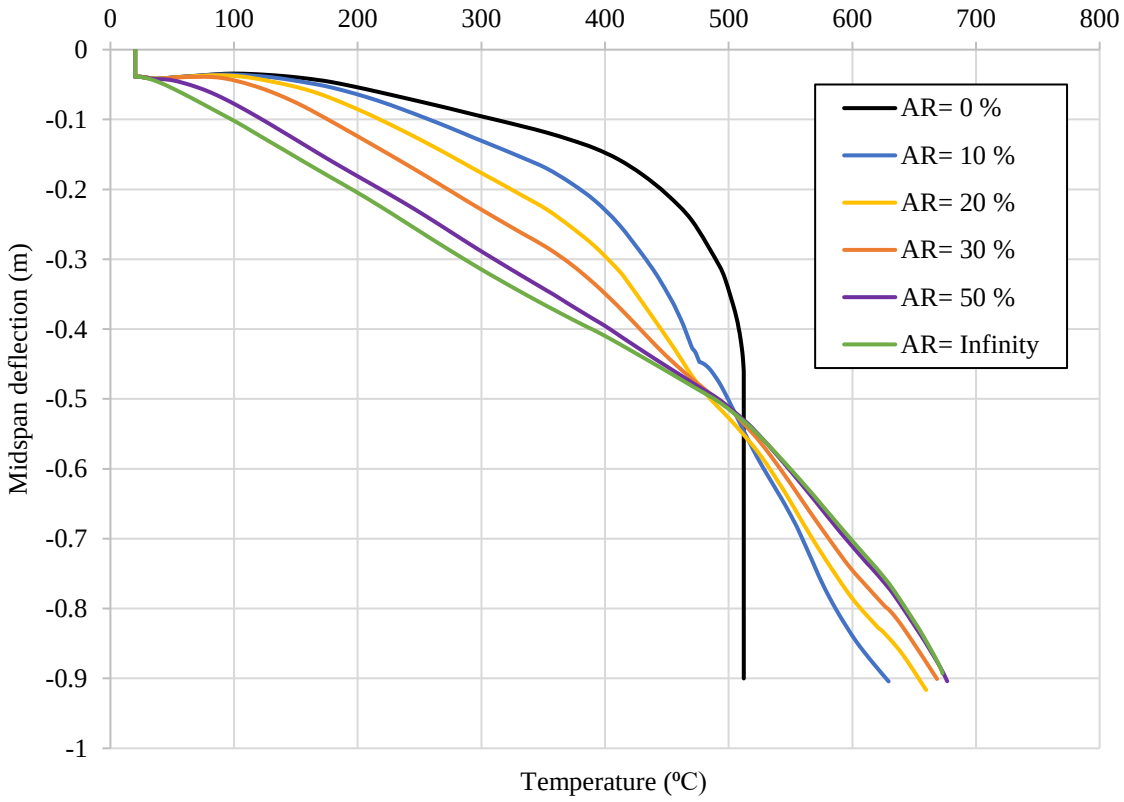

Fig. 0.4 Time- midspan deflection behaviour of different level of axial restraint

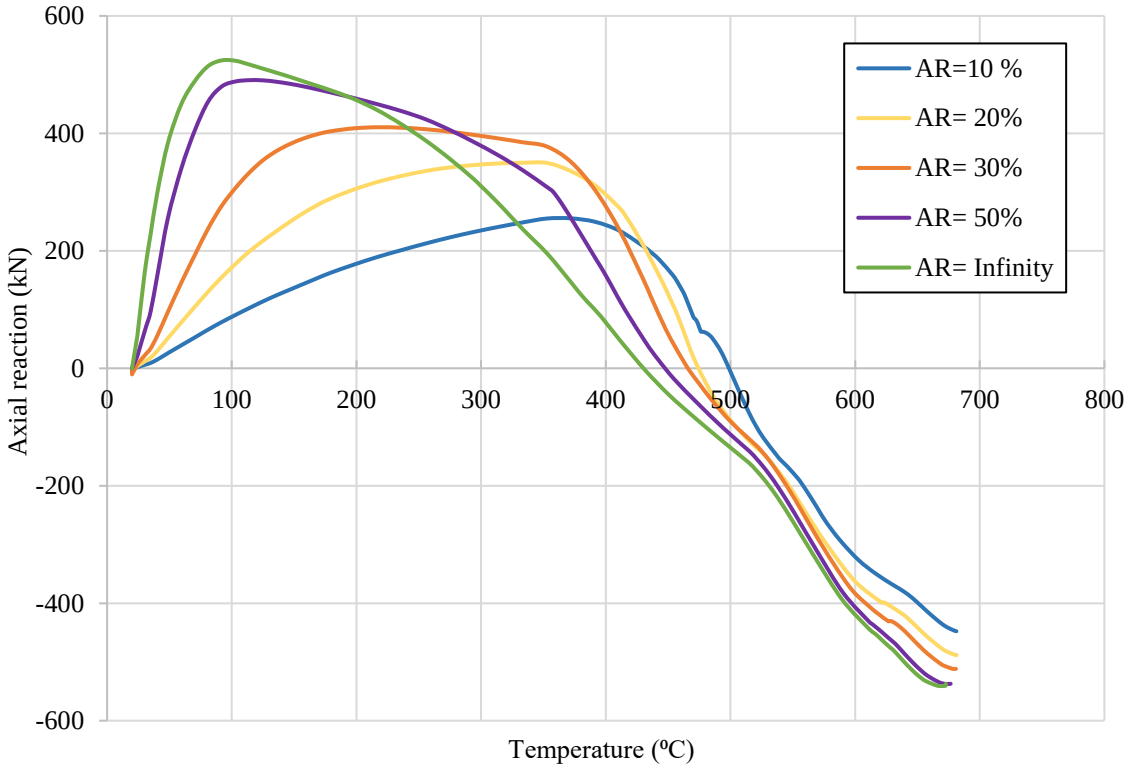

Fig. 0.5 Time- axial reaction behaviour of different level of axial restraint

In the later stage of fire, a higher level of axial restraint drives the beam to an early catenary action under a higher level of tensile force as shown in Fig. 4.5. It improves the overall performance of the perforated beams by carrying the load under tensile catenary action and slows the rate of increase of midspan deflection. The development of a high tensile catenary force enables the beam to sustain loads even at high temperatures without experiencing a collapse.

The trends in Fig. 4.5 show that at early stages of fire exposure, a higher compressive axial force is induced in the perforated beam with an increased level of the AR. This is due to the fact that the higher value of axial restraint arrests the thermal expansion of the beam more effectively. This high value of thermally induced compression may cause local buckling of the flange near the support. Overall, the catenary action helps the beam in carrying the load at a higher temperature but the magnitude of tensile force should be carefully monitored as it can adversely affect the performance of connections. At high temperature, the connections are subjected to a tensile force and its effect should be considered while designing for elevated temperature. However, if the connections are safely designed, the increase in the magnitude of axial restraint enhance the stability of

the perforated beams at elevated temperature and an improvement in the fire response is observed.

4.2. Effect of location of the axial restraint

The temperature variation, development of bending moment and axial forces at mid-section and support for different location of axial restraint are shown in Fig. 4.6. The bending moment acting at the mid-section comprises the moment coming from the gravity loads (M_g) and the moment developed because of the P- δ effect ($M_{p-\delta}$).

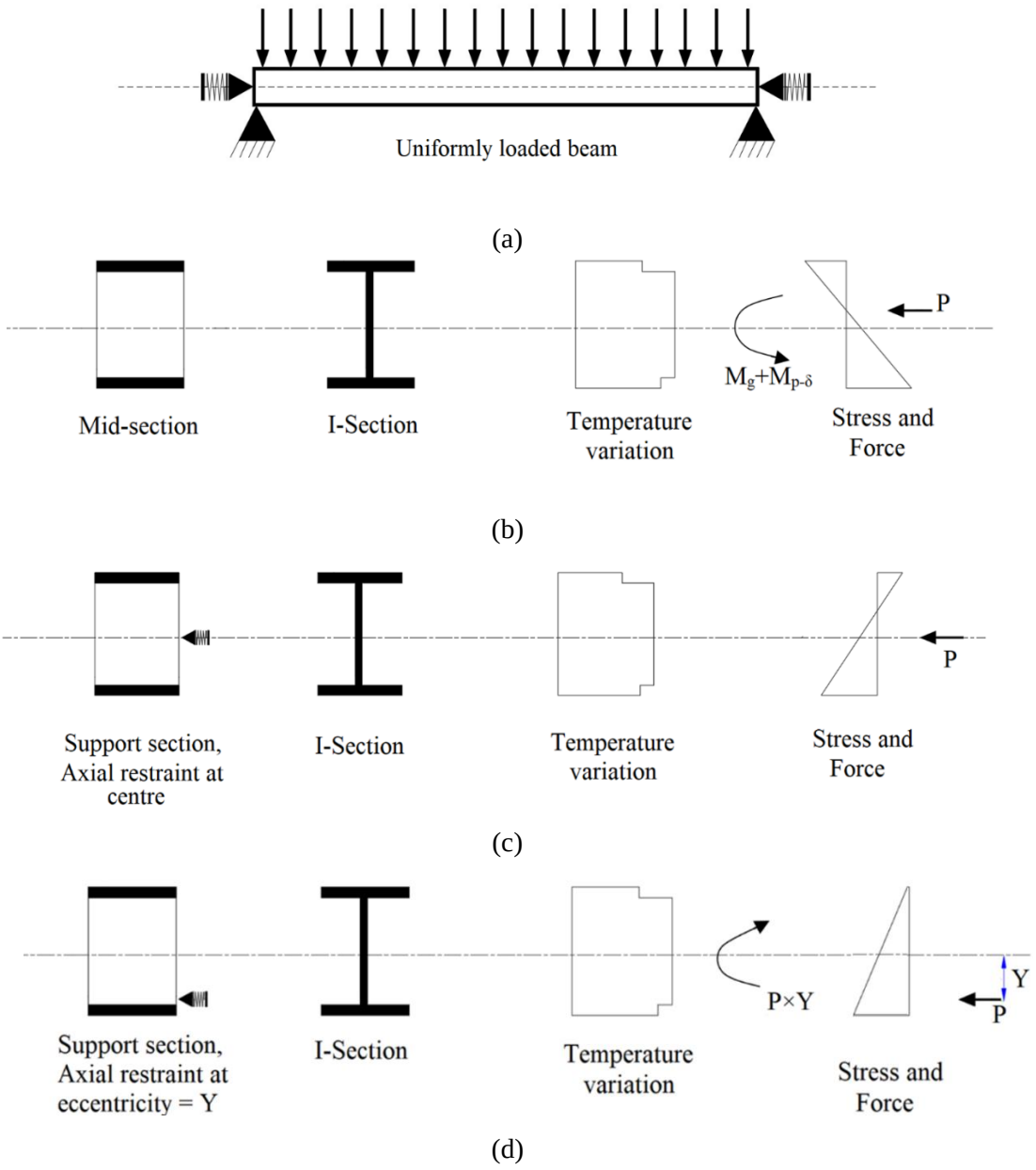

Fig. 0.6 Effect of restraint force location in a restrained perforated beam exposed to fire (a) Restrained perforated beam (b) Midspan section (c) Support section with central axial restraint (d) Support section with eccentric axial restraint

Owing to the downward midspan deflection, the moment induced from the P- δ effect is sagging and adds to the sagging moment developed due to the vertical loads (M_g+$M_{p-\delta}$) as can be seen in Fig. 4.6(b). The thermal variation and the stress variation at the support with axial restraint acting at the centre of the section is shown in Fig. 4.6(c). No counteracting moment is developed in this case due to the application of the axial force at the geometric centre of the section. However, when the location of the axial restraint is moved downward with an eccentricity of Y, it causes the development of a hogging moment at the support with a magnitude P×Y, which opposes the (M_g+$M_{p-\delta}$) as shown in Fig. 4.6(d). This leads to a reduction in the total moment at the midspan, and therefore, enhances the fire resistance of the perforated beams. Fig. 4.7 shows the effect of eccentric axial restraint on bending moment diagram of perforated beams.

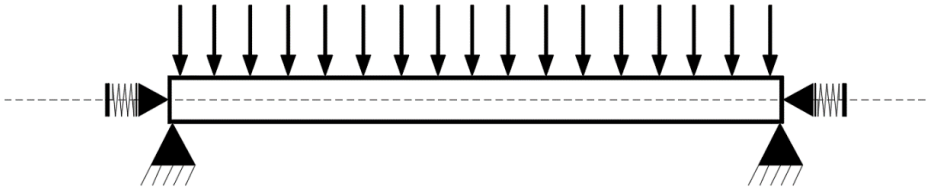

(a)

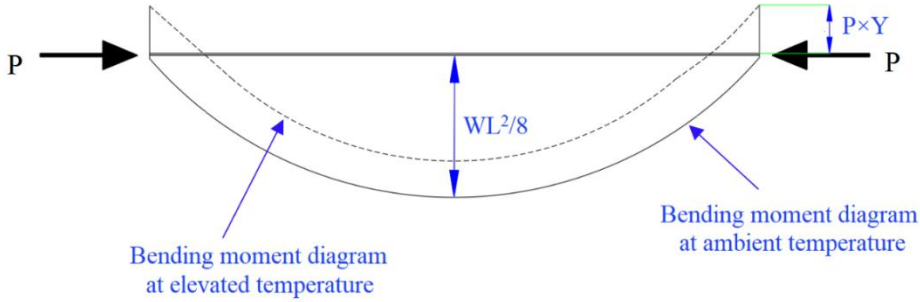

(b)

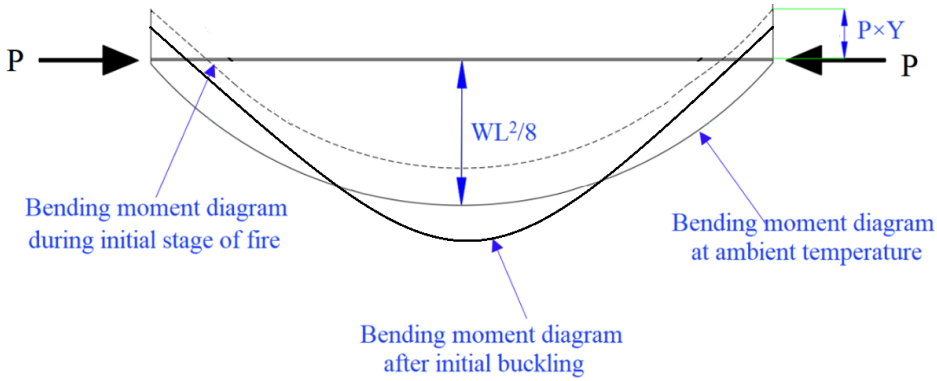

(c)

Fig. 0.7 Bending moment diagram of a uniformly distributed beam (a) Schematic of the beam (b) for non-slender perforated beams (c) for slender perforated beams

The effect of the development of the eccentric axial restraint in non-slender perforated beams on the bending moment diagram is shown in Fig. 4.7(b). The solid line shows the bending moment diagram at the ambient temperature. The eccentric axial restraint developed due to restrained thermal expansion shifts the bending moment diagram in an upward direction, which reduces the overall sagging moment; it is represented by a dotted line in Fig. 4.7(b). On the other hand, in slender perforated beams, the effect of eccentric axial restraint on the bending moment diagram is shown in Fig. 4.7(c). Slender perforated beams buckles at an early stage compared to non-slender perforated beams due to their lesser stiffness. The midspan deflection increases suddenly to a large value due to this early buckling. The P- δ effect developed due to the large deflection induces high magnitude of sagging moment, which shifts the bending moment diagram in a downward direction as shown in Fig. 4.7(c).

4.3. Parametric study

In previous studies conducted on fire exposed perforated beams, the location of the axial restraint is assumed at the geometric centre of the section. A finite element analysis is carried out to investigate the effect of various parameters on the response of restrained steel perforated beam at elevated temperature. The influence of the parameters investigated in this study is the slenderness ratio and the location of axial restraint. Fig. 4.8 illustrates the schematic for the beams investigated in this study.

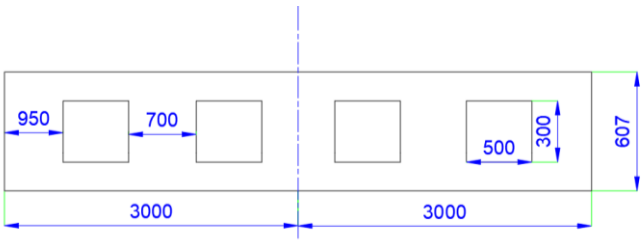

(a)

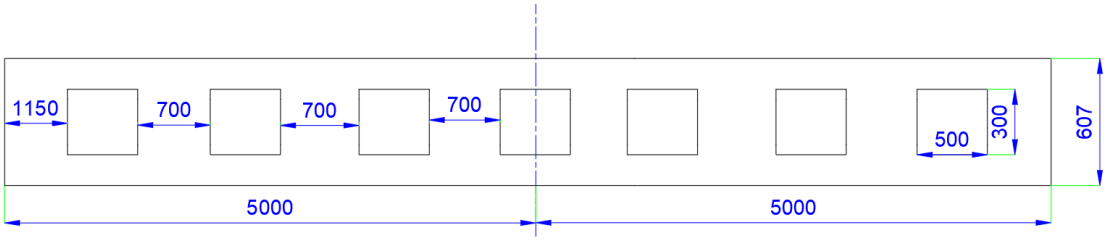

(b)

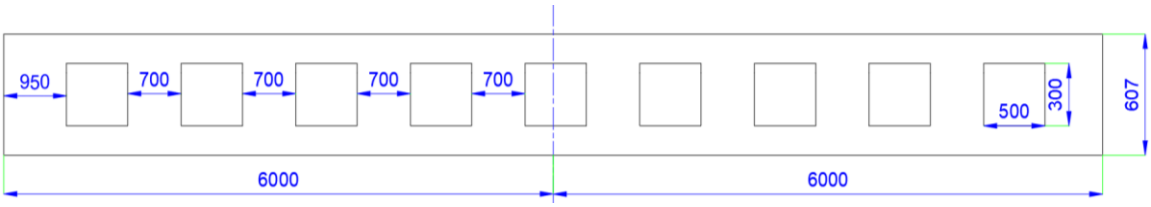

(c)

Fig. 0.8 Schematic for beams used in the parametric study (all dim. are in mm)
(a) 6 m perforated beam (b) 10 m perforated beam (c) 12 m perforated beam

The W24×76 section is used for all the cases in this study. The openings of size 500×300 mm are located at a spacing of 700 mm symmetrical to the centroidal axis of the section. Three different span lengths of 6 m, 10 m and 12 m are simulated in this study to vary the slenderness ratio (L/r) from 24.1 to 48.8. Beams with a slenderness ratio less than 30 ($L/r \leq 30$) are assumed as non-slender beams and beams having slenderness ratio greater than 30 ($L/r > 30$) are assumed as slender beams. Another parameter varied in this study is the location of the axial restraint. The location of axial restraint is varied by increasing the eccentricity of the axial support from the geometric centroid of the section towards the lower flange. Eccentricities of 0 mm, 100 mm, 150 mm and 200 mm are considered to vary the location of the axial restraint. The magnitude of axial restraint assumed for all the simulations is 50% AE/L (Area of the solid section). Table 4.1 summarises all the numerical simulation performed in this study.

Table 0.1 Beam parameters and results of the numerical study

S. No.	Beam Section	Span	Slenderness ratio	Axial restraint (distance from geometric centre)	Temperature (ºC) at L/20 deflection
1	W 24X76	6	24.1	0 mm	625
2	W 24X76	6	24.1	100 mm	680
3	W 24X76	6	24.1	150 mm	692
4	W 24X76	6	24.1	200 mm	705
5	W 24X76	10	40.6	0 mm	481
6	W 24X76	10	40.6	100 mm	355
7	W 24X76	10	40.6	150 mm	302
8	W 24X76	10	40.6	200 mm	250
9	W 24X76	12	48.8	0 mm	430
10	W 24X76	12	48.8	100 mm	321
11	W 24X76	12	48.8	150 mm	263
12	W 24X76	12	48.8	200 mm	218

Firstly, the ambient load carrying capacity of all the three beams under a uniformly distributed load is evaluated by increasing the load till failure and it is assumed that the axial restraint is located at the geometric centre of the section. This analysis evaluates the magnitude of the static load applied for carrying out the actual analysis in fire. The actual analysis is carried out in two steps. In the first step, all the beams are loaded with 30% of their ambient load carrying capacity. In the second step, the static load is kept constant and the temperatures profiles as shown in Fig. 4.3 are applied to various locations of the beams. Following sections represents the results and discussion of this study.

4.3.1. Thermo-mechanical behaviour of perforated beams with different location of axial restraint

The results presented in Table 4.1 indicate that the fire resistance of the non-slender restrained perforated beams improves when the point of application of the axial restraint moves away from the centroid towards the bottom flange. Whereas an opposite trend is observed for slender beams, i.e., a reduction in the fire resistance with an increased eccentricity of axial restraint from the centroid of the perforated beam (see Table 4.1).

The non-slender perforated beams are able to resist higher temperature if the location of axial restraint moves away from the geometric centre of the section as shown in Fig. 4.9. A rise of 80 ºC is observed for 6 m beams when the location of axial restraint changes from the centre of the section to 200 mm away from the centre (see Table 4.1). This enhancement in fire resistance of non-slender perforated beams can be attributed to the fact that a hogging moment is developed at the support due to the eccentric axial compression, which acts in the opposite direction to the bending moments developed due to the gravity loads and P-δ effect. The section is stiffer near the flanges due to the presence of openings in the web. This attributes to an increase in the axial compressive force developed in the section when the location of axial restraint is moved towards the bottom flange as shown in Fig. 4.10. The magnitude of the hogging moment developed in the section increase with an increase in the axial compression and the eccentricity of the axial restraint. This effect is analogous to the phenomenon of developing a counter-acting moment in the pre-stressed reinforced concrete beams. In pre-stressed beams, the compressive force developed in the tendons improves the load carrying capacity of the beams. Here in this study, the compressive force is induced due to the restrained thermal expansion.

For the initial duration of the fire, the magnitude of the compressive force increases with the increase in temperature. On further rise in temperature, buckling of the top tee is observed under high compressive force. The onset of buckling of the top tee leads to the compressive unloading of the perforated beams. The compressive unloading causes a reduction of the counter-acting moment in the beam. At the later stage of fire, the stiffness of the beam is significantly reduced and the sagging moments ($M_g+M_{p-\delta}$) exceed the fire-induced counter moment. This behaviour results in a sudden rise of midspan deflection (a runaway), which leads to the collapse of the beam.

However, for slender beams, an opposite trend is observed, i.e., a reduction in the fire resistance with an increased eccentricity of the location of axial restraint from the geometric centroid of the perforated beam. A significant increase in the axial compression is observed for slender beams when the location of axial restraint changes from Y = 0 to Y = 200 mm as illustrated in Fig. 4.12 and Fig. 4.14. The compressive axial reaction in 10 m perforated beam increases from 450 kN to 1070 kN when the location of the axial restraint changes from Y = 0 mm to Y = 200 mm as shown in Fig. 4.12. When the location of axial restraint is at the geometrical centroid of the section, the magnitude of the axial compression is the lowest which delays the buckling of the top tee under compression beyond 400 ºC until the material starts to lose the mechanical strength as illustrated in Fig. 4.12 and Fig. 4.14.

The high magnitude of axial compression develops when the location of axial restraint is more eccentric. This high compression causes a premature buckling of the less stiff slender perforated beam and a sudden rise in the midspan deflection is observed at the early stage of fire as shown in Fig. 4.11 and Fig. 4.13. A rise in the magnitude of the axial compression results in a greater midspan deflection at the early stage of fire. Due to high midspan deflection at an early stage, the sagging moments ($M_g+M_{p-\delta}$) exceed the fire-induced counter moment which reduces the fire performance of the slender beams.

The most sudden compression unloading takes place for the highest eccentric (200 mm) location of the axial restraint as shown in Fig. 4.12 and Fig. 4.14. Due to this unloading, the transition of axial force takes place from compression to tension and the load resisting mechanism of the perforated beams also changes from flexural action to a catenary (tensile) action. With high eccentric axial restraint, the perforated beams are forced to attain the catenary action at a lower temperature.

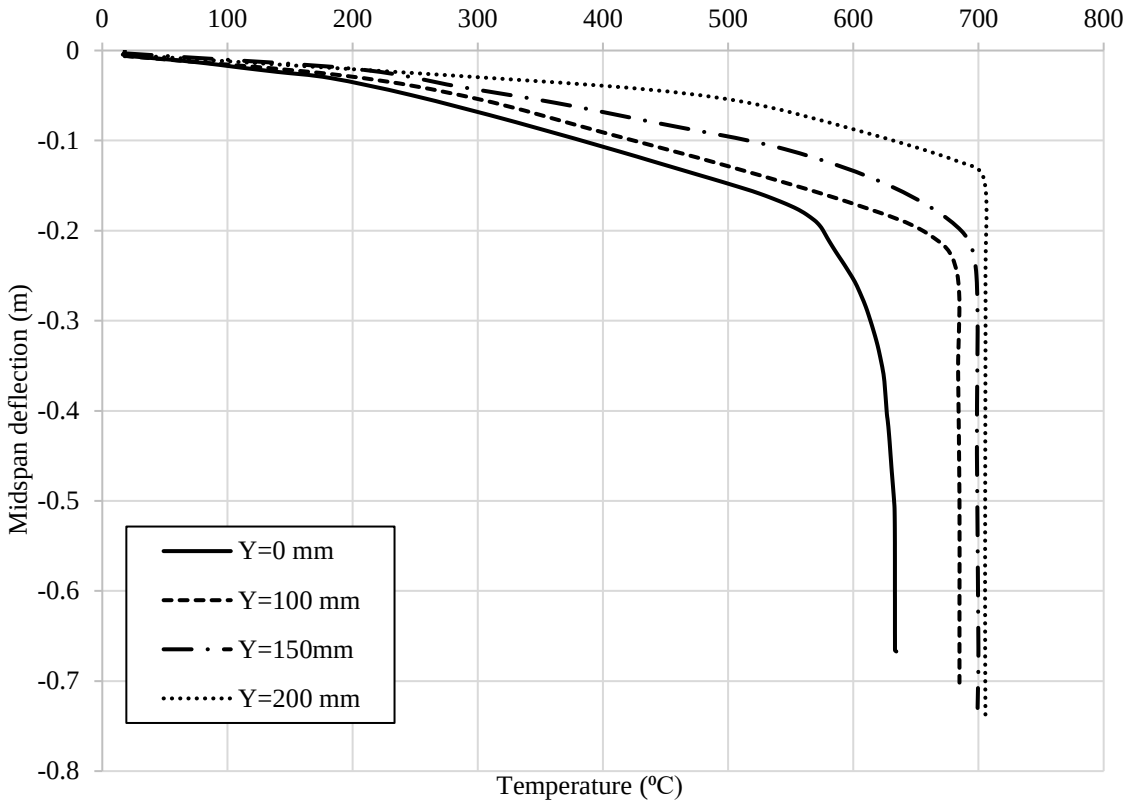

Fig. 0.9 Effect of varying location of axial restraint on midspan deflection in a 6 m perforated beam exposed to fire

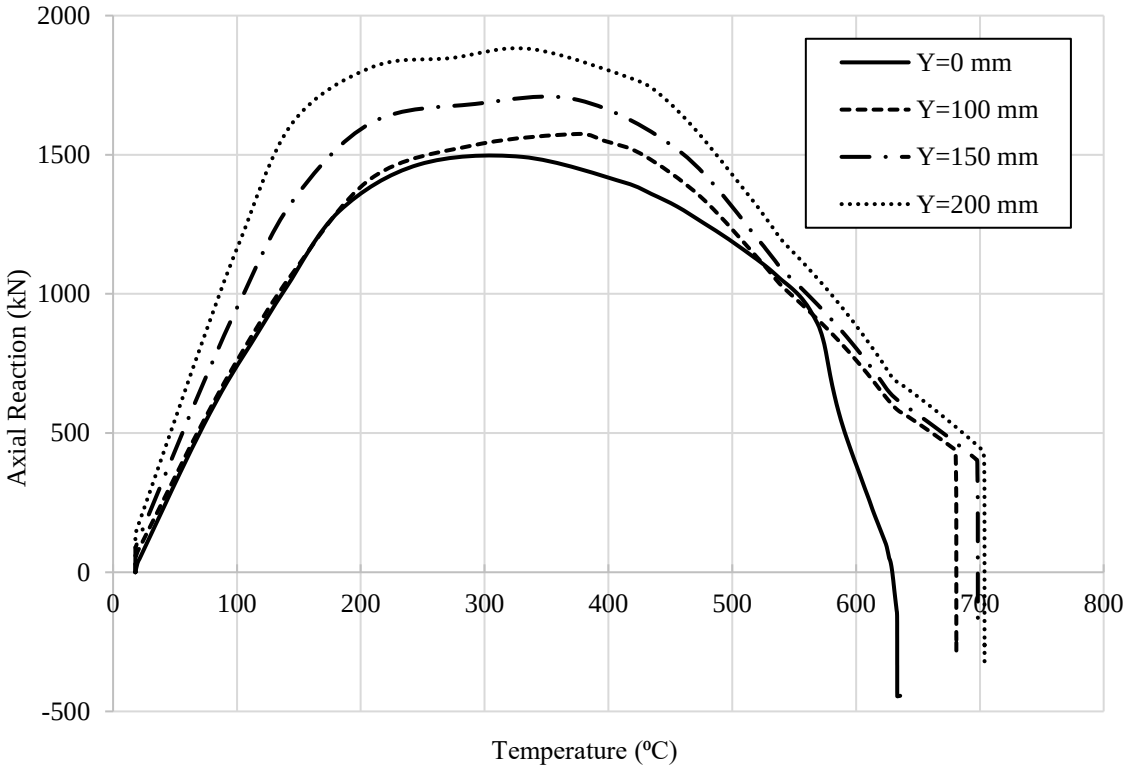

Fig. 0.10 Effect of varying location of axial restraint on the fire-induced axial force in a 6 m perforated beam exposed to fire

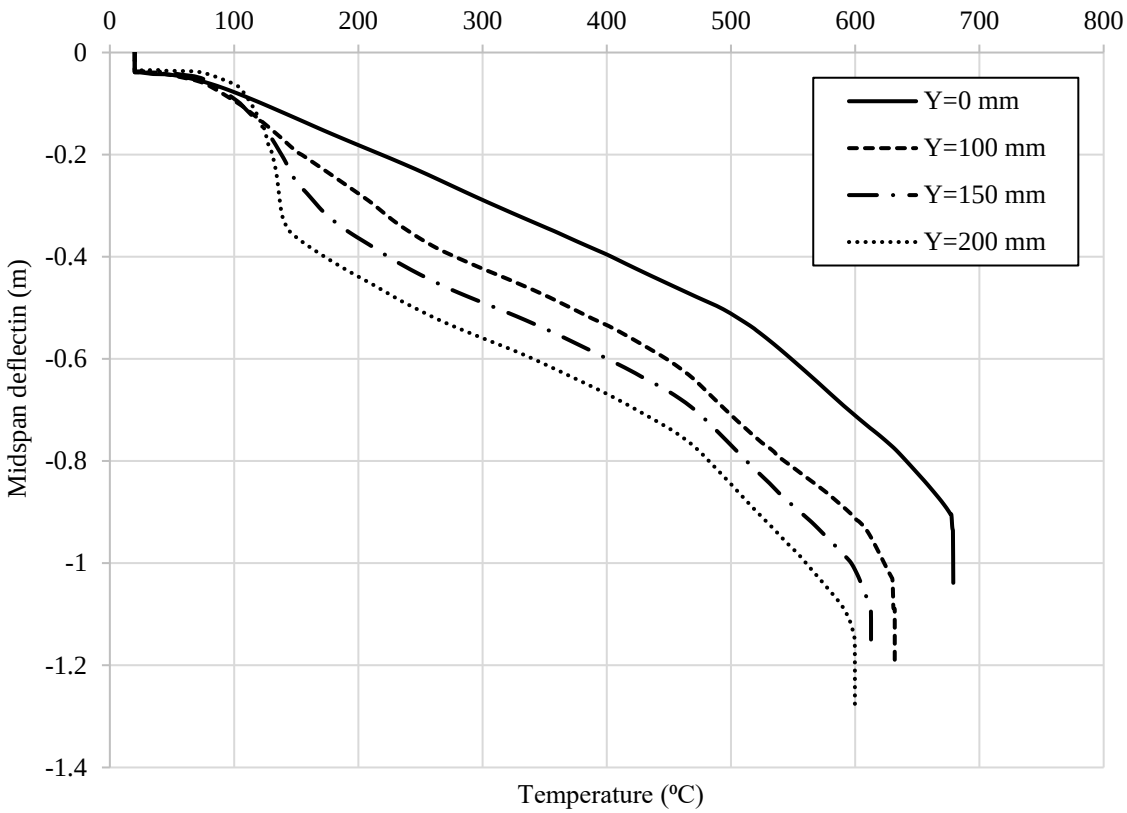

Fig. 0.11 Effect of varying location of axial restraint on midspan deflection in a 10 m perforated beam exposed to fire

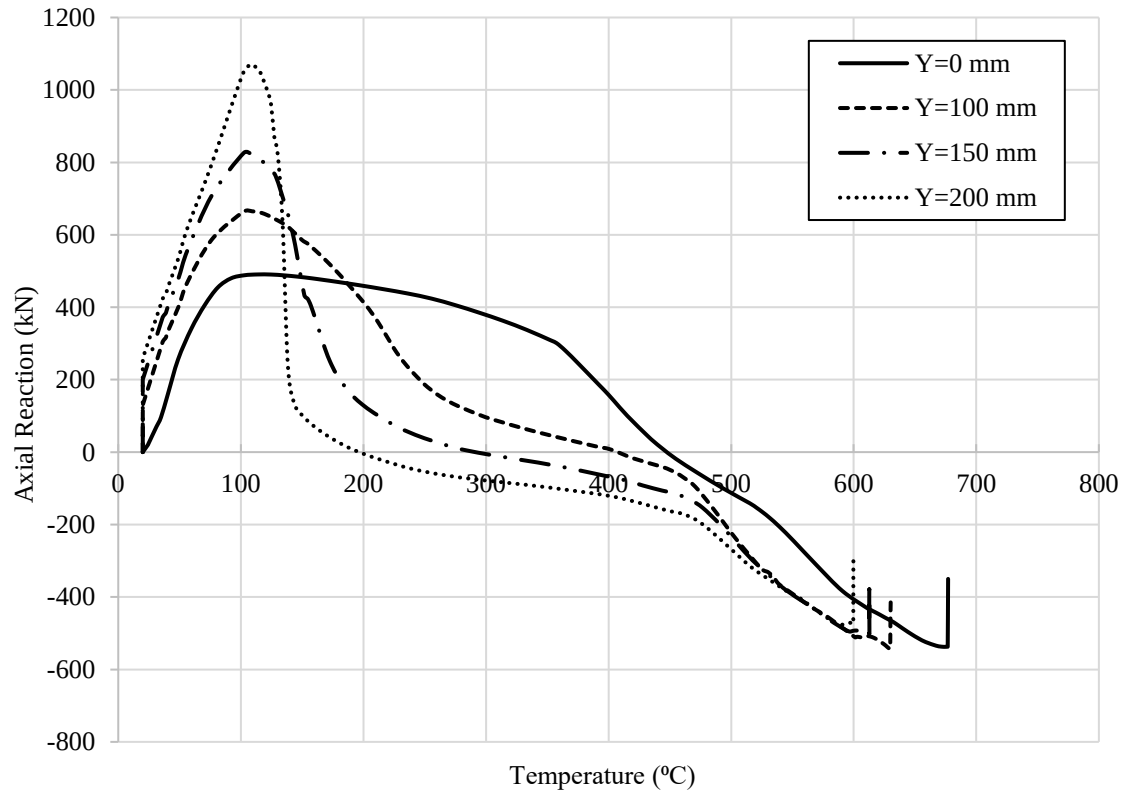

Fig. 0.12 Effect of varying location of axial restraint on the fire-induced axial force in a 10 m perforated beam exposed to fire

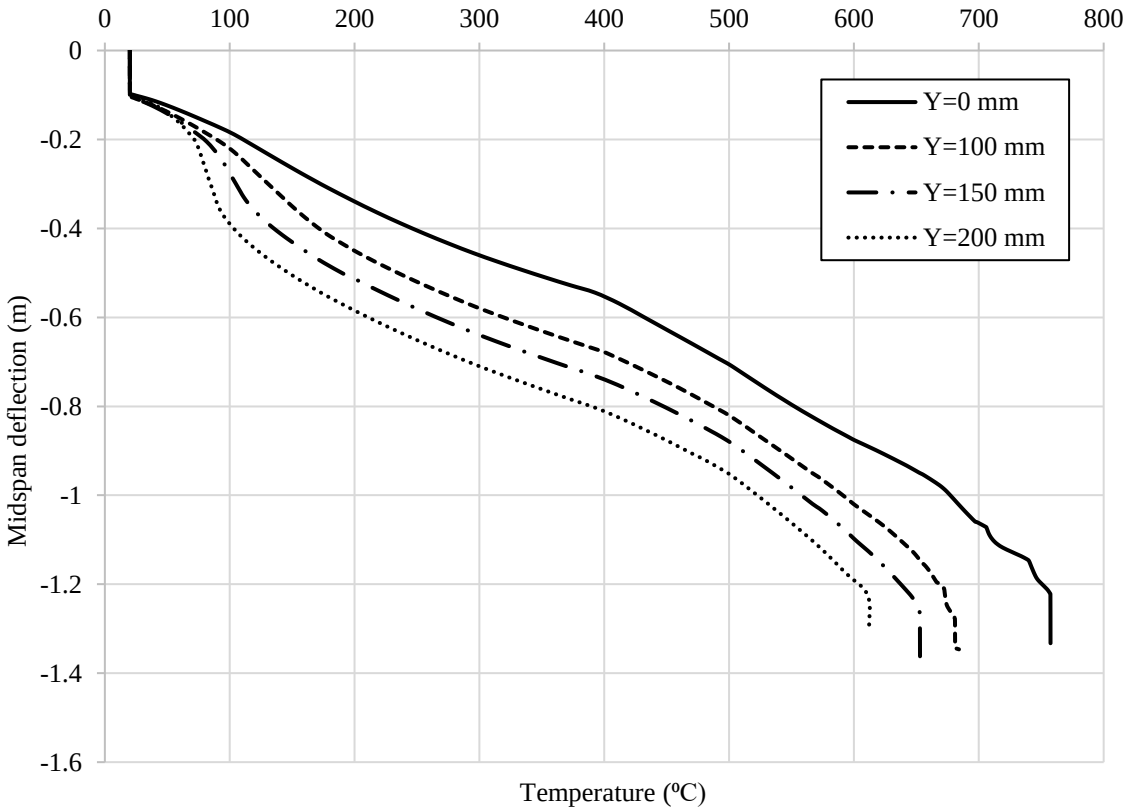

Fig. 0.13 Effect of varying location of axial restraint on midspan deflection in a 12 m perforated beam exposed to fire

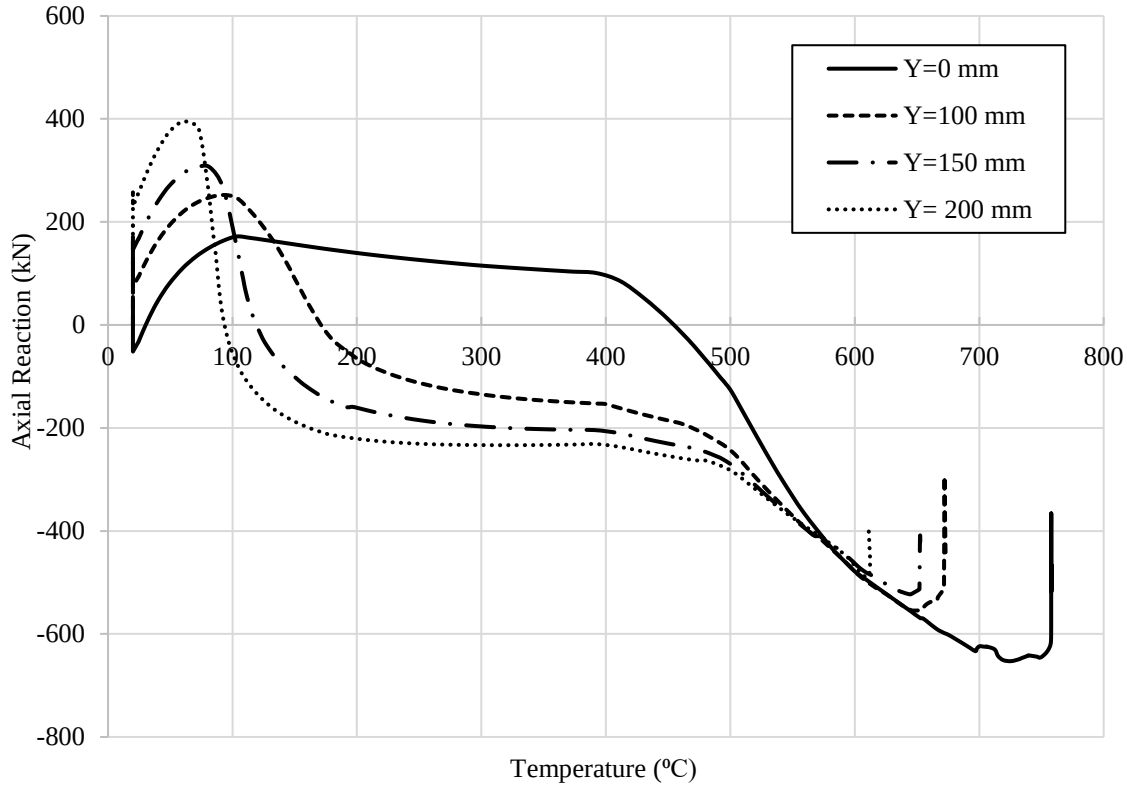

Fig. 0.14 Effect of varying location of axial restraint on the fire-induced axial force in a 12 m perforated beam exposed to fire

It can be seen from Fig. 4.14 that the transition temperature for the 0 mm eccentric axial restraint is 458 degrees and it reduces to 93 degrees at 200 mm eccentric axial restraint for 12 m perforated beam. On further increase in temperature, the material strength reduces significantly and the beam fails after reaching its full tensile capacity at elevated temperature. Hence, it can be concluded that the fire resistance of slender perforated beams reduces with an increase in the eccentricity of the location of the axial restraint. However, the analysed non-slender perforated beams showed an enhancement in the overall fire performance due to an increase in the eccentricity of the location of the axial restraint.

4.3.2. Effect of the slenderness ratio

A change in the slenderness ratio has a great influence on the performance of the restrained perforated beams exposed to fire. This influence is investigated by varying the slenderness ratio (L/r) of the perforated beams. The slenderness ratio is defined as the ratio of the span length (L) over the radius of gyration (r) of the beam section in the direction of bending. Beams with the span lengths of 6 m, 10 m and 12 m and the slenderness ratios of 24.1, 40.6 and 48.8, respectively are modelled in this study. The results of all the investigated cases in this study are presented in Table 4.1.

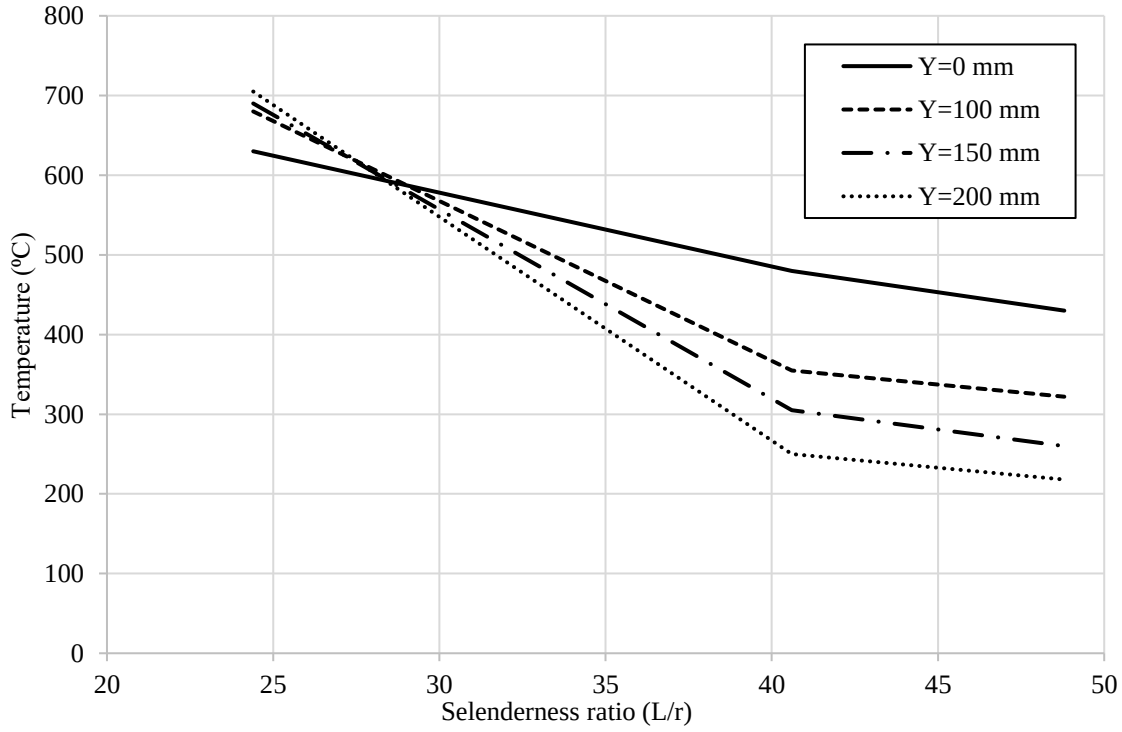

Fig. 0.15 Fire resistance of beams exposed to fire as a function of beam slenderness and locations of axial restraint.

The variation of the fire resistance temperature as a function of slenderness ratio for different location of axial restraint in the perforated beams is plotted in Fig. 4.15. For non-slender beams ($L/r \leq 30$), it is observed that the beams are able to resist higher temperature when the eccentricity of the axial restraint increases from 0 mm to 200 mm. It is noticed that at slenderness ratio ($L/r = 28$), the change in the location of the axial restraint has minimum effect on the fire resistance temperature as illustrated in Fig. 4.15. In non-slender beams, during the early stage of fire, the magnitude of the axial compression is high and the fire-induced hogging moment at support ($P \times Y$) is quite significant compared to the sagging moments due to the gravity load and P-δ effect ($M_g + M_{p-\delta}$). Therefore, this fire-induced hogging moment reduces the total sagging moment and an improvement in the fire resistance is observed with an increase in the eccentricity of the location of the axial restraint. For beams with a slenderness ratio of 24.1, a shift of location of the axial restraint from 0 mm to 200 mm improves the fire resistance by 80 ºC as illustrated in Fig. 4.15.

However, as the slenderness ratio of the perforated beams increases, i.e., slender beams ($L/r > 30$), the change in the location of the axial restraint has an adverse effect on the fire performance of the perforated beams. For slender perforated beams, the early buckling of the beams results in a sudden increase of midspan deflection, and thus the sagging moment due to P-δ effect ($M_{p-\delta}$) becomes significantly large compared to the moment due to the eccentric location of axial force ($P \times Y$). Therefore, the higher eccentricity of the axial restraint causes the early buckling in the beam and higher midspan deflections throughout the duration of fire as shown in Fig. 4.11 and Fig. 4.13. This behaviour illustrates the diminished fire performance of slender beams with an increase in the eccentricity of the location of the axial restraint.

Moreover, the fire resistance of the perforated beams decreases with the increase in the slenderness ratio. This behaviour is explained by the fact that an increase in the slenderness ratio reduces the axial stiffness of the perforated beams and more slender beams experiences buckling prior to the less slender beams under fire-induced compression. This early buckling results in large deflection during the initial stage of fire and the phenomenon of transformation of beam behaviour from flexure to catenary is also accelerated. Finally, the beam reaches its reduced tensile capacity and failure occurs.

However, any further increase in the slenderness ratio beyond 40 has a minimum effect on the fire resistance of perforated beams as illustrated in Fig. 4.15.

4.3.3. Design implications

Generally, during the initial stage of fire, a compressive axial force is induced in the restrained perforated beam. At the later stage of fire, this compressive force changes to tension if an adequate amount of axial restraint is provided. The axial compressive force has a great influence on the behaviour of perforated beams as they are more prone to buckling compared to solid beams. Effect of various crucial parameters which can influence the behaviour of restrained perforated beams in fire is not addressed in the available design codes. The parametric study presented here shows that the location of axial restraint with respect to the geometric centre of the section and the slenderness ratio affects the fire behaviour of perforated beams to a great extent. Importance of these parameters should be appreciated and accounted in the design standards to achieve a realistic design. In this study, it is presented that if a particular connection type is used for non-slender perforated beams than it can greatly enhance the fire behaviour of these beams. On the other hand, if the similar connection type is employed for slender perforated beams it could adversely affect the fire performance. The study presented here gives an idea about the influence of these important parameters on the fire behaviour of perforated beams and can be utilised to account for such effects in the current standards. However, to quantify the effects of a shift in the location of axial restraint and the effect of slenderness ratio on the fire response of a perforated beam, a more detailed study is required.

4.4. Concluding remarks

In this chapter, the developed modelling methodology of chapter 3 is used to analyse the effect of various parameters on the response of restrained perforated steel beams. Influence of magnitude of axial restraint, the location of axial restraint and the slenderness ratio on the fire behaviour of perforated steel beams has been investigated. A shift in the location of the axial restraint enhances and degrade the performance of perforated beams in fire conditions depending on their slenderness ratio. In non-slender perforated steel beams, shifting the location of the axial restraint towards the bottom flange can improve the fire performance of beams. Whereas for slender beams, it is observed that a shift in the location of the axial restraint has a negative impact on the fire performance of the

beams. The fire performance is more sensitive to slenderness ratio of range 25 to 40 and less sensitive to a further rise in the slenderness ratio.

Chapter 5

Virtual hybrid simulation framework in fire

5. Introduction

Obtaining an accurate simulation of the boundary conditions is a very challenging task but it is essential and in order to represent the real behaviour of the structural components in fire, real boundary conditions should be simulated by incorporating the whole system effects. To achieve this objective, a virtual hybrid simulation framework has been developed in this chapter. In recent years, hybrid simulation has been emerging as an efficient and economical method for simulating realistic boundary conditions in the field of earthquake engineering. In this chapter, a virtual hybrid simulation framework in fire has been established and successfully implemented using the OpenFresco and OpenSees software. In this framework, a sub-structuring is required, the fire-exposed part of the structure is modelled in one analysis (a 3D model) and the rest of the structure in another analysis (a 2D model). This kind of sub-structuring enables the behaviour of the structural system as a whole to be investigated. This approach enables the simulation of the correct restraint provided by the surrounding structure to the fire affected structural element. The Cardington restrained beam test (British Steel Plc 1999) is modelled and validated to demonstrate the potential of using the virtual hybrid simulation framework. A reasonably good agreement with the test results illustrate that using virtual hybrid simulation framework can be an effective method for studying the behaviour of the whole structural system in fire conditions.

5.1. Background to hybrid simulation

There are a number of finite element software packages available for commercial and research purposes and most of them are used by the structural engineering community to provide an efficient and inexpensive method for analysing the behaviour of structures exposed to extreme events, such as fire, earthquake, etc. However, most of the commonly

used software packages lack the required features for more customised applications and where they do, they do not allow developers to implement them in the source code.

In recent years, many researchers have focussed on modelling structural system response during extreme events, such as in the context of progressive collapse, or other such behaviour that is not achievable by simulating individual components. Simulating the whole structure in three dimensions (3D) is a complex and more computationally demanding task than simulating a single component, i.e. a beam or column, owing to the interactions present. On the other hand, testing large structures in fire is an expansive task and require specialised experimental facilities. Due to the complexities involved in 3D numerical modelling and challenges of structural fire testing, hybrid simulation has emerged as a promising technique in that it combines testing of fire exposed component with simulation of the surrounding structure to understand the global response of the structural system. Hybrid simulation is a popular approach in the seismic engineering community but is a new technique for analysing the behaviour of structures subjected to fire. In this chapter, a virtual hybrid simulation framework in fire is established in a fully numerical environment. This framework is validated by simulation and comparing results from tests conducted on large structures. One of the main objectives of developing this framework is to conduct real hybrid test of structural components exposed to fire under physical-numerical environment in future.

Two or more appropriate finite element analyses can be coupled for each portion of the structure to achieve more flexible and inexpensive simulation of large engineering systems, compared with simulating the whole structure in a single 3D finite element analysis. Although the study presented here is specifically related to the finite element analysis of structures exposed to fire, a similar approach can be applied to structures exposed to other types of severe loading conditions, such as earthquake, flooding and blast.

In this chapter, the behaviour of a composite beam exposed to fire is studied with the application of a new simulation method that is capable of coupling two or more finite element analyses together in order to create an accurate yet efficient simulation. The accuracy is measured by comparing against solutions obtained without sub-structuring and through validation against real experiments. Efficiency is achieved by coupling a high resolution model of the structural element exposed to fire with a dimensionally reduced

model of the rest of the structure, without loss of accuracy. Section 5.6 provides the results that corroborate this claim.

A virtual hybrid simulation framework has been established that involves the coupling of multiple instances of the same finite element program but modelled in different dimensions. The beam which is exposed to fire may experience large deformations and needs to be analysed in greater detail than other parts of the structure. So, it is modelled using 3D elements but the rest of the structure, which remains at ambient temperature, is modelled using 2D elements. OpenSees is used to model all the sub-structures to be coupled. Open-source software framework (OpenFresco) (Schellenberg et al. 2007; Takahashi and Fenves 2006) is employed as the middleware software to enable the coupling between the codes. The primary motivation of this work is to create a tool that would enable system level simulation of the response of structures subjected to fire with the added feature of multi-scale analysis by exploiting the hybrid simulation approach. The advantage of this approach is to enable the analyst to focus on the structural element of interest and modelling it at a higher resolution (such as the ones exposed to fire or other extreme loading) while modelling the rest of the structure at a lower resolution that is adequate to simulate the correct boundary restraint conditions. This approach produces an extremely powerful and versatile tool for efficient and accurate simulations of large structural systems subjected to complex fire scenarios in the context of performance based engineering.

In this chapter, the tool developed is used to simulate a composite steel and concrete beam subjected to fire where the correct representation of boundary restraint conditions is critical to obtain an accurate simulation of the behaviour. Most composite beams are axially and rotationally restrained in a composite steel-framed structure, and their behaviour in fire depends significantly on the nature and magnitude of the restraints. In the majority of the studies in this area, the behaviour of composite beams exposed to fire has been investigated by performing isolated fire tests or numerically modelling single elements (Dwaikat et al. 2011; Kodur and Naser 2015; Łukomski et al. 2017). Limited tests have been performed on composite beams exposed to fire as part of a structural frame (Dong and Prasad 2009; Liu et al. 2002; Zhao and Shen 1999). Applying accurate boundary conditions has a great influence on the behaviour of structures in fire. Section 5.2 focusses on the influence of the different boundary conditions on the fire

behaviour of a steel beam. The virtual hybrid simulation framework is used to model restrained composite beam behaviour in fire and is validated against a well referenced full scale test (Cardington restrained beam test) showing excellent agreement with the experiment both in terms of the beam response and restraint simulation measured using the horizontal displacement of the beam end against the restraint provided by the frame.

5.2. The influence of the boundary conditions on the fire behaviour of steel beams

This section illustrates the importance of applying correct boundary conditions to capture the real behaviour of the structures in fire condition. For this illustration, a steel beam exposed to fire is modelled and simulated with different configurations. A similar beam is also analysed as part of a moment resisting frame, which is common in construction. Most of the fire tests are conducted on isolated components under specific boundary conditions. So, different support conditions are possible, depending on the furnace facility. Fig. 5.1 presents various configurations of a beam exposed to fire which are analysed in this section. All the configurations are simulated under a uniformly distributed load (UDL) and a uniform temperature distribution along the length and across the depth of the beam is assumed.

Configuration 1

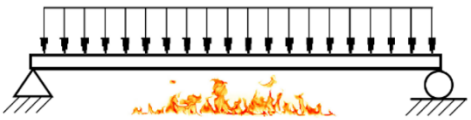

Configuration 2

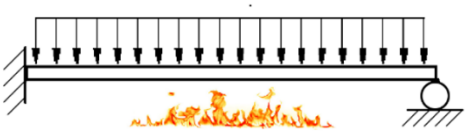

Configuration 3

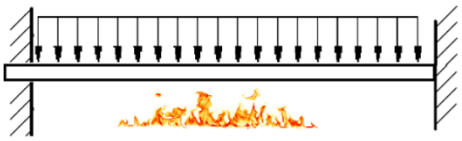

Configuration 4

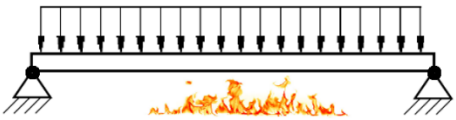

Configuration 5

Configuration 6

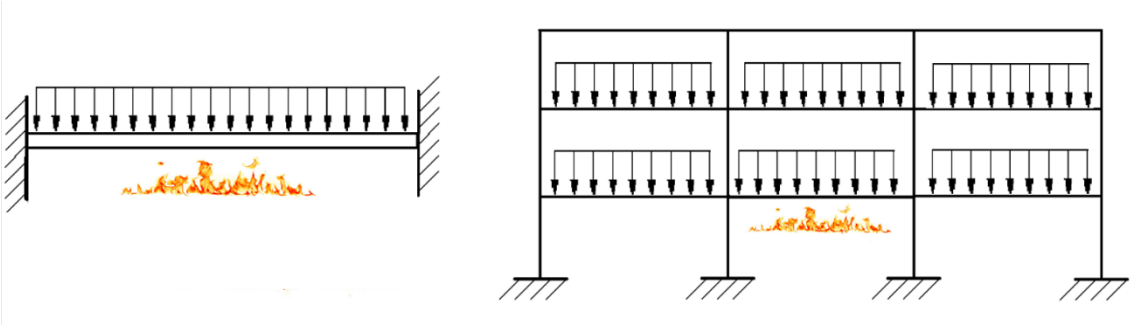

Fig. 5.1 Possible configurations of a beam exposed to fire

- Configuration 1 represents a simply supported beam exposed to fire.
- Configuration 2 represents a beam where one support is fixed and the other support is axially and rotationally unrestrained.
- Configuration 3 represents a beam where one end is fixed and the other end is axially unrestrained and rotationally restrained.
- Configuration 4, a beam is assumed with pin-pin boundary conditions with axially restrained and rotationally unrestrained supports.
- Configuration 5 represents a beam with completely fixed support conditions.
- Configuration 6 represents a moment resisting frame but only the central beam is exposed to fire as shown in Fig. 5.1.

All configurations are numerically modelled in OpenSees software to analyse the behaviour during a fire exposure. A section UB305×165×40 for beams in all configurations and a section UC254×254×89 is used for columns in Configuration 6. All the configurations are modelled with a span length of 9 m under a UDL of 4.5 kN/m. A 2DdispBeamColumnThermal element class available in OpenSees is utilised to model all the configurations. SteelECThermal material class is used with a yield strength of 275 N/mm^2. The standard fire exposure is considered for all configurations, i.e., ISO 834 (EN 1991-1-2 2005). The interest here is to access the failure temperatures and different modes of failure for all configurations. Fig. 5.2 presents the temperature-midspan deflection behaviour for all configurations simulated in this section.

The first three configurations (Configuration 1 to 3) behave in a similar way as shown in Fig. 5.2. The similarity in the behaviour of these configurations is due to their resemblance with regards to boundary conditions, i.e., the first three configurations are unrestrained in axial direction. During the initial stage of fire, no thermal bowing is observed due to a uniform temperature distribution across the depth of the section and all

three configurations expand freely in axial direction due to a uniform rise in temperature, which is attributed to a slow rate of increase of midspan deflection as displayed in Fig. 5.2. In the later stages of fire, when the material softens and loses its strength, a sudden increase in the midspan deflection is observed which leads to the collapse of the first three beam configurations. Comparing first three configurations, it is noticed that the temperature at the failure for Configuration 3 (755 °C) is the highest followed by Configuration 2 (673 °C) and Configuration 1 (625 °C) as shown in Fig. 5.2. This is due to the fact that the Configuration 3 has the maximum number of restraint at the support followed by Configuration 2 and Configuration 1. More is the number of restraints (high indeterminacy) at the support less is the midspan deflection and an improvement in the fire performance of the structural element is observed.

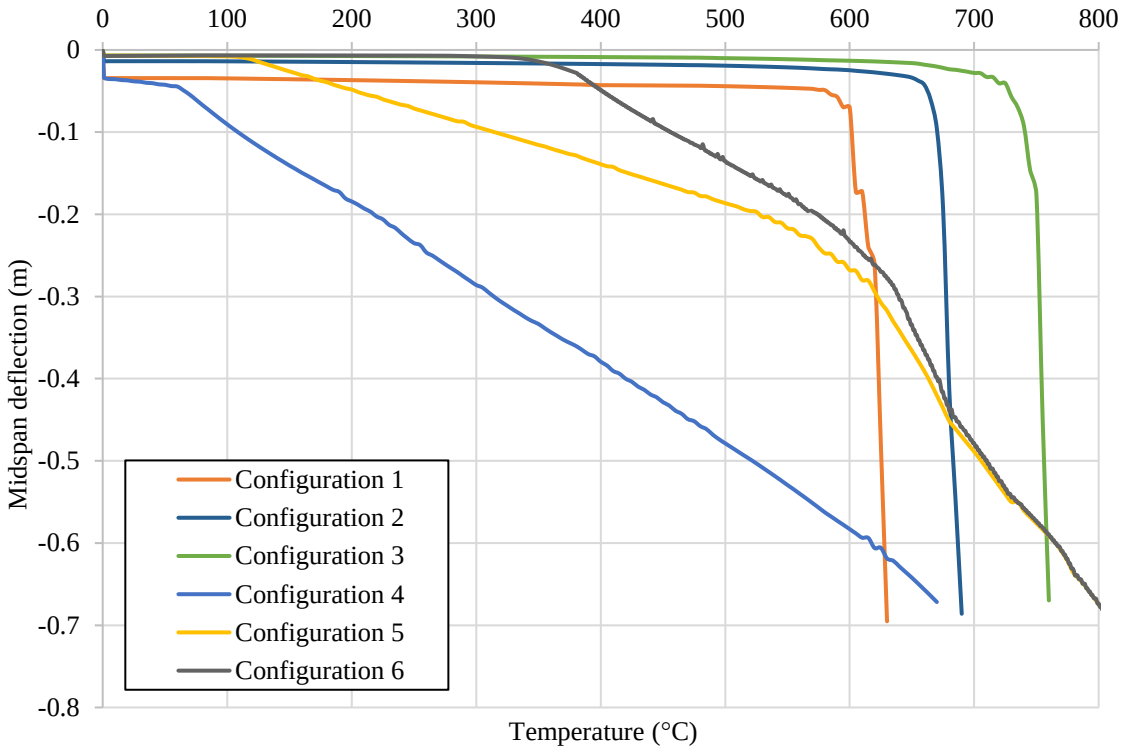

Fig. 5.2 Temperature-midspan deflection behaviour for different beam configurations in fire

For Configuration 4 and Configuration 5, the temperature-midspan deflection behaviour observed is also similar. The physical similarity between these two configurations is that they are axially restrained against thermal expansion. When the temperature rises, a compression is induced in the section due to restrained thermal expansion, which causes a compression buckling of these beams. The buckling in Configuration 4 and 5 initiates at 62 °C and 117 °C, respectively as shown in Fig. 5.2. During the initial stage of fire, the rate of increase of midspan deflection in these configurations is higher compared to

first three configurations owing to the restrained thermal expansion. However, at later stage of fire, the load carrying mechanism in these configurations changes from flexural action to tensile catenary action due to the presence of sufficient axial restraint. Due to the transformation of load carrying mechanism, axially restrained beams continue to carry load even at high temperature without a collapse and a better fire performance is observed compared to unrestrained beams (Configuration 1 to 3). Analysing the behaviour of these two configurations, it is observed that the Configuration 5 experiences less midspan deflection compared to Configuration 4 and results in a better fire performance as shown in Fig. 5.2. This behaviour is also attributed to the presence of more number of restraints provided in Configuration 5 compared to Configuration 4.

The fire response of Configuration 6 is observed as the most efficient of all configurations. The Configuration 6 is not completely fixed in axial direction which results in a slow development of axial compression during the initial stage of fire. Due to this delay in the development of compressive force, the initial buckling of the beam in Configuration 6 is also delayed and initiates at 348 °C compared to 62 °C and 117 °C for Configuration 4 and 5, respectively as illustrated in Fig. 5.2. Post buckling behaviour of Configuration 6 is similar to the behaviour of Configuration 4 and 5 but with less midspan deflections.

Analysing all the possible configurations presented in this section, it can be concluded that the fire behaviour of structural components is highly influenced with the number and magnitude of the restraints provided at the support. So, simulating the correct boundary conditions is vitally important in numerical modelling to study the real fire behaviour of the structural components. The Configuration 6 represents the real boundary conditions which exist in most of the steel frame structures. Using virtual hybrid simulation framework to assess the true behaviour of structural components in fire conditions could be a useful technique as the effect of the surrounding structure is also incorporated in the model.

5.3. Virtual hybrid simulation framework

Generally, hybrid simulation is quite popular amongst earthquake engineers and is commonly used to study the seismic behaviour of structures. In hybrid simulation, the structure is divided into two assemblies or substructures. The assembly which is expected to experience large deformations or whose seismic performance needs to be evaluated in

fine detail is tested physically in the laboratory and is known as the physical substructure (PS). The rest of the structure is modelled using a standard FE software in the other assembly which is referred to as the numerical substructure (NS). Both assemblies interact with each other at each time step using a communication software e.g., OpenFresco (Schellenberg et al. 2007; Takahashi and Fenves 2006). Typically, performing a hybrid simulation involves the following three steps. Firstly, the NS is started and calculates the displacements and rotations at the interface. In the second step, these calculated values are applied to the PS in the laboratory through the actuators, which are directly connected to the FE model (NS). In the third step, the reaction forces and moments as a result of the applied displacement and rotations in the physical test are recorded at the interface of the PS and then fed back to the NS to perform the next integration step and determine the new set of displacements and rotations. These steps are repeated until the end of the test. Using this technique, researchers are able to apply real boundary conditions owing to the surrounding structure to the PS in the laboratory and obtain an accurate depiction of the whole system behaviour.

In the context of this study the phrase 'Virtual hybrid simulation framework' refers to modelling a structure using different sub-assemblies, some of which may be represented in 2D or using standard FE elements in one assembly whilst the areas requiring more focussed attention are modelled using more complex elements (3D elements) in another assembly. Both assemblies are modelled in OpenSees (McKenna 1997) software and interact using a middleware software, such as OpenFresco (Schellenberg et al. 2007; Takahashi and Fenves 2006). The various sub-assemblies interact at every time step of the finite element analysis solution procedure. In virtual hybrid simulation, one of the assemblies is generally selected to act as the master assembly which solves the complete structure, while the other assembly is selected to act as slave assembly. An adapter element in the slave assembly and a super element in the master assembly is defined to couple the two substructures. Both the master and slave assemblies interact at interface nodes after each integration step using a middleware software.

5.3.1. Steps involved in establishing a virtual hybrid simulation framework in fire

The sequence of steps in exchanging the data between master and slave assembly to perform the hybrid simulation is shown in the Fig. 5.3. The steps required to couple the two analyses using OpenFresco are as follows:

(1) Run the analysis for the master program and, as a result, the super element receives a displacement vector of global trial displacements (u_{super}) for all of its degrees of freedom from the master integration program.

(2) The displacement vector obtained in the previous step is sent to OpenFresco using a TCP/IP socket (where TCP/IP means a Transmission Control Protocol/Internet Protocol which is the basic communication language or protocol of the Internet) as can be seen in Fig. 5.3. Here the SimAppSiteServer class is used to start the simulation server process.

(3) The storage and transformation tasks for the displacement vector are performed by the LocalExpSite and ExperimentalSetup objects (See Fig. 5.3). Transformation of the data is not required in this instance because no physical specimen (i.e. laboratory test specimen) is involved. So, the NoTransformation object as ExpSetup is utilised.

(4) The trial displacement vector is then transferred to the ExperimentalControl object which feeds the trial displacement vector to the adapter element in the slave assembly, using a TCP/IP socket. The adapter element then forms a resultant displacement vector by combining the trial displacements (u_{super}) with its own elemental displacements. Subsequently, corrosponding to the resultant displacement vector, a resultant force vector (P_{adpt}) for the adapter element is calculated and returned to the slave assembly.

(5) After the solution convergence from the slave program, the negative resultant force vector ($-P_{adpt}$) is sent to the ExperimentalControl object through the TCP/IP socket. Again, the storage and transformation of the force vector is carried out by the LocalExpSite and ExperimentalSetup objects (see Fig. 5.3).

(6) The SimAppSiteServer then sends the force vector to the super element in the master program through the TCP/IP socket.

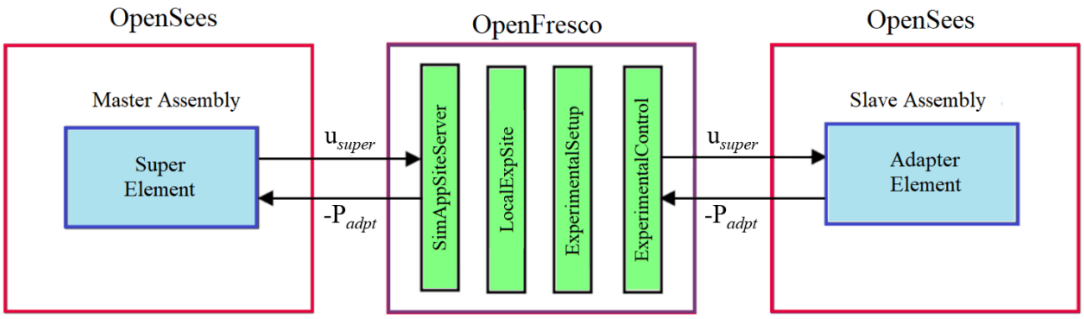

Fig. 5.3 Sequence of operations and data exchange

(7) The super element saves these values as element forces and returns them to the master integration method for the next step. The master program then determines the new trial displacements and Step 1 to Step 7 are repeated until the analysis is complete.

5.4. Implementation of virtual hybrid simulation framework in a 2D frame

In this section, an example frame is modelled in OpenSees in order to illustrate the process described in the previous section. The example consists of two instances, one slave program and a master program, as shown in Fig. 5.4. The whole structure comprises a three-storey, three-bay steel moment-resisting frame, with one column which is exposed to fire. The bay widths and story heights of the structure are 8 m and 3.5 m, respectively. In both assemblies, all components are modelled using section UB305×165×40 and section UC254×254×89 for beams and columns, respectively. A constant value of 0.000014/°C is used for the coefficient of thermal expansion of steel. The maser assembly is modelled using twenty dispBeamColumn elements and the slave column is modelled using one dispBeamColumnThermal element as it is exposed to fire. Fixed boundary conditions are assigned to all the columns at the base. For this simple example, all the beams and columns are assigned elastic material properties with Young's modulus of 2.1×10^5 N/mm^2 for steel. The total load applied to the beams is assumed to be 4.5 kN/m. As shown in Fig. 5.4, the master program performs the analysis of the majority of the structure (which does not experience fire loading) and the slave program analyse the ground floor column which is exposed to fire.

Master and slave structures are connected at one interface node using super and adapter element. The horizontal displacement, vertical displacement and rotation are the three degrees of freedoms at the interface node. A super element in the master assembly is required to communicate the above 3 degrees of freedom to adapter element in slave assembly. Therefore a super element is defined using a 3×3 stiffness matrix corresponding to the interface degrees of freedom. For the initial stiffness values in the matrix of the super element, a unit displacement is applied at one interface degree of freedom in the slave assembly while keeping the other degrees of freedom restrained. However, the stiffness matrix for the adapter element is defined by assigning a high stiffness value of 1×10^{12} N/mm to the diagonal elements, a very high stiffness value can cause convergence problems while a low stiffness value can lead to inaccurate results

(Schellenberg et al. 2008a). Accurate results are obtained and convergence problems are avoided by using the above stiffness values.

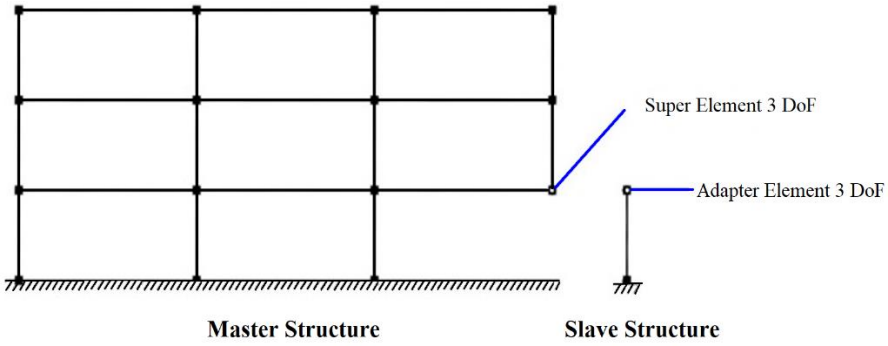

Fig. 5.4 Sub-structuring for the 2D building example

In this example, the column in the slave assembly is subjected to a uniform temperature of 800 °C while the rest of the structure in the master assembly remains at ambient temperature. Vertical displacements at the interface nodes are traced between the master and slave assemblies, as presented in Fig. 5.5. As the temperature increases, there is an elongation in the length of the column due to thermal expansion which is indicated by the upward movement of the interface node. As soon as the material softens, the column starts to buckle and the interface nodes start moving back downwards due to the load from the upper stories. For validation of the sub-structuring process, the whole building has also been analysed in a single assembly without sub-structuring into master and slave assemblies.

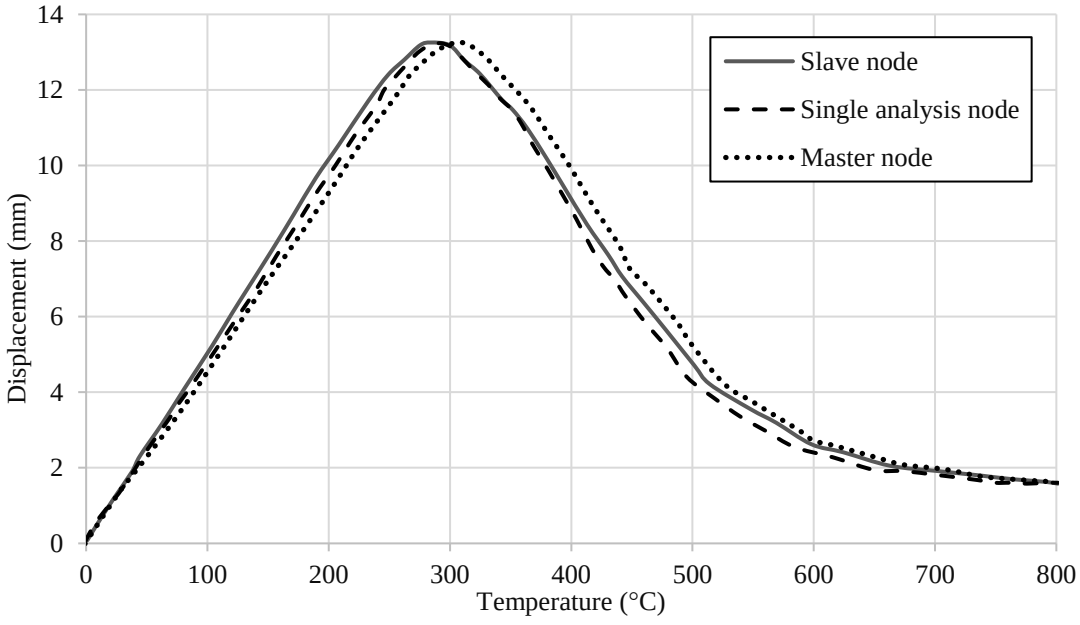

Fig. 5.5 Vertical displacement comparison at interface node

Results obtained from the single analysis (whole frame in single assembly) are compared with the partitioned analysis and presented in Fig. 5.5. It is evident from Fig. 5.5 that vertical deflection at the interface is very similar between the master assembly, slave assembly and whole building analysis. This agreement indicates that the master and slave assemblies are communicating successfully with each other at each time step and also confirms the kinematic compatibility of the framework. The agreement of the master and slave node displacements with the whole frame analysis shows the accuracy of the coupling method and the virtual hybrid simulation approach. This approach produces practically identical results as those obtained by analysing the whole structure in a single analysis. The slight difference in the vertical deflections at the master and slave nodes results from computational noise and can be reduced by choosing more stringent convergence criteria, however in practice this is not necessary for ordinary structural engineering simulations.

5.5. 3D Thermo-mechanical model in OpenSees

In the previous section, the hybrid simulation technique was applied to a simple 2D structure with one element exposed to a uniform fire. In the next section, the method is advanced in order to represent a structure using 3D elements and a more realistic fire exposure. In order to apply the aforementioned solution algorithm in OpenSees, it is necessary to validate the existing material classes including the temperature-dependent properties. This material class is originally development by Khan et al. (2018). Most of the previous thermo-mechanical analyses performed in OpenSees by other researchers have used 2D displacement beam-column elements (Jiang and Usmani 2018a). However, in this study, 3D thermal elements and material models are employed and therefore the newly developed 'J2PlasticityThermal' material class is utilised to analyse the thermal response of the structure. The J2Plasticity material class in OpenSees uses the von Mises yield criterion. In the following section, the J2PlasticityThermal material model accounting for thermal effects are described.

5.5.1. Modified material class

There are many types of material models available in OpenSees for steel, each of which defines the mechanical constitutive relationships. However, some of these require modifications to include temperature-dependent properties. In the current analysis, the effects of temperature on the properties of steel such as yield strength and elastic stiffness

are taken from the Eurocode design rules (EN 1993-1-2 2005). A temperature-dependent steel material model (J2PlasticityThermal) was created by Khan et al. (2018) based on the existing steel material model known as 'J2Plasticity', which represents the ambient temperature stress-strain relationship. For a J2Plasticity material model, the yield function follows the idealised von Mises yield criterion and is given as:

$$\emptyset(\sigma, q) = \|\mathrm{dev}(\sigma)\| - \sqrt{2/3} * q \tag{5.1}$$

where q is the yield strength with hardening and $\mathrm{dev}(\sigma)$ is the deviatoric stress.

It is necessary to mention that thermo-mechanical concrete materials are available in OpenSees to enable analyses performed for concrete or composite structures in fire. Users can refer to other literature (Gernay et al. 2013; Jiang and Usmani 2018b) and the website (Liming Jiang 2016) for further information about thermo-mechanical concrete materials.

5.5.1.1. Temperature dependent mechanical properties

The temperature dependent mechanical properties of the steel are determined as defined in Eurocode 3 (EN 1993-1-2 2005) for carbon steel at elevated temperatures. Reduction factors are defined for effective yield strength $f_{y,T}$, proportional limit stress $f_{p,T}$ and the modulus of elasticity E_T. The variation in reduction factors for the mechanical properties of steel at elevated temperature is shown in Fig. 5.6.

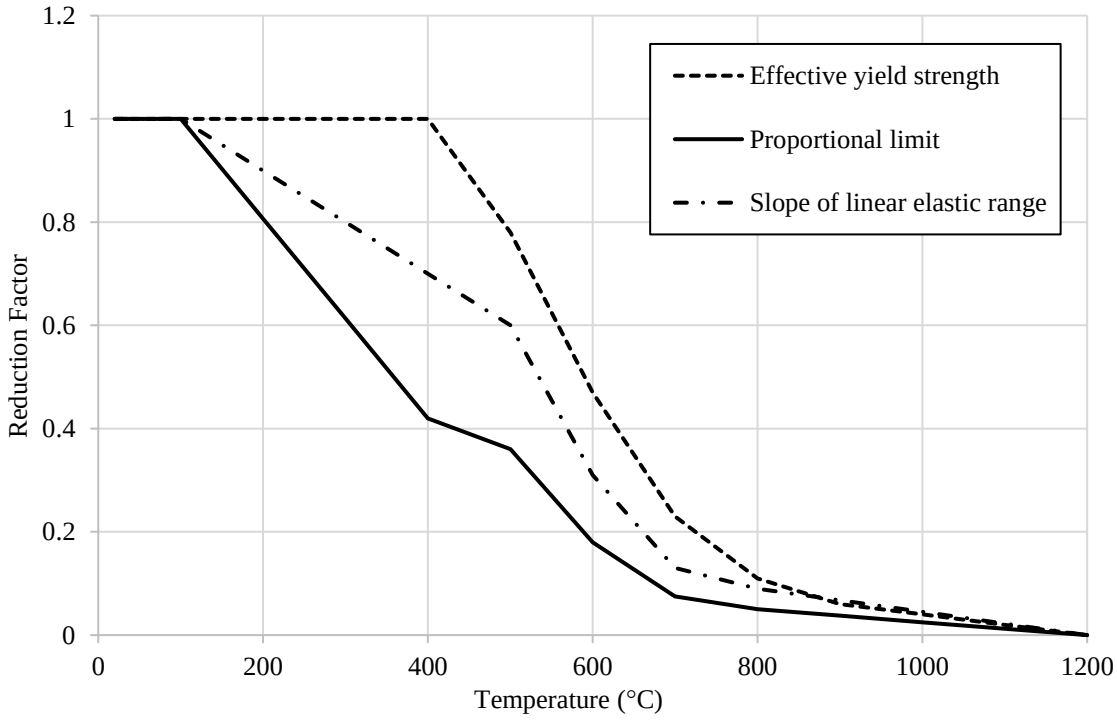

Fig. 5.6 Reduction factors for carbon steel at elevated temperatures (EN 1993-1-2 2005)

5.5.1.2. Thermal elongation strain

The values of thermal elongation strain are calculated in accordance with Eurocode 3 (EN 1993-1-2 2005). Fig. 5.7 shows the variation of thermal elongation strain of steel at elevated temperature. The thermal elongation strain of steel (ε_{sth}) can be determined according to different temperature range as follows:

$$\varepsilon_{sth} = -2.416\times10^{-4} + 1.2\times10^{-5}\,T + 0.4\times10^{-8}\,T^2 \quad \text{for } 20\,°C \leq T \leq 750\,°C \tag{5.2}$$

$$\varepsilon_{sth} = 11\times10^{-3} \quad \text{for } 750\,°C \leq T \leq 860\,°C \tag{5.3}$$

$$\varepsilon_{sth} = -6.2\times10^{-3} + 2\times10^{-5}\,T \quad \text{for } 860\,°C \leq T \leq 1200\,°C \tag{5.4}$$

where T is the temperature in °C.

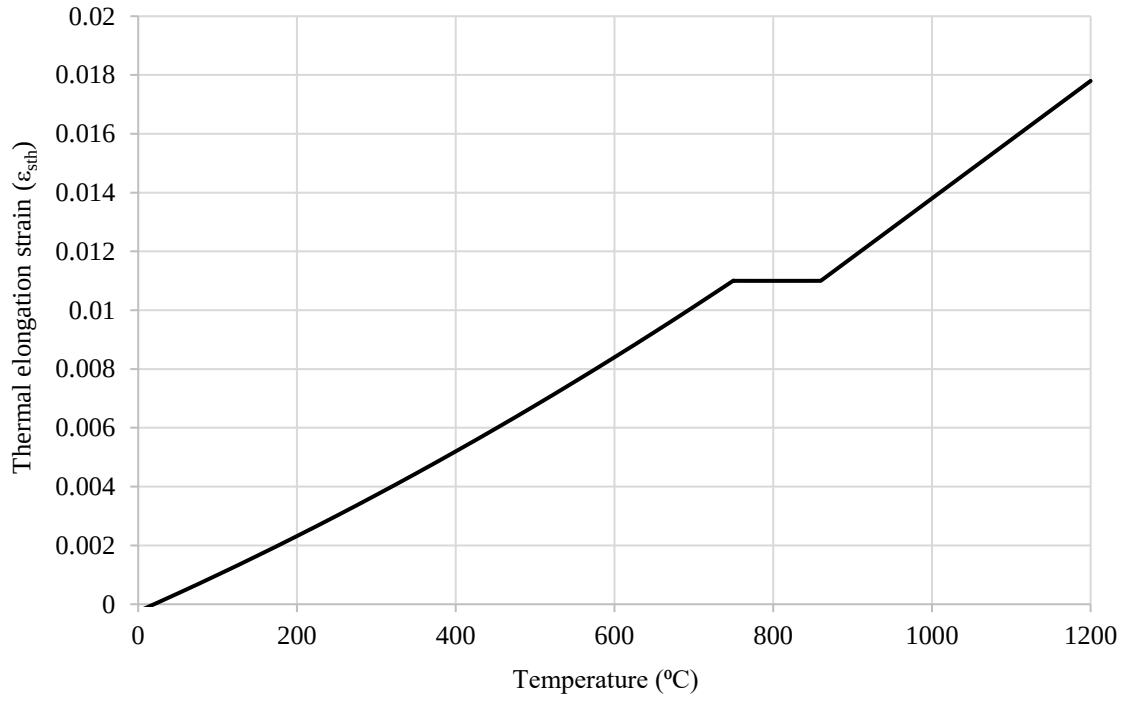

Fig. 5.7 Variation of thermal elongation strain of steel at elevated temperature

5.5.2. Material validation of J2PlasticityThermal at elevated temperature

A number of simply supported composite beams were subjected to an ISO 834 (EN 1991-1-2 2005) standard fire by Wainman and Kirby (1988) in a series of experiments conducted at the Swinden Laboratories. The structural configuration of one of these beams (Test 16 is selected for illustrative purposes herein) is shown in Fig. 5.8.

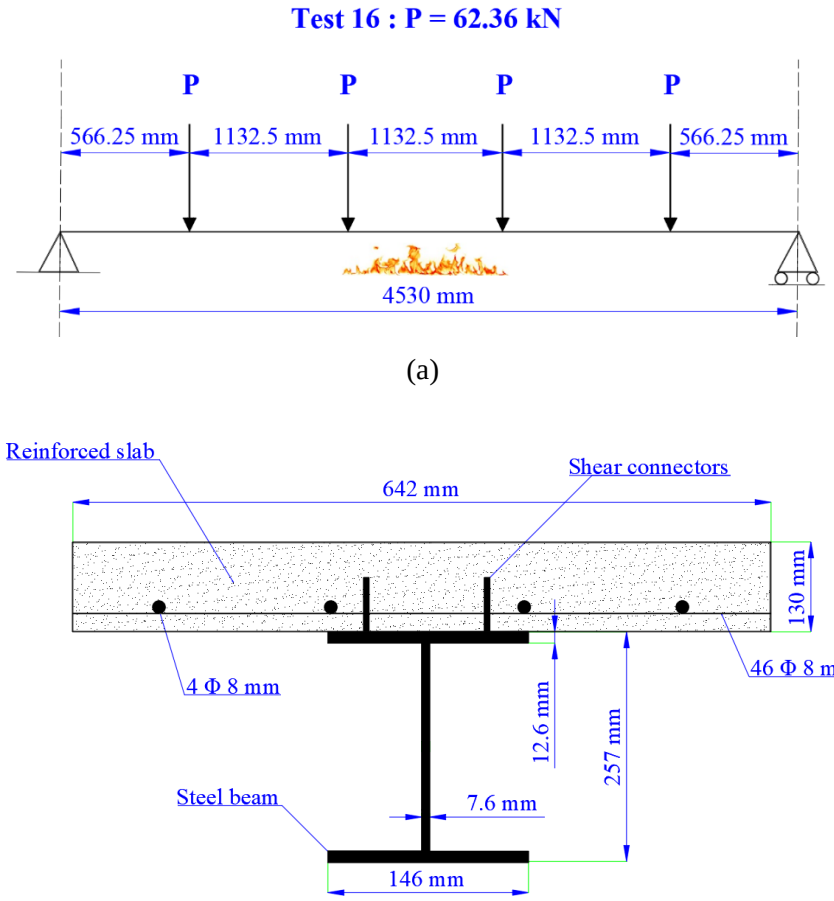

Fig. 5.8 Schematic view of tested beam. (a) beam setup; (b) beam section

Test 16 beam is used in the current analysis to validate the newly developed 'J2PlasticityThermal' material. The same beam was analysed using 2D beam-column elements in OpenSees (Jiang et al. 2015). The results from the tests and also the numerical analysis are used to validate the results obtained by 3D thermomechanical analysis performed in this section. The steel beam and slab are modelled using shell elements (ShellMITC4Thermal) with element size (35 × 30 mm). The 'J2PlasticityThermal' and 'DruckerPragerThermal' material models in OpenSees are selected to represent the steel and concrete material in the composite beam, respectively. Fig. 5.9 shows the temperature distribution in different components of the tested composite beams, during the experiment. No concrete slab temperature profiles were reported in the literature and therefore the temperature distributions through the thickness of the slabs are modelled based on the recommendations in Eurocode 4 (EN-1994-1-2 2005). Fig. 5.10 shows the midspan deflections that were measured during the test together with the predicted results using the OpenSees 3D model, as well as the results from the Jiang et al. (2015) analysis. The OpenSees predictions show reasonable agreement with both the test results and the

predictions made by Jiang et al. This agreement validates the behaviour of newly developed 'J2PlasticityThermal' material model, as well as the 3D modelling capabilities of OpenSees under thermomechanical loading.

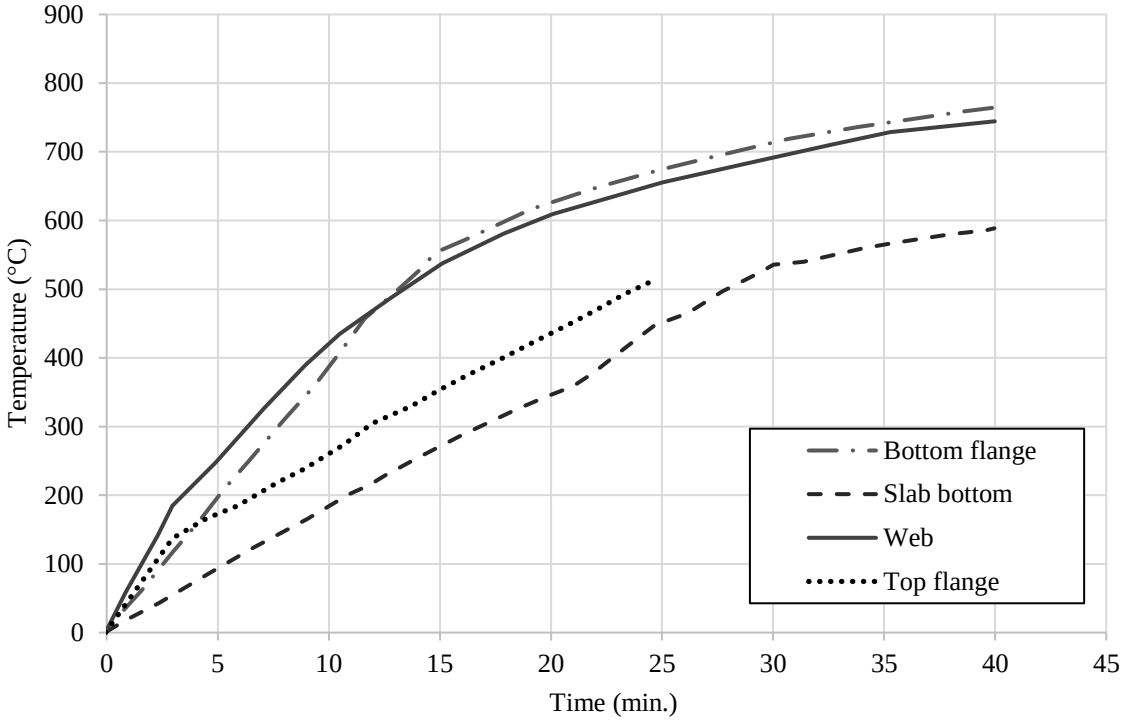

Fig. 5.9 Temperature distribution at midspan in test (Wainman and Kirby 1988)

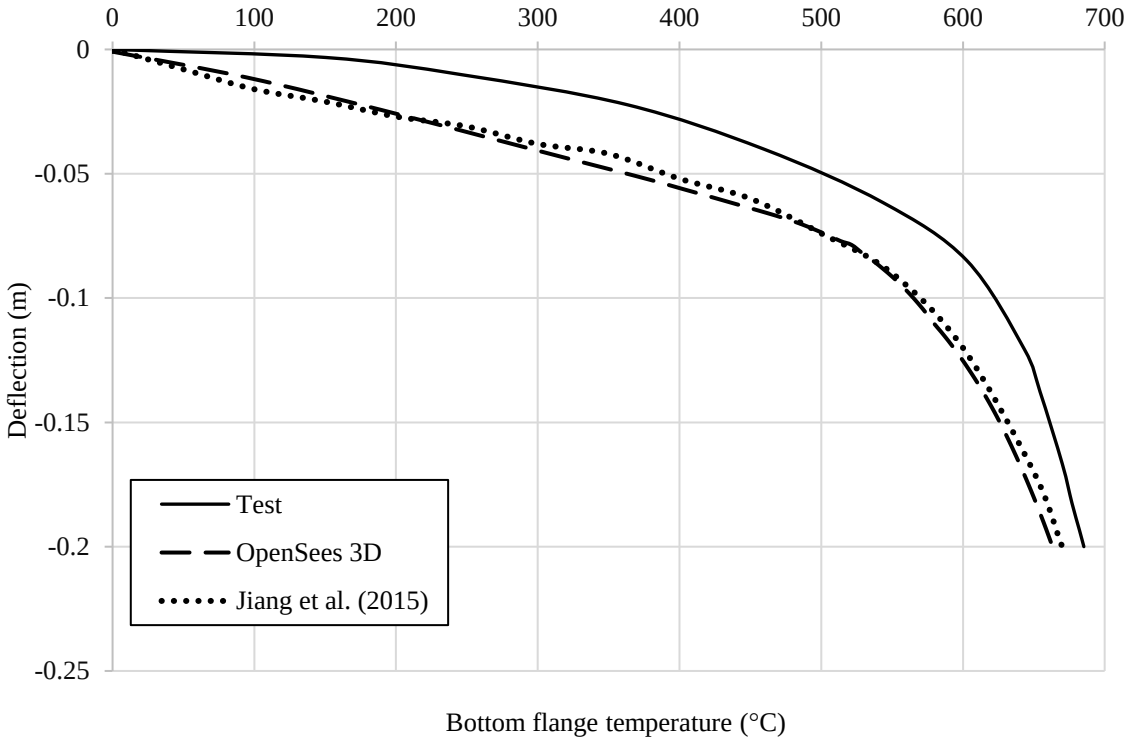

Fig. 5.10 Vertical deflection comparison at midspan

5.6. Efficiency of virtual hybrid simulation framework

As mentioned earlier, the virtual hybrid simulation approach provides a computationally efficient framework compared to detailed 3D modelling of the whole structure. In this section, a detailed 3D model of a three-storey, three-bay moment resisting steel frame is prepared in OpenSees software and the same frame is also analysed using the virtual hybrid simulation framework, to compare the time required to analyse the steel frame. The storey height and bay width assumed in this example are 9 m and 3.5 m, respectively. A UB305×165×40 and UC254×254×89 section is used for the beams and columns, respectively. The 3D shell element (ShellMITC4Thermal) available in OpenSees is utilised to model the detailed 3D frame. The J2PlasticityThermal material model which is described in the previous section is utilised for all the members with a yield strength of 275 N/mm^2. The analysis is conducted in two steps. In the first step, a static uniformly distributed load of 4.5 kN/m is applied to the beams. In the second step, the static load is kept constant and the first floor central beam is exposed to an ISO 834 fire (EN 1991-1-2 2005). In the virtual hybrid simulation framework, the fire exposed central beam is modelled using 3D shell elements in a slave assembly whereas the surrounding structure is modelled using beam-column elements in the master assembly. The J2PlasticityThermal and SteelECThermal material classes with a yield strength of 275 N/mm^2 are used for slave and master assembly, respectively.

Fig. 5.11 presents the temperature-midspan deflection behaviour for the central beam analysed using different approaches. A good agreement has been obtained between the two approaches which validates the accuracy of the virtual hybrid simulation framework. Moreover, as shown in Table 5.1, the detailed 3D model took 109 minutes to complete the analysis, compared with just 14 minutes for the hybrid model. This example highlights the computational efficiency of the proposed approach over 3D detailed modelling, yet with no associated loss of accuracy.

Table 5.1 Comparison of analysis time consumption

	Detailed 3D model	**Hybrid simulation**
Time elapsed	109 minutes	14 minutes

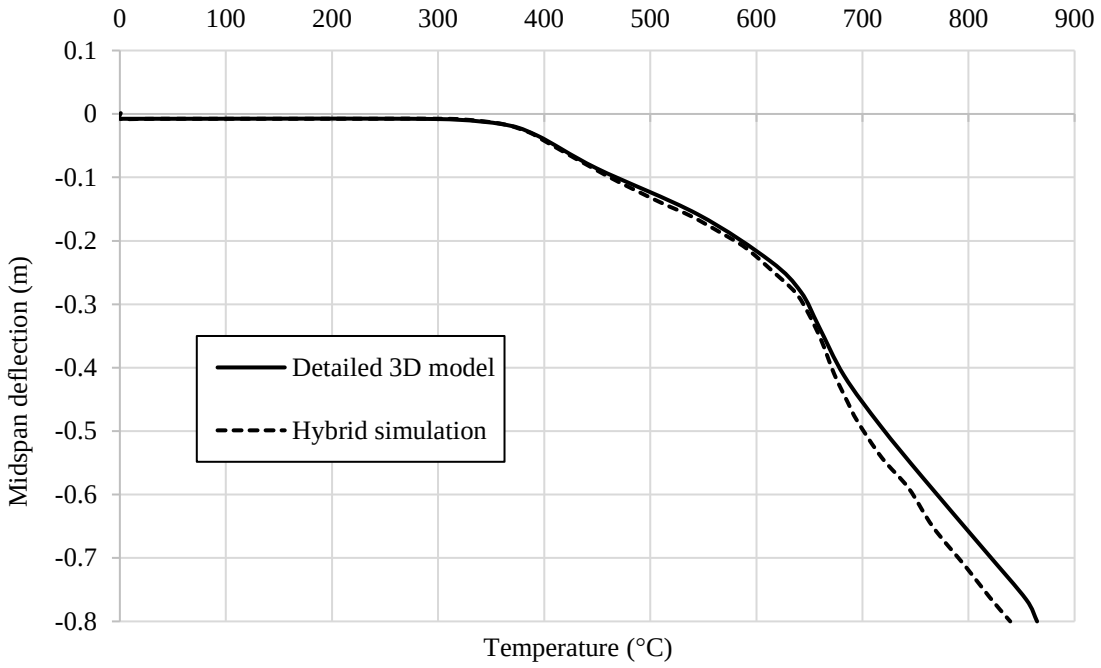

Fig. 5.11 Midspan deflection for 3D detailed model and hybrid simulation approach

5.7. Virtual hybrid simulation of a whole frame includes a 3D beam in fire

In this section, the restrained beam tested during the Cardington experiments is simulated and validated to establish the virtual hybrid simulation approach in 3D. These fire tests were performed by British Steel (1999) on the 7th floor of a composite steel framed structure at Cardington, as shown in Fig. 5.12. The objective of performing this fire test was to understand the structural behaviour when a single beam is heated and restrained by the surrounding steel frame which remains at room temperature. The new 3D thermomechanical material class described in the previous section is employed to model the steel beam. The restrained beam (which was a UB305×165×40 section) was heated over the middle 8.0 m of its 9.0 m length ensuring that the beam-column connection was at ambient temperature. In this section, a three-dimensional model of the Cardington restrained beam on the 7th floor is built in the slave assembly using OpenSees and the rest of the frame is modelled in a master assembly in a 2D OpenSees model as shown in Fig. 5.13. The composite restrained beam is modelled in the slave assembly and is connected to the rest of the structure at interface degrees of freedom through the adapter and super elements. The structure consists of a moment-resisting frame in the master assembly that is connected at interface nodes with the composite restrained beam modelled in the slave assembly. All beams in the master assembly are of length 9 m with section UB305×165×40 and columns are of height 4 m with section UC254×254×89.

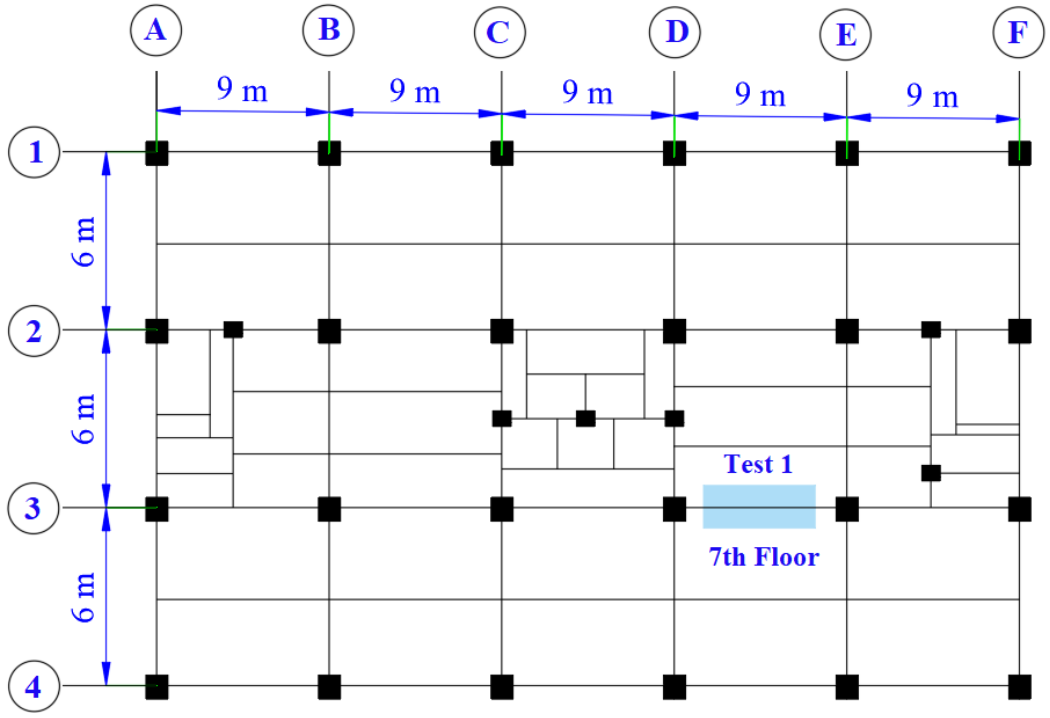

Fig. 5.12 Location of the restrained beam test

The profiled slab is modelled separately using shell elements (ShellMITC4Thermal) with an element size of 50 × 40 mm, for the flat part of the reinforced concrete slab and 3D beam-column elements (DispBeamColumn3DThermal) with an element length of 40 mm for the concrete ribs. The total number of shell elements used to model the flat portion of slab and 3D beam column elements to model the ribs are 13500 and 2325 respectively. The ShellMITC4Thermal elements with an element size of 50 × 40 mm for flange and 50 × 60 mm for web are used to model the steel beam. The steel beam is modelled using 2340 shell elements. The slab, ribs and beams are connected using the rigid link element (rigidLink beam). The rest of the columns and beams in the master assembly are modelled using 2D beam elements (DispBeamColumn2DThermal). The compressive strength of concrete is 48 N/mm^2 and the yield stress of the steel is 280 N/mm^2. The DruckerPragerThermal material class is used to model the concrete in the slab (modelled using shell elements, which require a biaxial material model) and Concrete02Thermal (Jiang et al. 2014) is used for the concrete in the ribs (modelled using beam-column elements, therefore a uniaxial material model is used). The 'J2PlasticityThermal' material model which was described in the previous section is used to model the steel beam. The slab reinforcement is modelled using a smeared layer distribution in the shell elements.

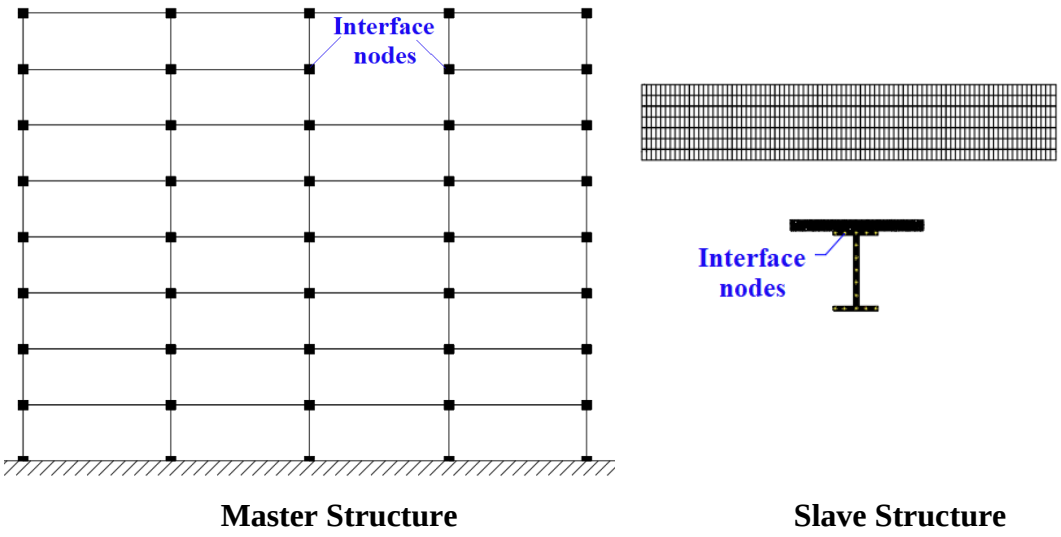

Fig. 5.13 Sub-structuring for Cardington restrained beam hybrid simulation

The slab is subjected to a uniformly distributed load of 5.48 kN/m^2 as reported in the literature (Gillie et al. 2002) and the temperature profile obtained from the test data (see Fig. 5.14) is applied as a thermal load to the beam and the slab. The structure is loaded in two steps. In the first step, the static load is applied while the rest of the structure is at ambient temperature. In the second step, the thermal load is applied to the restrained beam while the remaining structure at ambient temperature and constant static load. A nonlinear dynamic analysis is performed in OpenSees to investigate the behaviour of the restrained beam under fire.

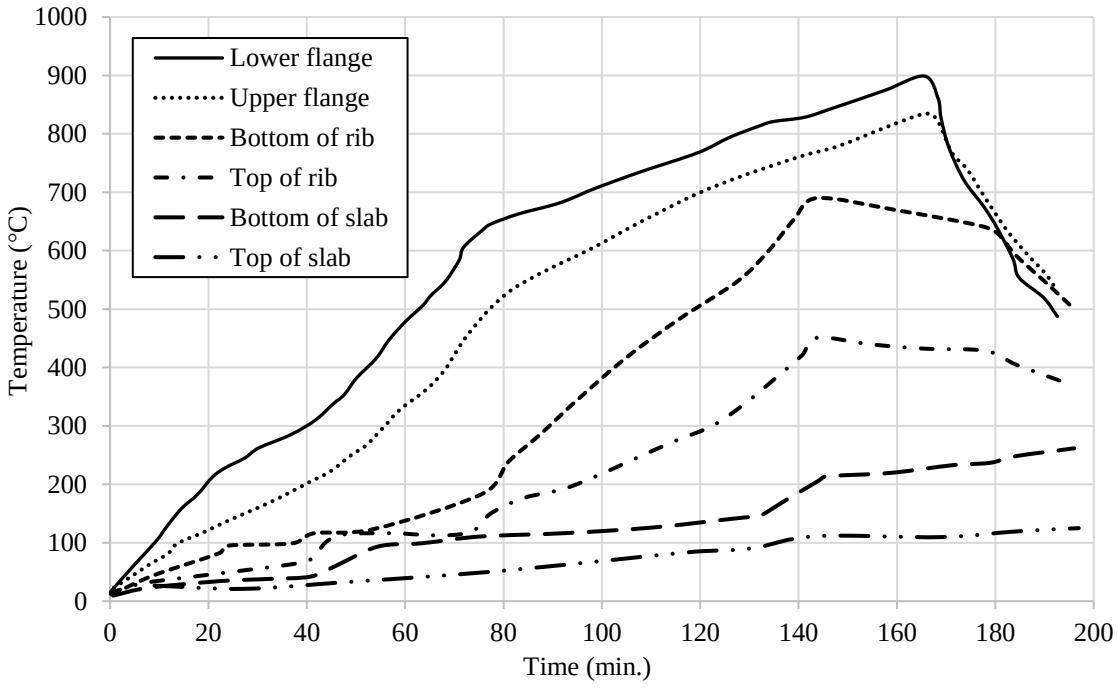

Fig. 5.14 Temperature distribution during restrained beam test (British Steel Plc 1999)

This structure is an ideal candidate for analysis using virtual hybrid simulation framework, where the frame is modelled using 2D displacement beam-column elements and the composite beam assembly is modelled with 3D elements. The steel moment-resisting frame assembly is analysed in the master FE software and the beam exposed to fire is analysed in the slave FE software. Both these assemblies are shown in Fig. 5.13. The moment-resisting frame is connected to the beam through 14 interface nodes at each end so, a 28-noded super element is added to the master program and a 28-noded adapter element is added to the slave program. Hence, the adapter element in the slave model connects to the interface node of the frame through the super-element in the master program. OpenFresco is used to transfer displacements and forces between slave and master assembly.

5.7.1. Vertical deflection

Fig. 5.15 shows the comparison of the midspan deflection of the restrained beam. It is evident that reasonable agreement with the test results is achieved by the virtual hybrid simulation. The vertical deflection increases at a constant rate during most of the fire test and no runaway deflection is observed. This is accurately depicted by the numerical model, as shown in Fig. 5.15.

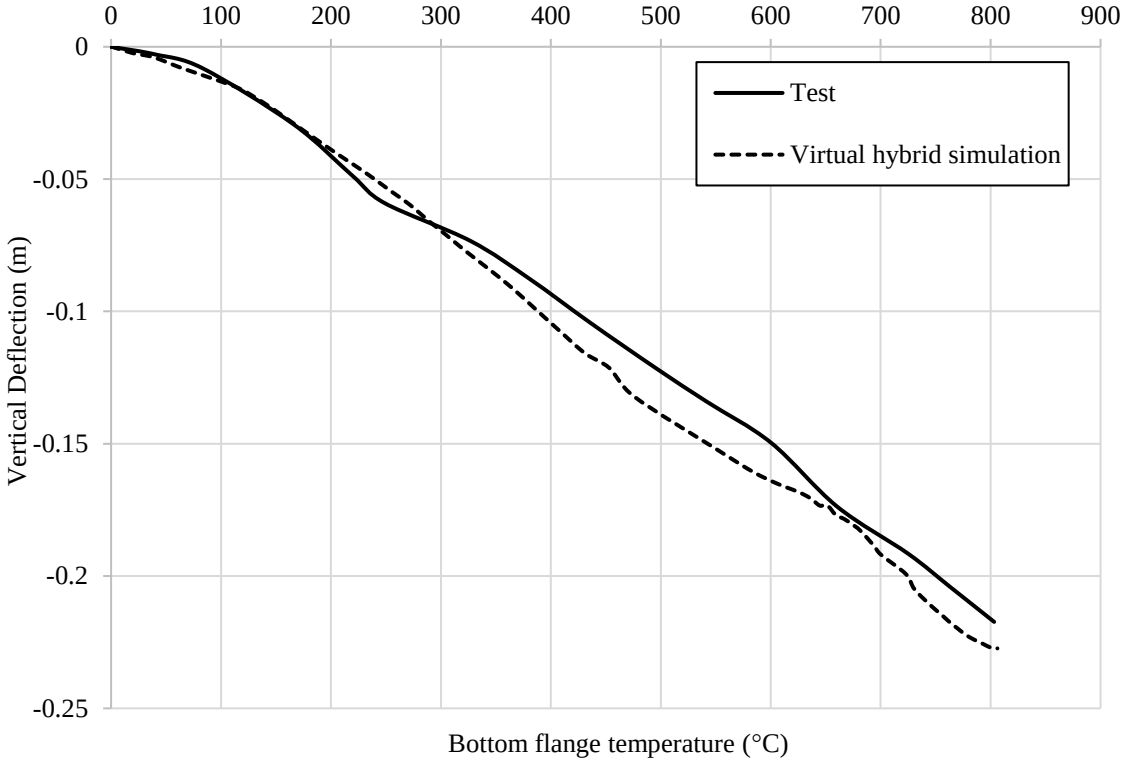

Fig. 5.15 Vertical deflection of the restrained beam at midspan

5.7.2. Horizontal displacement

The horizontal displacement of the column at floor level is also traced and compared with the test results. The plateau in the horizontal displacement of the column demonstrates a very interesting aspect of the behaviour during the test, as shown in Fig. 5.16. In the initial stages of the test, the horizontal displacement of the column increases with temperature, until about 250 °C. Then, it plateaus until around 600 °C after which it begins to increase again. The initial increase in horizontal displacement is dominated by thermal expansion of the steel beam. At about 250 °C, the bottom flange of the steel beam yields and a reduction in the restraint to thermal expansion is observed which results in no further increase in horizontal displacement and is evidenced by the plateau in Fig. 5.16, which is also shown in the OpenSees predictions. The increase in the column horizontal displacement in the second phase is due to the thermal expansion of the concrete slab because the temperature in the slab rises at a relatively slower rate than the steel beam and expands later than the steel beam.

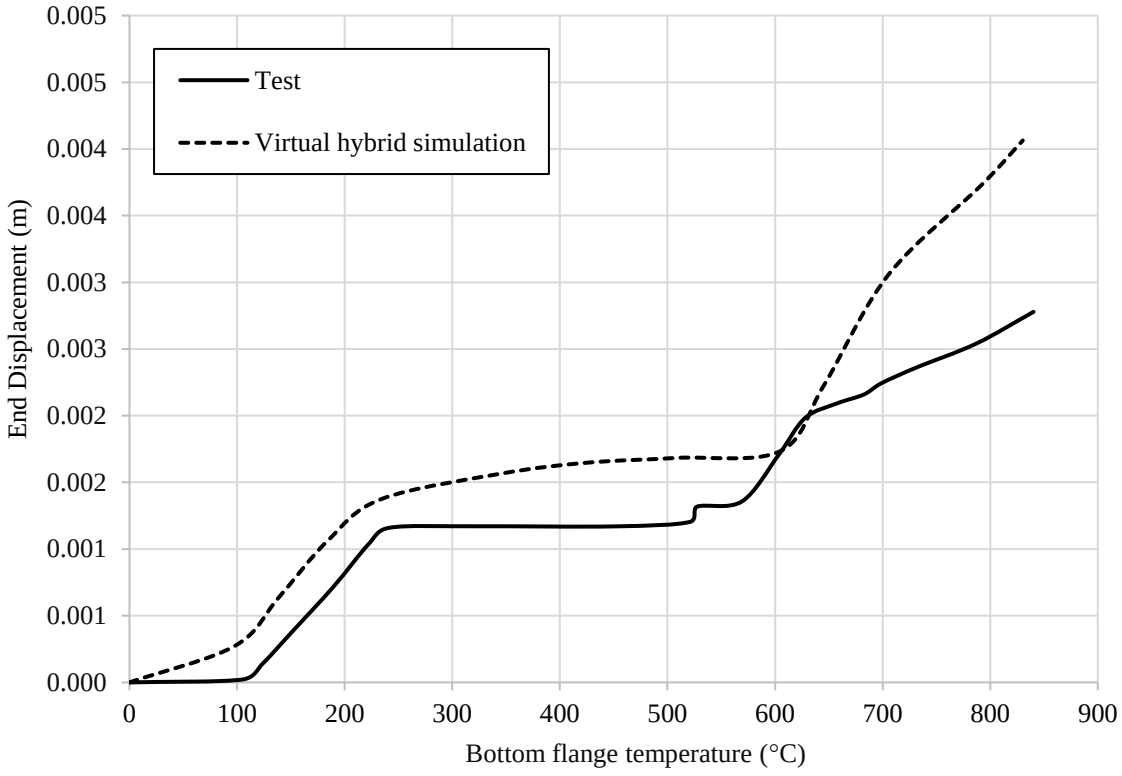

Fig. 5.16 Horizontal displacement at end of the restrained beam

In accordance with the general behaviour expected of restrained beams under fire, when the beam reaches runaway, it behaves as a catenary and the ends of the beam exert an

inward “pull” force on the restraints, which results in a reduction in the horizontal displacement. However, in this case, it can be clearly seen in Fig. 5.15 that the test beam does not experience runaway and the horizontal displacement continues to increase without experiencing any reduction.

5.7.3. Rotation

In addition to the vertical and horizontal displacements, virtual hybrid simulation also predicts the end rotations of the beam during the fire. These values are compared with the corresponding test data (British Steel Plc 1999) in Fig. 5.17, and it is evident that a good agreement has been achieved by the numerical analysis. It is noteworthy, with reference to Figs 5.15-5.17, that the midspan deflection (Fig. 5.15) and end rotations (Fig. 5.17) continue to increase even during the plateau stage in the horizontal displacements (Fig. 5.16). This is because of thermal bowing which develops due to the steep thermal gradient in the composite beam floor system.

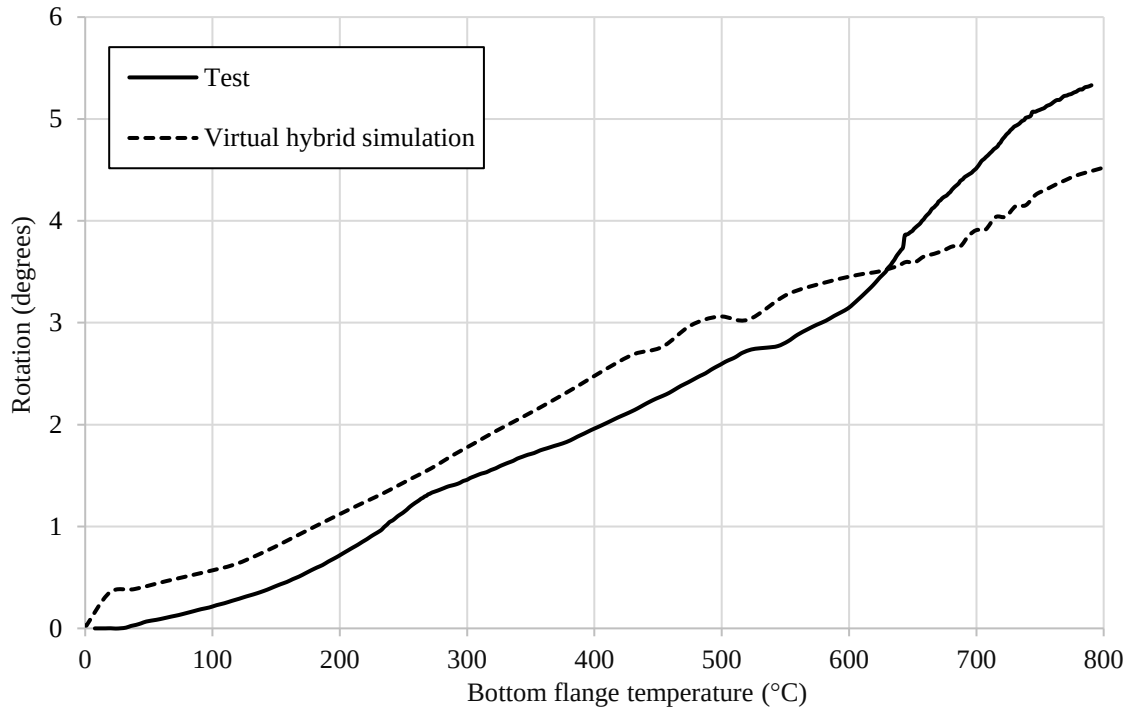

Fig. 5.17 End rotation of the restrained beam

5.8. Concluding remarks

A virtual hybrid simulation approach for thermo-mechanical analysis is established and verified by studying the behaviour of a three bay, three-storey frame under thermal and

mechanical loads. The virtual hybrid simulation approach simulates the actual restraint provided by the unheated structure. The performance of the capacity developed in OpenSees is validated by predicting the midspan deflection of a tested composite beam under thermomechanical loading as part of the Cardington restrained beam test. An additional feature of this analysis is that the tested composite beam is modelled in 3D but taking advantage of the directional nature of the tested element, the rest of the system is reduced to a 2D representation in order to save computation time. Excellent agreement is achieved between the virtual hybrid simulation predictions and the experimental measurements of the midspan deflection of the tested beam and horizontal displacement of the column, which is an excellent measure of the restraint provided by the cold structure. A dimensionally reduced hybrid simulation approach has therefore been established and verified. Next chapters will focus on the modelling of perforated beams exposed to fire using virtual hybrid simulation framework, in order to study the local buckling behaviour.

Chapter 6

Restrained perforated beams exposed to different fire scenarios

6. Introduction

Composite perforated beams are an increasingly popular choice in the construction of long-span floor systems as they provide a structurally and materially efficient design solution and provide space for placement of building services. The behaviour of restrained composite perforated beams with a profiled slab exposed to fire has not been considered in great detail to date and is the focus of the current study. A finite element model is developed utilising the virtual hybrid simulation framework, and the accuracy of the model is validated using available fire test data whereby the temperatures measured during the experiments are directly applied in the numerical model at various locations. The effect of axial and rotational restraints due to the connection type between the beams and columns is also incorporated in the model. Furthermore, the effect of using the different modelling approach i.e., virtual hybrid simulation and isolated beam modelling on the overall beam behaviour is investigated. It is observed that the perforated beams behave differently with different modelling approaches and the virtual hybrid simulation approach predicts the true behaviour of the perforated beams. In the next section of this chapter, the effect of different fire scenarios on the behaviour of perforated beams is assessed. Three fire scenarios are considered, a standard fire, a fast parametric fire and a slow parametric fire.

6.1. Perforated beams in fire

Perforated steel beams are synonymous with modern long-span construction, and are regularly specified in sports arenas, airport terminals and multi-storey buildings. They are typically manufactured either by cutting openings of the desired shape in the web of a hot-rolled steel section or by fabricating the section from steel plates similar to a plate girder. The most popular shapes for the web openings are circular (to give a cellular beam), rectangular, elongated and sinusoidal openings. The solid region between two

adjacent openings is called the web-post, and its dimensions vary depending on the opening arrangement. Perforated beams are often preferred in high-rise buildings to regular I-shaped sections as longer spans can be achieved resulting in large column-free spaces and reduced construction time. In addition, building services such as electrical cables and heating/ventilation pipework can easily pass through the web openings, thus reducing the overall height of the building and requirements for additional materials. It has been noted previously that perforated beams often provide a more economical solution compared with solid beams and result in significantly lower material requirements (Nadjai et al. 2017).

The fire behaviour of structures has been the subject of intensive research in recent decades (British Steel Plc 1999; Dwaikat and Kodur 2011; Li and Guo 2008; Liu et al. 2002) and is particularly topical for high-rise structures at the current time following the fire at Grenfell Tower in London in 2017 (McKenna et al. 2019). Owing to the many complexities involved in fire conditions, most research focusses on the behaviour of isolated structural components, without necessarily including the whole structure in the analysis, usually idealising the effect of the surrounding structure. In fact, the majority of research studies on perforated beams to date have concentrated on beams with simply-supported boundary conditions (Ellobody and Young 2015; Nadjai et al. 2007a, 2016; Wong et al. 2009). This has been a valid and necessary step towards gaining a greater understanding of the behaviour, although it has been noted that the majority of composite perforated beams in practice experience some degree of both axial and rotational restraint (Najafi and Wang 2017a). Moreover, the behaviour of the beams during a fire is very much dependent on the type and magnitude of the restraint developed by the surrounding structure (Najafi and Wang 2017b; a).

In this context, the current study is focused on the fire behaviour of perforated steel beams which are acting compositely with a profiled slab, and have various degrees of axial and/or rotational support. One of the largest studies into restrained perforated beams in fire was conducted at the Czech Technical University and the University of Ulster (Nadjai et al. 2011; Wald et al. 2011). This project included large-scale fire tests as shown in Fig. 6.1 and Fig. 6.2, however some important parameters which give an insight into the overall behaviour such as the beam end displacements were not measured. Further numerical and analytical analyses were conducted in which different levels of axial

restraint were considered and uniform temperature distribution was assumed (Najafi and Wang 2017a; b), but the influence of rotational restraint, composite action due to the slab and different fire scenarios was not included.

Fig. 0.1 Fire test conducted by the Czech Technical University (Wald et al. 2011)

Fig. 0.2 Fire test conducted by the University of Ulster (Nadjai et al. 2011)

6.2. Unrestrained composite perforated beams in fire

Nadjai et al. (2007b) conducted experiments on two simply supported composite cellular beams with symmetric (Beam A) and asymmetric (Beam B) placement of openings. The geometrical detail of both specimens is shown in Fig. 6.3. The steel grade and span length used for both these beams was S355 and 4.5 m respectively. Universal beam section UB406×140×39 was used as top and bottom tees to fabricate the symmetric Beam "A" with an overall depth of 575 mm. Whereas, the asymmetric beam "B" was fabricated using sections UB457×152×52 and UB406×140×39 for the bottom tee and top tee, respectively with an overall depth of 630 mm. A reinforced concrete slab of 150 mm thick and 1200 m wide was constructed over both the beams with 35 N/mm^2 grade of concrete.

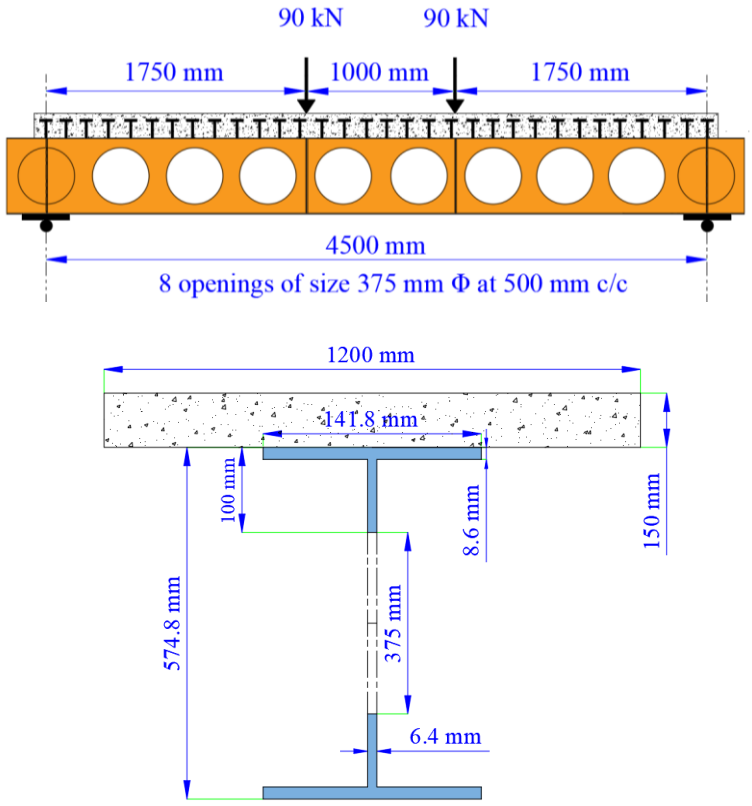

(a)

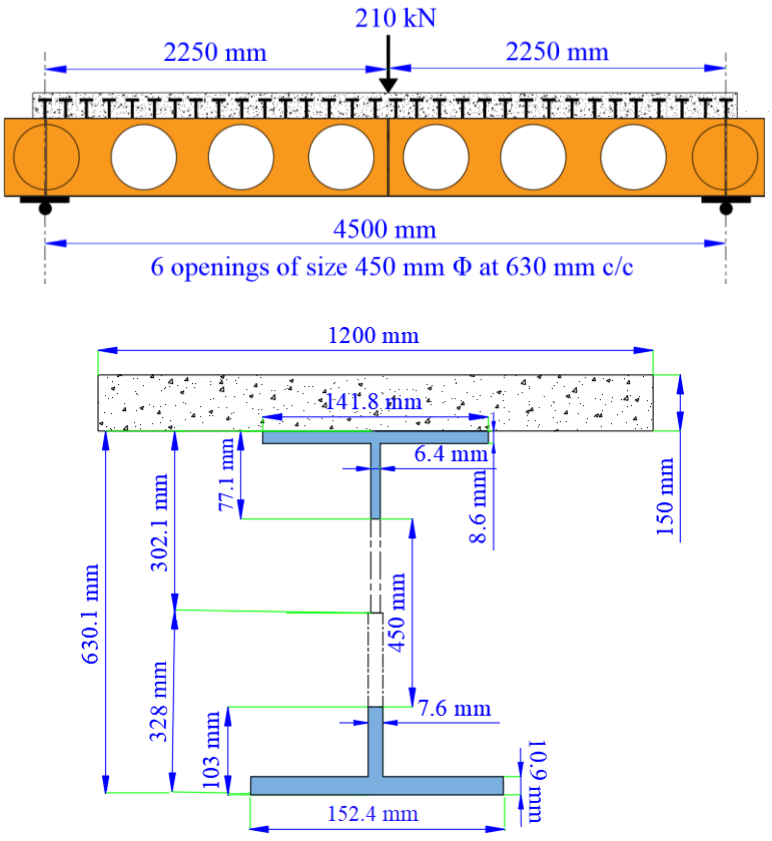

(b)

Fig. 0.3 General arrangements and geometric details of (a) test beam A and (b) test beam B (Nadjai et al. 2007b)

A welded reinforcement mesh A142 with a yield strength of 460 N/mm^2 was provided. Shear connectors of 19 mm diameter and 120 mm height were distributed at 150 mm spacing along the span of the test beams. A full shear connection between the slab and the beam was ensured because of the high density of shear connectors. Beam "A" was subjected to a four-point loading with two concentrated loads of 90 kN each and beam "B" was tested under a three-point loading arrangement with a concentrated load of 210 kN as shown in Fig. 6.3. Web Stiffeners were provided at loading locations and at the supports.

The steel cellular beam is modelled using the thermal shell elements (ShellMITC4Thermal) available in OpenSees. The shape of the openings is approximated to rectangular openings with a size of 170×340 mm for test beam A and 200×400 mm for test beam B in accordance with SCI 355 design guide. The 'J2PlasticityThermal' material model is used for steel cellular beam. The profiled slab is modelled separately using shell elements (ShellMITC4Thermal) for the flat part of the reinforced concrete slab and 3D beam-column elements (DispBeamColumn3DThermal) for the concrete ribs. The DruckerPragerThermal material class is used to model the concrete in the flat part of the slab (modelled using shell elements, which require a biaxial material model) and Concrete02Thermal material class (Jiang et al. 2014) is used for the concrete in the ribs (modelled using beam-column elements, therefore a uniaxial material model is used). The slab reinforcement is modelled using a smeared layer distribution in the shell elements. Since full shear connection was achieved during the tests, the shear connectors are not modelled. Instead, the rigid link element provided in OpenSees is used to connect the steel cellular beam and the concrete slab.

The structure is loaded in two steps. In the first step, the static load is applied while the structure is at ambient temperature. In the second step, the thermal load is applied to the cellular beam maintaining the constant static load. A nonlinear analysis is performed in OpenSees to investigate the behaviour of the cellular beams under fire. The measured temperatures at different locations after 80 minutes of fire exposure are presented in Table 6.1 as reported by Wong et al. (2009). A linear variation of temperatures from the start to 80 minutes of fire exposure is assumed in numerical modelling for all locations (top flange, web, bottom flange, top and bottom of the slab). A linear thermal variation across the depth of the slab is assumed. The temperature-midspan deflection behaviour

of both tests is compared against the simulation results and a reasonable agreement is achieved as shown in Fig. 6.4 and Fig. 6.5.

Table 0.1 Temperatures (°C) of different parts of the test beams after 80 minutes of fire exposure.

Test Beam	Slab top	Slab bottom	Top flange	Web	Bottom flange
A	92	388	520	646	667
B	88	408	511	634	635

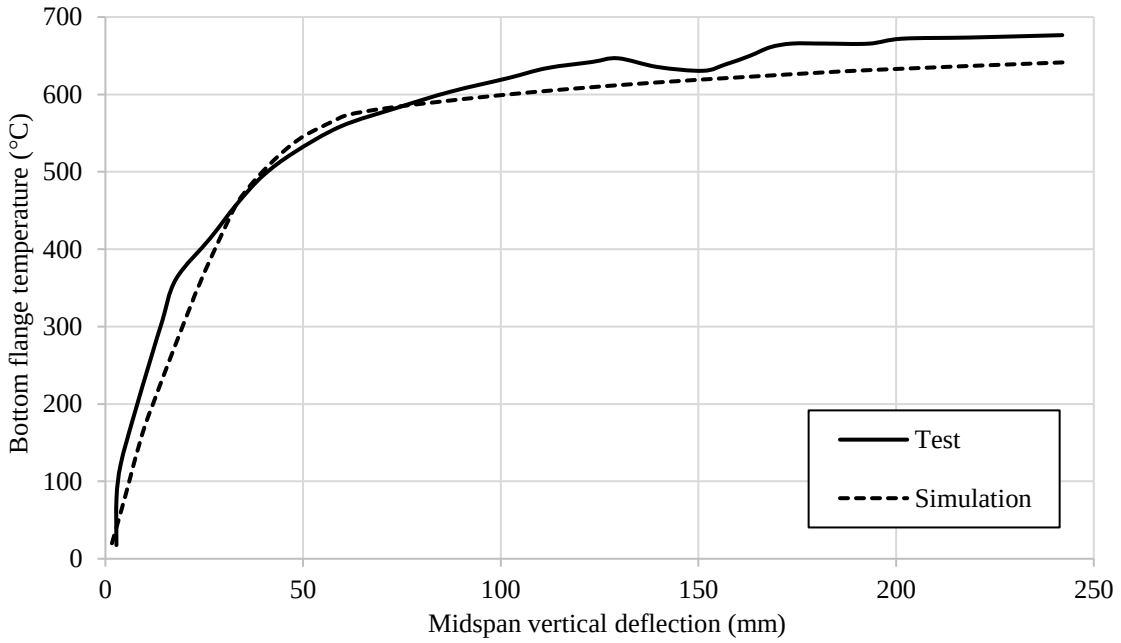

Fig. 0.4 Comparison between simulation results and test results of Nadjai et al. (2007b)-Beam A

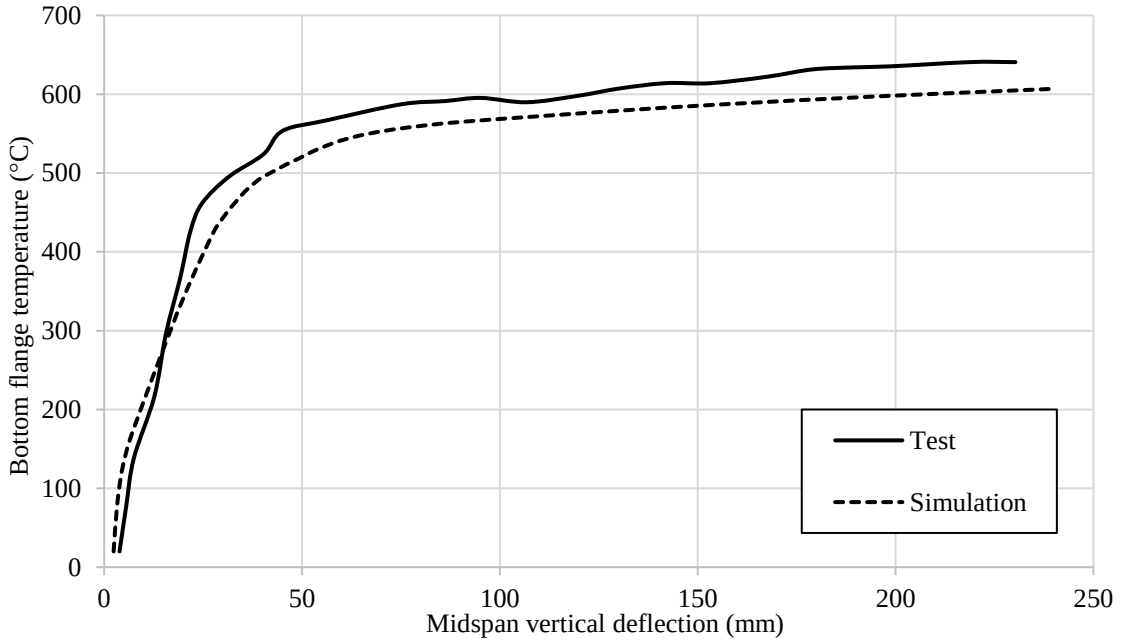

Fig. 0.5 Comparison between simulation results and test results of Nadjai et al. (2007b)-Beam B

6.3. Restrained composite perforated beam validation

In this section, a restrained perforated beam exposed to fire is modelled and validated using the previously explained virtual hybrid simulation framework. In virtual hybrid simulation, the structure is divided into two substructures. The part of the structure which is exposed to fire and expected to experience large deformations is modelled using complex 3D elements (shell and brick elements) in a substructure named the slave assembly whilst the remainder of the structure is modelled using simpler elements (beam-column elements) in another substructure named the master assembly. This section proceeds with the details of the numerical model and validation with the test results.

6.3.1. Numerical modelling

The numerical model is developed based on the fire test at an administrative building in Mokrsko, Poland, which included a composite cellular beam subjected to fire (Wald et al. 2011). The beam was made using an IPE 270 profile with an overall length and depth of 9 m and 395 mm, respectively, using grade S235 steel, and was named AS2 in the study. There were 8 sinusoidal openings at equal spacing along the span. The profiled slab had an overall depth of 120 mm, including a flat portion and ribs which were 60 mm each in depth, and was made using concrete with a compressive strength of 32.5 MPa. The slab was lightly reinforced with 5 mm diameter bars, at 100 mm spacing in both directions, located at the mid-depth of the flat portion of the cross-section. IPE 400 sections were used for the edge beams, also in grade S235 steel, whilst the columns were made using HEB 180 sections.

In the virtual hybrid simulation model, the part of the structure exposed to the fire (i.e. the AS2 composite beam) is represented using high-resolution 3D elements in a slave assembly whilst less detailed elements are employed for the rest of the structure in a master assembly. OpenSees is utilised to model both the slave and master assemblies. The cellular steel beam is modelled using 3D shell elements (ShellMITC4Thermal) available in OpenSees. The composite slab is modelled using 3D beam-column elements for the ribs (3DbeamcolumnThermal), and 3D shell elements (ShellMITC4Thermal) for the flat portion. The reinforcement is modelled using a smeared layer approach. The cellular beam is connected to the slab using link elements called rigidlink in OpenSees. The thermal and mechanical properties for both concrete and steel at elevated temperature are defined in accordance with the Eurocode (EN 1992-1-2 2004; EN 1993-1-2 2005) and

implemented to the model through the material classes available in OpenSees. The J2plasticityThermal material class (Khan et al. 2018) is employed for representing the structural steel response at elevated temperature and the SteelECThermal class is used for the steel reinforcement. For the concrete slab, the Concrete02Thermal and ConcreteDamagedPlasticity material classes which are available in OpenSees are utilised to model the material in the ribs and slab, respectively, at elevated temperature. In the fire test, the openings were sinusoidal in shape. However, in order to simplify the model, the openings are idealised herein as rectangles with equivalent opening areas to the test specimens, in accordance with the guidelines given in SCI P355 design manual (Lawson and Hicks 1998). In the model, each rectangular opening has dimensions of 625 × 250 mm. The remainder of the frame comprising the adjacent primary beams (IPE 400) and columns (HEB 180) are modelled using 3D beam-column elements in the master assembly in OpenSees.

The frame in the master assembly and the composite perforated beam in the slave assembly are connected using a middleware software OpenFresco. Both the substructures are connected at interface nodes. A super-element at the interface nodes in the master assembly and an adapter element at the interface nodes in the slave assembly are defined to connect the two FE assemblies. The communication between the two codes takes place according to a sequence of steps. The sequence of steps in exchanging the data between the master and slave assemblies to perform the virtual hybrid simulation is same as explained in Chapter 5.

The analysis is performed in two stages, similar to the Mokrsko test. In the first stage, a static load of 5.6 kN/m^2 with a load ratio of 0.26 is applied uniformly on the beam. In the second stage, the time-temperature curves obtained from the test are applied at various locations along the beam, in accordance with the available information (see Fig. 6.6) (Wald et al. 2011).

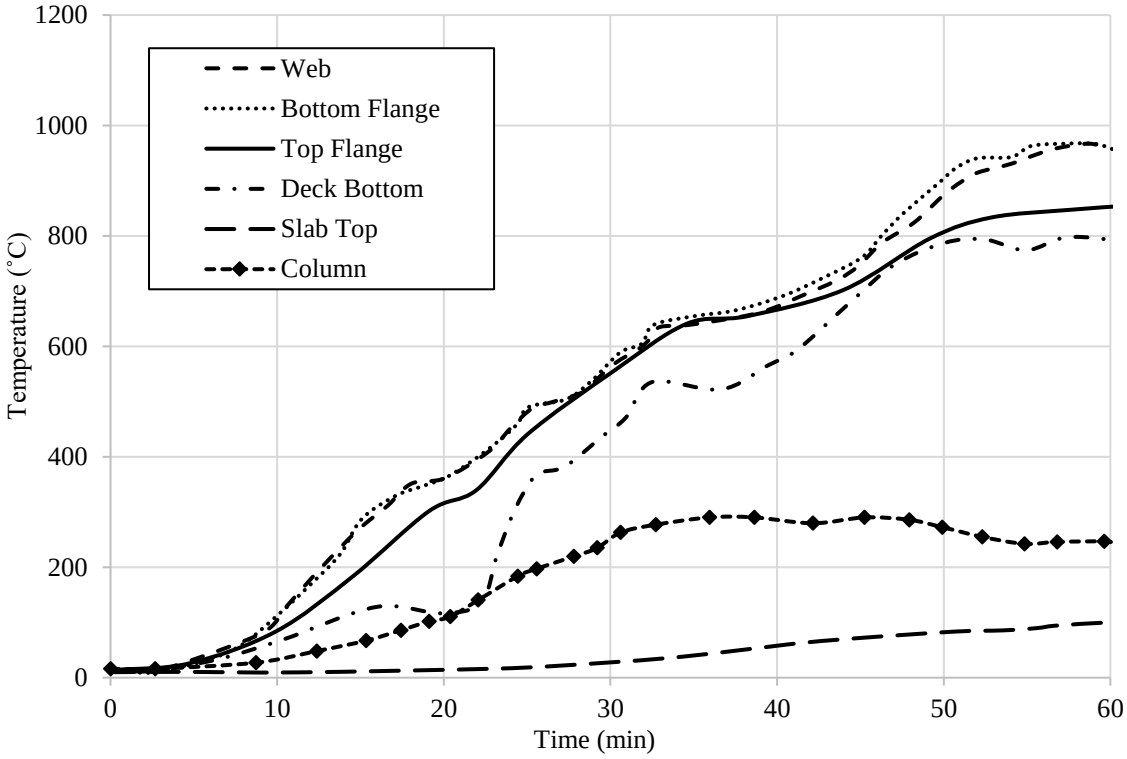

Fig. 0.6 Temperature profile at the various location (Wald et al. 2011)

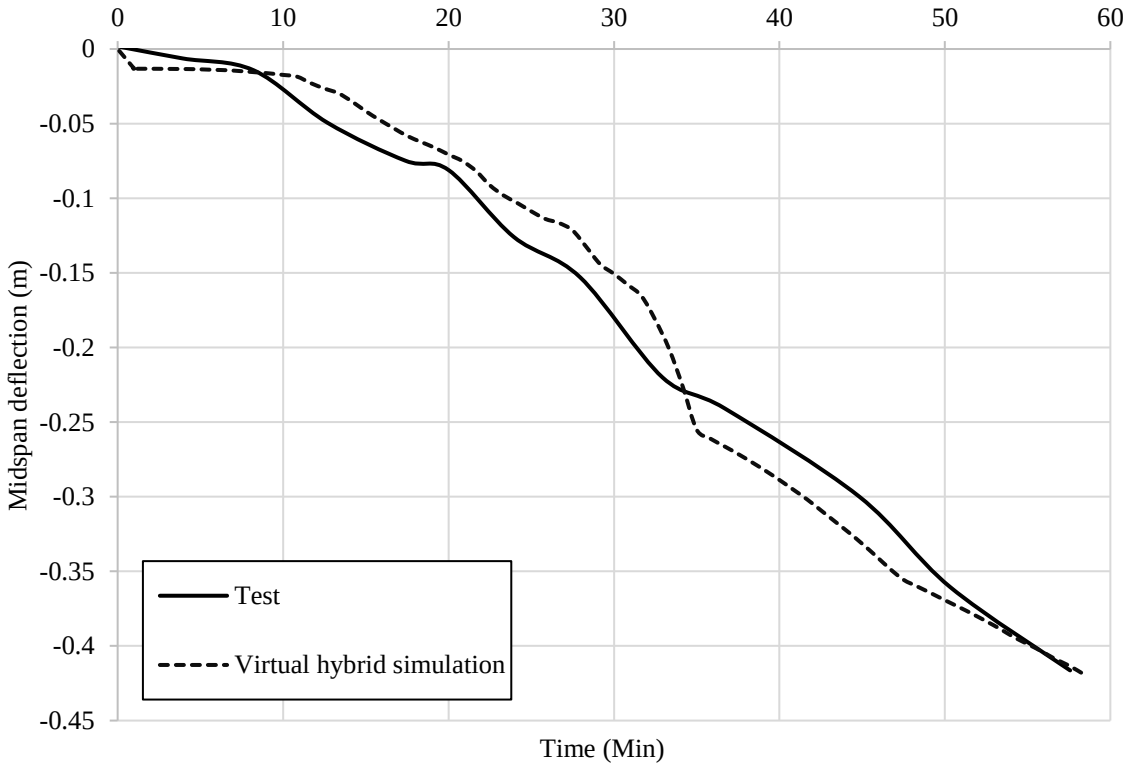

Fig. 0.7 Vertical deflection comparison at midspan

Fig. 6.7 presents the midspan vertical deflections of the restrained composite cellular beam (AS2) with increasing time, as predicted by the numerical simulation together with

the experimental results. It is clear that a reasonable agreement is achieved and the virtual hybrid simulation framework is capable of providing a good prediction of the true response.

6.4. Parametric study

Following the validation of the framework, the effect of using the different modelling approach i.e., virtual hybrid simulation and isolated modelling using simply supported boundary conditions on the overall behaviour of perforated beams in fire conditions is investigated. In terms of the opening arrangements and surrounding structure interaction (modelling approach), four cases are included in the investigation, as follows:

- Case 1: Openings in the centre (bending zone) of a composite perforated beam with axial and rotational support through virtual hybrid simulation;
- Case 2: Openings 500 mm from the end (shear zone) of a composite perforated beam with axial and rotational support through virtual hybrid simulation;
- Case 3: Openings in the centre (bending zone) of a simply supported composite perforated beam; and
- Case 4: Openings 500 mm from the end (shear zone) of a simply supported composite perforated beam.

Fig. 6.8 presents a graphical representation of the beam, indicating the size and positions of the openings. All other section properties are same to the beam modelled in section 6.3.1. All of the cases are analysed in two phases whereby the mechanical load is first applied and this is then followed by the application of thermal loading. The beam in each case is exposed to the same mechanical and thermal loading as experienced by AS2 test beam, as previously described. In terms of investigating the effect of the interaction of the AS2 beam with the surrounding structure, both restrained beams, using virtual hybrid simulation (Case 1 and 2), and simply supported beam arrangements (Case 3 and 4) are considered. For Case 1 and 2, the framework outlined in Chapter 5 of this thesis is utilised. On the other hand, in the simply supported simulations, an isolated simply supported beam is modelled without including the rest of the structure. Another important parameter which is investigated in this chapter is the effect of different fire scenarios. Three fire scenarios are considered for this study, including a standard fire, a slow

parametric fire and a fast parametric fire. The time-temperature curves for the parametric fires are generated in accordance with the Eurocode guidelines (EN 1991-1-2 2005).

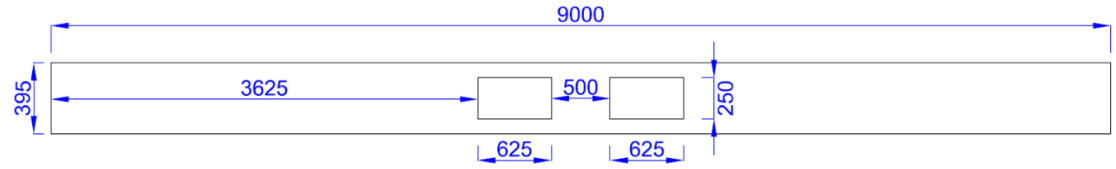

(a)

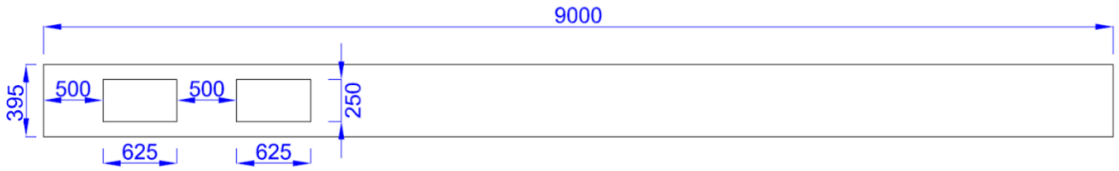

(b)

Fig. 0.8 Opening layout for (a) Case 1 and 3 and (b) Case 2 and 4 (all dimensions are in mm)

6.4.1. Behaviour with virtual hybrid simulation framework

In order to analyse the behaviour of restrained perforated beams simulated using virtual hybrid simulation framework, Fig. 6.9 presents the development of midspan vertical defections as a function of time for both arrangements, while the axial forces in the members is presented in Fig. 6.10. This sub-section focuses only on the effect of axial and rotational restraint provided by virtual hybrid simulation framework by analysing Case 1 and Case 2, whereas the following sub-section deals with simulation of the isolated composite perforate beams, and assesses Case 3 and 4.

Fig. 6.9 illustrates that for Case 1, the beam deflects in an upward direction initially. This behaviour is explained by inspecting the thermal profiles across the depth of the beam (See Fig. 6.6), which show that the temperature in the bottom flange increases at a rapid rate compared with the temperature of the web, top flange and slab. As a result, for the initial 20 minutes, the compressive force that develops in the bottom tee-section of the perforated beam due to the restrained thermal expansion exceeds the combined compressive force, which develops in the top tee and slab, as shown in Fig. 6.10(a). This unbalanced compressive force generates a hogging moment in the beam causing the beam to deflect in an upward direction.

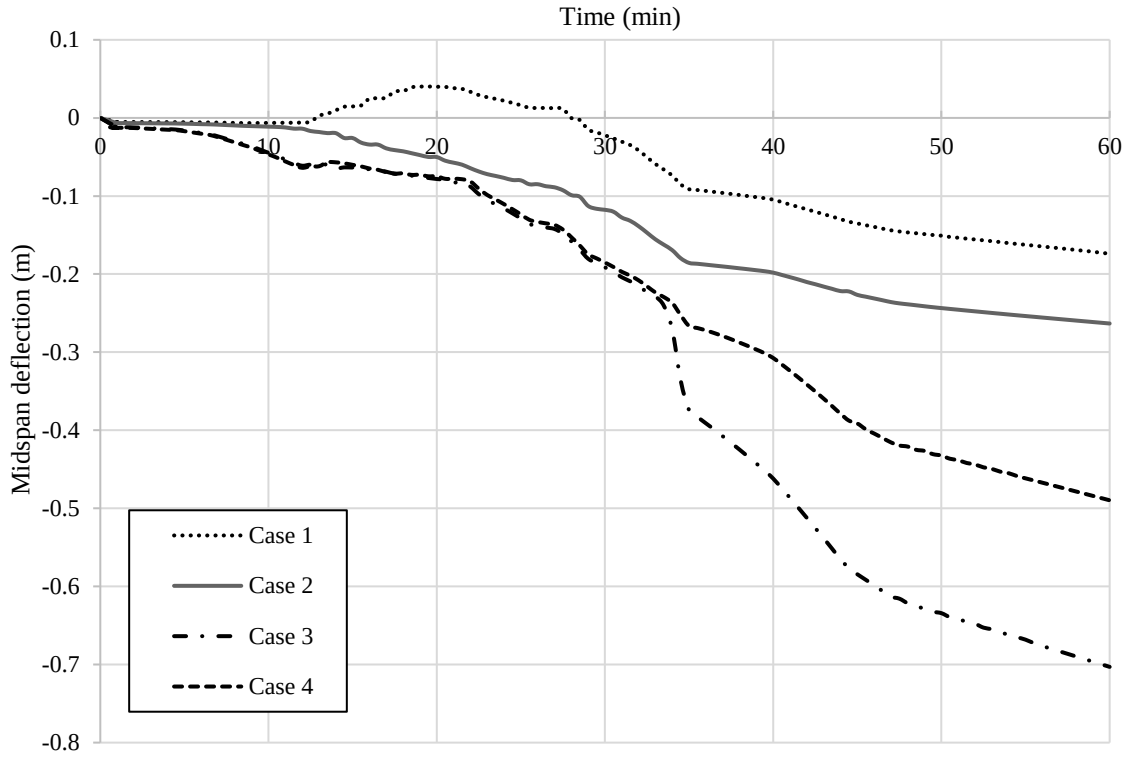

Fig. 0.9 Time-deflection behaviour of various cases

However, at the onset of yielding of the bottom tee under the compressive force, it starts to deflect in the downward direction. The level of ultimate downward deflection is reduced owing to the initial upward movement. On the other hand, for Case 2 the opening is present near the end of the beam in the shear zone and therefore partial axial and rotational restraint develops in this region. The lower levels of compressive and tensile forces for Case 2 compared with Case 1 during the initial phase of the analysis can be seen in Fig. 6.10(a) and (b). As a result of this restraint, any hogging moments which develop are not significant enough to cause upward deflections in the member, as occurred for Case 1.

Therefore, as well as the presence of a solid web at the midsection of the beam, the Case 2 beam deflects downwards for the entire duration of the fire. This behaviour is further shown with reference to Fig. 6.10(a) and (b) for Case 1 and 2, respectively. In addition, Fig. 6.10(b) shows that for most of the duration of the fire, the combined compressive force in the slab and the top flange is greater than the compressive force that develops in the bottom flange of the composite beam. This distribution of forces makes the beam to deflect in a downward direction for the whole of the duration of the fire.

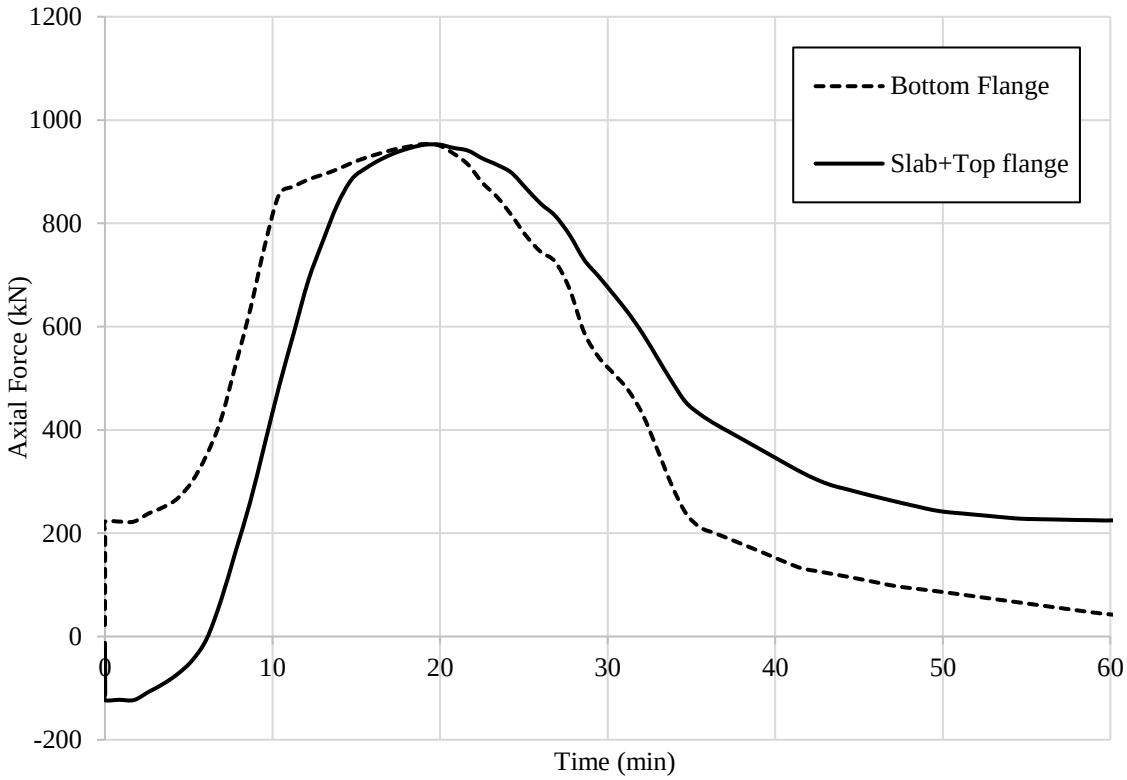

(a)

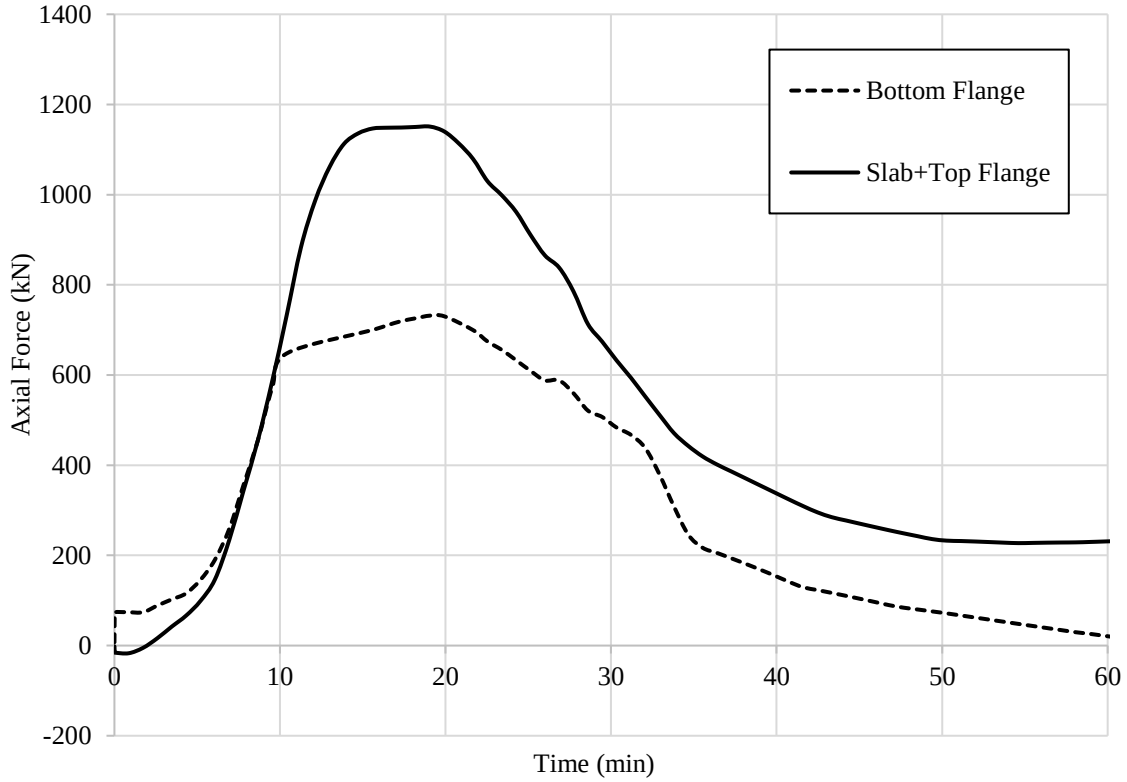

(b)

Fig. 0.10 Time- Axial force behaviour (a) for Case 1 (b) for Case 2

There is a fundamental difference in the behaviour between restrained composite perforated beams with openings in the bending zone (Case 1) and shear zone (Case 2). The Case 2 beams are required to resist larger hogging moments and shear forces compared with the Case 1 beam at the location of the openings, in addition to axial forces and Vierendeel bending. As a result, the beams with openings in the shear zone (Case 2) experience greater midspan deflection and perform in a more critical manner when analysed using virtual hybrid simulation framework. On the other hand, similar beams in the Case 1 arrangement experience lower levels of hogging moments and shear force and no Vierendeel bending develops at the openings location. In this instance, due to the presence of high axial compressive force, a yielding of the bottom tee-section is observed. Based on the data and analysis presented in this section, it is concluded that for restrained composite beams, an improved fire performance is obtained for members that have openings in the bending zone rather than in the shear zone.

6.4.2. Behaviour with simply supported support conditions

In this sub-section, the fire behaviour of restrained composite perforated beams as in Case 1 and 2 are compared with similar beams with simply-supported end conditions (Case 3 and Case 4) as presented in Fig. 6.9. With reference to Fig. 6.9, it is clear that the behaviour is very different, depending on the support conditions. In the analysis of the restrained beams in the previous sub-section, it is shown that members with openings in the shear zone (Case 2) are more critical compared with Case 1, with higher midspan deflections and inferior fire performance. However, for the simply supported members, Case 3 (with openings in the bending zone) exhibits greater midspan deflections and poorer fire resistance compared with Case 4 (openings in the shear zone). The absence of axial and rotational restraint does not allow the development of hogging moments in the simply supported beams. Accordingly, there is no initial upward movement in the Case 3 beam, as was observed in Case 1. Due to the openings at the midspan, the section becomes weak in this region as the temperature rises and the moment resisting capacity decreases which result in greater midspan deflections. This is further shown with reference to the vertical and end displacements presented in Figs. 6.9 and 6.11, respectively, where Case 3 experiences greater vertical deflection but lesser horizontal displacements, compared with Case 4. Therefore, it is concluded that for simply supported perforated composite beams, members with openings in the shear zone perform better in fire conditions, compared with beams that have openings in the middle of the members.

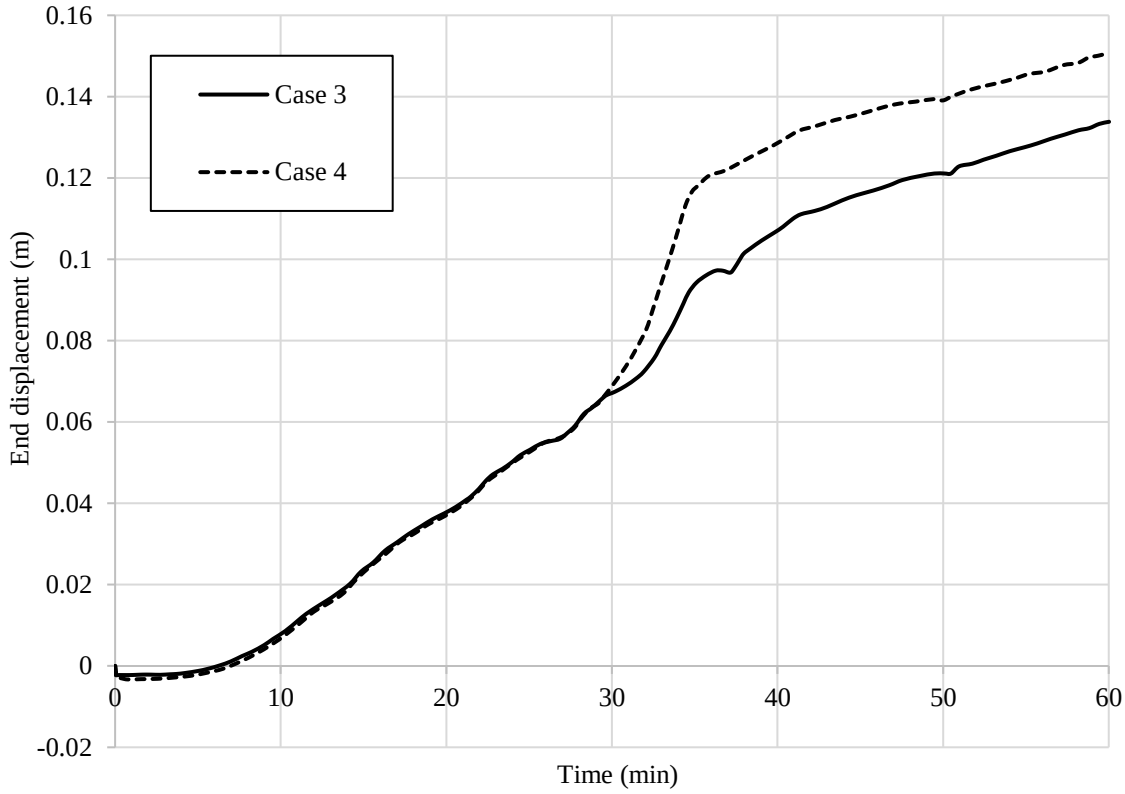

Fig. 0.11 Variation of the end displacement in the member for simply supported beams

It is noteworthy that using different modelling approach can make the same beams behave differently in fire conditions. Moreover, using the correct modelling technique is vitally important to predict the real behaviour of the structural elements. The virtual hybrid simulation approach includes the interaction between the surrounding structure and the fire exposed part of the structure so it provides a more accurate modelling technique to predict the behaviour of structures in fire conditions.

6.5. Effect of different fire scenario

In this section, the virtual hybrid simulation model is employed to assess the behaviour of restrained composite perforated beams exposed to three different types of fire scenario as shown in Fig. 6.12, namely a standard fire, a fast parametric fire and a slow parametric fire. A number of different fire models are available in the literature but these are selected as they are the most commonly found in the research literature and also in design methods (Dwaikat and Kodur 2010) . The parametric fires (both fast and slow) have been generated in accordance with the Eurocodes (EN 1991-1-2 2005) by adopting the following values.

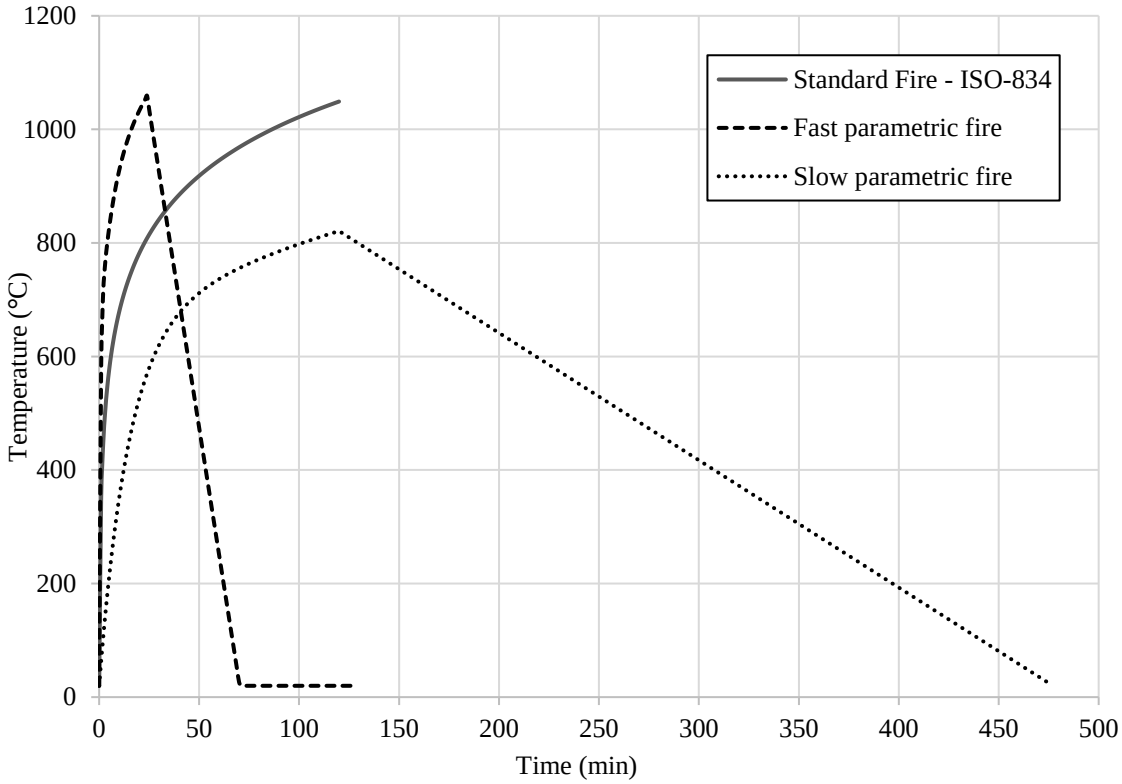

Fig. 0.12 Standard fire and parametric fires

It is assumed that the compartment represents a typical office building and the design value of fire load density ($q_{t,d}$) is 200 MJ/m^2 in both parametric fire scenarios. An opening factor of 0.02 m$^{1/2}$ is used to achieve the slow fire time-temperature curve, which is the minimum value in accordance with the Eurocodes (EN 1991-1-2 2005), whereas for the fast fire exposure a higher opening factor of 0.1 m$^{1/2}$ is used. The density, specific heat and thermal conductivity of the compartment boundaries are represented by the 'b' factor and the value used for both the fire scenarios is 1250 J/M^{2}s$^{1/2}$K. The time-temperature curves for all three fire scenarios, i.e. standard fire, slow parametric fire and a fast parametric fire are shown in Fig. 6.12. As before, the analysis is conducted in two phases. In the first phase, a heat transfer analysis is conducted to determine the temperature history at various locations in the beam and this temperature information is then inputted into to the model and a thermomechanical analysis is completed.

6.5.1. Heat transfer analysis in OpenSees

Heat transfer analysis in OpenSees is based on the finite element method to solve the transient governing equations. In OpenSees, it is conducted by following the flowchart

shown in Fig. 6.13 and the model is created using the required Tcl commands. Following steps are involved in conducting a heat transfer analysis is OpenSees.

(1) First and foremost, the HeatTransfer module is activated to enable the application of the relevant commands and facilities. The argument following the HeatTransfer command defines the number of dimensions that can be either 1D, 2D or 3D, which is useful in cases where the dimension reduction is applied.

(2) Heat transfer mesh (HTmesh) is created in association with HTmaterial and HTEntity, which accepts a wide range of entity types that are linked to the subclasses in the SimpleEntity family. The available types of entities and their usage can be found in detail at OpenSees for Fire website (Liming Jiang 2016). Seed distribution for the mesh can be refined if necessary by providing a vector containing element size and number. The final mesh is completed once HTMeshAll is detected.

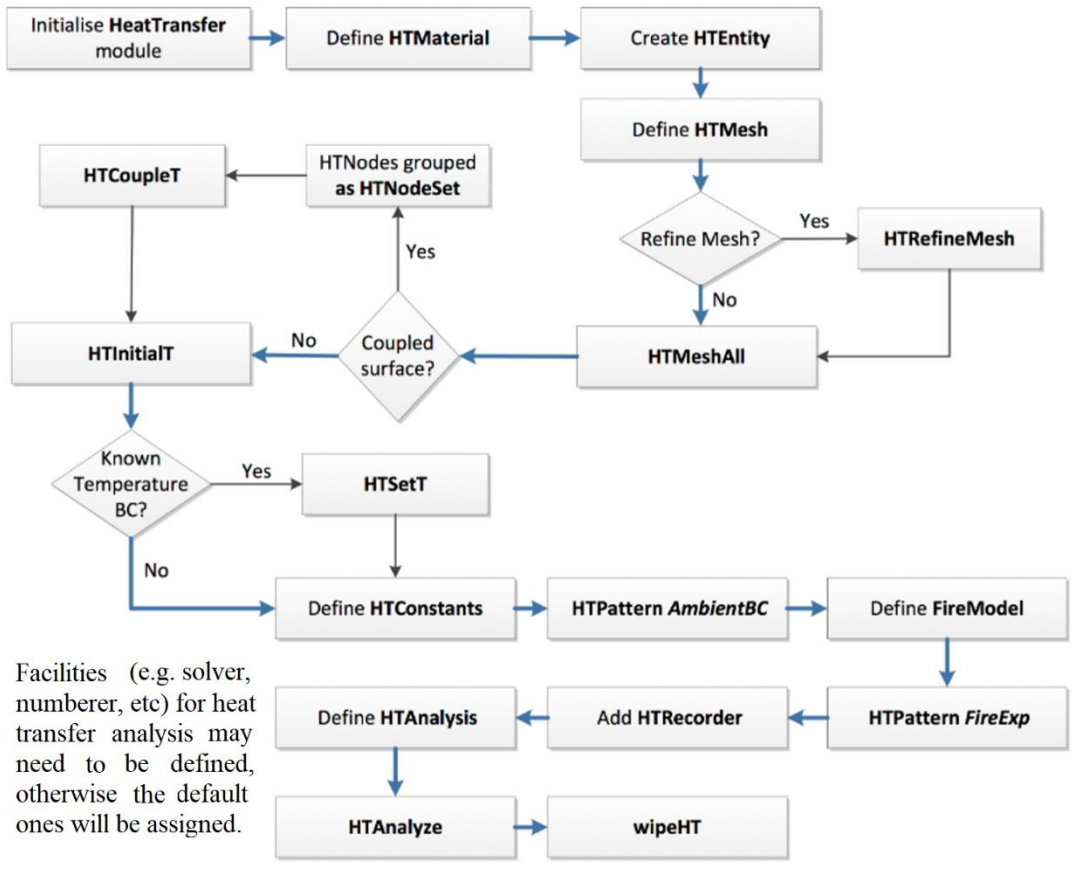

Fig. 0.13 Heat transfer algorithm in OpenSees (Liming Jiang 2016)

(3) This is followed by a few commands to declare the appropriate boundary conditions, as either fixed (HTSetT) or coupled (HTcoupleT) temperatures. Constants are defined before the heat flux boundary conditions are specified which list the coefficient of convection to or from ambient, ambient air temperature and the resultant emissivity of the fire plume.

(4) HTPattern is then used in association with AmbientBC for describing the heat loss to the ambient environment, while the keyword FireExp is used to invoke fire exposure defined as a specified fire model ranging from uniform fire action to localised fire exposure. Before proceeding to heat transfer analysis definition, heat transfer results can be requested via HTRecorder command.

(5) Heat transfer analysis is finally completed after receiving HTAnalyze and thereafter the model can be wiped out using command wipeHT.

6.5.2. Assessment of the heat transfer analysis

A thermal heat transfer analysis has been conducted for all three fire scenarios, resulting in the distribution of elevated temperatures and thermal gradients across the depth of the section. The thermal gradient in a portion or the whole section is determined as the maximum difference in temperature across that element. The results are presented in Figs. 6.14 to 6.16 and it is clear that in a standard fire, the average temperatures and thermal gradients continue to rise for the whole duration of the fire because of the absence of a cooling branch. On the other hand, for the parametric fires, the average temperature as well as the thermal gradient decrease after reaching a maximum value due to the rapid cooling of the steel section compared with the concrete slab. Due to relatively high thermal conductivity, low specific heat and thin elements, the steel section develops very high temperatures and relatively little thermal gradient during any of the three fire scenarios. On the other hand, a more significant thermal gradient develops across the concrete slab and the whole composite beam.

As expected, the greatest thermal gradient is found for the beam subjected to a fast parametric fire. In the first 30 minutes of the fire, the thermal gradient is very high with a maximum temperature difference of 972 °C. This thermal gradient decreases suddenly to a very small value of 206 °C after 80 minutes of fire exposure due to the sharp cooling branch of the fast fire time-temperature curve, as illustrated in Fig. 6.15.

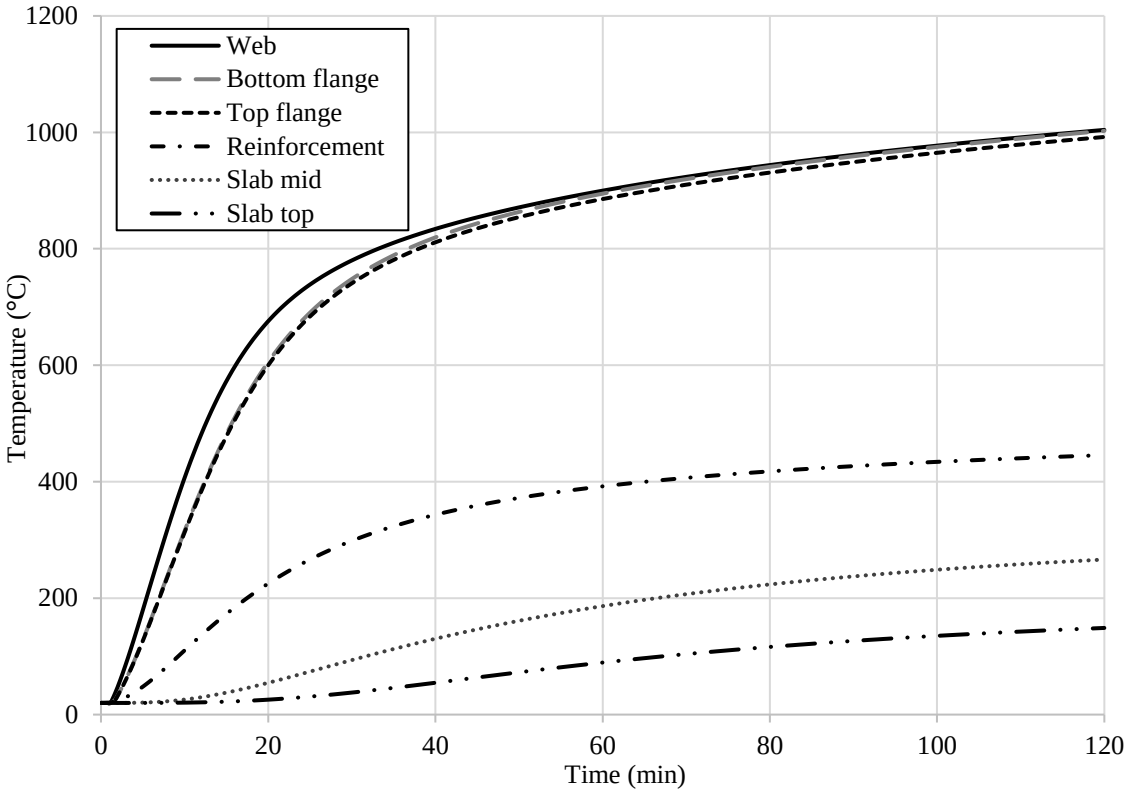

Fig. 0.14 Temperatures at various location of the beam exposed to the standard fire

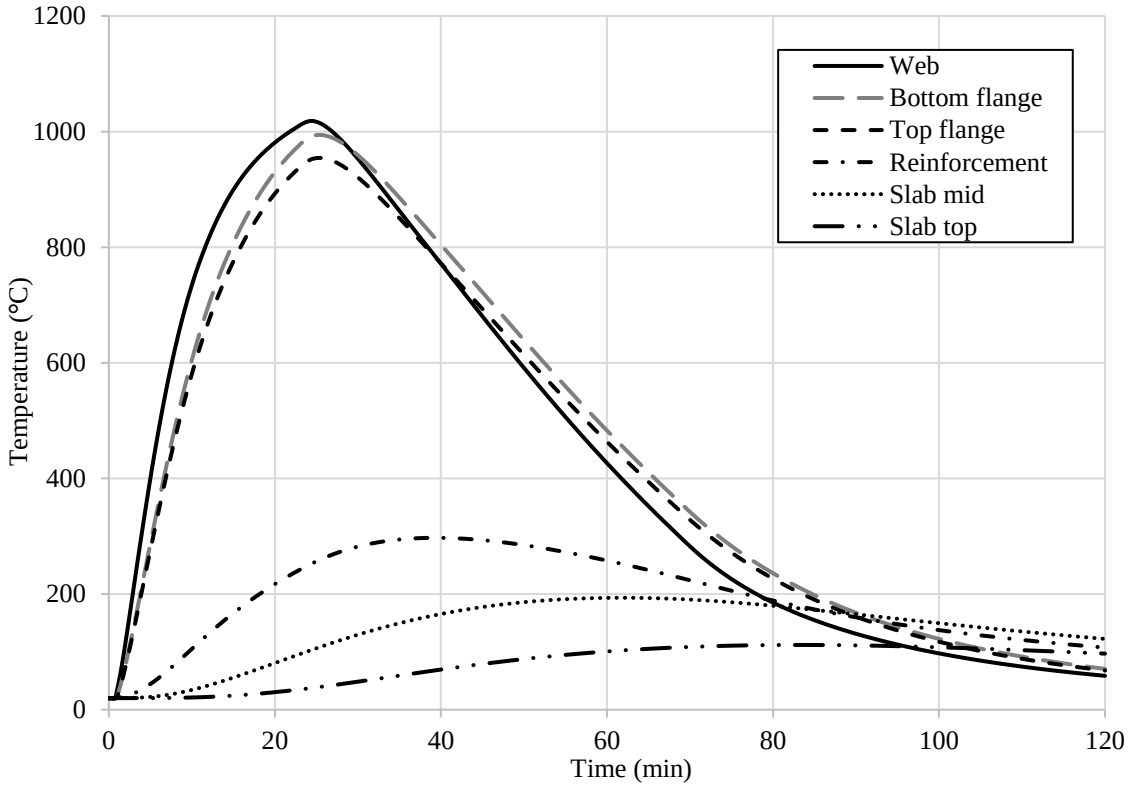

Fig. 0.15 Temperatures at various location of the beam exposed to fast parametric fire

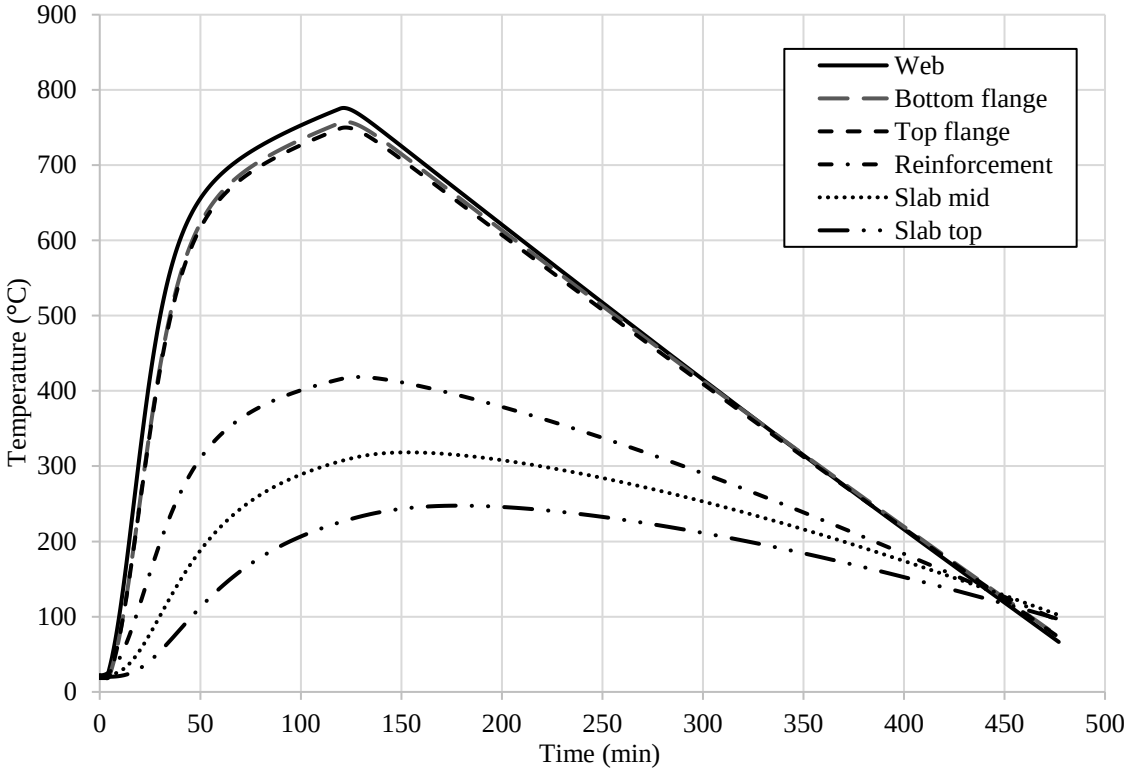

Fig. 0.16 Temperatures at various location of the beam exposed to slow parametric fire

On the other hand, for the standard fire, both the thermal gradient and the average temperature in the section increases for the whole duration of the fire because of the absence of a cooling branch. The maximum temperature difference in this case is 847 °C after 120 minutes of the standard fire exposure, as illustrated in Fig. 6.14. For comparison, it is worth noting that at 30 minutes, the maximum temperature difference is 743 °C, whereas it is 972 °C for the fast parametric fire, and in general, the rate of development of a thermal gradient across the section is slower compared with the fast fire.

When the structure is exposed to a slow parametric fire, the development of the thermal gradient in the section is the least significant of the three scenarios examined. The maximum temperature difference obtained is 532 °C after 120 minutes of heating as shown in Fig. 6.16. After 30 minutes, the temperature difference is 452 °C. In the cooling phase, greater average temperatures and thermal gradients are observed in the slow parametric fire compared with the fast fire, owing to a slower rate of cooling.

6.5.3. The thermomechanical analysis

The effect of different fire scenarios on the structural response of the restrained composite perforated beams is analysed in terms of the midspan deflections predicted for the

standard and parametric fire exposures. The failure criteria employed herein are adopted based on the British Standard (BS 476-20 1987), and employ a deflection limit of L/20 and limit rate of deflection, where L is the length of the beam. Fig. 6.17 presents the time versus midspan deflection behaviour for perforated beams with openings in the bending zone which are exposed to different fire scenarios. It is clear that the fast parametric fire leads to the greatest levels of deflection, followed by the standard fire whilst the slow parametric fire generally results in the lowest defections.

As stated before, Case 1 beams experience an initial upward deflection due to the development of a thermal gradient in the section. Due to the relatively high average temperature and thermal gradients, the midspan deflections for the structure exposed to a fast parametric fire is greater than for the other fire types for most of the fire duration. The maximum deflection obtained during the heating branch of fast fire exposure is 262 mm. On the other hand, for the slow fire exposure, the midspan deflections are significantly lower than for the fast parametric or standard fire which is attributed to the lower thermal gradient and lower average temperature. The deflection limit of 450 mm, corresponding to L/20, is reached after 64 and 80 minutes for the fast parametric and standard fires, respectively. The maximum deflection obtained for the slow parametric fire is 100 mm and it does not reach limiting deflection as shown in Fig. 6.17. A runaway deflection is observed only in the case of standard fire exposure, and this occurs after 95 minutes. Due to the continual increase of the average temperature of the section in the standard fire, the strength of concrete and steel are reduced significantly which results in a runaway deflection.

As shown in Fig. 6.18, similar behaviour is observed for beams with openings in the shear zone although the beams reach to the limiting deflection and runaway failure at an earlier point. The limiting deflections are reached after 60 and 65 minutes for the fast parametric and standard fire exposures, respectively. For both fire exposures, the Case 2 beams reaches the limiting deflection prior to the Case 1 beam. Again, the beam exposed to slow parametric fire does not reach the limiting deflection and the maximum deflection is 205 mm when the openings are in the shear zone compared with 100 mm for the members with openings in the bending zone. It is noteworthy that only the beam subjected to a standard fire experiences runaway failure which occurs after 73 minutes.

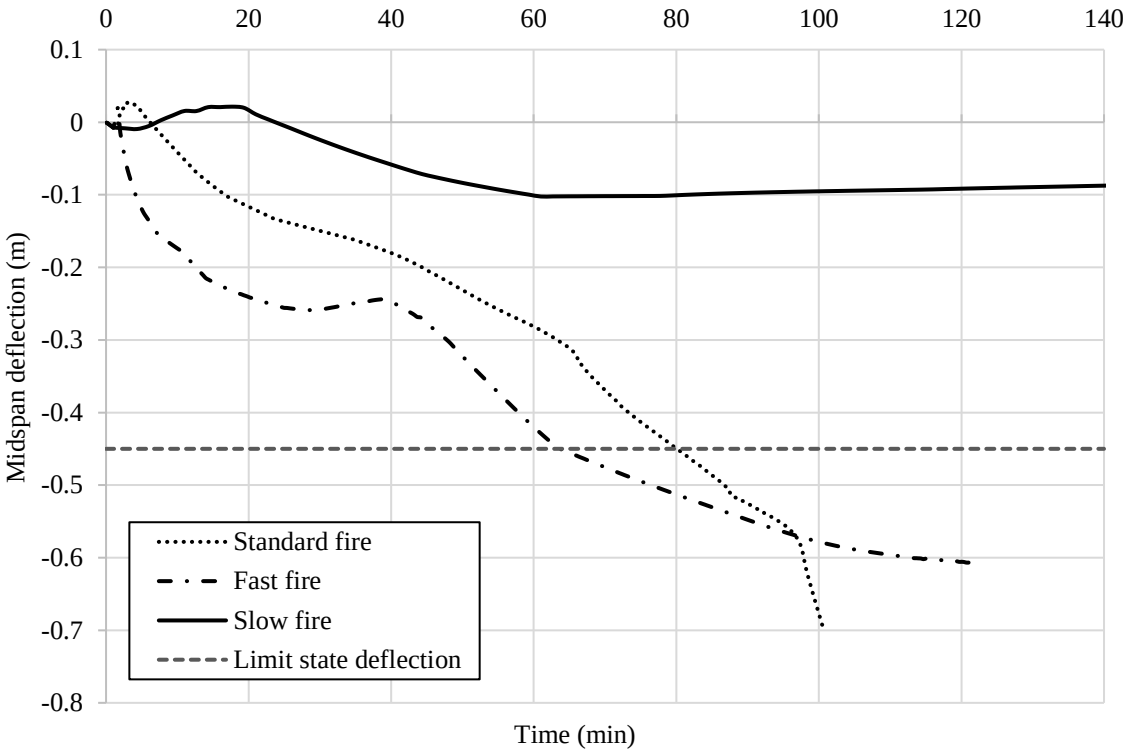

Fig. 0.17 Midspan deflection of the beam with the openings in the bending zone for different fire exposures

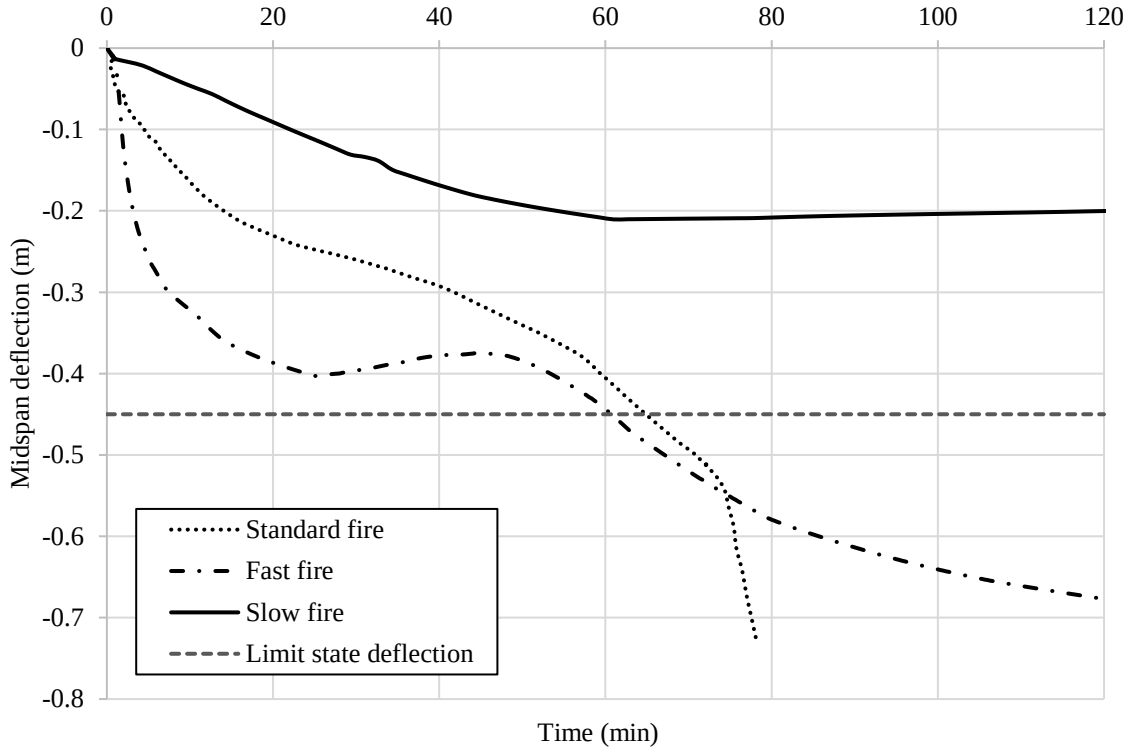

Fig. 0.18 Midspan deflection of the beam with openings in the shear zone for different fire exposures

In summary, it is clear that during the initial stages of fire, the behaviour of composite perforated beams is governed by the rate of heating and the thermal gradients that develop in the section. Greater thermal gradients result in higher midspan deflections and earlier attainment of the prescribed deflection limits. On the other hand, the ultimate failure of composite perforated beams is mainly governed by the average temperature of the section which reduces the overall strength of the section and causes a collapse in the form of runaway deflection. This implies that the structural response of composite perforated beams is a function of the average temperatures and thermal gradient across the composite beam section.

6.6. Concluding remarks

This chapter presents a study of the behaviour of restrained perforated beams exposed to fire using a virtual hybrid simulation technique. Simply supported boundary conditions are also assessed, using a straight forward, single-analysis, finite element model. For the restrained beams simulated using the virtual hybrid simulation technique, compressive forces develop initially in the whole section and, as the material properties gradually degrade, the distribution of forces returns to its original state, which is compression at the top and tension in the lower portion of the beam, at the midspan. The combined effect of bending moments, shear forces, axial forces and Vierendeel bending results in the beams with openings in the shear zone (Case 2) perform in a more critical manner for the restrained beams. On the other hand, for beams simulated with simply-supported boundary conditions, the nature of the force distribution in the cross-section remains the same throughout the fire, which is compression in the top portion and tension in the lower section. For the simply-supported beams, the beams with openings in the bending zone (Case 3) experience higher midspan deflections and have less fire resistance compared with the beams with openings in the shear zone, which is converse to the findings for the virtual hybrid simulation framework. It is concluded that the virtual hybrid simulation framework represents the whole system behaviour, so it is closer to reality and provides a more accurate modelling approach compared to the modelling of isolated structural component without considering the effects of the surrounding structure. Finally, the effect of different fire scenarios on the perforated beams modelled using virtual hybrid simulation framework is analysed. It is shown that during the initial stages of a fire, the thermal gradient developed across the section is greatly influenced by the fire model which is used in the numerical analysis. Of the three different fire scenarios studied

herein, due to high average temperature and thermal gradient, the fast parametric fire results in greater midspan deflections during the heating phase and the beams reach the limiting deflection earlier than for the standard fire or the slow parametric fire. In both cases, the limiting deflection is not achieved when the beams are exposed to a slow parametric fire. The strength reduction of concrete and steel in standard fire exposure is significant due to the continual increase in the temperature. Consequently, for both locations of openings, a runaway deflection is observed only in the case of a standard fire exposure. It is concluded that the structural response of composite perforated beams in fire is a function of the thermal gradient across the composite beam section and the average temperature of the section.

Chapter 7

Fire response of restrained perforated beams using a modified virtual hybrid simulation framework

7. Introduction

This chapter is concerned with the behaviour of restrained perforated beams acting compositely with a profiled slab during a fire. In this work, a modified virtual hybrid simulation approach is adopted using a combination of the OpenSees, Abaqus and OpenFresco softwares. This framework is a further development of the framework used in chapter 5. In this chapter, the 3D model of the perforated beam is prepared in Abaqus software. Abaqus is used because the material and element library available in Abaqus for elevated temperature is well defined and widely used by many researchers. The non-linear model prepared in Abaqus is capable of capturing all the important failure modes associated with perforated beams in fire conditions i.e., web-post buckling, lateral movement of the web, top and bottom tee buckling, yielding of the top and bottom tee, concrete crushing and Vierendeel bending. The accuracy of the model is validated using available fire test data whereby the temperatures measured during the experiments are directly applied in the numerical model at various locations. The axial force developed at the beam interface is investigated and its variation with time helps in understanding the overall behaviour of the perforated beams. Furthermore, this approach is employed to study a number of salient parameters, including load level, material grade and the location of the openings. Various local and global failure modes are observed during the analysis including flexural and shear failure, failure of the web-post, concrete crushing and also a Vierendeel mechanism.

In the final section of this chapter, the analytical model proposed by Steel Construction Institute SCI P355 (Lawson and Hicks 1998) for composite perforated beams at ambient temperature is discussed and modified for elevated temperature by implementing the strength reduction factors of concrete and steel in accordance with Eurocode (EN-1994-

1-2 2005). The fire resistance of the analysed beams is compared with the values obtained from the analytical model. Due to the consideration of restraint forces, which are not included in the design codes, the resistances predicted by the finite element simulations are more favourable. It is found that the distribution of the openings along the span and also the axial restraint have a considerable effect on the time-displacement behaviour, axial reactions, web-post buckling behaviour as well as the overall fire performance of the perforated beam.

7.1. Modified virtual hybrid simulation framework in fire

In this chapter, the 3D model of the composite perforated beam (slave assembly) is now being modelled in Abaqus. The 3D assembly which is expected to experience large deformations or whose fire performance needs to be evaluated in fine detail is modelled in Abaqus and is known as the slave assembly. The rest of the structure is modelled using a standard FE software in the other assembly which is referred to as the master assembly in OpenSees. Both assemblies interact with each other at each time step using a communication software e.g., OpenFresco. Typically, performing a modified virtual hybrid simulation in fire will involve the following three steps:

(1) The master assembly in OpenSees is started and calculates the displacements and rotations at the interface for the first time-step.

(2) These displacements and rotations are applied to the 3D slave assembly in Abaqus through the middleware software (OpenFresco).

(3) The reaction forces and moments as a result of the applied displacement and rotations in the slave assembly in Abaqus are recorded at the interface nodes then fed back to the master assembly in OpenSees to perform the next integration step and determine the new set of displacements and rotations. These steps are repeated until the end of the simulation.

Using this technique, researchers are able to apply real boundary conditions owing to the surrounding structure to the specimen exposed to fire and obtain an accurate depiction of the whole system behaviour. Once numerically validated, this approach could be used to perform experiments involving hybrid simulations in fire conditions. Although this approach is relatively common in seismic engineering, there are few examples in the literature of hybrid simulation being applied to analyse structures exposed to fire.

Mostafaei (2013) conducted a hybrid analysis of a reinforced concrete frame, including a fire test of the first floor central column. The rest of the structure was modelled in the non-linear finite element software SAFIR (Nwosu et al. 1999). Utilising the symmetry of the structure, the substructures interacted with each other through manual control of the axial force at the column ends. The interaction between the physical and numerical substructures was not automatic but was user-controlled, meaning that the user paused the physical test every five minutes to log the numerical data and then the simulation was re-started. The accuracy of this approach was compromised due to the manual nature of the test.

Hybrid simulation in a real fire testing scenario is very complex, particularly if it is necessary to apply manual control to more than one interface. There are up to six unknowns (i.e. degrees of freedom in the NS and forces and moments in the PS) requiring control and communication at each interface. Manual control of these quantities increases the complexity of the tests and can introduce error into the process. So, before conducting a hybrid simulation in fire it is necessary to establish a hybrid simulation framework in a numerical environment. This means replacing the physical testing element of the hybrid simulation with another numerical model which uses high resolution elements such as 3D shell and brick elements to create a so-called virtual hybrid simulation approach. The successful implementation of a virtual hybrid simulation framework eliminates the requirement for manual involvement between the two assemblies and this system can then be employed with a physical substructure in place of the detailed FE model in future work. In this approach, a multiple number of responses can be controlled and communicated at the interface between the two assemblies.

In the previous chapters, a virtual hybrid simulation framework is established using OpenSees and OpenFresco. This framework is utilised to study the behaviour of composite solid beams and composite perforated beams in fire. There are various failure modes associated with the perforated beams in fire conditions such as flange buckling, web-post buckling, concrete crushing and Vierendeel bending. To understand the true behaviour of the perforated beams at elevated temperature, these failure modes need to be traced accurately. Various failure modes and behavioural aspects (catenary action) are difficult to capture with the existing modelling capabilities of OpenSees in 3D module, i.e. solid elements in OpenSees are not yet developed to be used at elevated temperature

and lack of a visual interface. So, the 3D slave model of the perforated beams is required to be modelled in much detail with geometrically non-linear shell elements for the steel beam and solid elements for the concrete slab to achieve an accurate simulation. Abaqus is widely used to model the behaviour of structural components in fire conditions. So, in this chapter, the 3D slave model of the perforated beam is modelled in greater depth using Abaqus while the surrounding structure (master assembly) is modelled in OpenSees. In this technique, two different finite element software are coupled together to utilise their distinct modelling capabilities and results in a modified virtual hybrid simulation framework. In the future, the travelling fire feature of the OpenSees can be utilised in combination with the 3D modelling capabilities of Abaqus or other finite element software. The detail of the numerical modelling and implementation of this approach using Abaqus and OpenSees is provided in the next section.

7.1.1. Implementation of the modified virtual hybrid simulation framework

The modified virtual hybrid simulation modelling approach is validated using the fire test which was conducted on an administrative building in Mokrsko by the Czech Technical University (Wald et al. 2011). This included a composite cellular beam which was subjected to fire, known as the AS4 composite cellular beam (Wald et al. 2011). Beam AS4 was made using an IPE 270 I-beam in grade S235 steel which was cut to create sinusoidal openings giving an overall depth of 395 mm. The concrete slab had an overall depth of 120 mm, comprising a flat portion and ribs which were 60 mm each in depth, as shown in Fig. 7.1. The compressive strength of the concrete was 32.5 N/mm^2 with a mass density of 2400 kg/m^3. The slab reinforcement was located at the mid-depth of the flat portion, was 5 mm in diameter and was positioned at 100 mm centres in both directions. IPE 400 sections were used for the edge beams, also in grade S235 steel whilst the columns were made using HEB 180 sections.

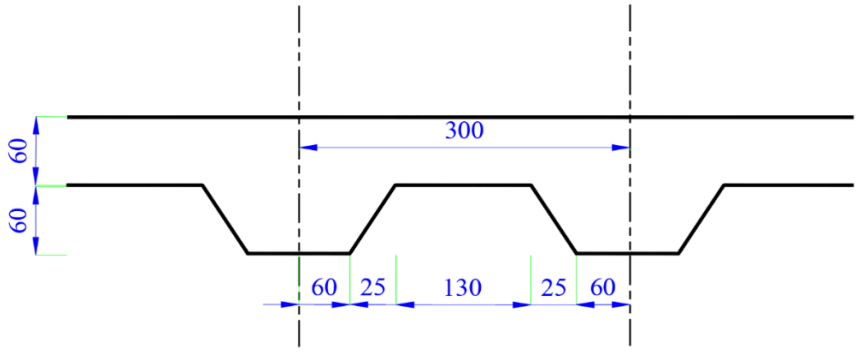

Fig. 7.1 Profiled deck slab (all dimensions are in mm)

The test was performed in two stages. Firstly, a mechanical load of 5.6 kN/m^2 was applied uniformly to the floor, representing a load ratio of 0.26. Then, the load was maintained at a constant level whilst the elevated temperature was applied as represented in Fig. 7.2 (Wald et al. 2011). In order to represent this test arrangement in the modified virtual hybrid simulation, the perforated beam AS4 is modelled using complex 3D elements in a slave assembly in Abaqus whilst less detailed elements are utilised to model the rest of the structure in the master assembly in Opensees. The schematic for both master and slave assemblies is shown in Fig. 7.3. The steel beam is represented using S4R shell elements which are available in the Abaqus library, and each element is 25 × 25 mm in size, based on a mesh sensitivity study. The concrete slab is modelled using C3D8R solid elements while the reinforcement is modelled using T3D2 truss elements. The steel decking is not included in the model as it is not expected to have a significant influence on the fire behaviour. The connection between the perforated beam and the deck slab is represented using the tie constraint in Abaqus. In terms of material modelling, it is assumed that the steel behaves in an elastic-plastic manner whilst the concrete damaged plasticity model is employed to represent the concrete. The stress-strain relationship for both concrete and steel at elevated temperature is adopted from the Eurocode (EN 1992-1-2 2004; EN 1993-1-2 2005). For the thermal properties, constant values of 0.000014 /°C and 0.000009 /°C are used for the coefficient of thermal expansion of steel and concrete, respectively. The remainder of the frame comprising the edge beams and the adjacent beams (IPE 400) and columns (HEB 180) is modelled using 3D beam-column elements in the master assembly in OpenSees.

At the interface between the master and slave assemblies, OpenFresco requires that an adapter element and a super element are defined in the slave and master assemblies, respectively. For the 2-node adapter element in the slave assembly, the nodes at the left and right of the perforated beam are constrained as shown in Fig. 7.3. The distributing coupling constraint type available in Abaqus is utilised to constrain the nodes at the interface and a user-defined element of type U1 is defined between the two reference nodes. This element effectively applies the displacements and rotations at the interface degrees of freedom of the perforated beam. A very high stiffness value of 1×10^{12} N/mm is employed for the diagonal element of the stiffness matrix to ensure that the boundary conditions are accurately represented (Schellenberg et al. 2008b). The kinematic compatibility of the approach has already been described in more detail in Chapter 5.

Similarly, a 2-node super element is defined at the interface nodes in the master assembly. The initial stiffness matrix for the super element is defined by applying a unit displacement to the perforated beam model in Abaqus and measuring the resulting force. As in the test, the analysis is performed in two stages, with a mechanical load applied first, followed by the thermal loading.

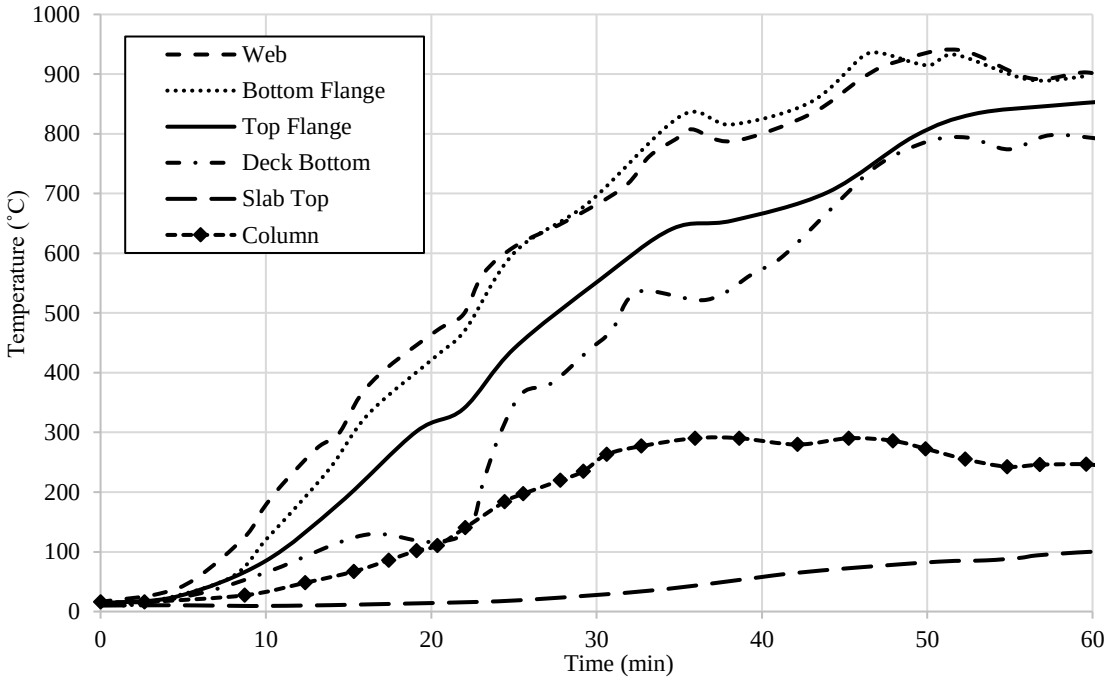

Fig. 7.2 Temperature profile at the various location (Wald et al. 2011)

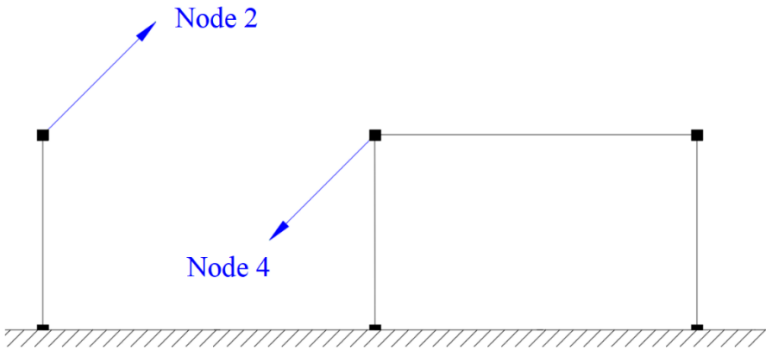

Master structure

Slave structure

Fig. 7.3 Sub-structuring for modified virtual hybrid simulation

During the simulation, firstly the displacements at the interface nodes are determined in the master assembly. Then, these displacements are communicated and applied at the interface nodes in the slave assembly. The reaction forces are calculated in the slave assembly and applied at the interface nodes of the master assembly for the determination of the new displacement. The communication between the two codes and the development of the framework is presented in Fig. 7.4 and the sequence of steps involved in the communication are the same as described in Chapter 5.

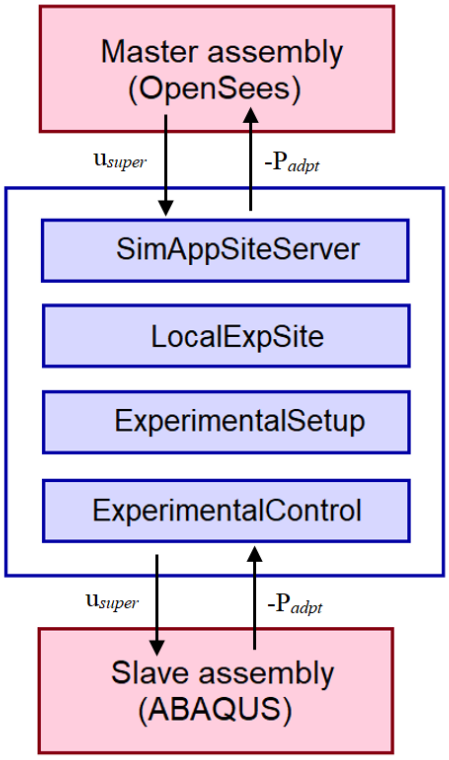

Fig. 7.4 Sequence of operations and data exchange

7.1.2. Validation

In this section, the modified virtual hybrid simulation approach is applied to the experiment conducted at Mokrsko and described previously (Wald et al. 2011). Fig. 7.5 presents the deformed shape of (a) the test beam and (b) the finite element simulation. The images show that during the fire, the bottom flange of the beam displaced laterally which caused the steel web to bend. Meanwhile, the top flange was restrained by the composite slab. The midspan vertical deflection of the restrained composite perforated beam (AS4) as predicted by the modified virtual hybrid simulation is plotted against time and compared with the test results in Fig. 7.6 and it is shown that a good agreement is obtained. Fig. 7.7 presents the variation in axial reaction during the fire, as predicted by

the modified virtual hybrid simulation (measurements from the test are not available). Initially, it is shown that the beam experiences axial compression (indicated by a positive value in Fig. 7.7) due to restrained thermal expansion which increases until the onset of local buckling in the steel section. Subsequently, the compressive forces reduce due to the significant changes in material stiffness at high temperature, and the axial forces change from compression to tension as the full cross-section goes into tension and behaves like a tensile catenary.

(a)

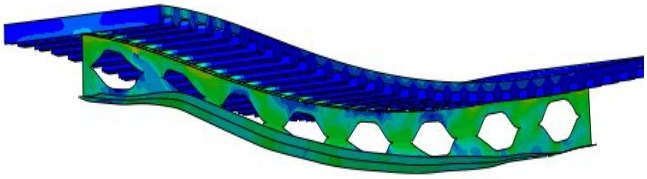

(b)

Fig. 7.5 Deformed shape of (a) the test beam (Wald et al. 2011) and (b) the FE model

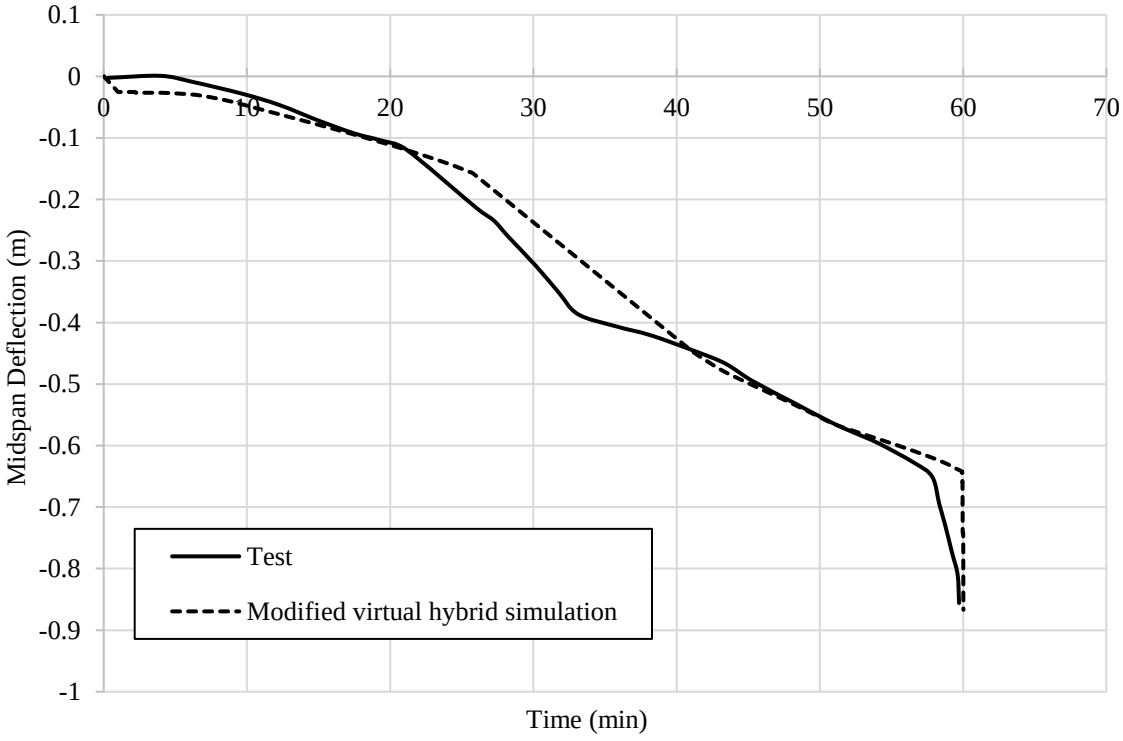

Fig. 7.6 Vertical deflection of the AS4 beam during the fire

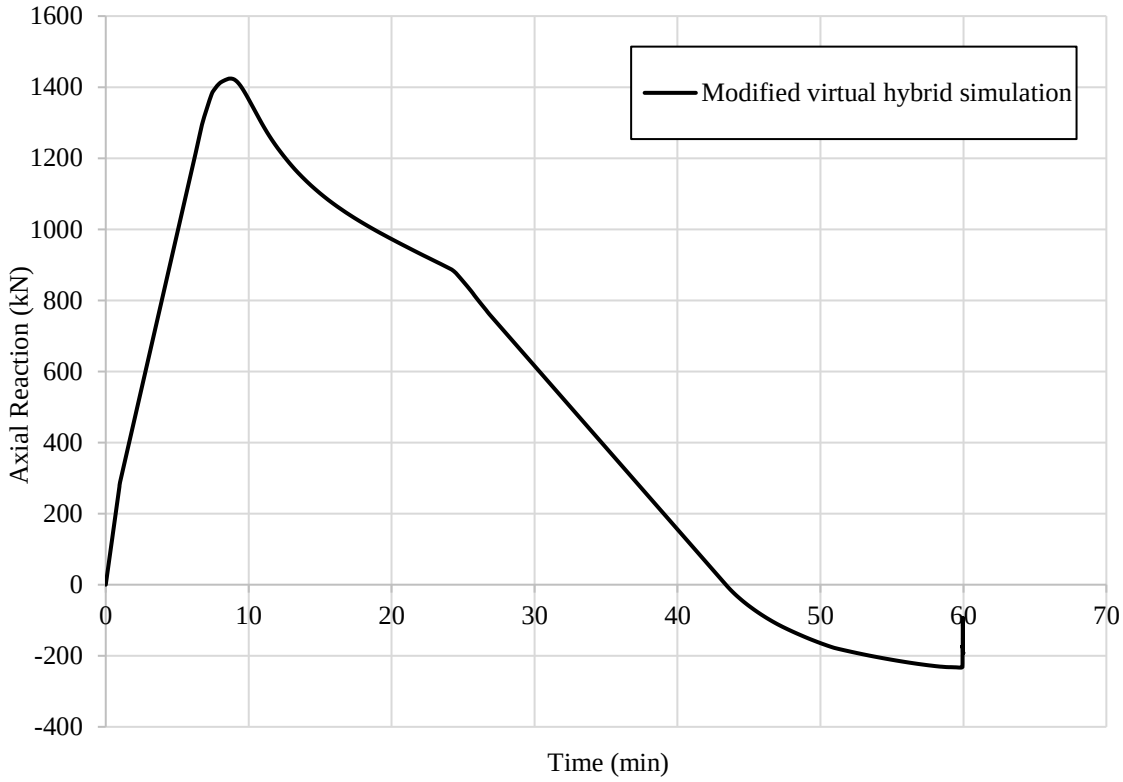

Fig. 7.7 Axial reaction at the beam support, with time, for beam AS4

7.2. Parametric study

Following this validation, the model is employed to conduct an extensive parametric study to analyse the response of restrained composite perforated beams in fire. The effect of load level, steel strength and opening layout on the behaviour is studied. The various parameters considered in the study are summarised in Table 7.1, including three different load levels (namely LL1=3.1 kN/m^2, LL2=4.3 kN/m^2 and LL3=5.6 kN/m^2, respectively) and three grades of steel (with yield strengths of 275, 450 and 550 N/mm^2, respectively). Four opening layouts are considered in the parametric study which are presented in Fig. 7.8, and described as follows:

Layout 1: Openings in the centre of the beam (bending zone);
Layout 2: Openings at 250 mm from the one end (one shear zone);
Layout 3: Openings at 250 mm from both the ends (both shear zones); and
Layout 4: Combination of layout 1 and layout 3 (bending and shear zone).

It is noteworthy that the load levels mentioned above result in different load ratios for each beam in the parametric study as the member capacity is related to the opening arrangement, steel grade, etc. The parametric study is divided into twelve different groups

for ease of analysis. Each group comprises 3 simulations, all of which have the same opening layout and steel grade but a different applied load level (i.e. LL1, LL2 or LL3). Accordingly, groups 1, 5 and 9 correspond to beams with opening layout 1 and steel strength of 275, 450 and 550 N/mm^2, respectively. Similarly, groups 2, 6 and 10 investigate opening layout 2 whilst groups 3, 7 and 11 study layout 3 and groups 4, 8 and 12 contain beams with opening layout 4. All other materials and geometric properties of the beam and surrounding structure are identical to that described earlier in the model validation and the Mokrsko AS4 test.

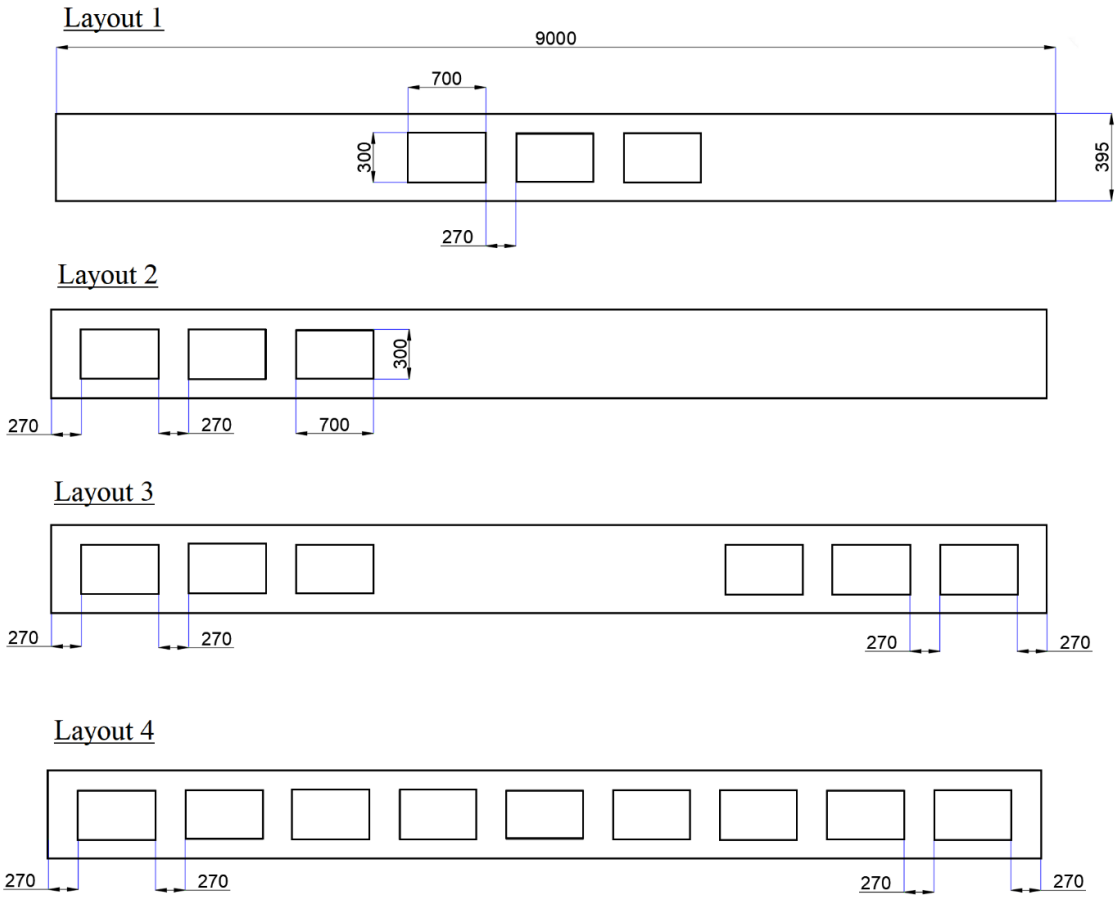

Fig. 7.8 Schematic of opening layout (all dimensions are in mm)

All of these analyses are conducted in two stages whereby the mechanical load is first applied to the whole structure in both the OpenSees and Abaqus models and this is then followed by the application of the thermal load in the detailed Abaqus model of the perforated beam. The same fire model (i.e. time-temperature relationship) as used in the model validation previously described, is applied in all cases. Accordingly, the temperatures obtained from the AS4 beam test are applied to all the groups as shown in Fig. 7.2.

Table 7.1 Composite frames investigated in the parametric study

Group No.	Beam	Opening Layout	Steel Grade (N/mm^2)	LL
Group 1	Beam-1	Layout 1	275	LL1
	Beam-2	Layout 1	275	LL2
	Beam-3	Layout 1	275	LL3
Group 2	Beam-4	Layout 2	275	LL1
	Beam-5	Layout 2	275	LL2
	Beam-6	Layout 2	275	LL3
Group 3	Beam-7	Layout 3	275	LL1
	Beam-8	Layout 3	275	LL2
	Beam-9	Layout 3	275	LL3
Group 4	Beam-10	Layout 4	275	LL1
	Beam-11	Layout 4	275	LL2
	Beam-12	Layout 4	275	LL3
Group 5	Beam-13	Layout 1	450	LL1
	Beam-14	Layout 1	450	LL2
	Beam-15	Layout 1	450	LL3
Group 6	Beam-16	Layout 2	450	LL1
	Beam-17	Layout 2	450	LL2
	Beam-18	Layout 2	450	LL3
Group 7	Beam-19	Layout 3	450	LL1
	Beam-20	Layout 3	450	LL2
	Beam-21	Layout 3	450	LL3
Group 8	Beam-22	Layout 4	450	LL1
	Beam-23	Layout 4	450	LL2
	Beam-24	Layout 4	450	LL3
Group 9	Beam-25	Layout 1	550	LL1
	Beam-26	Layout 1	550	LL2
	Beam-27	Layout 1	550	LL3
Group 10	Beam-28	Layout 2	550	LL1
	Beam-29	Layout 2	550	LL2
	Beam-30	Layout 2	550	LL3
Group 11	Beam-31	Layout 3	550	LL1
	Beam-32	Layout 3	550	LL2
	Beam-33	Layout 3	550	LL3
Group 12	Beam-34	Layout 4	550	LL1
	Beam-35	Layout 4	550	LL2
	Beam-36	Layout 4	550	LL3

7.2.1. Results and discussion

In this section, the results of the parametric study using modified virtual hybrid simulation are presented and discussed. Particular attention is given to analysing the fire resistance, vertical displacement, axial restraint, local buckling and deflected shape in order to understand the behaviour and assess the influence of the most critical parameters.

7.2.1.1. Transition time and temperature

The transition time refers to the point in the response at which the axial force in the beam changes from compression to tension, as observed in Fig. 7.7. For a typical restrained perforated beam in bending, as the load is applied at ambient temperature, the top tee-section and slab experience compression forces whereas the lower part of the beam goes into tension. With the addition of fire loading, initially, the restraint against thermal expansion results in an increase in the compressive forces in the top of the beam and a reduction of the tensile forces in the lower portion. Then, as the deflection increases and due to the thermal gradient across the depth of the section, compressive arching occurs and the whole cross-section is in compression. Local failure may occur either if the bottom tee-section buckles or yields under this compressive stress or through the formation of a Vierendeel mechanism, depending on the position of the opening; both of these local mechanisms are presented in Fig. 7.9 for the 4 opening layouts. As deflections increase further, the compressive forces begin to reduce in the section. Web-post buckling and web buckling due to lateral movement of the lower flange may develop and the axial force in the beam changes from compression to tension. The time at which this occurs is known as the transition time and the temperature at which this change takes place is the transition temperature.

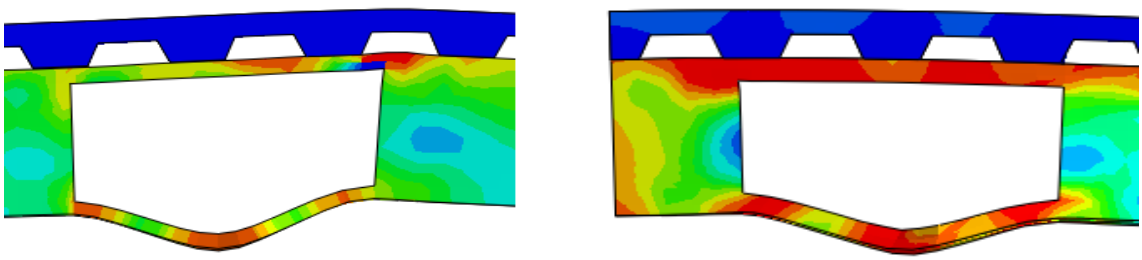

(a) (b)

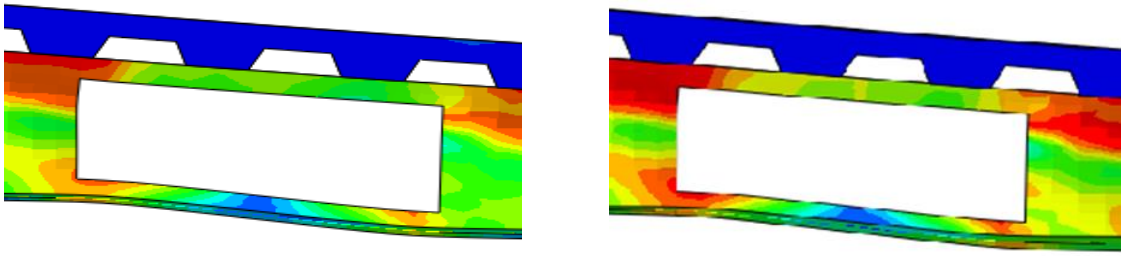

(c) (d)

Fig. 7.9 Local failure modes for beams made with steel S275 for opening layout (a) 1, (b) 2, (c) 3 and (d) 4

7.2.1.2. Load level

Fig. 7.10 presents the midspan deflection versus time responses for beams in Group 1 to Group 12 with different opening layouts and load levels for steel strengths S275. Fig. A.1 and Fig. A.3 of Appendix A presents the similar responses for steel strength S450 and S550 respectively. Fig. 7.11 illustrates the axial force response against time for the S275 beams while Fig. A.2 and Fig. A.4 of Appendix A presents the similar responses for steel strength S450 and S550 respectively. With reference firstly to Fig. 7.10, it is observed that in general, the overall behaviour remains unchanged irrespective of the load level. The response is quite different depending on the opening layout and each of the figures in Fig. 7.10 (a) to (d) presents differently shaped curves (this will be discussed further in Section Opening Layout). As expected, an increase in the load level results in greater midspan deflections for a given time, as well as an earlier transition time and ultimate failure. It is observed that for layout 2, 3 and 4, presented in Fig. 7.10 (b) to (d), respectively, the beam deflects in a downward direction from the beginning of the analysis. However, for layout 1 (Fig. 7.10 (a)), the beam initially deflects upwards for all load levels. For layout 1, the opening is at the centre of the beam and therefore the section is weaker at this location and the beam tends to deflect in an upward direction as it initially behaves somewhat like two separate cantilever beams under hogging moments. The reason for this upward curvature has already been explained in Chapter 6. Due to this upward curvature, an arching action also develops in the beam and the applied load induces more compressive forces in the section. Owing to this, the bottom tee section yields and the web-post begins to buckle causing the beam to deflect in a downward direction. The web-post buckling behaviour for different opening layouts with steel grade S275 is shown in Fig. 7.12.

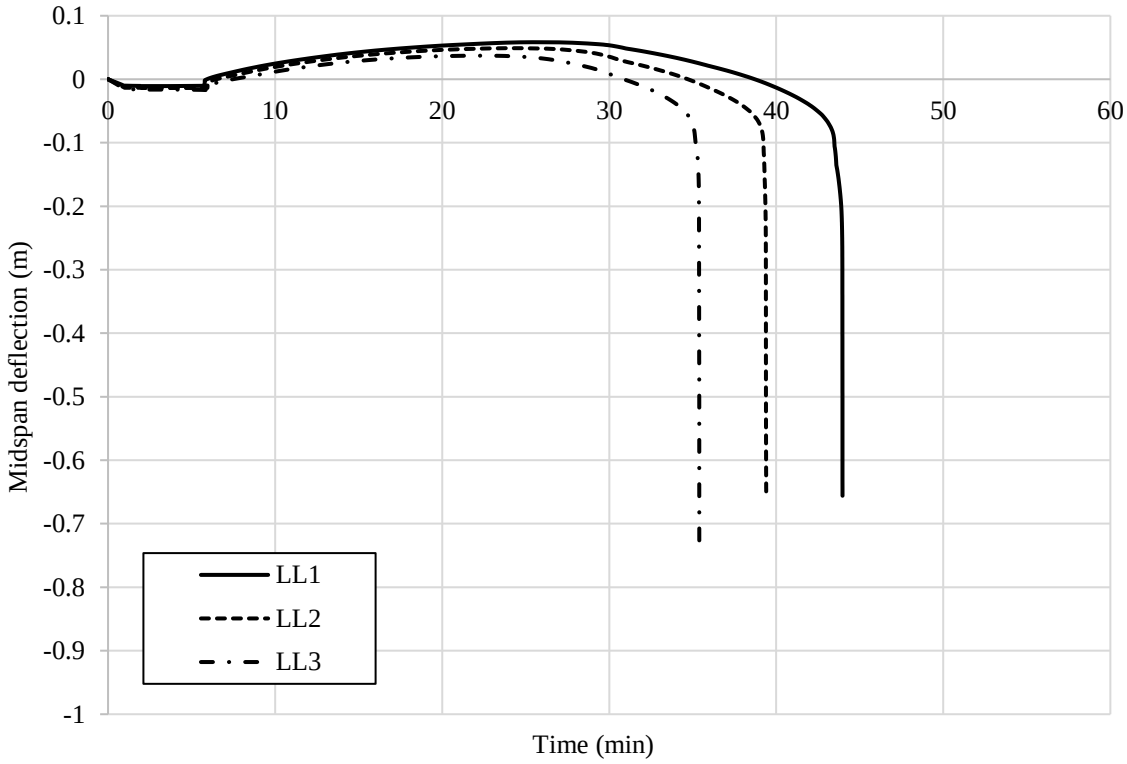
0.1
0
-0.1
-0.2
-0.3
-0.4
-0.5
-0.6
-0.7
-0.8
-0.9
-1
0
10
20
30
40
50
60
Midspan deflection (m)
Time (min)
LL1
LL2
LL3

(a)

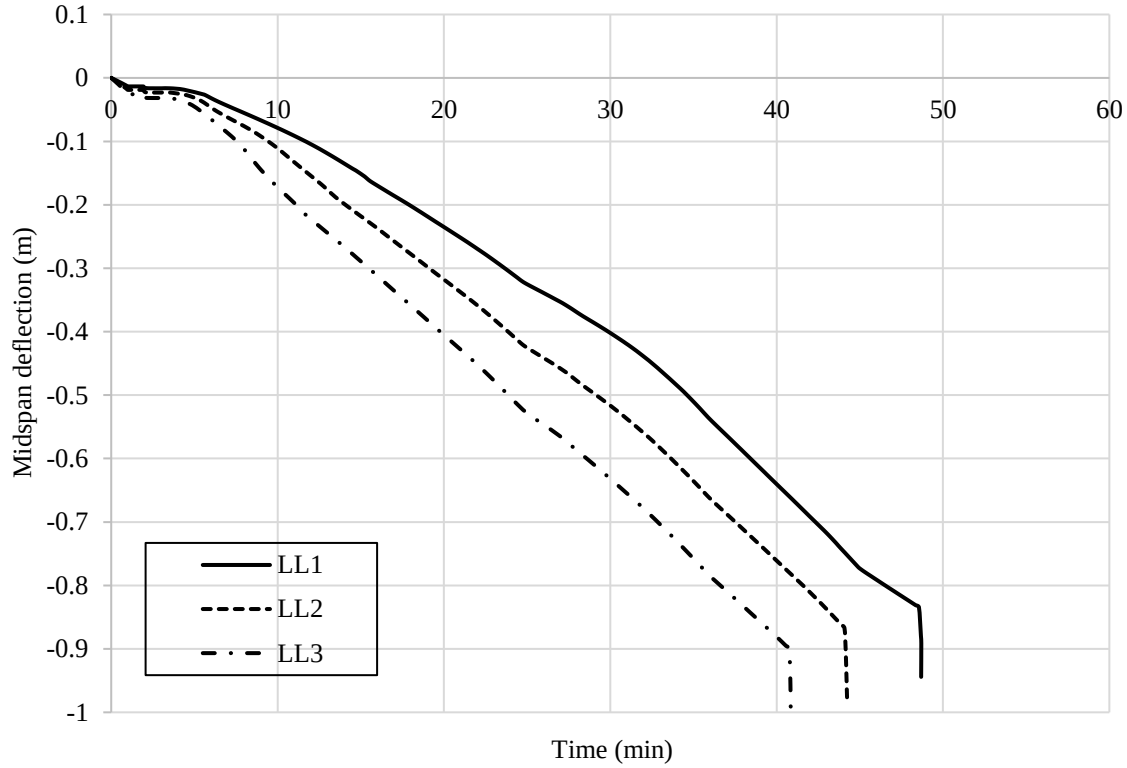
0.1
0
-0.1
-0.2
-0.3
-0.4
-0.5
-0.6
-0.7
-0.8
-0.9
-1
0
10
20
30
40
50
60
Midspan deflection (m)
Time (min)
LL1
LL2
LL3

(b)

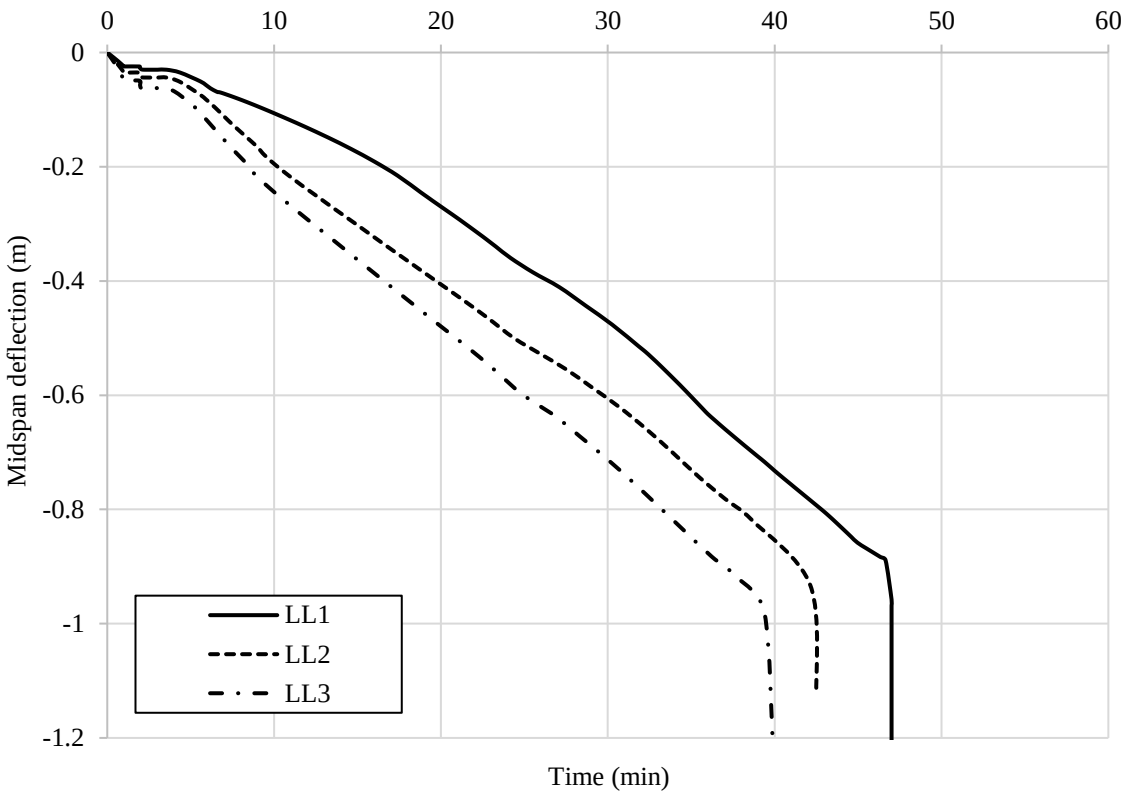

(c)

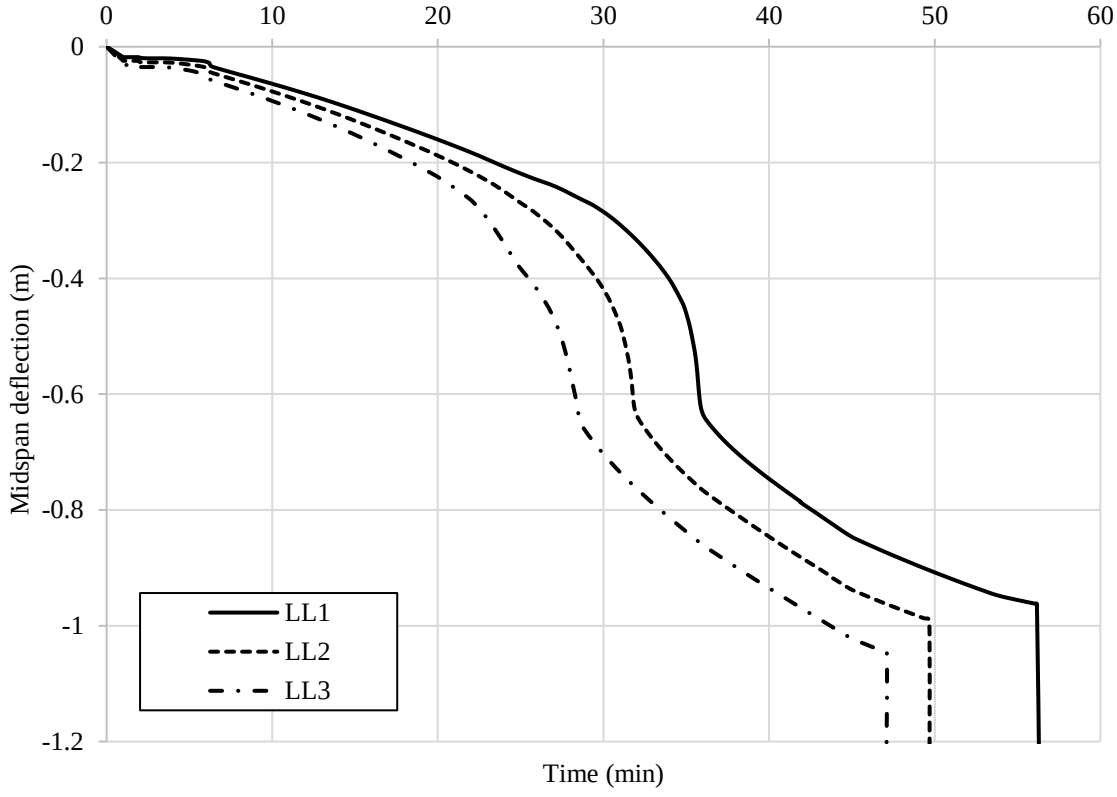

(d)

Fig. 7.10 Time-deflection behaviour for beams made with steel strength S275 and opening layout (a) 1, (b) 2, (c) 3 and (d) 4.

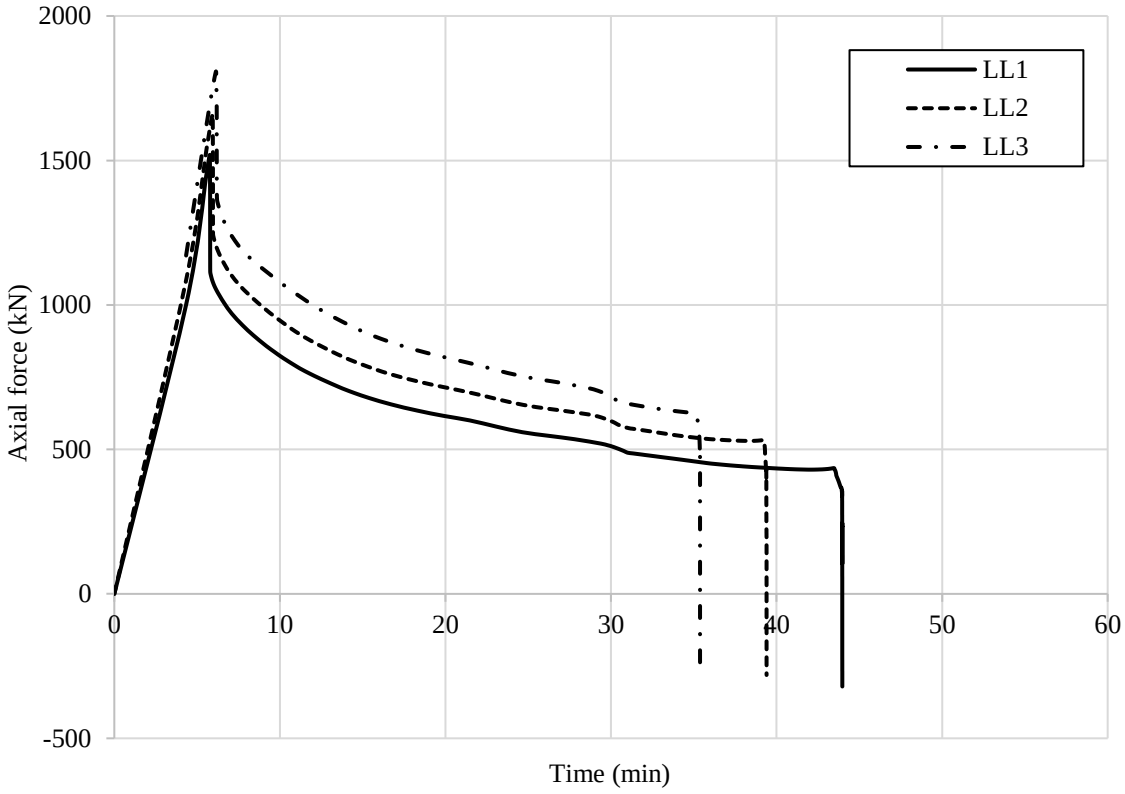
2000
1500
1000
500
0
-500
Axial force (kN)
0
10
20
30
40
50
60
Time (min)
LL1
LL2
LL3

(a)

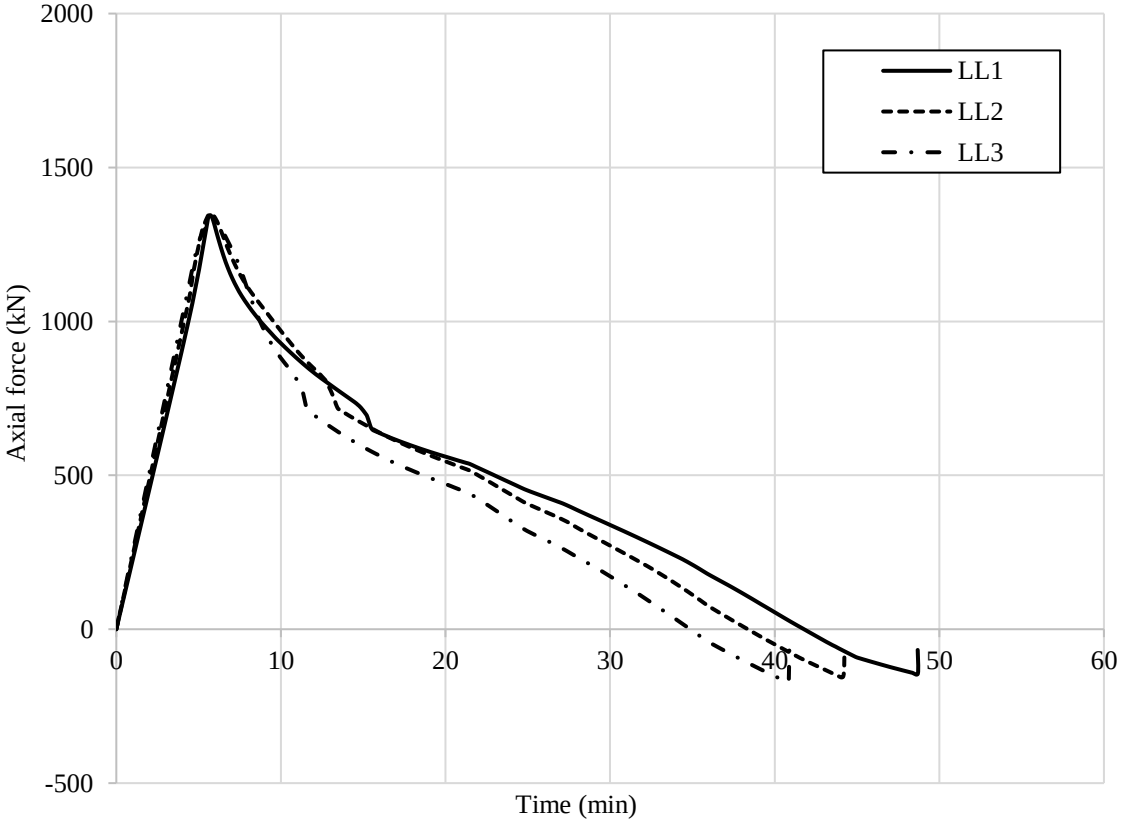
2000
1500
1000
500
0
-500
Axial force (kN)
0
10
20
30
40
50
60
Time (min)
LL1
LL2
LL3

(b)

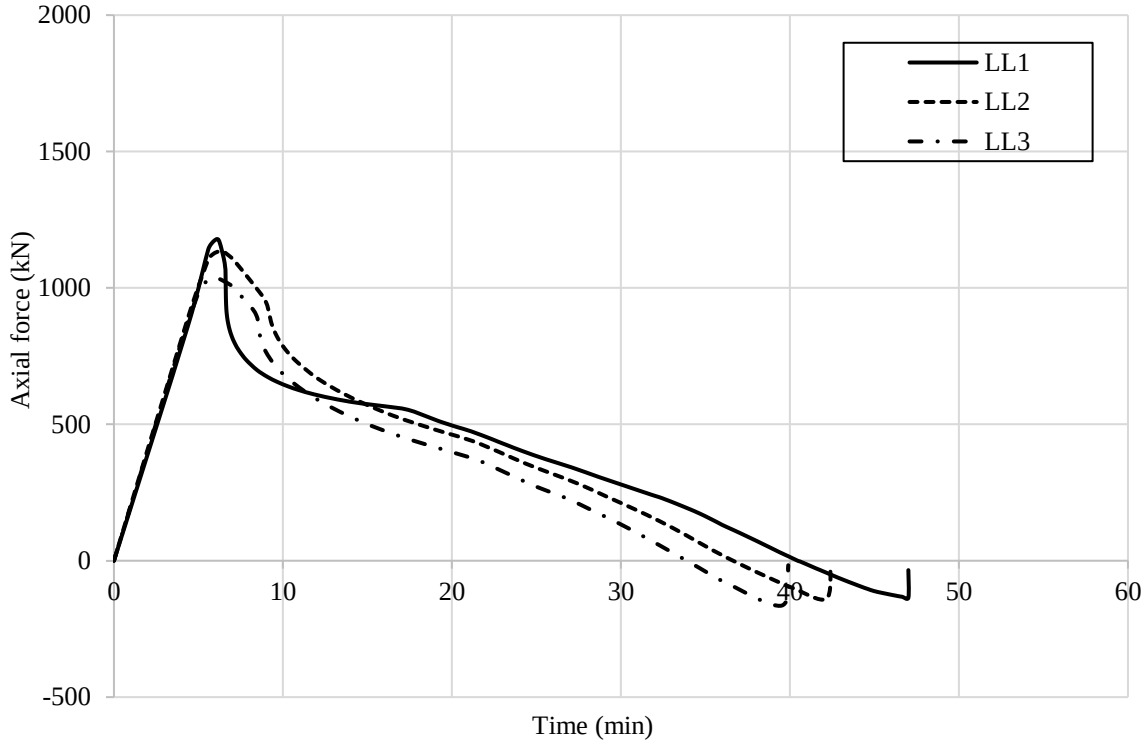

(c)

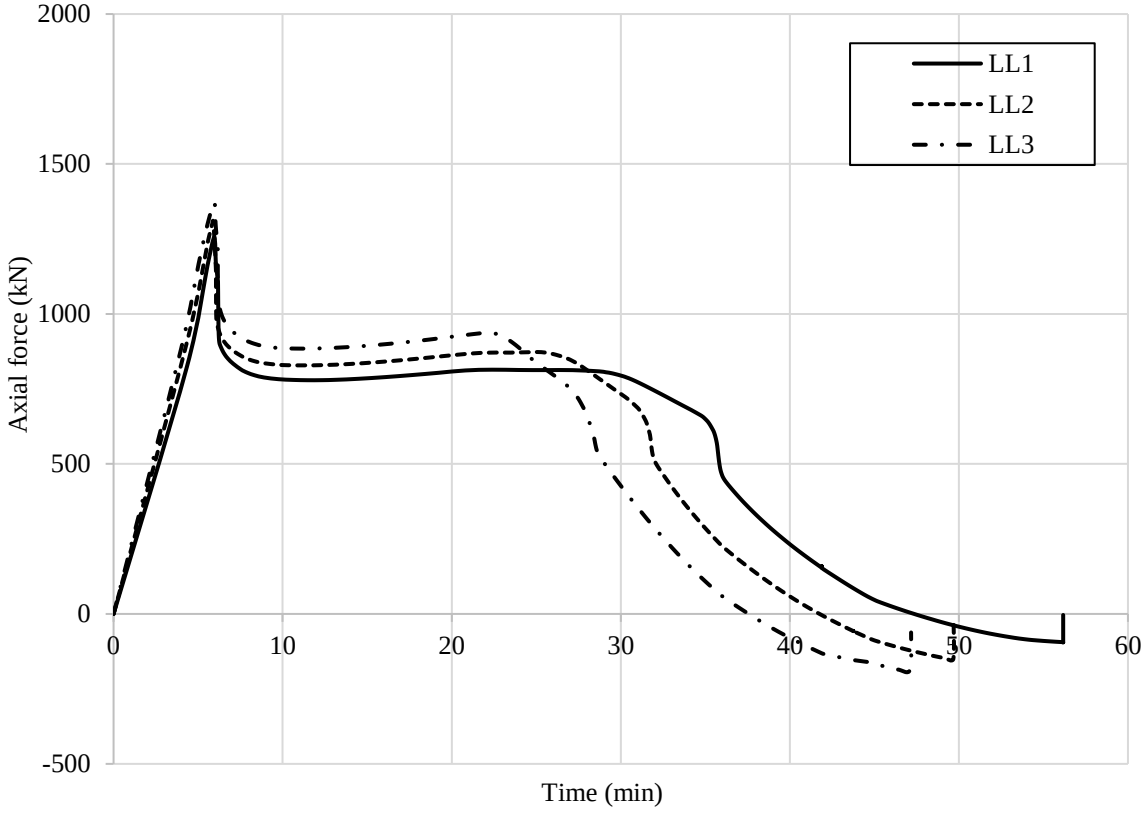

(d)

Fig. 7.11 Development of axial force for beams made with S275 at different load level and opening layout (a) 1, (b) 2, (c) 3 and (d) 4.

With reference to Fig. 7.11, similar behaviour is observed for all perforated composite beams with the same opening layout, regardless of steel strength and load level applied. In general, it is noteworthy that the peak axial force value in the beams is much greater for layout 1 than for the other opening arrangements. These beams have openings in the bending zone, which results in the development of arching action and a greater axial force. For layouts 2 and 3 which have openings in the shear zone only, arching action does not develop and therefore the levels of axial forces in the beam are lower. For beams with opening layout 4, some arching action does develop but because the relative stiffness of the section is similar along the whole length of the beam, only a small portion of the hogging moment is transferred to the mid-section, which leads to the development of partial arch action. The local failure modes including web-post buckling, buckling of the bottom flange and the lateral displacement of the web are presented in Fig. 7.12 for each of the layouts.

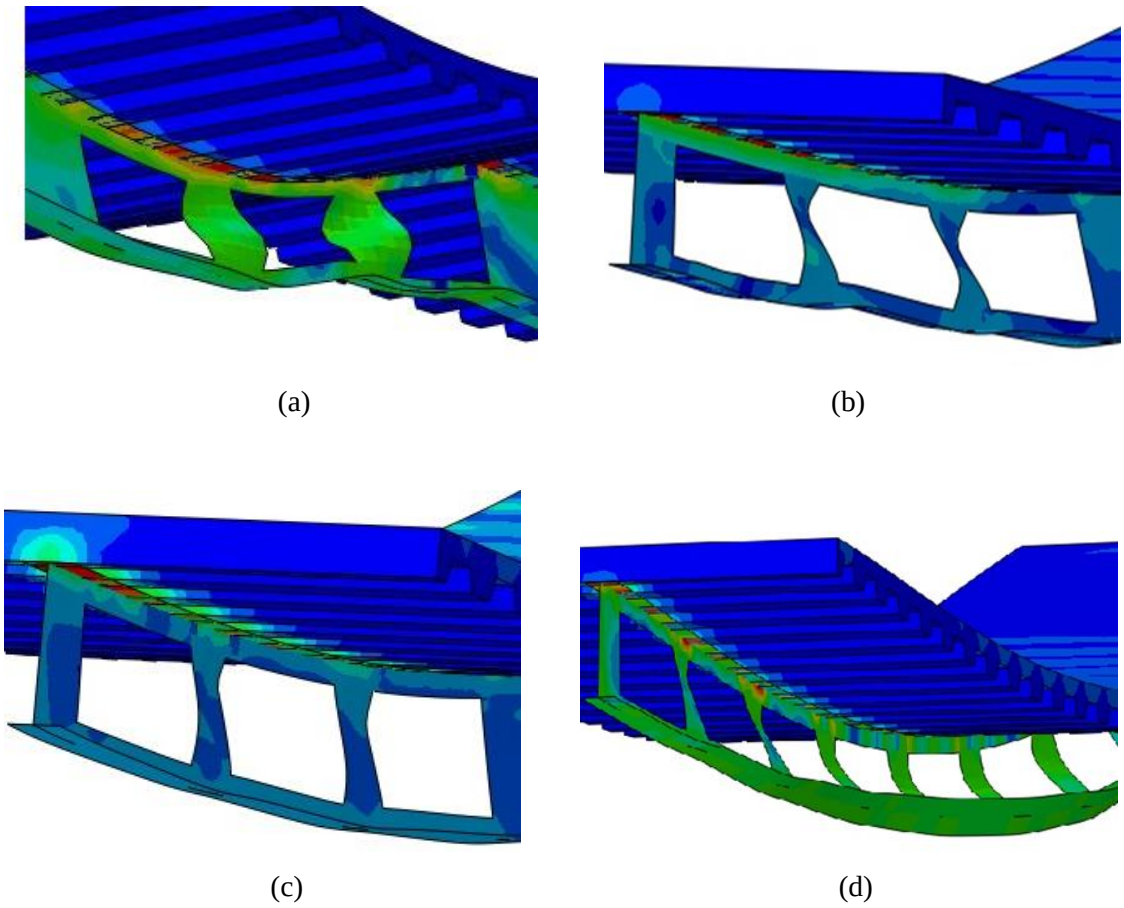

Fig. 7.12 Web-post buckling and lateral torsional displacement for beams made with S275 and opening layout (a) 1, (b) 2, (c) 3 and (d) 4.

Buckling of the web-post and lower flange is observed for all the opening layouts due to the narrow width of the web-post. The extent of web-post buckling increases with increase in load level from LL1 to LL3 for all the opening layouts. On the other hand, the top flange remains straight and buckling is prevented by the slab. Of the four layouts studied, only layout 4 results in lateral displacement of the web (See Fig. 7.12) which is attributed to the reduced stiffness of the web in this arrangement owing to the presence of openings along the whole span. The extent of the lateral displacement of the web increases with increase in load level and the maximum lateral displacement of the web is observed when the beam is loaded under LL3.

7.2.1.3. Steel grade

In this section, the influence of different grades of steel on the overall behaviour is assessed. As given in Table 7.1, three different grades are included in the study, with yield strengths of 275, 450 and 550 N/mm^2, respectively. Fig. 7.13 presents the development of axial force in the beam for each steel type, in the 4 different layout arrangements. It is shown that greater axial force develops in the beams made from relatively stronger steel, as expected. Moreover, the beams made from S275 steel start behaving as a tensile catenary earlier than the beams with higher steel strength.

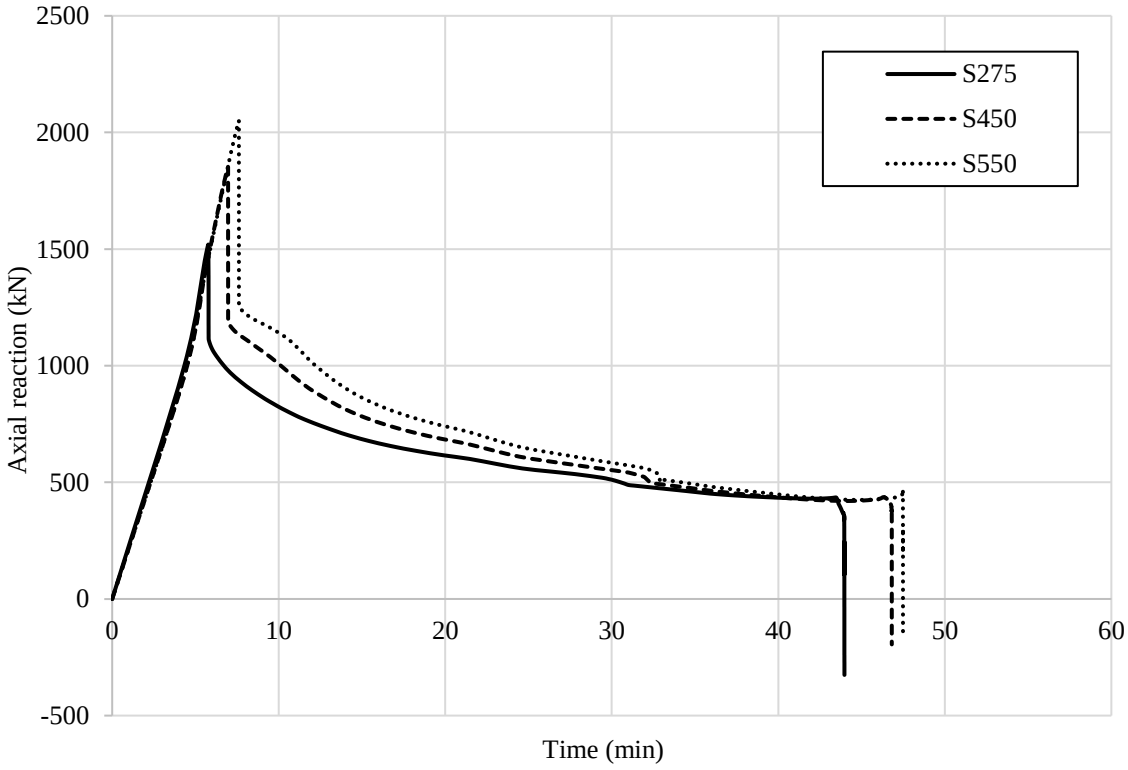

(a)

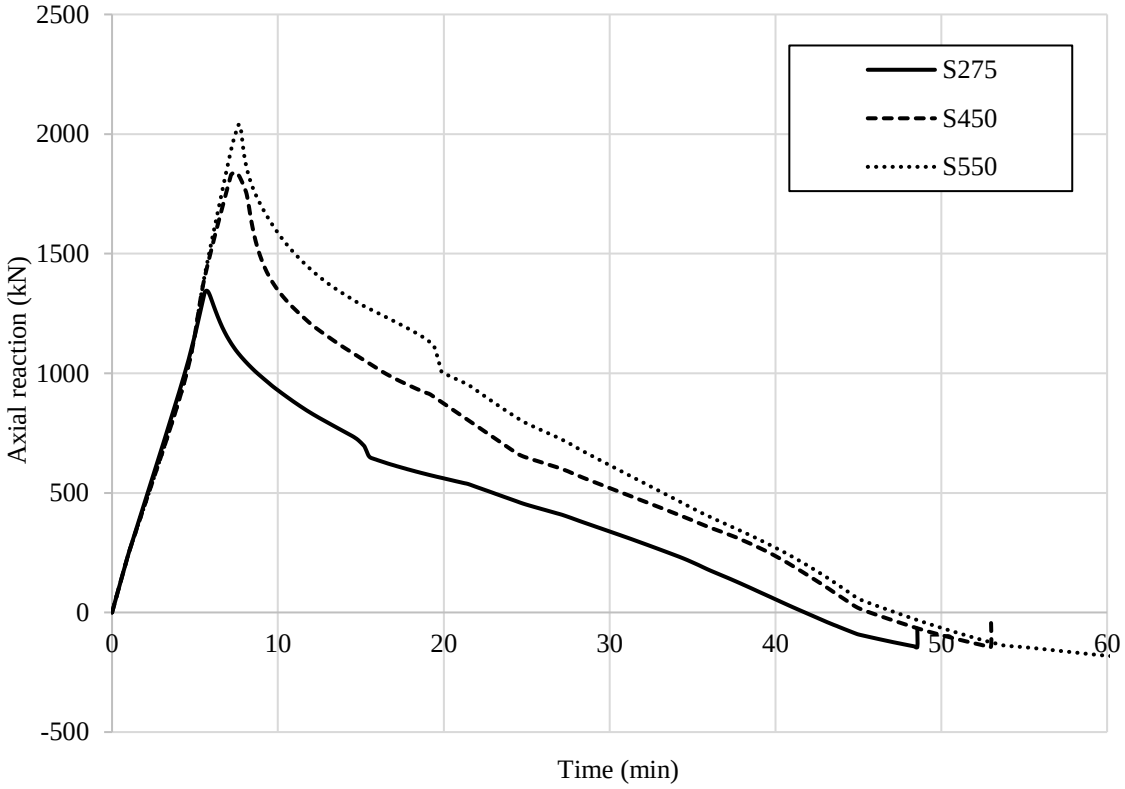
2500
2000
1500
1000
500
0
-500
0
10
20
30
40
50
60
Axial reaction (kN)
Time (min)
S275
S450
S550

(b)

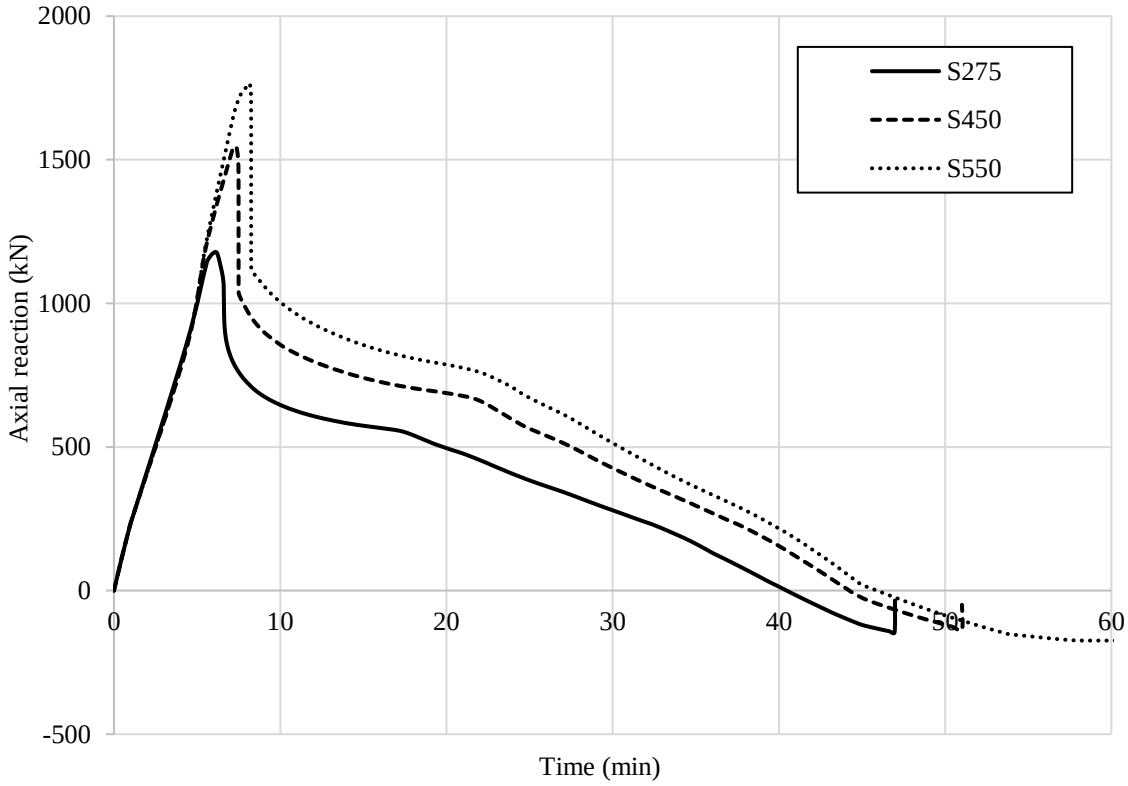
2000
1500
1000
500
0
-500
0
10
20
30
40
50
60
Axial reaction (kN)
Time (min)
S275
S450
S550

(c)

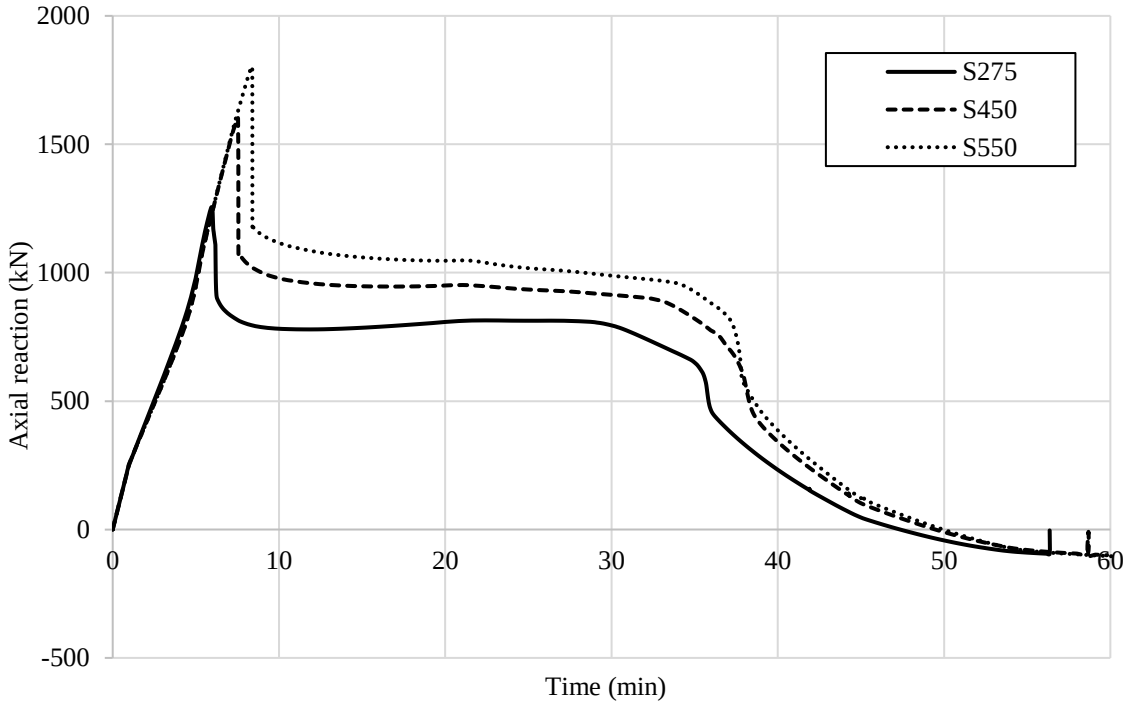

(d)

Fig. 7.13 Development of axial force for beams made with different strength steels and opening layout (a) 1, (b) 2, (c) 3 and (d) 4.

The magnitude of the axial reaction provides an indication of the stiffness and strength of the beam relative to the surrounding structure. An increase in steel strength has a positive effect on the web-post buckling and lateral torsional buckling behaviour and the out-of-plane displacements of the web-post are reduced. It is noteworthy that although there is a difference in the axial force between beams made from S450 and S550, the transition time is almost identical. Therefore, any further increase in the steel strength may not give any improvement in terms of fire resistance for perforated beams.

7.2.1.4. Opening layout

It has already been presented that the arrangement of openings in the perforated beam can be highly influential to the overall performance in fire and this will be discussed further in this section. Towards the end, Fig. 7.14 presents the development of both axial force and vertical midspan deflection, with time, for perforated composite beams made from S275, S450 and S550 steel, respectively. From these figures, it is clear that the presence of openings is very influential to the behaviour and a number of observations are made, as follows:

- All beams with layout 1 (which has an opening in the bending zone only) experience an initial upward deflection initially before the beam changes direction and starts moving downwards. This then results in the development of less arching action and a later transition time as well as a lower ultimate displacement, compared with beams that do not have openings in the bending area.

- The area of the openings in layout 1 is identical to that in layout 2 as shown in Fig. 7.8, but the midspan deflections are much lower for the former arrangement, irrespective of load ratio or steel strength which is illustrated in Fig. 7.14. This is because the beam with opening layout 1 experiences high axial compression due to arching action and the behaviour is influenced by buckling of the bottom tee as well as web-post buckling. On the other hand, beam with openings in layout 2 develops relatively less axial compression in the absence of arching action. The development of an arching action in the beams with layout 1 reduces the midspan deflection considerably.

- For beams that have openings in the bending zone (i.e. layout 1 and 4), the behaviour is governed by the buckling resistance of the bottom tee at the openings. On the other hand, for beams with openings in the shear zone, these must be able to resist Vierendeel bending in addition to bending and axial compression. In the Vierendeel mechanism, transverse shear is transferred across the opening leading to the formation of plastic hinges at the corners of the opening. In the later stages of a fire (i.e. after 15 minutes), the reduction in compression forces for Layout 1 and 4 is gradual and the transition time is relatively high compared to Layout 2 and 3, as shown in Fig. 7.15.

- The degree of web-post buckling in layout 1 is greater than the beams with opening layout 2 or 3 due to the presence of the openings in the bending zone. Due to the openings at the midspan, beams with opening layout 1 experience high axial compression, which results in buckling of top and bottom tee at midsection and leads to a sudden failure of the beam. In layout 4, the presence of openings along the whole span results in a weaker web and leads to lateral displacement of the web as shown in Fig. 7.12 (d).

- Transition time is an important concept in structural fire engineering as it indicates the fire resistance of the beam in a given fire scenario. For the cases considered herein, at the transition time, the beam is no longer resisting the applied loads through bending action but by acting as a tensile catenary. The transition time is greatest for opening layout 4, followed by layout 1, 2 and 3, respectively. It is clear that beams with openings in layout 1 fail suddenly as shown in Fig. 7.14 and Fig. 7.15, whereas all other cases considered in this study continue to carry load through the development of catenary action. For layout 4, the presence of openings along the whole length of the beam helps in distributing the load uniformly across the span, which delays failure, compared with the other layouts. The development of arching action reduces the midspan deflections and keeps the beam in compression for longer, which delays the transition time and therefore improves the fire resistance. It is noteworthy that layouts 2 and 3 behave very similarly with similar transition times, despite layout 3 having an additional set of openings.

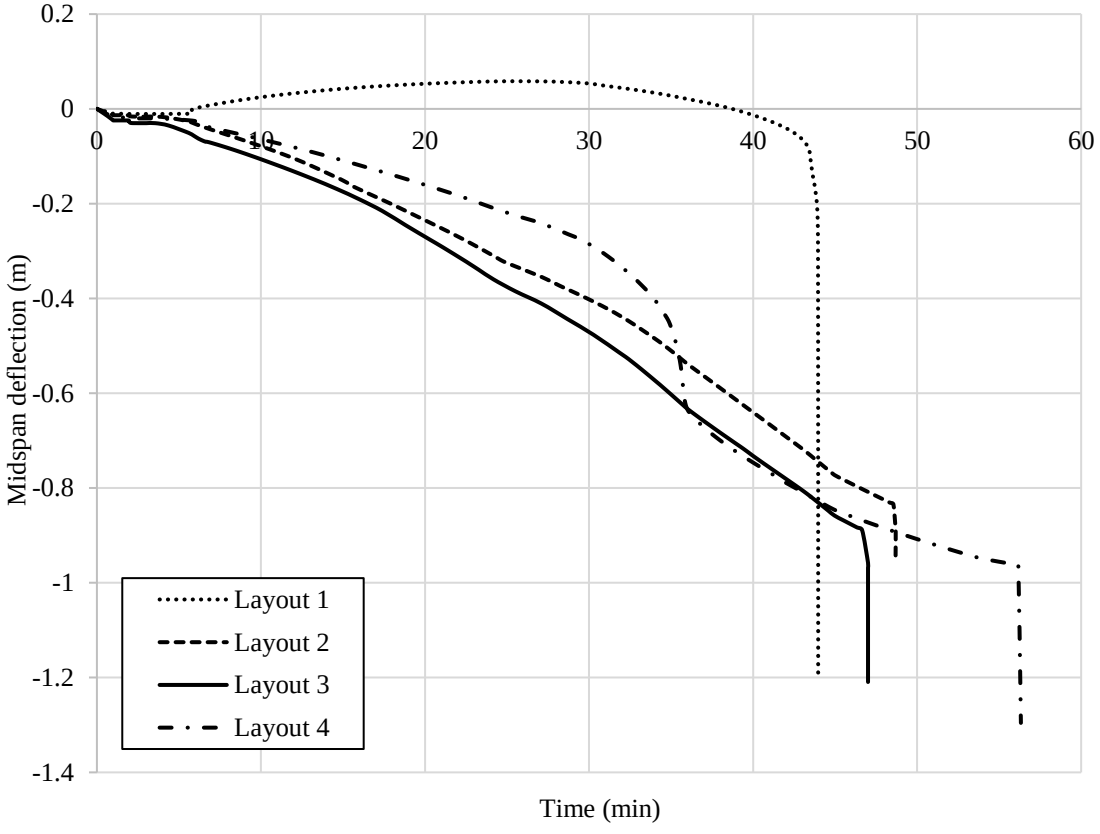

(a)

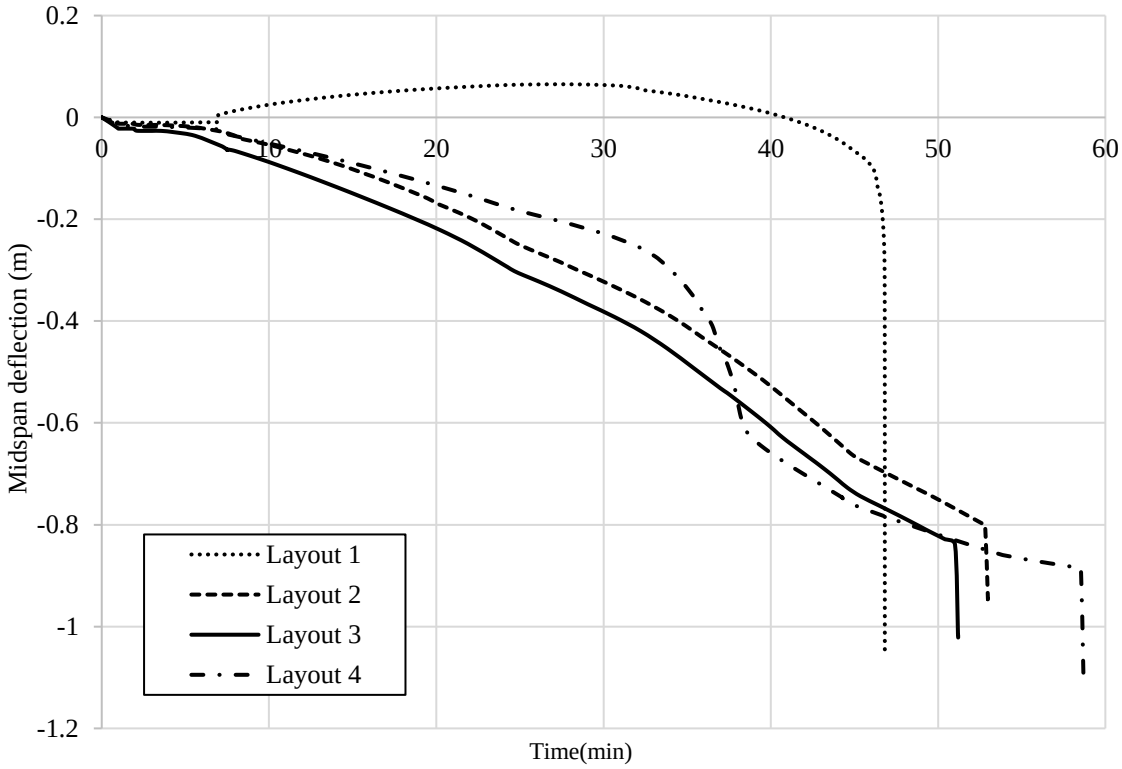

(b)

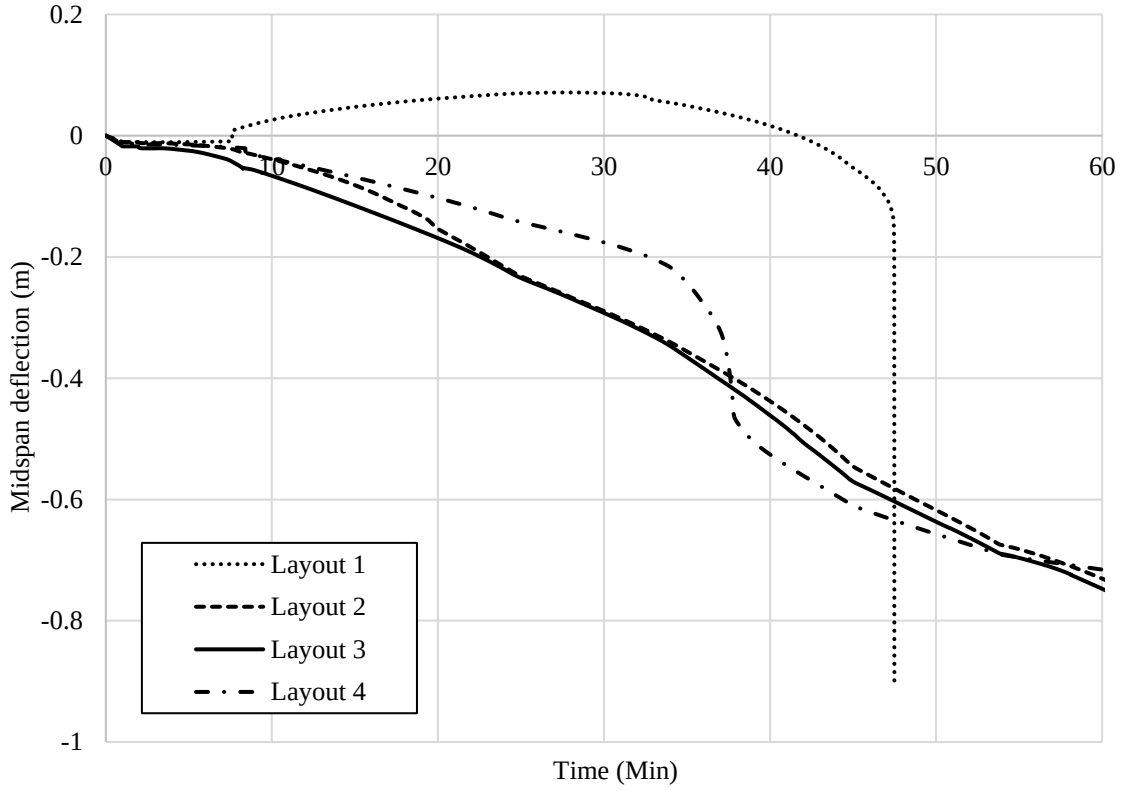

(c)

Fig. 7.14 Midspan deflection and axial reaction variation for all layouts, a) Steel grade 275 N/mm2 b) Steel grade 450 N/mm2 c) Steel grade 550 N/mm2

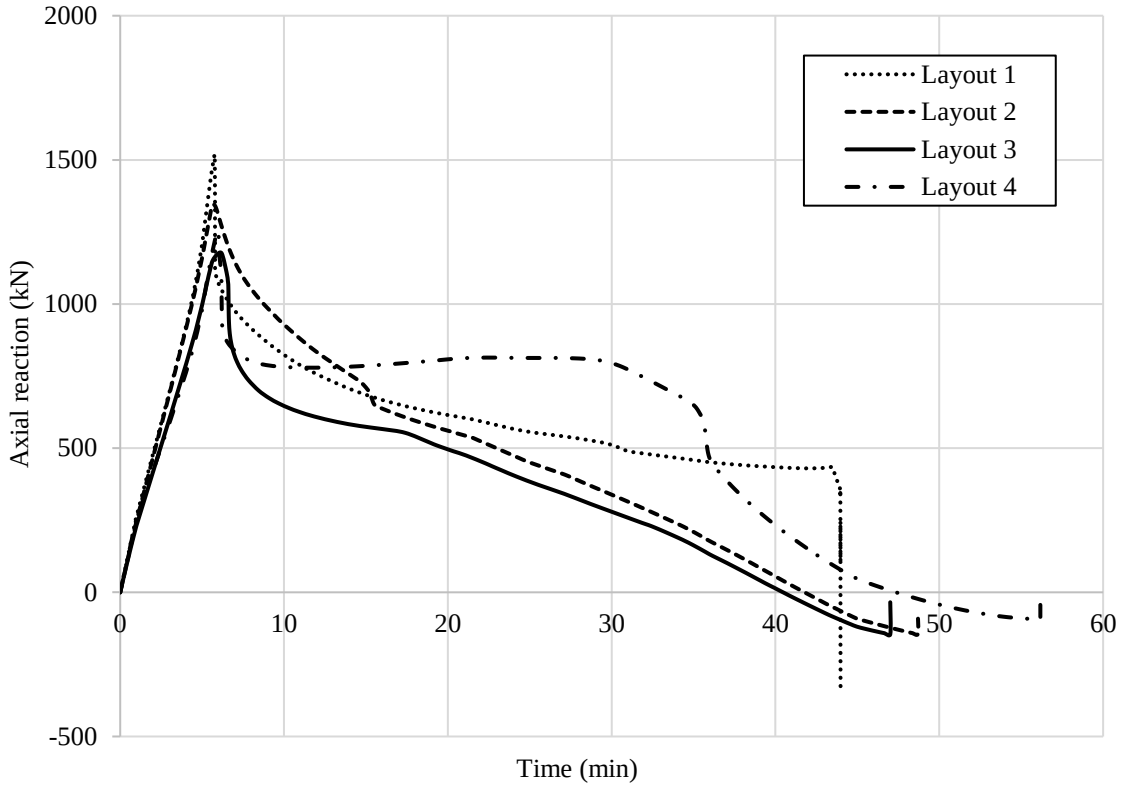
2000
1500
1000
500
0
-500
0
10
20
30
40
50
60
Axial reaction (kN)
Time (min)
Layout 1
Layout 2
Layout 3
Layout 4

(a)

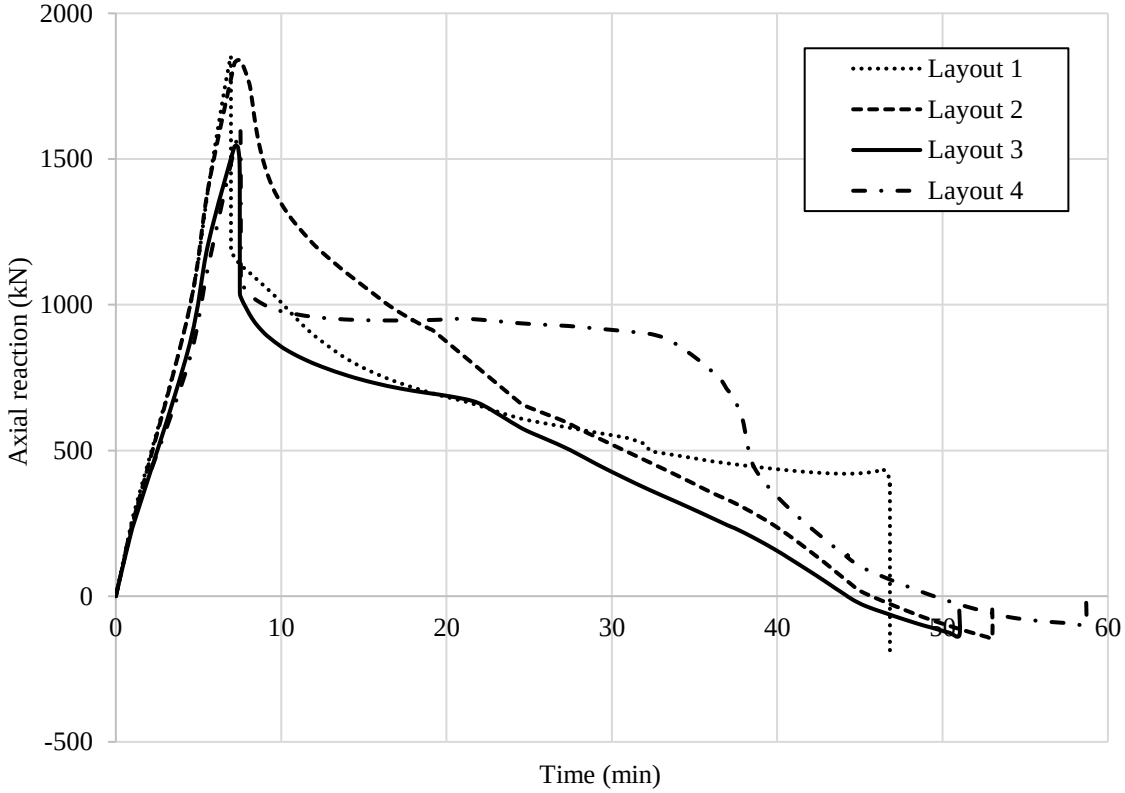
2000
1500
1000
500
0
-500
0
10
20
30
40
50
60
Axial reaction (kN)
Time (min)
Layout 1
Layout 2
Layout 3
Layout 4

(b)

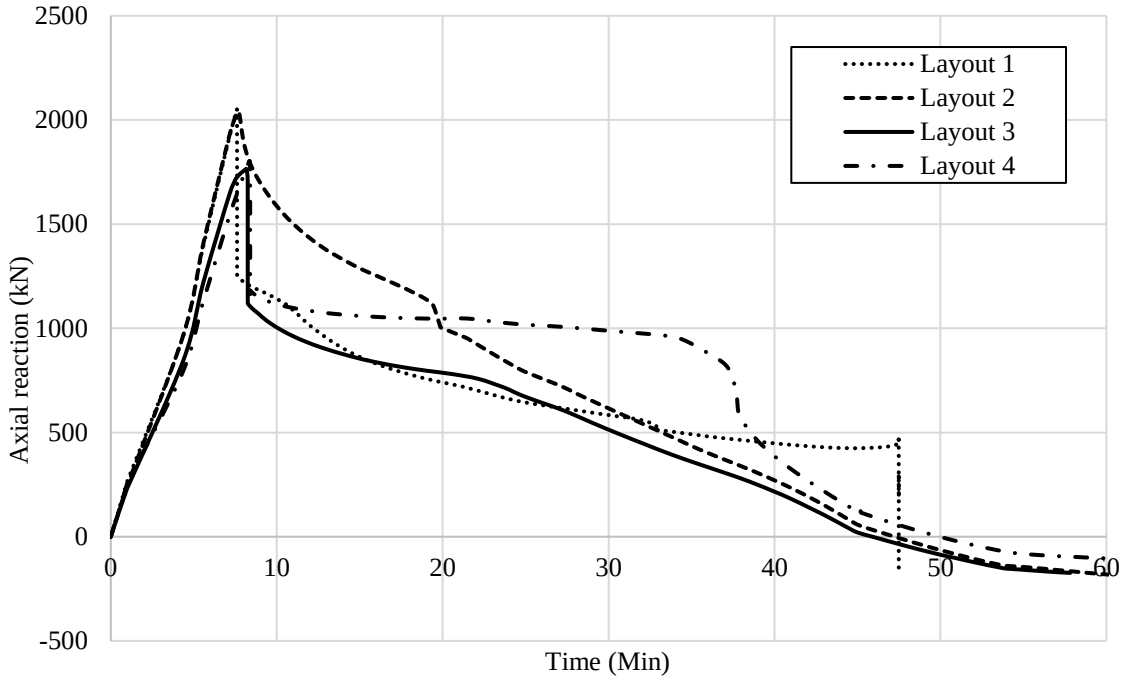

(c)

Fig. 7.15 Midspan deflection and axial reaction variation for all layouts, a) Steel grade 275 N/mm^2 b) Steel grade 450 N/mm^2 c) Steel grade 550 N/mm^2

7.3. Analytical model

In this section, an analytical model proposed by Steel Construction Institute SCI P355 design guide (Lawson and Hicks 1998) is modified to calculate the fire resistance of the perforated composite beams. The SCI P355 covers only the ambient temperature response and the design equations are modified by applying the elevated temperature reduction factors for the material strength in accordance with Eurocode 4 (EN-1994-1-2 2005) as shown in Fig. 7.16.

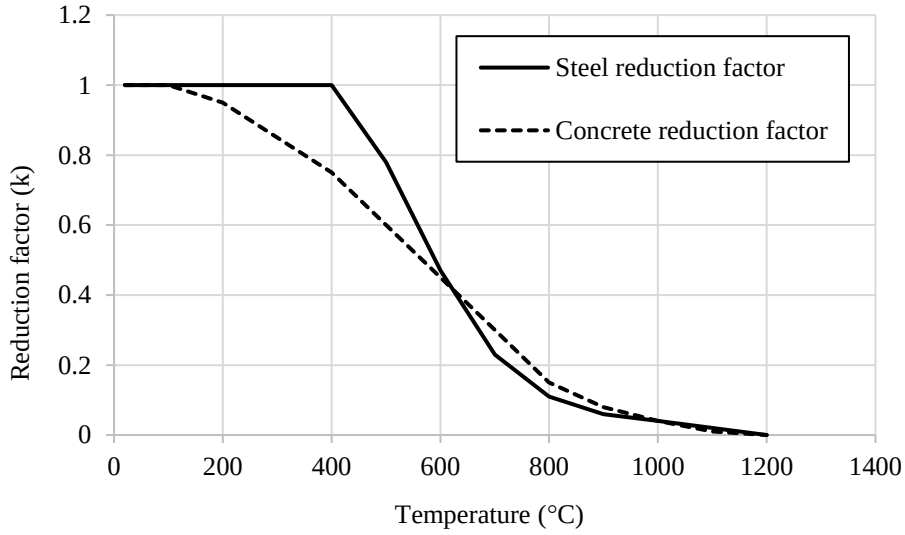

Fig. 7.16 Reduction factors for the yield strength of concrete and steel (EN-1994-1-2 2005)

The critical temperature is defined as the point at which the beam fails and the failure modes considered in the analytical model are global bending, global shear, Vierendeel bending, web-post shear and the web-post buckling. Once the critical temperature is established, the fire resistance can be estimated by recording the time for the critical temperature.

7.3.1. Bending resistance at the opening

According to the SCI P355 design guide, it is suggested that the bending resistance of a composite perforated beam should be calculated at the centre of the opening. For a solid composite beam, it is generally observed that the plastic neutral axis (PNA) lies in the top flange and slab. This observation also holds good for the composite perforated beams and location of PNA is higher as compared to solid composite beams. As per the analytical solution to estimate the bending resistance of the section, the location of the neutral axis is found out. There are two possible locations of the PNA which are in the slab and in the top tee. Both the cases estimate the bending resistance as below.

7.3.1.1. Location of PNA in the slab ($N_{cRd} > N_{bTRd}$)

For this condition to holds good, the compressive resistance of the slab must be more than the tensile resistance of the bottom tee. It is assumed that all the concrete above the PNA develops stress of $0.85f_{cd}$.

The tensile strength of the bottom tee is given as:

$$N_{bT,Rd} = \frac{A_{bT} f_y}{\gamma_{M0}} \tag{7.1}$$

where A_{bT} is the area of cross section of the bottom tee and f_y is the yield strength of steel.

The compressive resistance of the slab ($N_{c,Rd}$) is assumed to be minimum of the resistance due to the shear connector from nearest support to centre of the opening and the compressive resistance provided by the effective width of the slab, according to:

$$N_{c,Rd} = \min \{0.85\, f_{cd} b_{eff,o} h_c;\ n_{sc} P_{rd}\} \tag{7.2}$$

where f_{cd} is the design strength of concrete.

$b_{eff,o}$ is the effective width of the slab at the opening, determined as:

$$b_{eff,o} = \frac{3L_e}{16} + \frac{x}{4} \text{ for } x \leq L_e/4 \quad (7.3)$$

$$b_{eff,o} = \frac{L_e}{4} \text{ for } x > L_e/4 \quad (7.4)$$

x is the distance of the opening from the support. In these expressions, the following terms are used:

L_e is the effective span; h_c is the depth of concrete topping ($h_c = h_s - h_d$); h_s is the depth of the flat part of the slab; h_d is the overall depth of the profiled deck; n_{sc} is the number of the shear connector between the nearest support and the centre of the opening; and P_{rd} is the design resistance of the shear connector.

The plastic moment of resistance is given by the following equation:

$$M_{o,Rd} = N_{bT,Rd}(h_{eff} + z_t + h_s - 0.5\, z_c) \quad (7.5)$$

where h_{eff} is the effective depth of the beam between the centroids of two tees;

z_t is the distance of centroid of the top tee from the outer surface of the flange; and

z_c is the concrete depth in compression, found from:

$$z_c = \frac{N_{c,Rd}}{0.85 f_{cd} b_{eff,o}} \leq h_c \quad (7.6)$$

As a simplification, z_c may be assumed as equal to h_c.

7.3.1.2. Location of PNA in the top tee ($N_{cRd} < N_{bTRd}$)

$$M_{o,Rd} = N_{bT,Rd} h_{eff} + N_{c,Rd}(z_t + h_s - 0.5\, z_c) \quad (7.7)$$

where h_{eff}, z_t, h_s and z_c are already defined.

7.3.2. Shear resistance of perforated steel section

According to SCI P355 design guide, the shear resistance of a composite perforated beam is the sum of the shear resistance of the steel section and shear resistance of the narrow width of the slab. It is assumed that most part of the shear is resisted by the top tee as it is attached to the concrete slab and not severely stresses as bottom tee to resist the global bending.

The shear resistance of the steel section is given as follows:

$$V_{pl,Rd} = \frac{A_v f_y/\sqrt{3}}{\gamma_{M0}} \tag{7.8}$$

A_v is the shear area (area of two tees), found from:

$$A_v = [A - b_f t_f + (2r + t_w) \times 0.5 t_f] \tag{7.9}$$

where A is the cross-sectional area; b_f is the overall width of the tee; t_f is the thickness of the flange; t_w is the thickness of the web; and r is the root radius of the tee.

To find out the plastic shear resistance of a composite perforated beam the contribution from the slab should also be included. The shear resistance of a reinforced concrete section without any shear reinforcement is given as the minimum of Eqs. 7.10 and 7.11:

$$V_{c,Rd} = [\, C_{Rd,c} k (100 \rho_1 f_{ck})^{\frac{1}{3}} + k_1 \sigma_{cp}] b_w d \tag{7.10}$$

and

$$V_{c,Rd} = [\, V_{min} + k_1 \sigma_{cp}] b_w d \tag{7.11}$$

where $C_{Rd,c}$ is defined as per national annex to BS EN 1992-1-1:

$$C_{Rd,c} = 0.18/\gamma_c \tag{7.12}$$

$$K = 1 + \sqrt{\frac{200}{d}} \text{ but } \leq 2.0 \text{ (with d in mm)} \tag{7.13}$$

$$\rho_1 = \frac{A_{sl}}{b_w d} \text{ but } \leq 0.02 \tag{7.14}$$

In these expressions, A_{sl} is the area of tensile reinforcement, which extends $\geq (l_{bd} + d)$ beyond the section considered; l_{bd} is the encourage length for tensile reinforcement; d is the effective depth of the slab which is assumed as equal to h_c; $k_1 = 0.15$ as per national annex to BS EN 1992-1-1; and σ_{cp} is found from the Eq. 7.15:

$$\sigma_{cp} = \frac{N_{c,Ed}}{b_{eff} h_c} < 0.2 f_{cd} \tag{7.15}$$

b_w is the effective width of the concrete flange in shear $= b_f + 2h_{s,eff}$;

b_f is the flange width of the top tee; and

$h_{s,eff}$ is the effective depth of the slab for punching shear $\approx 0.75\ h_s$

V_{min} is determined as:

$$V_{min} = 0.035k^{3/2}{f_{ck}}^{1/2} \tag{7.16}$$

7.3.3. Resistance to Vierendeel bending

The vertical shear across the opening is transferred through the Vierendeel bending. At failure, a mechanism is formed by the development of four hinges at the corner of a rectangular opening and at the corners of an inscribed rectangular in case of an elongated and Angelina opening. The composite action due to the top tee and slab enhances the Vierndeel bending resistance of the section. So, the sum of the Vierndeel bending resistance at the four corners and due to the composite action of the slab and top tee must not be less than bending moment from one side of the opening to the other due to the vertical shear.

The Vierndeel bending resistance is expressed as follows:

$$2M_{bT,RD} + 2M_{tT,RD} + M_{vc,RD} \geq V_{Ed}l_e \tag{7.17}$$

where $M_{tT,RD}$ is the bending resistance of the top tee, found from Eq 5.18:

$$M_{tT,RD} = \frac{A_{w,T}f_y}{\gamma_{M0}}\left(0.5h_{w,T} + t_f - z_{pl}\right) + \frac{A_f f_y}{\gamma_{M0}}\left(0.5h_f - z_{pl} + {z_{pl}}^2/t_f\right) \tag{7.18}$$

z_{pl} is the distance of the extreme steel surface of the top flange from the plastic neutral axis, found from Eq. 7.19:

$$z_{pl} = (A_f + A_{w,T})/2b_f \tag{7.19}$$

$A_{w,T}$ is the cross section area of the web in top tee; A_f is the cross section are of the top flange; b_f is the width of the flange; $h_{w,T}$ is the depth of the web of top tee; and t_f is the thickness of the top flange.

$M_{bT,RD}$ is the bending resistance of the bottom tee, which is reduced due to axial tension.

$$M_{bT,RD} = M_{tT,RD}\left[1 - \left(\frac{N_{ED}}{N_{pl,RD}}\right)^2\right] \quad (7.20)$$

$N_{pl,RD}$ is the axial resistance of the tee section; N_{ED} is the axial tensile force due to global bending action (due to design moment); and

$M_{vc,RD}$ is the bending resistance due to the composite action of the top tee and the slab, determined as:

$$M_{vc,RD} = n_s P_{Rd}(h_s + z_t - 0.5h_c)k_0 \quad (7.21)$$

where n_s is the number of shear connectors above the opening; P_{Rd} is the shear resistance of the shear connector; h_s is the overall depth of deck slab; z_t is the distance between the extreme surface of the top flange and centroid of the top tee; h_c the depth of the flat part of the slab above decking; and k_0 is the reduction factor for the flexibility of the opening due to longer openings, determined as:

$$k_0 = \left(1 - \frac{l_o}{25h_t}\right) \quad (7.22)$$

where l_o is the effective length of the opening; and h_t is the depth of the top tee.

7.3.4. Web-post shear, and buckling resistance

In the case of closely spaced openings, the behaviour may be governed by the shear bending and buckling resistance of the web post. In the study conducted here, the web post at the critical location is checked for resistance against shear and buckling. The location of maximum applied shear is considered as the critical location.

7.3.4.1. Web-post shear resistance

The shear resistance of a web post is defined as:

$$V_{wp,ED=} \frac{(S_0 t_w) f_y/\sqrt{3}}{\gamma_{M_0}} \quad (7.23)$$

where S_0 is the clear distance between the two openings; and t_w is the thickness of the web.

7.3.4.2. Web-post buckling resistance

In the case of closely spaced rectangular openings, the web-post buckling resistance is defined as:

$$N_{wp,Rd} = \chi \frac{S_0 t_w f_y}{\gamma_{M1}} \tag{7.24}$$

where

$$\chi = \frac{1}{\phi + (\phi^2 - \lambda^2)^{0.5}} \tag{7.25}$$

$$\phi = 0.5\,[1 + 0.49(\lambda - 0.2) + \lambda^2] \tag{7.26}$$

$$\lambda = \frac{2.5\sqrt{{S_0}^2 + {h_0}^2}}{t_w} \frac{1}{\lambda_1} \tag{7.27}$$

λ is the slenderness ratio for the web-post and λ_1 is defined according to the grade of steel in BS EN 1993-1-1; and h_0 is the height of the opening.

7.4. Comparison with design codes

In this section, the fire resistance of the 36 perforated composite beams presented in Table 7.2 is compared with the design values obtained using the SCI P355 design guide (Lawson and Hicks 1998) by applying reduction factors from Eurocode 4 (EN-1994-1-2 2005). Table 7.2 presents the results including the fire resistance predicted by the finite element simulation ($R_{fi,FEM}$), SCI P355 ($R_{fi,P355}$) and also the ratio of these two values. It is shown that in almost all cases, the finite element analysis predicts that the beams will last for a longer period of time before failure occurs, compared with the design code. It is important to note that the design equations do not account for axial restraint and assume simply-supported boundary conditions. It has been shown in previous studies that restrained beams offer greater fire resistance compared with unrestrained beams (British Steel Plc 1999; Izzuddin and Moore 2002). With reference to Table 7.2, it can be seen that beams with opening layout 2, 3 or 4 have identical fire resistance's according to the design equations because the behaviour is governed by the Vierendeel mechanism and buckling of the web-post in the shear zone.

Table 7.2 Finite element analysis results and SCI-P355/EC-4 fire resistance

Group No.	**Beam**	**$R_{fi,FEM}$ (min)**	**$R_{fi,P355}$ (min)**	**$R_{fi,FEM}$ / $R_{fi,P355}$**
Group 1	Beam-1	43	43	1
	Beam-2	39	41	*0.95*
	Beam-3	35	37	*0.95*
Group 2	Beam-4	48	43	1.12
	Beam-5	44	39	1.13
	Beam-6	41	33	1.24
Group 3	Beam-7	47	43	1.09
	Beam-8	42	39	1.08
	Beam-9	39	33	1.18
Group 4	Beam-10	56	43	1.3
	Beam-11	49	39	1.26
	Beam-12	47	33	1.42
Group 5	Beam-13	47	50	*0.94*
	Beam-14	43	47	*0.91*
	Beam-15	39	44	*0.89*
Group 6	Beam-16	52	50	1.04
	Beam-17	49	43	1.14
	Beam-18	46	39	1.18
Group 7	Beam-19	51	50	1.02
	Beam-20	47	43	1.09
	Beam-21	45	39	1.15
Group 8	Beam-22	58	50	1.16
	Beam-23	52	43	1.21
	Beam-24	48	39	1.23
Group 9	Beam-25	50	60	*0.83*
	Beam-26	46	50	*0.92*
	Beam-27	43	46	*0.93*
Group 10	Beam-28	60	60	1
	Beam-29	60	46	1.3
	Beam-30	56	42	1.33
Group 11	Beam-31	60	60	1
	Beam-32	55	46	1.2
	Beam-33	52	42	1.24
Group 12	Beam-34	60	60	1
	Beam-35	60	46	1.3
	Beam-36	57	42	1.36

Therefore, these equations do not account for the effect of multiple openings at various locations. On the other hand, the finite element analysis considers all of the influential aspects such as opening shape and location as well as the arching effect due to axial restraint. For opening layout 1, the fire resistance estimated using finite element simulation is lower than the fire resistance computed using design equations. This behaviour is due to the sudden failure of these beams at the onset of the axial force transition from compression to tension.

7.5. Concluding remarks

This chapter has presented the framework for performing a hybrid simulation type approach for the analysis of restrained perforated beams subjected to fire, in a real building. Firstly, a detailed description of the novel modified virtual hybrid simulation method in fire is presented. This includes the slave assembly, in Abaqus, and the master assembly, implemented using the open-source software OpenSees. This modified virtual hybrid simulation approach offers both accuracy and excellent computational efficiency, particularly for complex problems such as modelling a whole building which is subjected to fire. Hybrid simulation, which includes physical testing, has been extensively applied to seismic engineering applications. However, in order to develop a framework for examining other extreme conditions such as fire, it is convenient to replace the physical testing element with a detailed numerical assembly, as is developed herein.

The modified virtual hybrid simulation approach is validated for perforated beams subjected to fire using available test data. Thereafter, the model is employed to conduct a parametric study. The key variables included in the study are the opening position, steel strength and load level. During the analysis of the results, it is noted that for axially restrained perforated composite beams, there are a number of distinct stages during the response. Initially, at ambient temperature, the section is in pure bending. Then, as the temperature increases, the whole section starts experiencing axial compression owing to the restraint provided. As soon as initial yielding occurs either by buckling of the bottom tee and web-post or by the Vierendeel mechanism, these compression forces reduce. Beams with openings in the bending zone experience a more rapid unloading compared with beams that have openings in the shear zone only. Thereafter, with increasing deflection, the axial force in the section transitions from compression to tension as the beam behaves as a tensile catenary. It is noted that compressive arching action develops

for all beams that have openings in the bending zone which delays the transition time of the beam giving greater fire resistance.

The effect of load level on the fire behaviour of perforated beams has also been studied and it is found that an increase in the load applied to the beam results in a relative reduction in the transition time i.e., a reduction in the fire resistance of the beam. The overall behaviour remains the same with a change in the load level and steel strength. As expected, beams made using a higher strength steel grade demonstrate a greater capacity to develop axial forces. Interestingly, beams which have openings throughout their length are shown to offer the greatest fire resistance of those examined in this study. This is due to the fact that the stresses and loads are more evenly distributed across the length and the development of arching action provides a significant mechanism for resisting the applied loads, supplementing the bending resistance. On the other hand, beams which have openings in the bending zone only are shown to offer the lowest fire resistance.

Finally, the analytical model proposed by Steel Construction Institute SCI P355 (Lawson and Hicks 1998) design guide to analysing the beams with web openings at room temperature has been discussed and modified to estimate the fire resistance of the perforated beams at elevated temperature. This analytical model is utilised to estimate the fire resistance of perforated beams and compared with the fire resistance estimated using modified virtual hybrid simulation. It is shown that virtual hybrid simulation approach provides a good estimation of the fire resistance for most cases, apart from layout 1 of the studied arrangements due to the sudden failure of the beams with opening layout 1. In all other cases, the fire resistance predicted by the modified virtual hybrid simulation is greater compared with the fire resistance calculated using design equations i.e., fire resistance estimated by design equations is conservative. This is mainly because the effects of axial and rotational restraint are neglected in design equations and accounted for in the FE model.

Chapter 8

Conclusions

In this chapter, the key research findings and principal conclusions reached in this thesis are summarised. Recommendations for future research, building on the work conducted herein, are made thereafter.

8. Conclusions

The research presented in this thesis investigates the thermal and structural response of perforated beams in fire conditions, taking into account the effects of the surrounding structure. Focus is given to establishing a virtual hybrid simulation framework to simulate the restraint developed at the support of a fire-exposed perforated beam, in a structural frame. Following conclusions have been made in this study.

- In Chapter 3, a numerical model for an isolated perforated beam exposed to fire is developed. It is shown that the numerical model is able to capture the important aspects associated with the behaviour of unrestrained and restrained perforated beams in fire conditions such as local buckling of the flanges, thermal bowing, runaway deflection, catenary action and the detailed deformation patterns of the beams.
- The developed model is then used to analyse the effect of various parameters on the response of perforated steel beams. It is observed that in the early stages of fire, local buckling of the top flange near the support occurs due to high axial restraint. If sufficient axial restraint is provided, catenary action then develops and helps the beam to continue to carry loads at high temperatures. It is concluded that high levels of axial restraint assists the beam to develop catenary action, but the magnitude of the induced tensile force should be carefully monitored as it can adversely affect the performance of the connections.
- Chapter 4 analyse the effect of location of axial restraint developed in a perforated steel beam. A shift in the location of the axial restraint may either enhance or adversely affect the performance of perforated beams in fire conditions,

depending on their slenderness ratio. For non-slender perforated steel beams, shifting the location of the axial restraint towards the bottom flange improve the fire performance. On the other hand, for slender beams, it is observed that a downward shift in the location of the axial restraint has a negative impact on the fire performance of the beams.

- In order to apply the actual end restraints that would develop in a steel framed building, a virtual hybrid simulation framework for thermo-mechanical analysis is established in Chapter 5. This framework can be utilised to conduct real hybrid fire test using a physical specimen in place of the 3D detailed model. Due to the use of OpenFresco middleware software, this framework is capable of communicating many responses at the interface of PS and NS. This approach presents a fully automated procedure to conduct the hybrid fire test without manual involvement after every integration step.
- Developed framework is also capable to simulate the whole structure behaviour in an efficient yet accurate manner. Only the fire exposed part of the structure is required to be modelled in fine detail using 3D solid and shell elements while detailed modelling of the remainder structure is not required to understand the whole system behaviour. In other words, this framework is presents a computationally efficient approach to understand the behaviour of structural components exposed to fire.
- In Chapter 6, the behaviour of restrained perforated beams exposed to fire is investigated using the virtual hybrid simulation technique. The beams with openings in the shear zone perform in a more critical manner than beams with openings in the bending zone for the restrained beams i.e., less fire resistance and more midspan deflections are observed. On the other hand, for beams with simply-supported boundary conditions, the beams with openings in the bending zone experience higher mid-span deflections and have less fire resistance compared with the beams with openings in the shear zone, which is converse to the findings for the restrained beams. It is concluded that the virtual hybrid simulation approach is capable of simulating the actual end restraint that are developed due to the surrounding structure, and thus provides a more accurate depiction of the structural response, compared with modelling isolated structural components.

- Furthermore, the virtual hybrid simulation model is used to investigate the effect of different fire scenarios on the response of perforated beams. It is observed that during the initial stages of a fire, the thermal gradient developed across the section is greatest in fast parametric fire exposure and least in slow parametric fire exposure. Of the three different fire scenarios studied herein, the fast parametric fire results in the greatest midspan deflections during the heating phase and the beams reach the limiting deflection earlier than other fire exposures.
- For both locations of openings, a runaway deflection is observed only in the case of a standard fire exposure due to the strength reduction of concrete and steel at elevated temperature; this does not occur for either parametric fire. It is concluded that the structural response of composite perforated beams in fire is a function of the thermal gradient across the composite beam section and the average temperatures developed due to different fire exposures.
- In Chapter 7, the virtual hybrid simulation framework is modified by modelling the fire exposed part of the structure in Abaqus software. The modified virtual hybrid simulation framework offers both accuracy and excellent computational efficiency. The modified framework is capable of capturing local effects which are particularly important in perforated beams i.e., web-post buckling, lateral torsional buckling and Vierendeel bending.
- An increase in the load level results in greater midspan deflections for a given time, as well as an earlier transition time and ultimate failure. Only for layout 1, the beam tends to deflect in an upward direction and it initially behaves somewhat like two separate cantilever beams under hogging moments. Due to this upward curvature, an arching action also develops in the beam and the applied load contribute to compressive axial forces as a result layout 1 experiences highest magnitude of compression.
- The dominating failure mode in layout 1 is observed as the top tee buckling along with the web-post buckling whereas in layout 2 and 3, Vierendeel bending in combination of web-post buckling is noticed as the main failure mode. Moreover, lateral torsional buckling is only observed in layout 4 beam and they fails due to the combined effect of web-post buckling and lateral torsional buckling.
- The extent of web-post buckling increases with increase in load level from LL1 to LL3 for all the opening layouts and the extent of the lateral displacement of

the web also increases with increase in load level and the maximum lateral displacement of the web is observed when the beam is loaded under LL3.

- It is concluded that greater axial force develops in the beams made from relatively stronger steel i.e., connections in high steel strength beams experiences greater axial pull, which should be carefully considered while designing the connections.
- The beams made from S275 steel start behaving as a tensile catenary earlier than the beams with higher steel strength i.e., less transition time. Beams with steel strength S550 experiences least extent of web-post buckling and lateral torsional buckling. It is noticed that although there is a difference in the axial force between beams made from S450 and S550, the transition time is almost identical. Therefore, it is concluded that any further increase in the steel strength does not give any improvement in terms of fire resistance for perforated beams.
- To compare the results from numerical simulations, the analytical model proposed in the SCI P355 design guide (Lawson and Hicks 1998) has been modified to estimate the fire resistance of the perforated beams at elevated temperature. It is concluded that this modified approach provides a good estimation of the fire resistance for most cases, apart from layout 1 of the studied arrangements. In all other cases, the fire resistance predicted by the modified virtual hybrid simulation is greater compared with the fire resistance calculated using design equations i.e., the fire resistance estimated by design equations is conservative. This is mainly because the effects of axial and rotational restraint are accounted for in the FE model.

8.1. Suggestions for future research

As evidenced throughout this thesis, considerable advancements have been made in the analysis of structures in fire. However, as is usual in research, some reasonable limitations and assumptions were made. To thoroughly understand this topic and to enable practical application of the research, the following further research studies are recommended:

- The application of fire protection material is a common practice for many types of structural components, to improve the fire performance. The effects of fire protection are outside the scope of this research, and therefore it is recommended to include the effects of fire protection in the virtual hybrid simulation model to analyse the behaviour of protected perforated beams in fire conditions.

- Many studies conducted over the past two decades to analyse the thermal and structural behaviour of large compartments in fire show that fires in such compartments have a great deal of non-uniformity, unlike the homogeneous compartment temperature assumption in the current fire safety engineering practice. To incorporate the non-homogeneity of temperature, a travelling fire model is required. As OpenSees is an open source software and is being continually developed by the research community, it is recommended to further include the travelling fire model which is recently developed in OpenSees, to simulate a more realistic fire scenario for future research.

- All hybrid fire simulations performed in the past involve testing a central column. This type of hybrid simulation communicates only the axial degree of freedom at the interface due to its symmetric location. However, hybrid simulation of other structural components have not been performed due the complexity involved in communicating more than one degree of freedom at the interface. If the 3D Abaqus model in the modified virtual hybrid simulation framework is replaced with a physical specimen in the laboratory, multiple degrees of freedom can be communicated at the interface. Hence, hybrid simulations of structural components other than central columns are recommended using the developed framework for future research.

- It has been observed that the presence of axial and rotational restraint have a great influence on the fire behaviour of perforated beams in steel framed structures. The analytical models for perforated beams available in the literature generally consider simply supported boundary conditions and do not incorporate the effect of axial and rotational restraint. The presence of web openings at multiple location also affects the fire performance of a perforated beam and has not been considered in the analytical models. Hence, there is a requirement to develop analytical models that incorporate the effect of axial and rotational restraints as well as the presence of web openings at multiple locations for future research.

- Stainless steel has superior stiffness and strength relative to carbon steel at elevated temperature, as well as other attributes such as durability and pleasant aesthetics. The research into stainless steel perforated beams is extremely limited, but in the few studies available in the literature, simply supported boundary

conditions are always assumed. It is recommended that an experimental and numerical study is performed to analyse restrained stainless steel perforated beams, or stainless steel perforated beams in a structural frame. The modified virtual hybrid simulation framework can be utilised to analyse the behaviour of restrained stainless steel perforated beams in fire conditions by simulating the real restraint provided by a surrounding structure and hence this is recommended for future research.

References:

Abu, A., Block, F., Butterworth, N., and Burgess, I. (2009). "Structural fire engineering assessments of the Fracof and Moksko fire tests: An Engineering prediction." *Application of Structural Fire Engineering*, Prague, Czech Republic.

AISC. (2005). "Steel construction manual." *American Institute of Steel Construction*, Inc, Chicago, Illinois.

AISC. (2016). "AISC 360-16: Specification for Structural Steel Buildings." *American Institute of Steel Construction*, Chikago, Illinois.

Alam, N., Nadjai, A., Maraveas, C., Tsavdaridis, K. D., and Ali, F. (2017). "Response of Asymmetric Slim Floor Beams in Parametric-Fires." *Conference on Structural Safety under Fire and Blast Loading - 2017*, London.

Anderberg, Y. (1988). ""Modeling steel behavior." *Fire Safety Journal*, 13, 17–26.

Boissonnade, N., Nseir, J., Moussa, L., and Somja, H. (2013). "Design of cellular beams against lateral torsional buckling." *ICE Proceedings-Structures and Buildings*, 167(SB7), 436–444.

British Steel Plc. (1999). *The behaviour of multi-storey steel framed buildings in fire*. Swinden Technology centre, Rotherham.

BS 476-20. (1987). "Fire tests on building materials and structures. Method for determination of the fire resistance of elements of construction (general principles)." *British Standard Institution*, London, United Kingdom.

Burgess, I. W., El Rimawi, J., and Plank, R. J. (1991). "Studies of the Behaviour of Steel Beams in Fire." *Journal of Construction Research*, 19, 285–312.

Campbell, S., and Stojadinovic, B. (1998). "A system for simultaneous pseudodynamic testing of multiple substructures." *National Conference on Earthquake Engineering*, U.S, Proceeding.

Chen, L., and Wang, Y. C. (2012). "Efficient modelling of large deflection behaviour of restrained steel structures with realistic endplate beam/column connections in fire." *Engineering Structures*, 43, 194–209.

Chung, K. F., Liu, C. H., and Ko, A. C. H. (2003). "Steel beams with large web openings of various shapes and sizes: An empirical design method using a generalised moment-shear interaction curve." *Journal of Constructional Steel Research*, 59(9), 1177–1200.

Chung, K. F., Liu, T. C. H., and Ko, A. C. H. (2001). "Investigation on vierendeel

mechanism in steel beams with circular web openings." *Journal of Constructional Steel Research*, 57(5), 467–490.

Cooke, G. M. E. (1988). "An introduction to the mechanical properties of structural steel at elevated temperature." *Fire Safety Journal*, 13(1), 45–54.

Dai, X. H., Wang, Y. C., and Bailey, C. G. (2010). "Numerical modelling of structural fire behaviour of restrained steel beam-column assemblies using typical joint types." *Engineering Structures*, 32(8), 2337–2351.

Dai, X., Welch, S., and Usmani, A. (2017). "A critical review of 'travelling fire' scenarios for performance-based structural engineering." *Fire Safety Journal*, 91, 568–578.

Deng, H., Pu, W., Li, T., and Chen, D. (2015). "Analysis on Behavior of web buckling of Hexagonal Castellated Beams with Transverse Stiffeners Under Uniform Loads." (Iccet), 380–384.

Dermitzakis, S. N., and Mahin, S. A. (1985). "Development of substructuring techniques for on-line computer controlled seismic performance testing." *Earthquake Engineering Research Center*, Berkeley, California.

Dong, Y., and Prasad, K. (2009). "Experimental Study on the Behavior of Full-Scale Composite Steel Frames under Furnace Loading." *Journal of Structural Engineering*, 135(10), 1278–1289.

Durif, S., Bouchaïr, A. H., and Vassart, O. (2013). "Validation of an analytical model for curved and tapered cellular beams at normal and fire conditions." *Periodica Polytechnica Civil Engineering*, 57(1), 83–95.

Dwaikat, M., and Kodur, V. (2010). "Effect of location of restraint on fire response of steel beams." *Fire Technology*, 46(1), 109–128.

Dwaikat, M. M. S., and Kodur, V. K. R. (2011). "A performance based methodology for fire design of restrained steel beams." *Journal of Constructional Steel Research*, 67, 510–524.

Dwaikat, M. M. S., Kodur, V. K. R., Quiel, S. E., and Garlock, M. E. M. (2011). "Experimental behavior of steel beam-columns subjected to fire-induced thermal gradients." *Journal of Constructional Steel Research*, Elsevier Ltd, 67(1), 30–38.

El-Rimawi, J. A., Burgess, I. W., and Plank, R. J. (1997). "The Influence of Connection Stiffness on the Behaviour of Steel Beams in Fire." *Journal of Constructional Steel Research*, 43(1–3), 1–15.

Ellobody, E. (2011). "Interaction of buckling modes in castellated steel beams." *Journal of Constructional Steel Research*, Elsevier Ltd, 67(5), 814–825.

Ellobody, E. (2012). “Nonlinear analysis of cellular steel beams under combined buckling modes.” *Thin-Walled Structures*, Elsevier, 52, 66–79.

Ellobody, E., and Young, B. (2015). “Nonlinear analysis of composite castellated beams with profiled steel sheeting exposed to different fire conditions.” *Journal of Constructional Steel Research*, 113, 247–260.

Elsawaf, S., Wang, Y. C., and Mandal, P. (2011). “Numerical modelling of restrained structural subassemblies of steel beam and CFT columns connected using reverse channels in fire.” *Engineering Structures*, 33(4), 1217–1231.

EN-1994-1-2. (2005). “Eurocode 4: Design of composite steel and concrete structures - Part 1-2 General rules - Structural fire design.” *European Commitee for Standardization*, Brussels.

EN 13501-1. (2007). “Fire classification of construction products and building elements - Part 1: Classification using test data from reaction to fire tests.” *British Standards Institution*, Brussels.

EN 1991-1-2. (2005). “Eurocode 1: Actions on structures - Part 1-2: General actions - Actions on structures exposed to fire.” *European Commitee for Standardization*, Brussels.

EN 1992-1-2. (2004). “Eurocode 2: Design of concrete structures - Part 1-2: General rules - Structural fire design.” *European Commitee for Standardization*, Brussels.

EN 1993-1-1. (2005). “Eurocode 3: Design of steel structures - Part 1-1: General rules and rules for buildings.” *European Commitee for Standardization*, Brussels.

EN 1993-1-2. (2005). “Eurocode 3: Design of steel structures - Part 1-2: General rules - Structural fire design.” *European Commitee for Standardization*, Brussels.

Gernay, T., Millard, A., and Franssen, J. M. (2013). “A multiaxial constitutive model for concrete in the fire situation: Theoretical formulation.” *International Journal of Solids and Structures*, Elsevier Ltd, 50(22–23), 3659–3673.

Gillie, M., Usmani, A. S., and Rotter, J. M. (2001). “A structural analysis of the first Cardington test.” *Journal of Constructional Steel Research*, 57(6), 581–601.

Gillie, M., Usmani, A. S., and Rotter, J. M. (2002). “A structural analysis of the Cardington British steel corner test.” *Journal of Constructional Steel Research*, 58(4), 427–442.

Halleux, P. (1967). “Limit analysis of castellated steel beams.” *Acier-Stahl-Steel*, 32(3), 133–144.

Hicks, S., Feeney, M., and Clifton, G. C. (2012). “Fire performance of an office building

with long-span cellular floor beams-Britomart East, Auckland." *Journal of the International Association for Bridge and Structural Engineering*, 22(4), 533–540.

Izzuddin, B. A., and Moore, D. B. (2002). "Lessons from a full-scale fire test." *Proceedings of the ICE - Structures and Buildings*, 152(4), 319–329.

Jiang, J., Li, G.-Q., and Usmani, A. (2015). "Analysis of Composite Steel-concrete Beams Exposed to Fire using OpenSees." *Journal of Structural Fire Engineering*, 6(1), 1–20.

Jiang, J., Usmani, A., and Li, G.-Q. (2014). "Modelling of Steel-Concrete Composite Structures in Fire Using OpenSees." *Advances in Structural Engineering*, 17(2), 249–264.

Jiang, L., and Usmani, A. (2018a). "Computational performance of beam-column elements in modelling structural members subjected to localised fire." *Engineering Structures*, 156, 490–502.

Jiang, L., and Usmani, A. (2018b). "Towards scenario fires – modelling structural response to fire using an integrated computational tool." *Advances in Structural Engineering*, 21(13), 2056–2067.

Jiang, S. C., Ranzi, G., Chen, L. Z., and Li, G. Q. (2017). "Behaviour and design of composite beams with composite slabs at elevated temperatures." *Advances in Structural Engineering*, 20(10), 1451–1465.

Kerdal, D., and Nethercot, D. A. (1984). "Failure modes for castellated beams." *Journal of Constructional Steel Research*, 4(4), 295–315.

Khaliq, W., and Kodur, V. (2012). "High temperature mechanical properties of high strength fly ash concrete with and without fibers." *ACI Materials Journal*, 109(6), 665–674.

Khan, M. A., Jiang, L., Cashell, K. A., and Usmani, A. (2018). "Analysis of restrained composite beams exposed to fire using a hybrid simulation approach." *Engineering Structures*, Elsevier, 172(May), 956–966.

Kirby, B. R. (1988). "High temperature properties of hot rolled structural steel for use in fire design studies." *Fire Safety Journal*, 13(1), 27–37.

Kodur, V. K. R., and Naser, M. Z. (2015). "Effect of local instability on capacity of steel beams exposed to fire." *Journal of Constructional Steel Research*, 111, 31–42.

Kolozvari, K., Orakcal, K., and Wallace, J. W. (2018). "New OpenSEES models for simulating nonlinear flexural and coupled shear-flexural behavior of RC walls and columns." *Computers and Structures*, 196, 246–262.

Korzen, M., Magonette, G., and Buchet, P. (1999). “Mechanical loading of columns in fire tests by means of the substructuring method.” *Journal of applied mathematics and mechanics*, 79(S2), S617-- S618.

Korzen, M., Rodrigues, J. P., and M Correia, A. (2010). “Composite Columns Made of Partially Encased Steel Sections Subjected to Fire.” *Structures in Fire - 2010*, Michigan, USA.

Kuchta, K., and Maślak, M. (2015). “Failure Modes Determining the Resistance and the Stability of Steel Cellular Beams.” *Journal of Civil Engineering, Environment and Architecture*, 32(4), 263–280.

Kwani, S., and Wijaya, P. (2017). “Lateral Torsional Buckling of Castellated Beams Analyzed using the Collapse Analysis.” *Procedia Engineering*, 171, 813–820.

Kwon, O.-S., Nakata, N., Park, K., Elnashai, A., and Spencer, B. (2007). *User Manual and Examples for UI-SIMCOR v2.6 (Multi-Site Substructure Pseudo-Dynamic Simulation Coordinator) and NEES-SAM v2.0 (Static Analysis Module for NEESgrid)*.

Lamont, S., Gillie, M., and Usmani, A. S. (2007). “Composite steel-framed structures in fire with protected and unprotected edge beams.” *Journal of Constructional Steel Research*, 63(8), 1138–1150.

Lawson, R. M. (1990). “Behaviour of steel beam-to-column connections in fire.” *The Structural Engineer*, 68(14), 263–271.

Lawson, R. M. (2006). “Design of FABSEC Cellular Beams in Non-composite and Composite Applications for Both Normal Temperature and Fire Engineering Conditions.” *Steel Construction Institute*, Fabsec Limited.

Lawson, R. M., and Hicks, S. J. (1998). “Design of beams with large web openings.” *Steel Construction Institute*, Berkshire.

Lawson, R. M., Lim, J., Hicks, S. J., and Simms, W. I. (2006). “Design of composite asymmetric cellular beams and beams with large web openings.” *Journal of Constructional Steel Research*, 62(6), 614–629.

Lennon, T. (1997). “BRE Cardington Steel Framed Building Fire Tests.” *British Steel*, Watford, UK.

Li, G. Q., and Guo, S. X. (2008). “Experiment on restrained steel beams subjected to heating and cooling.” *Journal of Constructional Steel Research*, 64, 268–274.

Liming Jiang. (2016). “http://openseesforfire.github.io/Subpages/heattransfer.html.” *OpenSees for Fire*.

Liu, T. C. H. (1998). “Effect of connection flexibility on fire resistance of steel beams.” *Journal of Constructional Steel Research*, 45(1), 99–118.

Liu, T. C. H. (1999). “Fire resistance of unprotected steel beams with moment connections.” *Journal of Constructional Steel Research*, 51(1), 61–77.

Liu, T. C. H., Fahad, M. K., and Davies, J. M. (2002). “Experimental investigation of behaviour of axially restrained steel beams in fire.” *Journal of Constructional Steel Research*, 58, 1211–1230.

Łukomski, M., Turkowski, P., Roszkowski, P., and Papis, B. (2017). “Fire Resistance of Unprotected Steel Beams-Comparison between Fire Tests and Calculation Models.” *Procedia Engineering*, The Author(s), 172, 665–672.

Magonette, G. E., and Negro, P. (1998). “Verification of the pseudodynamic test method.” *European Earthquake Engineering*, XII(1), 40–50.

Mahin, S. A., and Shing, P. S. B. (1985). “Pseudodynamic method for seismic testing.” *Journal of Structural Engineering*, 111(7), 1482–1503.

Manal, D. (2017). “Thermomechanical behaviour of cellular beams.” *Polytechnic Institute of Bragança*, Portugal.

McKenna, F. T. (1997). “Object-oriented finite element programming: Frameworks for analysis, algorithms and parallel computing.” *ProQuest Dissertations and Theses*.

McKenna, S. T., Jones, N., Peck, G., Dickens, K., Pawelec, W., Oradei, S., Harris, S., A Stec, A., and Hull, T. R. (2019). “Fire behaviour of modern façade materials – understanding the Grenfell Tower fire.” *Journal of Hazardous Materials*, 368, 115–123.

Mehta, P. K., and Monteiro, P. J. M. (2006). *Concrete: Microstructure, Properties, and Materials*. McGraw-Hil, New York, USA.

Menkulasi, F., Moen, C. D., and Eatherton, M. R. (2017). “Investigation of Web Post Compression Buckling Limit State and Stiffener Requirements in Castellated Beams.” (2015), 21–43.

Mindess, S., Young, J. F., and Darwin, D. (2003). “Concrete.” *Pearson Education*, Upper saddle river, NJ, USA.

Moss, P. J., Buchanan, A. H., Seputro, J., Wastney, C., and Welsh, R. (2004). “Effect of support conditions on the fire behaviour of steel and composite beams.” *Fire and Materials*, 28(24), 159–175.

Mostafaei, H. (2012). “A New Testing Capability for Seismic Resistance Assessment of Structures Damaged Due to a Fire.” *15th World Conference on Earthquake*

Engineering, Lisbon Portugal.

Mostafaei, H. (2013). "Hybrid fire testing for assessing performance of structures in fire - Methodology." *Fire Safety Journal*, Elsevier, 58, 170–179.

Nadjai, A., Bailey, C. G., Vassart, O., Han, S., Zhao, B., Hawes, M., Franssen, J. M., and Simms, I. (2011). "Full-scale fire test on a composite floor slab incorporating long span cellular steel beams." *Structural Engineer*, 89(21), 18–25.

Nadjai, A., Han, S., Ali, F., Alam, N., and Allam, A. (2017). "Fire resistance of axial restraint composite floor steel cellular beams." *Journal of Constructional Steel Research*, 136, 229–237.

Nadjai, A., Petrou, K., Han, S., and Ali, F. (2016). "Performance of unprotected and protected cellular beams in fire conditions." *Construction and Building Materials*, Elsevier Ltd, 105, 579–588.

Nadjai, A., Vassart, O., Ali, F., Talamona, D., Allam, A., and Hawes, M. (2007a). "Performance of cellular composite floor beams at elevated temperatures." *Fire Safety Journal*, 42(6–7), 489–497.

Nadjai, A., Vassart, O., Ali, F., Talamona, D., Allam, A., and Hawes, M. (2007b). "Performance of cellular composite floor beams at elevated temperatures." *Fire Safety Journal*, 42(6–7), 489–497.

Najafi, M. (2014). "Behaviour of Axially Restrained Steel Beams With Web Openings At Elevated Temperatures." *University of Manchester*, Manchester.

Najafi, M., and Wang, Y. C. (2017a). "Axially restrained steel beams with web openings at elevated temperatures, Part 1: Behaviour and numerical simulation results." *Journal of Constructional Steel Research*, 128, 745–761.

Najafi, M., and Wang, Y. C. (2017b). "Axially restrained steel beams with web openings at elevated temperatures, Part 2: Development of an analytical method." *Journal of Constructional Steel Research*, 128, 687–705.

Nakashima, M. (1992). "Development of real-time pseudo dynamic testing." *Earthquake Engineering & Structural Dynamics*, 21(1), 79–92.

Nakata, N., Spencer, Jr., B. F., and Elnashai, A. S. (2007). "Multi-dimensional Mixed-mode Hybrid Simulation Control and Applications." *Newmark Structural Engineering Laboratory*, Urbana, Illinois, USA.

Newmark, N. M. (1959). "A method of computation for structural dynamics." *Journal of Engineering Mechanics*, ASCE 67.

Nwosu, D. I., Kodur, V. R., Franssen, J., and Hum, J. K. (1999). *User Manual for SAFIR :*

A Computer Program for Analysis of Structures at Elevated Temperature Conditions NRC Publications Archive. *National Research Council*, Canada.

Outinen, J., and Mäkeläinen, P. (2004). "Mechanical properties of structural steel at elevated temperatures and after cooling down." *Fire and Materials*, 28(2–4), 237–251.

Pachpor, P. D., Gupta, L. M., and Deshpande, N. V. (2014). "Analysis and Design of Cellular Beam and its Verification." *IERI Procedia*, 7, 120–127.

Pan, P. (2005). "Online test using displacement-force mixed control." *Earthquake Engineering & Structural Dynamics*, 34(8), 869–888.

Pegon, P., and Pinto, A. (2000). "Pseudo-dynamic testing with substructuring at the ELSA Laboratory." *Earthquake Engineering & Structural Dynamics*, 29, 905–925.

Purkiss, J. A., and Li, L.-Y. (2013). "Fire Safety Engineering Design of Structures." *CRC Press*, 3 edition.

Redwood, R., Zaarour, W., and Megharief, J. (2007). "Web Post Buckling in Castellated Beams." *Advances in Steel Structures (ICASS '96)*, Hong Kong, 67–71.

Schellenberg, A. H., Mahin, S. A., Fenves, G. L., and Center, P. E. E. R. (2009). "Advanced Implementation of Hybrid Simulation." (November), 286.

Schellenberg, A., Huang, Y., and Mahin, S. A. (2008a). "Structural FE-Software Coupling through the Experimental Software Framework, OpenFresco." *The 14th World Conference on Earthquake Engineering*, Beijing.

Schellenberg, A., Huang, Y., and Mahin, S. A. (2008b). "Structural FE-software coupling through the experimental software framework , openfresco." *The 14th World Conference on Earthquake Engineering*, 1–8.

Schellenberg, A., Mahin, S. A., and Fenves, G. L. (2007). "A Software Framework for Hybrid Simulation of Large Structural Systems." *Structural Engineering Research Frontiers*.

Schneider, U. (1988). "Concrete at high temperatures: A general review." *Fire Safety Journal*, 13(1), 55–68.

Shah, S. P. (1991). "Do fibers increase the tensile strength of cementbased matrixes?" *ACI Materials Journal*, 88(6), 595–602.

Shing, P. S. B., and Mahin, S. A. (1984). "Pseudodynamic test method for seismic performance evaluation: theory and implementation." *Earthquake Engineering Research Center*, Earthquake Engineering Research Center, Berkeley, California, 164.

Simms, W. I. (2008). “REP RT1187 Guidance on the fire protection of beams with web openings.” *Steel Construction Institute*, Ascot, UK.

Sofias, C. E., Kalfas, C. N., and Pachoumis, D. T. (2014). “Experimental and FEM analysis of reduced beam section moment endplate connections under cyclic loading.” *Engineering Structures*, Elsevier Ltd, 59, 320–329.

Sonck, D., and Belis, J. (2015). “Lateral-torsional buckling resistance of cellular beams.” *Journal of Constructional Steel Research*, Elsevier Ltd, 105, 119–128.

Sonck, D., Vanlaere, W., and Van Impe, R. (2011). “Influence of plasticity on lateral–torsional buckling behaviour of cellular beams.” *Materials Research Innovations*, 15(s1), s158–s161.

Stern-Gottfried, J. (2011). “Travelling Fires for Structural Design.” *Fire Safety Journal*, 54, 74–85.

Stern-Gottfried, J., and Rein, G. (2012). “Travelling fires for structural design-Part II: Design methodology.” *Fire Safety Journal*, 54, 96–112.

Surtees, J. O., and Liu, Z. (1995). “Loading Tests on Cellform Beams : Research Report.” *University of Leeds*, Leeds.

Takahashi, Y., and Fenves, G. L. (2006). “Software framework for distributed experimental-computational simulation of structural systems.” *Earthquake Engineering and Structural Dynamics*, 35(3), 267–291.

Takanashi, K., and Nakashima, M. (1987). “Japanese activities on on-line testing.” *Journal of Engineering Mechanics*, 113(7), 1014–1032.

Takanashi, K., and Nakashima, M. (1988). “On-line computer test control method and its application to earthquake response simulation of steel structural models.” *Journal of Constructional Steel Research*, 11(1), 27–40.

Tan, K.-H., and Huang, Z.-F. (2005). “Structural Responses of Axially Restrained Steel Beams with Semirigid Moment Connection in Fire.” *Journal of Structural Engineering*, 131(April), 541–551.

Thewalt, C. R., and Mahin, S. A. (1987). “Hybrid solution techniques for generalized pseudodynamic testing.” *Earthquake Engineering Research Center*, Berkeley, California, 112.

Toprac, A. A., and Cooke, B. R. (1959). “An experimental investigation of open-web beams.” *Welding research council bulletin series*, 47.

Tsavdaridis, K. D., and D’Mello, C. (2011a). “Web buckling study of the behaviour and strength of perforated steel beams with different novel web opening shapes.” *Journal*

of Constructional Steel Research, Elsevier Ltd, 67(10), 1605–1620.

Tsavdaridis, K. D., and D'Mello, C. (2011b). *Fe Modelling Techniques for Web-Post Buckling Response*. *6th European Conference on Steel and Composite Structures*, Budapest, Hungary.

Twilt, L. (1991). "Stress-strain relationships of structural steel at elevated temperatures: Analysis of various options and European proposal–Part F: mechanical properties." *TNO Rep. No. BI-91-015*, Delft, The Netherlands.

Usmani, A., Drysdale, D. D., Rotter, J. M., Sanad, A. M., Gillie, M., and Lamont, S. (2000). "PIT Project, Main Report : Behaviour of steel framed structures under fire conditions." *University of Edinburgh*, Edinburgh.

Usmani, A. S., Rotter, J. M., Lamont, S., Sanad, A. M., and Gillie, M. (2001). "Fundamental principles of structural behaviour under thermal effects." *Fire Safety Journal*, 36(8), 721–744.

Usmani, A., Zhang, J., Jiang, J., Jiang, Y., Kotsovinos, P., Zhang, J., and May, I. (2010). "Using OpenSEES for structures in fire." *Structures in Fire*, 3(1), 919–926.

Vassart, O. (2009). "Cellular Beam Solutions." *Arcelor Mittal*.

Vassart, O., Hawes, M., Simms, I., Zhao, B., Franssen, J. M., and Nadjai, A. (2010). "Fire resistance of long span cellular beam made of rolled profiles (FICEB)." *Research Fund for Coal and Steel*, Brussels.

Wainman, D. E., and Kirby, B. R. (1988). "Compendium of UK standard fire test data unprotected structural steel-1." *British Steel Corporation*, Swinden Laboratories, Rotherdam.

Wald, F., Kallerová, P., Chlouba, P., and Sokol, Z. (2011). *Fire test on administrative building*. *Steel and Aluminium Structures*, Mokrsko.

Wang, P., Liu, C., Liu, M., and Wang, X. (2016). "Numerical studies on large deflection behaviour of axially restrained corrugated web steel beams at elevated temperatures." *Thin-Walled Structures*, Elsevier, 98, 58–74.

Wang, P., Wang, X., and Ma, N. (2014). "Vertical shear buckling capacity of web-posts in castellated steel beams with fillet corner hexagonal web openings." *Engineering Structures*, Elsevier Ltd, 75, 315–326.

Wang, T., Nakashima, M., and Pan, P. (2006). "On-line hybrid test combining with general-purpose finite element software." *Earthquake Engineering and Structural Dynamics*, 35(12), 1471–1488.

Wang, Y. (2002). "Steel and Composite Structures: Behaviour and Design for Fire

Safety.” *Taylor and Francis group*, London, 1, 1829–1841.

Wang, Y. C., and Burgess, I. W. (2008). “The safety of common steel beam / column connections in fire.” *Structural Engineer*, 88(21), 26–35.

Warren, J. (2001). “Ultimate load and deflection behaviour of cellular beams.” *University of Natal*, Durban.

Withers, P. J., and Bhadeshia, H. K. D. H. (2001). “Residual stress. Part 1 – Measurement techniques.” *Materials Science and Technology*, Taylor & Francis, 17(4), 355–365.

Wong, V. B., Brugess, I., and Plank, R. (2009). “Behaviour of composite cellular steel - concrete beams at elevated temperatures.” *Steel Structures*, 9, 29–37.

Yin, Y. Z. (2004). “Advanced behaviour of steel beams under fire conditions.” *University of Manchester*, Manchester.

Yin, Y. Z., and Wang, Y. C. (2004). “A numerical study of large deflection behaviour of restrained steel beams at elevated temperatures.” *Journal of Constructional Steel Research*, 60(7), 1029–1047.

Yin, Y. Z., and Wang, Y. C. (2006). “Analysis of behaviour of steel beams with web openings at elevated temperatures.” *Steel and Composite Structures*, 6, 15–31.

Zhao, J. C., and Shen, Z. Y. (1999). “Experimental studies of the behaviour of unprotected steel frames in fire.” *Journal of Constructional Steel Research*, 50(2), 137–150.

Zhu, M., McKenna, F., and Scott, M. H. (2018). “OpenSEESPy: Python library for the OpenSEES finite element framework.” *SoftwareX*, Elsevier B.V., 7, 6–11.

Appendix A.

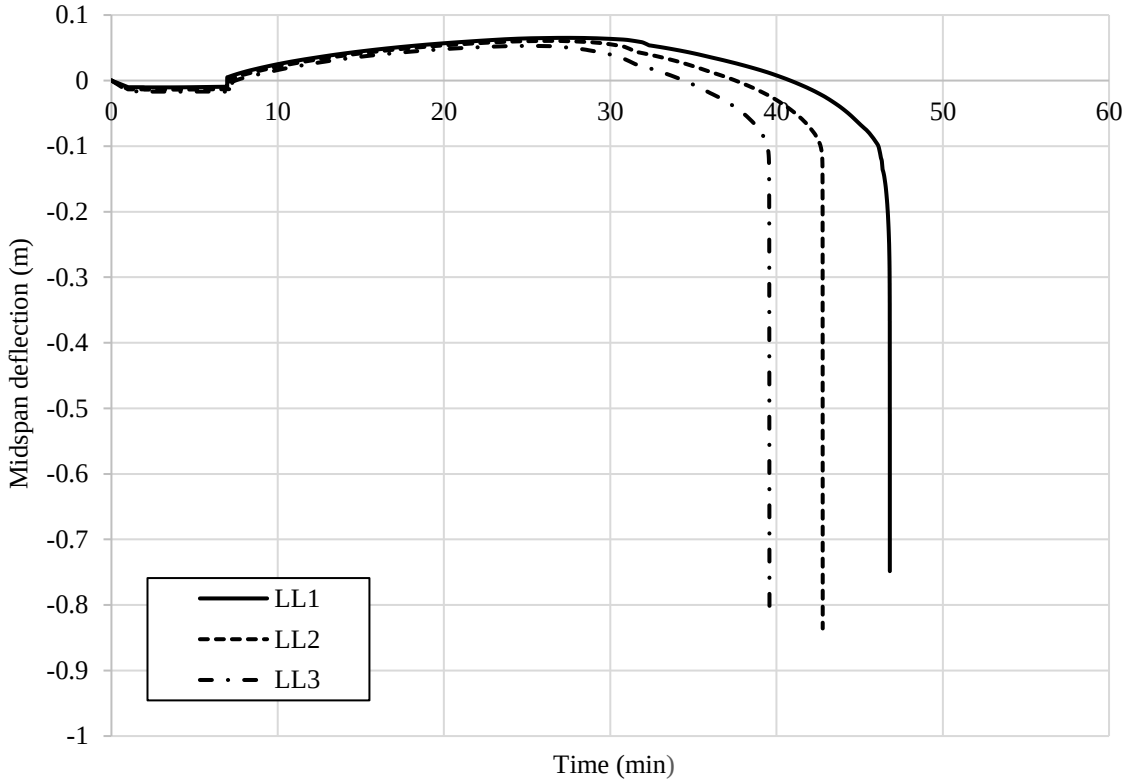

(a)

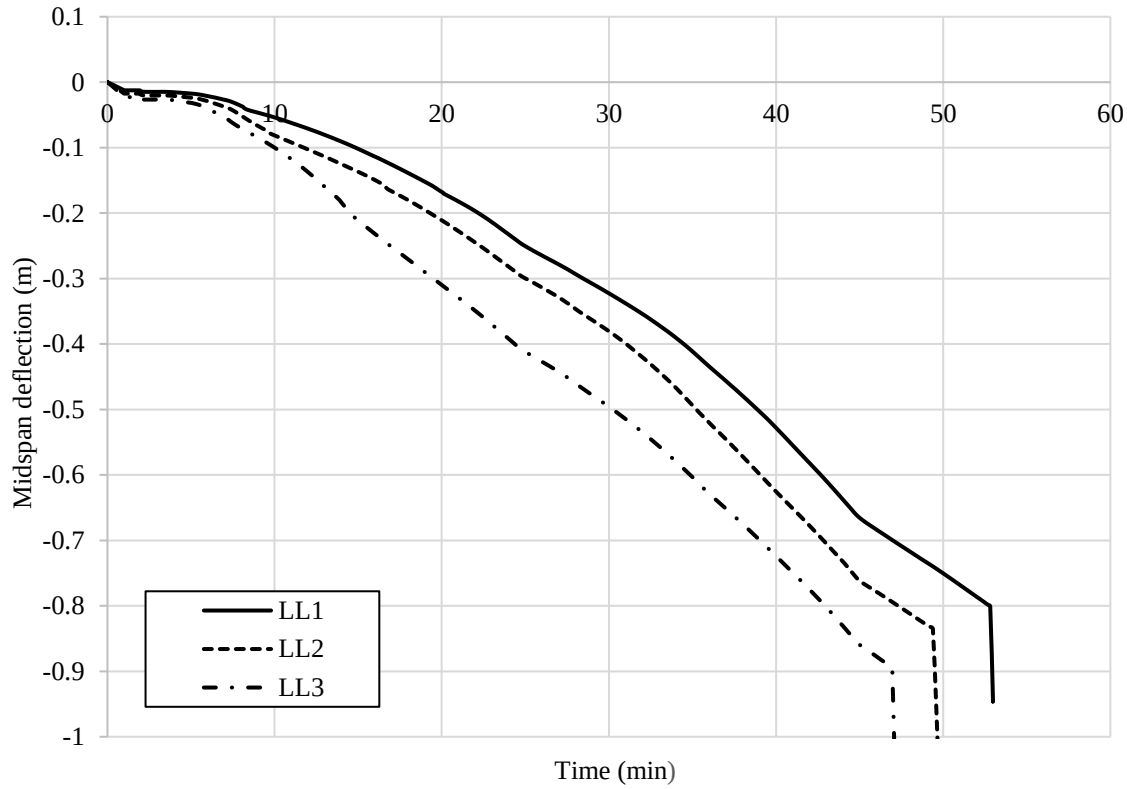

(b)

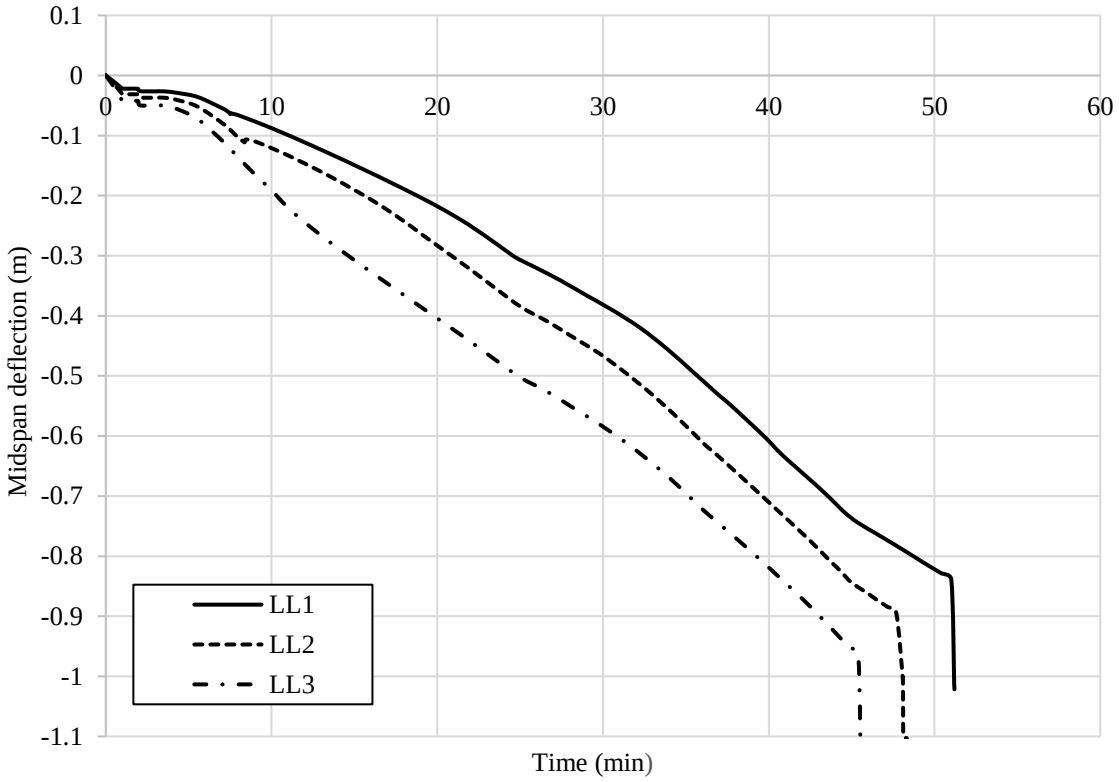

(c)

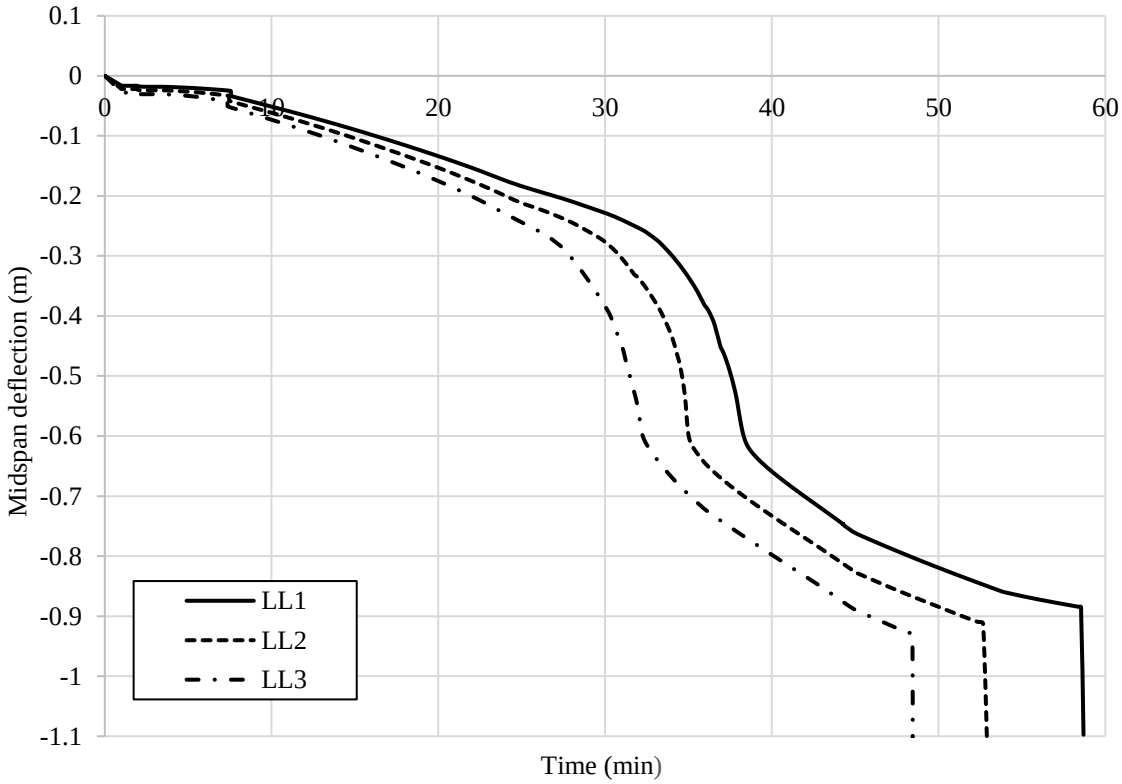

(d)

Fig. A.1 Time-deflection behaviour for beams made with steel strength S450 and opening layout (a) 1, (b) 2, (c) 3 and (d) 4.

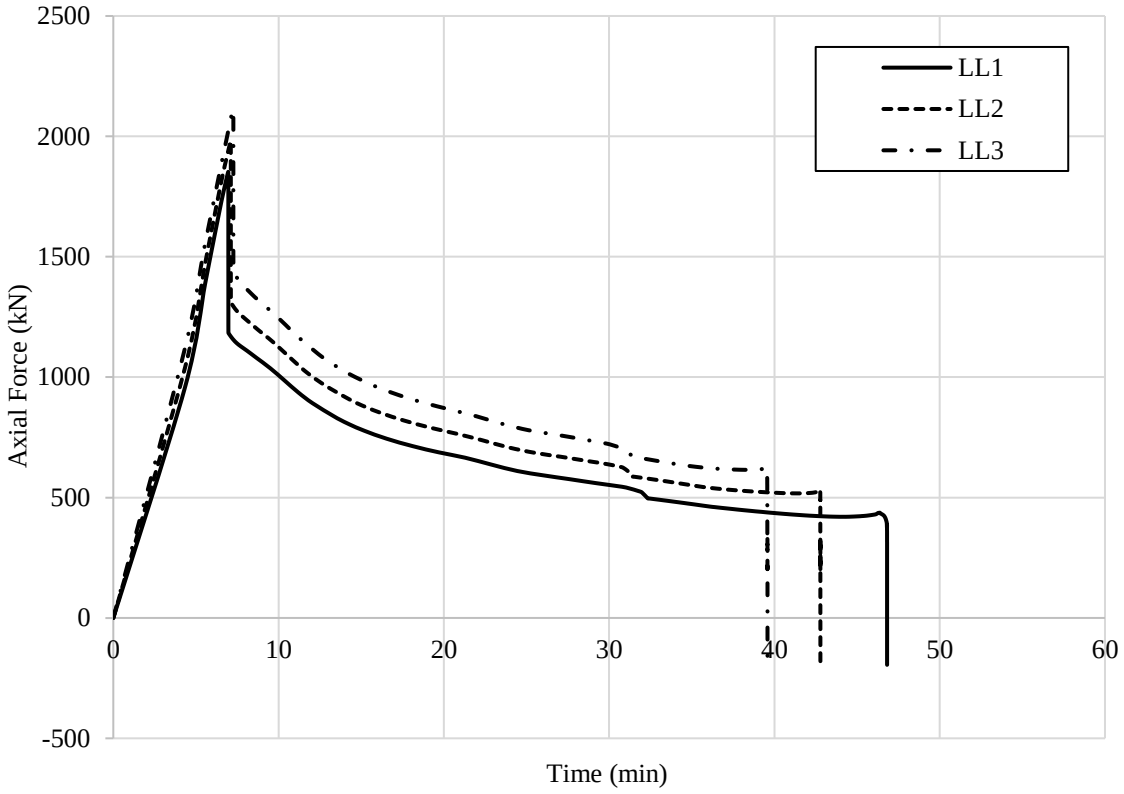
2500
2000
1500
1000
500
0
-500
Axial Force (kN)
0
10
20
30
40
50
60
Time (min)
LL1
LL2
LL3

(a)

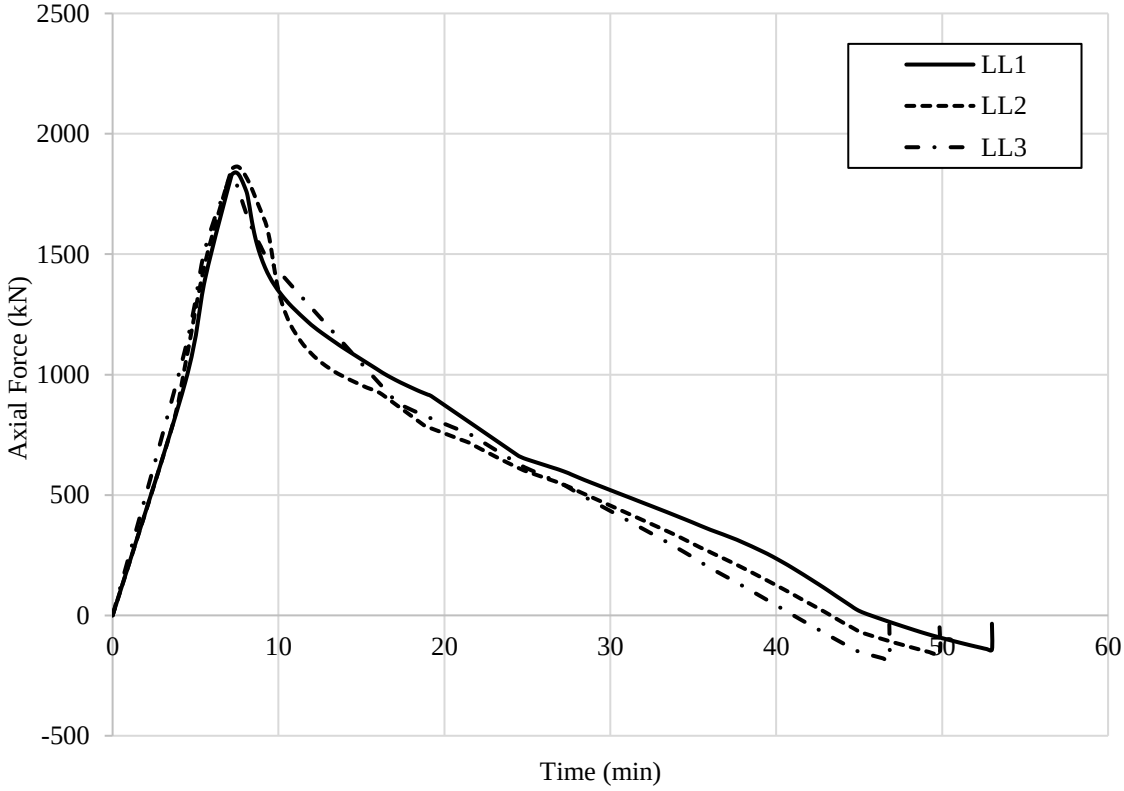
2500
2000
1500
1000
500
0
-500
Axial Force (kN)
0
10
20
30
40
50
60
Time (min)
LL1
LL2
LL3

(b)

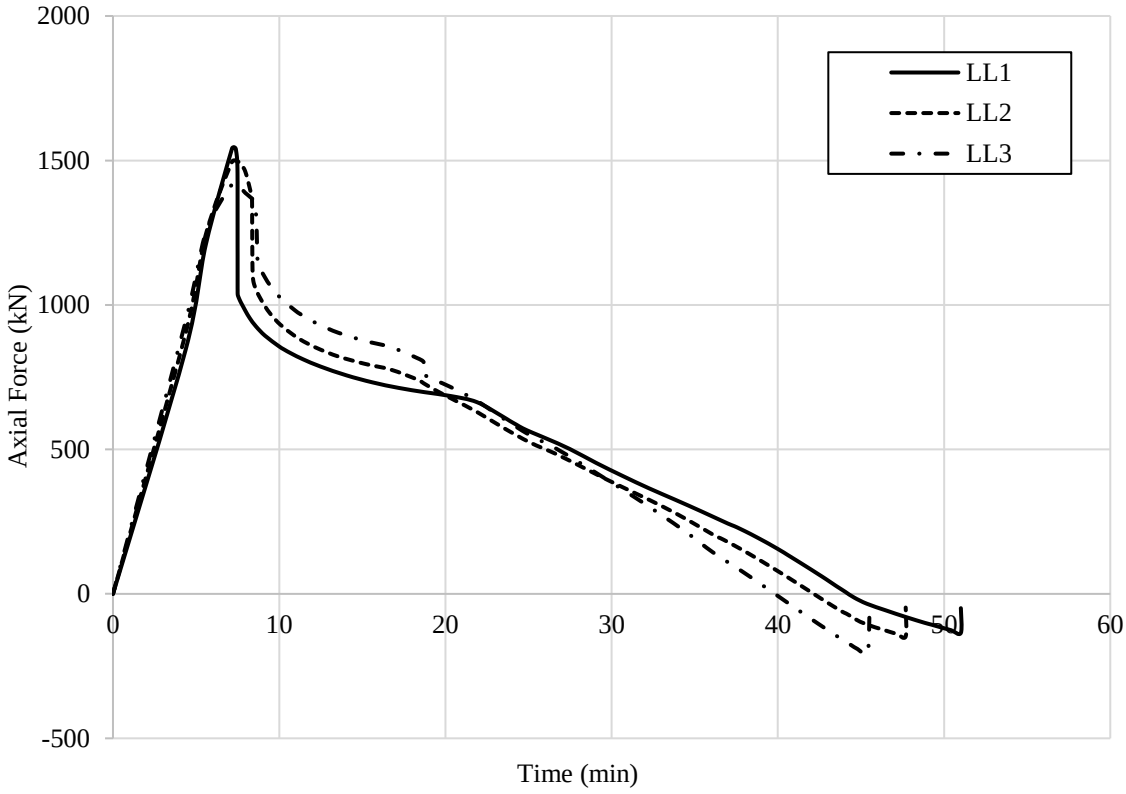

(c)

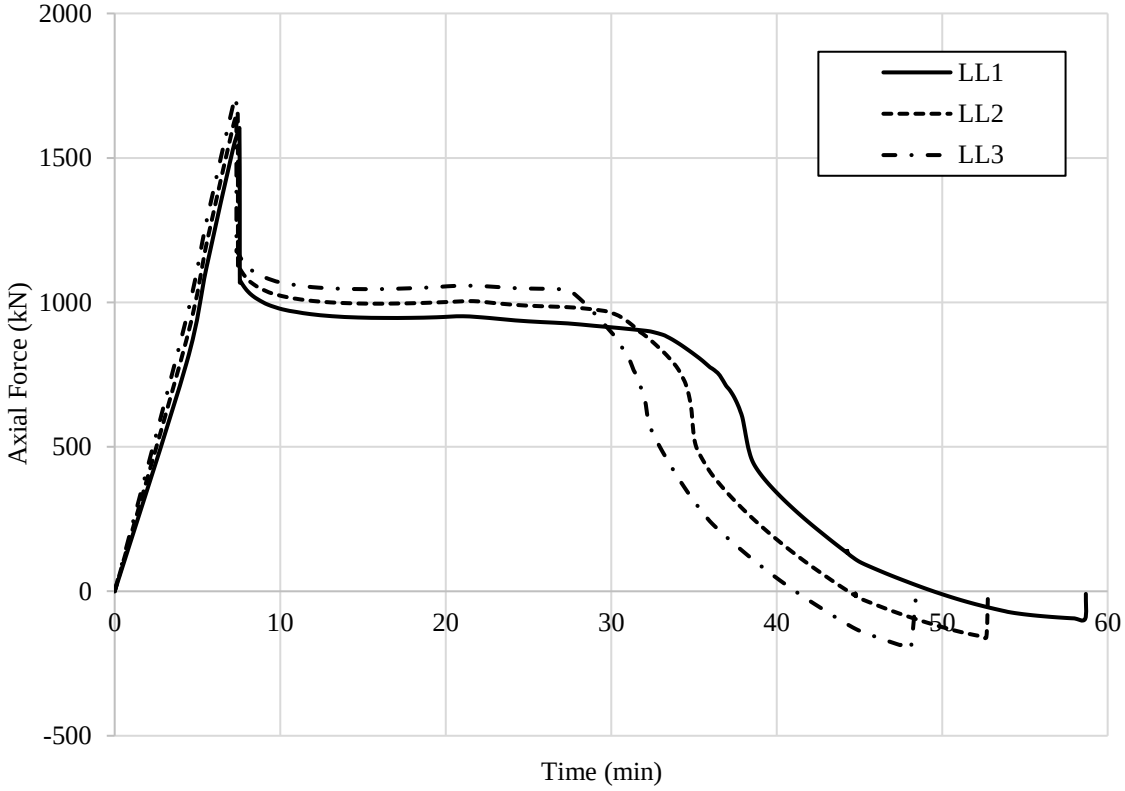

(d)

Fig. A.2 Development of axial force for beams made with S450 at different load level and opening layout (a) 1, (b) 2, (c) 3 and (d) 4.

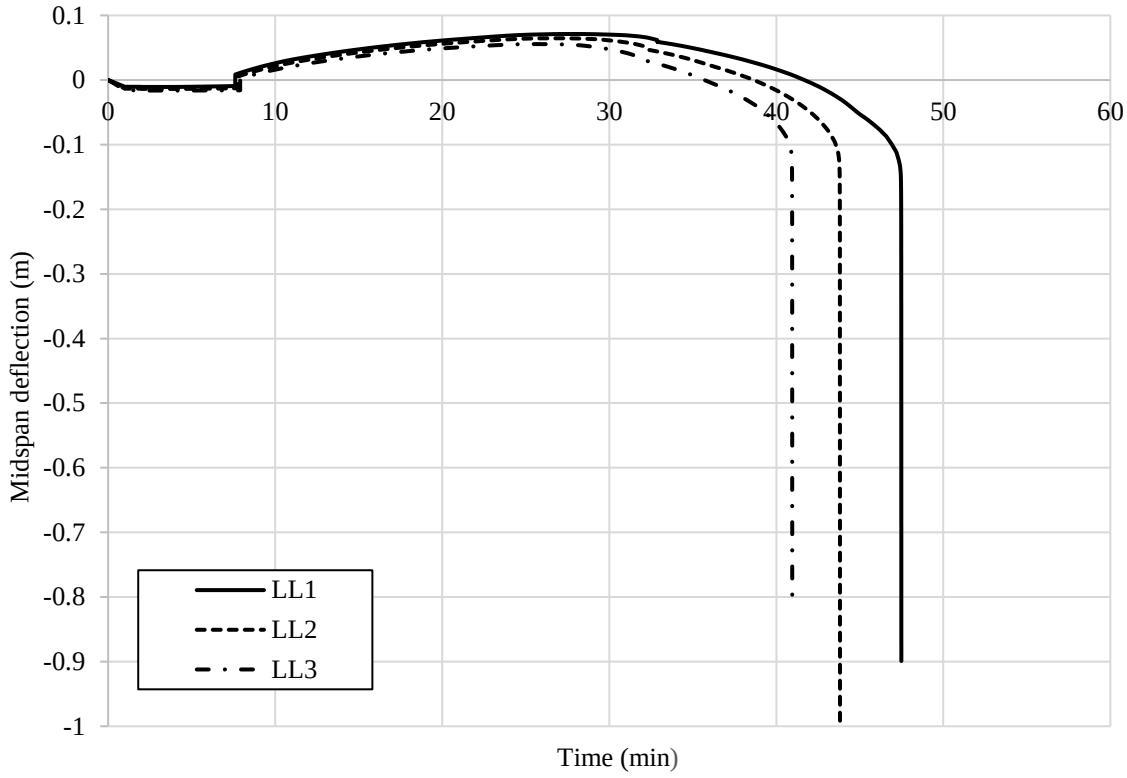
0.1
0
-0.1
-0.2
-0.3
-0.4
-0.5
-0.6
-0.7
-0.8
-0.9
-1
0
10
20
30
40
50
60
Midspan deflection (m)
Time (min)
LL1
LL2
LL3

(a)

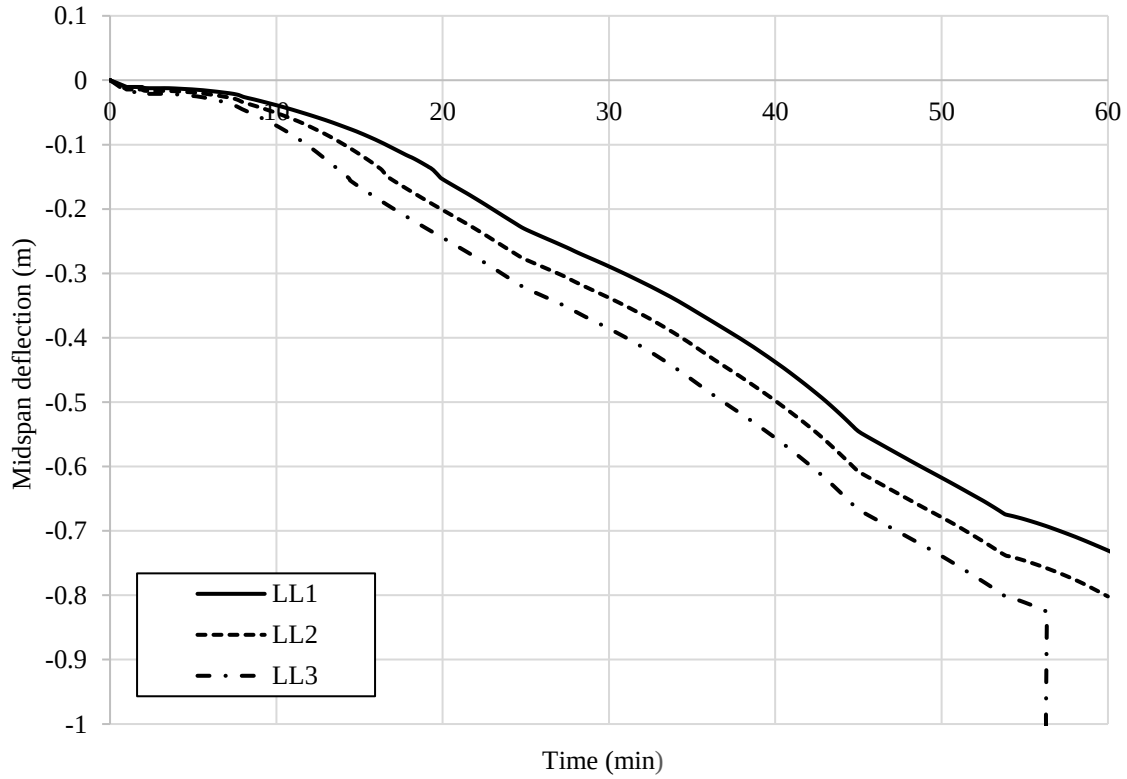
0.1
0
-0.1
-0.2
-0.3
-0.4
-0.5
-0.6
-0.7
-0.8
-0.9
-1
0
10
20
30
40
50
60
Midspan deflection (m)
Time (min)
LL1
LL2
LL3

(b)

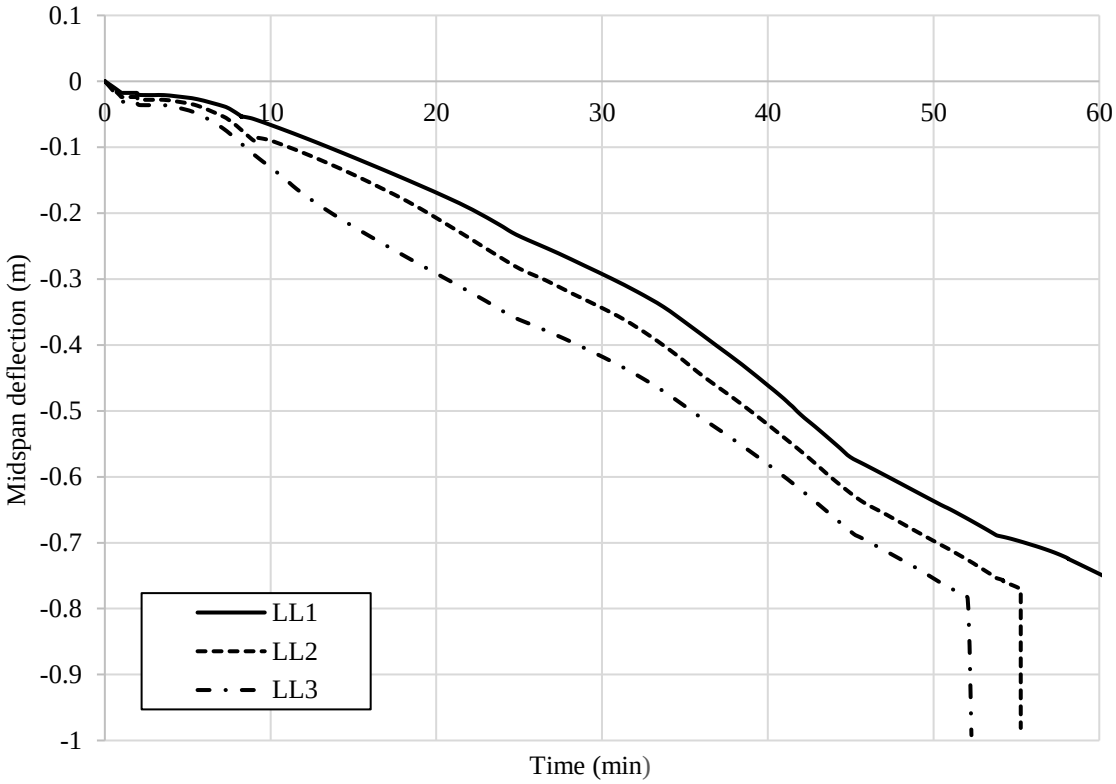

(a)

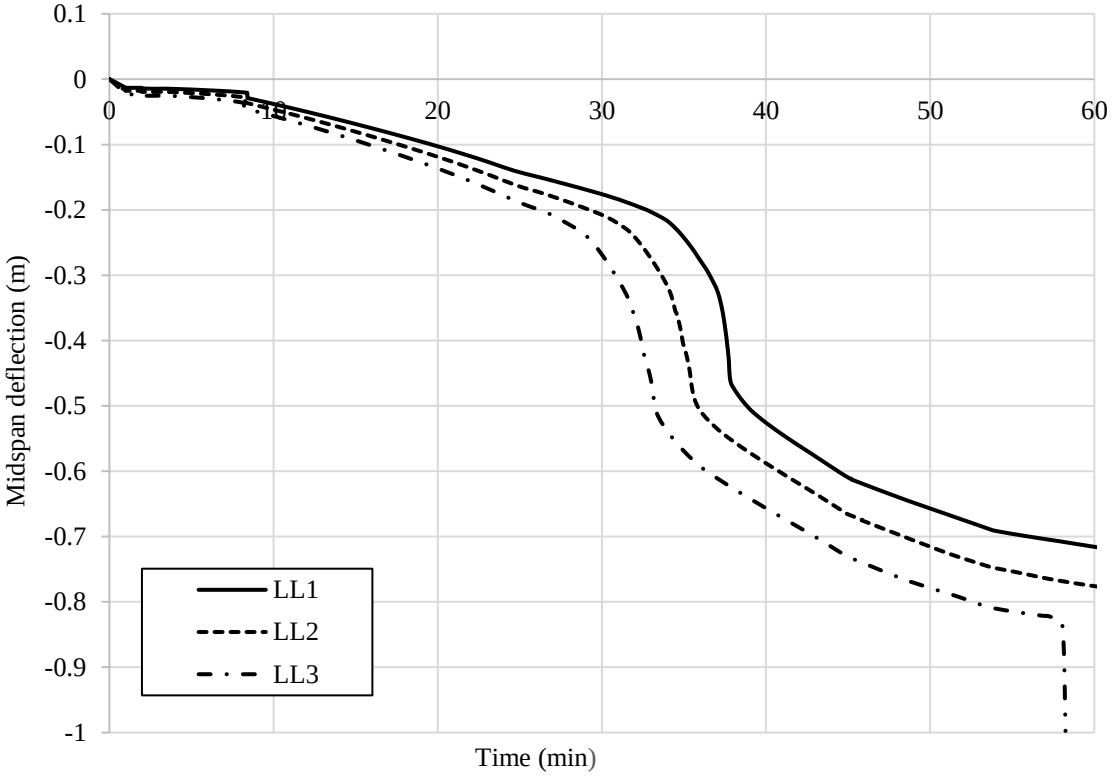

(d)

Fig. A.3 Time-deflection behaviour for beams made with steel strength S550 and opening layout (a) 1, (b) 2, (c) 3 and (d) 4.

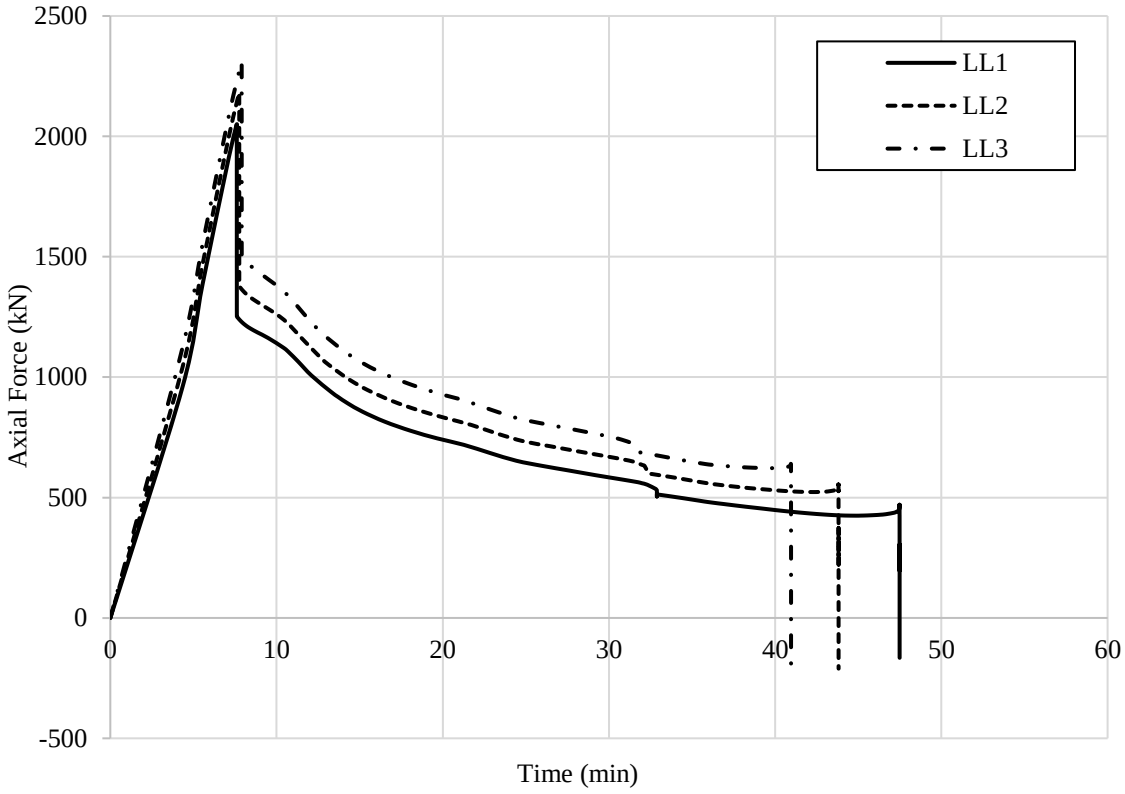
2500
2000
1500
1000
500
0
-500
Axial Force (kN)
0
10
20
30
40
50
60
Time (min)
LL1
LL2
LL3

(a)

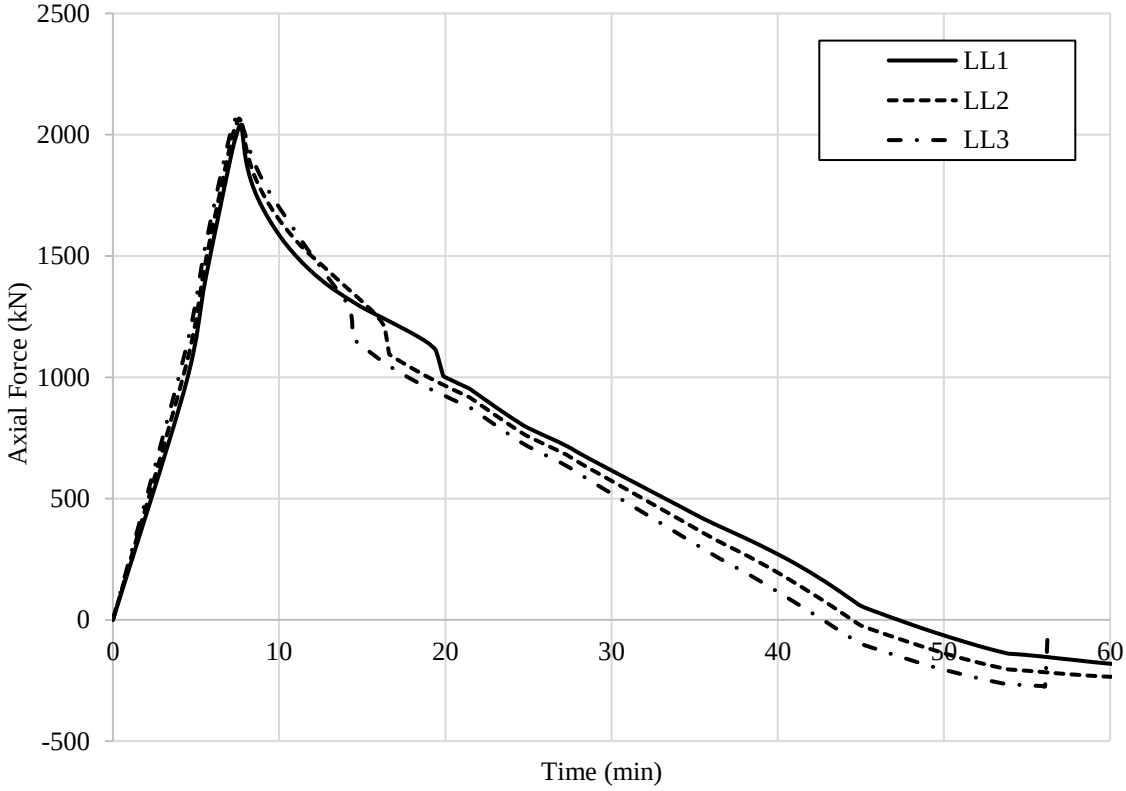
2500
2000
1500
1000
500
0
-500
Axial Force (kN)
0
10
20
30
40
50
60
Time (min)
LL1
LL2
LL3

(b)

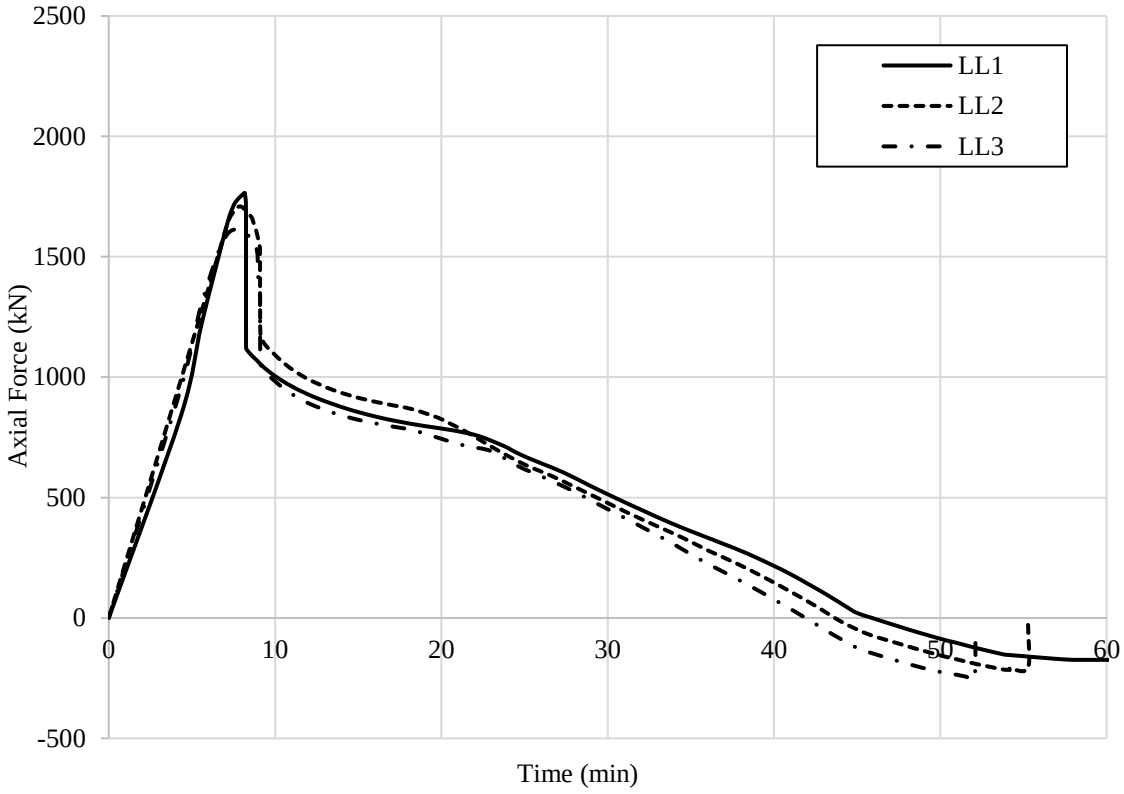

(c)

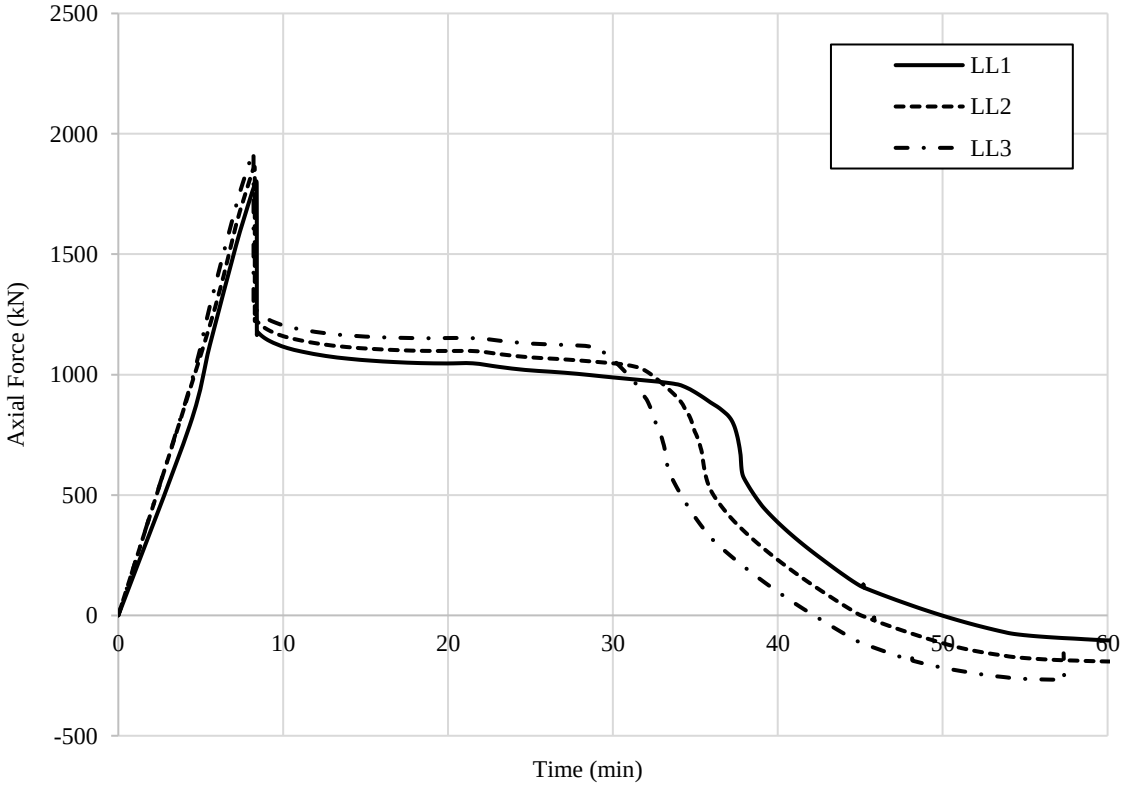

(d)

Fig. A.4 Development of axial force for beams made with S550 at different load level and opening layout (a) 1, (b) 2, (c) 3 and (d) 4.